THE UNIVERSITY OF QUEENSLAND

AUSTRALIA

Investigation of Control of the Incremental Forming Processes

Haibo Lu

Bachelor of Engineering

A thesis submitted for the degree of Doctor of Philosophy at

The University of Queensland in 2016

School of Mechanical and Mining Engineering

Abstract

Incremental Sheet Forming (ISF) is a new-emerging sheet forming process that promises high flexibility and formability because it does not need any dedicated dies or tooling. This makes ISF well suited for small scale and customised production. ISF uses a simple tool with a smooth end to deform sheets along a toolpath typically generated from CAM software. In ISF, the part is fabricated incrementally by orderly accumulation of plastic deformations localised around the ball end of the tool. Without using dedicated tooling, ISF can quickly adapt to new and modified product shapes via toolpath alteration. Hence, ISF is a promising sheet forming process for quick and low-cost production for small batch manufacturing. In spite of these outstanding characteristics, ISF still suffers from some drawbacks including long processing time and low geometric accuracy. The latter one is the major cause of low take-up of ISF in the forming industry. Therefore, the work presented in this thesis is mainly focused on the improvement of geometric accuracy of the formed parts via in-process toolpath correction using feedback control. In this thesis, Model Predictive Control (MPC), an advanced model-based control technology, was adopted to develop feedback control strategies for ISF toolpath control and correction to improve geometric accuracy.

The first research aspect of this thesis is focused on the development of a simple MPC algorithm to optimise the step depth, a critical toolpath parameter defined by the user in the toolpath generation. Firstly, a parameter investigation was performed to experimentally study the influences of the step depth on geometric accuracy, surface finish, and thickness distribution. Two sets of experimental tests with varying step depth values were conducted in the typical Single Point Incremental Forming (SPIF) process that is without toolpath control. The results showed that a smaller step depth led to better geometric accuracy and part surface quality in the ISF process, while the material formability decreased with the step depth value. Too small step depth values would lead to material failure. The parameter investigation work provided significant fundamental information for the development of feedback control strategies for toolpath correction. Then, a simple MPC algorithm was developed for in-process toolpath control/correction in SPIF. During the forming process using the simple MPC algorithm, the step depth of the contour toolpath was optimised at each forming step by solving a receding optimal problem based on the measured shape feedback during the forming process. The developed algorithm was experimentally verified in two case studies to form two different shapes. Results show that the geometric accuracy in ISF with feedback control has been greatly improved (from ±3 mm to ±0.3 mm) at the bottom area of the formed parts compared with a standard ISF approach without control. Improved geometric accuracy has been achieved on the wall of the parts as well, but the errors in the wall areas are still relatively large.

In the second research objective of this thesis, a two-directional MPC algorithm was developed by augmenting the simple MPC algorithm with a horizontal control module for horizontal toolpath correction. With two separate MPC modules in vertical and horizontal directions, the toolpath was corrected by optimising the step depth and the horizontal step increment at each step during the forming process. Two case studies were conducted to experimentally verify the developed two-directional MPC algorithm. In the first case study (a truncated pyramid), two control approaches with different assumptions for the horizontal springback distribution along the horizontal cross-sectional profile were tested and compared. Then, the developed MPC control algorithm was applied to form an asymmetric cone. Results show that the developed strategy can reduce the forming errors in the wall and base of the formed shape compared to the existing works. The SPIF process with two-directional MPC control leads to significant accuracy improvement (from ±3 mm to ±0.3 mm) in the base and most wall areas of the formed shapes in comparison with the typical SPIF process that is without toolpath control.

The last research objective of this thesis is focused on an enhanced MPC algorithm specially developed for Two Point Incremental Forming (TPIF) with a partial die to conduct in-process toolpath correction. In the horizontal control module, dense profile points in the evenly distributed radial directions of the horizontal section were used to estimate the horizontal error distribution along the horizontal sectional profile during the forming process. The toolpath correction was performed through properly adjusting the toolpath in the horizontal and vertical directions based on the optimised toolpath parameters at each step. A case study for forming a non-axisymmetric shape was conducted to experimentally verify the developed toolpath correction strategy. Experiment results indicate that the two-directional toolpath correction approach contributes to part accuracy improvement of about 90% (from ±3 mm to ±0.3 mm) in TPIF compared with the uncontrolled TPIF process.

The work in this thesis explores various aspects of ISF research, although the most important contribution is the feedback control of ISF processes and the experimental validation, which helps to achieve great improvement in ISF geometric accuracy and provides good approaches for in-process control and optimisation in the field of advanced manufacturing.

Declaration by author

This thesis is composed of my original work, and contains no material previously published or written by another person except where due reference has been made in the text. I have clearly stated the contribution by others to jointly-authored works that I have included in my thesis.

I have clearly stated the contribution of others to my thesis as a whole, including statistical assistance, survey design, data analysis, significant technical procedures, professional editorial advice, and any other original research work used or reported in my thesis. The content of my thesis is the result of work I have carried out since the commencement of my research higher degree candidature and does not include a substantial part of work that has been submitted to qualify for the award of any other degree or diploma in any university or other tertiary institution. I have clearly stated which parts of my thesis, if any, have been submitted to qualify for another award.

I acknowledge that an electronic copy of my thesis must be lodged with the University Library and, subject to the policy and procedures of The University of Queensland, the thesis be made available for research and study in accordance with the Copyright Act 1968 unless a period of embargo has been approved by the Dean of the Graduate School.

I acknowledge that copyright of all material contained in my thesis resides with the copyright holder(s) of that material. Where appropriate I have obtained copyright permission from the copyright holder to reproduce material in this thesis.

Publications during candidature

Published/Accepted papers

1. **Lu, H. B.**, Li, Y. L., Liu, Z. B., Liu, S., & Meehan, P. A. (2014). Study on step depth for part accuracy improvement in incremental sheet forming process. *Advanced Materials Research*, 939, 274-280.

2. **Lu, H.**, Kearney, M., Li, Y., Liu, S., Daniel, W. J., & Meehan, P. A. (2015). Model predictive control of incremental sheet forming for geometric accuracy improvement. *The International Journal of Advanced Manufacturing Technology*, *82*(9-12), 1781-1794.

3. **Lu, H.,** Kearney, M, Liu, S., Daniel, W. J., & Meehan, P. A (2016). Two-directional toolpath correction in single point incremental forming using Model predictive control. *The International Journal of Advanced Manufacturing Technology*, 1-16.

4. **Lu, H.**, Kearney, M., Wang, C., Liu, S., & Meehan, P. A. (2017). Part accuracy improvement in two point incremental forming with a partial die using a model predictive control algorithm. *Precision Engineering*, 49, 179-188.

5. Li, Y., **Lu, H.**, Daniel, W. J., & Meehan, P. A. (2015). Investigation and optimisation of deformation energy and geometric accuracy in the incremental sheet forming process using response surface methodology. *The International Journal of Advanced Manufacturing Technology*, 79(9-12), 2041-2055.

6. Li, Y., Daniel, W. J., Liu, Z., **Lu, H.**, & Meehan, P. A. (2015). Deformation mechanics and efficient force prediction in single point incremental forming. *Journal of Materials Processing Technology*, *221*, 100-111.

7. Li, Y., Liu, Z., **Lu, H.**, Daniel, W. B., Liu, S., & Meehan, P. A. (2014). Efficient force prediction for incremental sheet forming and experimental validation. *The International Journal of Advanced Manufacturing Technology*, *73*(1-4), 571-587.

8. Li, Y. L., Liu, Z. B., **Lu, H.**, Daniel, W. J. T., & Meehan, P. A. (2014). Experimental study and efficient prediction on forming forces in incremental sheet forming. *Advanced Materials Research,* 939, 313-321.

9. Wang, C. H., Daniel, W. J., **Lu, H. B.**, Liu, S., & Meehan, P. A. (2017). An Experimental and Numerical Study on Forming Force, Fracture Behavior, and Strain States in Two Point Incremental Forming Process. *Key Engineering Materials*, 725, 586-591.

Conference presentations

- **Lu, H,** Study on step depth for part accuracy improvement in incremental sheet forming process. The 16th International conference on Advances in Materials & Processing Technologies. Taipei, Taiwan. 22-26 Sep. 2013.

Publications included in this thesis

The following publications have been appended at the end of this thesis.

1. **Lu, H.**, Li, Y., Liu, Z., Liu, S., & Meehan, P. A. (2014). Study on step depth for part accuracy improvement in incremental sheet forming process. *Advanced Materials Research*, 939, 274-280.

Contributor	Statement of contribution
Author H. Lu (Candidate)	Conception and design (75%) Data analysis and interpretation (70%) Wrote and edited the paper (80%)
Author Y. Li	Conception and design (10%) Data analysis and interpretation (10%) Wrote and edited the paper (5%)
Author Z. Liu	Conception and design (5%) Data analysis and interpretation (5%)
Author S. Liu	Data analysis and interpretation (5%) Wrote and edited the paper (5%)
Author P.A. Meehan	Conception and design (10%) Data analysis and interpretation (10%) Wrote and edited the paper (10%)

2. **Lu, H.**, Kearney, M., Li, Y., Liu, S., Daniel, W. J., & Meehan, P. A. (2015). Model predictive control of incremental sheet forming for geometric accuracy improvement. *The International Journal of Advanced Manufacturing Technology*, *82*(9-12), 1781-1794.

Contributor	Statement of contribution
Author H. Lu (Candidate)	Conception and design (70%) Data analysis and interpretation (70%) Wrote and edited the paper (75%)
Author M. Kearney	Conception and design (20%) Data analysis and interpretation (10%) Wrote and edited the paper (10%)
Author Y. Li	Data analysis and interpretation (5%) Wrote and edited the paper (5%)
Author S. Liu	Data analysis and interpretation (5%)
Author W. J. T. Daniel	Data analysis and interpretation (5%) Wrote and edited the paper (5%)
Author P.A. Meehan	Conception and design (10%) Data analysis and interpretation (5%) Wrote and edited the paper (5%)

3. **Lu, H.,** Kearney, M, Liu, S., Daniel, W. J., & Meehan, P. A (2016). Two-directional toolpath correction in single point incremental forming using Model predictive control. *The International Journal of Advanced Manufacturing Technology*, 1-16.

Contributor	Statement of contribution
Author H. Lu (Candidate)	Conception and design (70%) Data analysis and interpretation (70%) Wrote and edited the paper (75%)
Author M. Kearney	Conception and design (20%) Data analysis and interpretation (10%) Wrote and edited the paper (10%)
Author S. Liu	Data analysis and interpretation (5%) Wrote and edited the paper (5%)
Author W. J. T. Daniel	Data analysis and interpretation (5%) Wrote and edited the paper (5%)
Author P.A. Meehan	Conception and design (10%) Data analysis and interpretation (10%) Wrote and edited the paper (5%)

4. **Lu, H.**, Kearney, M., Wang, C., Liu, S., & Meehan, P. A. (2017). Part accuracy improvement in two point incremental forming with a partial die using a model predictive control algorithm. *Precision Engineering*, 49, 179-188.

Contributor	Statement of contribution
Author H. Lu (Candidate)	Conception and design (70%) Data analysis and interpretation (75%) Wrote and edited the paper (75%)
Author M. Kearney	Conception and design (20%) Data analysis and interpretation (10%) Wrote and edited the paper (10%)
Author C. Wang	Data analysis and interpretation (5%) Wrote and edited the paper (5%)
Author S. Liu	Data analysis and interpretation (5%)
Author P.A. Meehan	Conception and design (10%) Data analysis and interpretation (5%) Wrote and edited the paper (10%)

Contributions by others to the thesis

My principal supervisor Prof. Paul Meehan offered extensive assistance in writing the thesis draft and revising the thesis so as to contribute to the interpretation. Dr Michael Kearney provided useful comments on the development of the control algorithms and the revision of this thesis. Dr. Bill Daniel provided helpful comments on the structure and the revision of thesis.

Statement of parts of the thesis submitted to qualify for the award of another degree

None.

Acknowledgements

First of all, I would like to give my sincere appreciation to my principal supervisor Prof. Paul Meehan for the great guidance and support in my research throughout my PhD studies, for the continuous help in the completion of this thesis.

My great gratitude also goes to my co-supervisors Dr. Michael Kearney, and Dr. Bill Daniel. Dr. Michael Kearney is a very nice man who smiles a lot every time I meet him. I really appreciate his extensive guidance in developing the control algorithms, his insightful ideas and suggestions in the weekly discussions during the past three years and more, and his great help in the revision of this thesis. I would like to thank Dr. Bill Daniel for his enlightening discussions and suggestions on the analytical modelling aspects.

I also appreciate the time and helpful comments from the review committee members of my milestones: Prof. Mingxing Zhang, Dr. Michael Bermingham, and Dr. Bo Feng during the course of my candidature.

Special thanks are given to Dr. Sheng Liu, Dr. Zhaobing Liu, Dr. Yanle Li, Mr. Chenhao Wang, and all the other group members for their extensive discussions and assistance.

The scholarship received from the Chinese Scholarship Council (CSC) and The University of Queensland International Scholarship (UQI) are gratefully acknowledged.

I had a great time studying at The University of Queensland and staying in Australia for four years. I am grateful for the enjoyable time and support from all my friends.

Finally, I would like to thank my parents, my wife, and all the other families for their love, continuous encouragement over the years.

Keywords

Incremental sheet forming, Model predictive control, Feedback control, Geometric accuracy, Analytical predictive model, Toolpath correction, Toolpath optimisation, Formability.

Australian and New Zealand Standard Research Classifications (ANZSRC)

ANZSRC code: 091006, Manufacturing Processes and Technologies, 30%

ANZSRC code: 091302, Automation and Control Engineering, 50%

ANZSRC code: 091399, Mechanical Engineering not elsewhere classified, 20%

Fields of Research (FoR) Classification

FoR code: 0913, Mechanical Engineering, 55%

FoR code: 0910, Manufacturing Engineering, 45%

Table of Contents

List of Figures

List of Tables

List of Abbreviations used in the thesis

3D	Three dimensional
CAD	Computer-aided design
CAM	Computer-aided manufacturing
CNC	Computer numerically controlled
DSIF	Double-sided incremental forming
FE	Finite element
FEA	Finite element analysis
FEM	Finite element method
FLC	Forming limit curve
ISF	Incremental sheet forming
MPC	Model predictive control
NN	Neural network
PID	Proportional-Integral-Derivative
QP	Quadratic programming
SPIF	Single point incremental forming
TPIF	Two point incremental forming

Chapter 1 Introduction

The work presented in this thesis is focused on the investigation of control of Incremental Sheet Forming (ISF) technology, which includes: process investigation, and development and validation of the feedback control algorithms for ISF. This research facilitates the development of ISF technology and its industry application for the fabrication of complex sheet parts, such as vehicle and aircraft body panels, and fairings. This chapter summarises the background, research scope, and the contents of this thesis. A general introduction to ISF is first presented to provide the background and the motivation of this thesis. Then, the objectives and structure of this thesis is introduced.

1.1 Background and Motivation

Sheet metal forming plays a significant role in the manufacturing field and has been widely used in manufacturing industries such as automobile and aircraft industries. There is a wide range of conventional sheet metal forming processes, including stamping, pressing, drawing, etc. These processes require dedicated dies and/or punches to manufacture sheet metal components. The time and economic costs for the fabrication, storage, and maintenance of the dies and/or punches are quite high [1,]. Hence, conventional sheet metal forming methods are efficient for mass production but less competitive for multi-product and small-batch production due to the high cost of die fabrication and storage, and the lack of flexibility [3]. As the market demand in the sheet forming area is becoming increasingly customer-oriented and diversified, more flexible manufacturing technologies for custom part fabrication or small batch production are demanded [4].

ISF is an emerging flexible forming technology targeted at the cost-effective production of small-batch or customised sheet parts because dedicated dies and tooling are not required. This makes ISF a promising alternative to conventional sheet forming technologies to meet the new market demand [5, 6]. In the past two decades, intensive research and development of ISF have been performed in both academia and industry. In ISF, sheet metal parts are formed by a smooth-end tool, generally mounted on a three-axis computer numerically controlled (CNC) machine, with the plastic deformations accumulated in a stepwise manner. During the forming process, the simple forming tool moves over the surface of the clamped metal sheet along a predefined toolpath so that the plastic deformation is highly localized around the tool end. Figure 1-1 schematically illustrates the process principles for different variants of ISF. ISF has no need of dedicated tooling and/or dies so that various shapes can be fabricated using the same tooling [7]. The product design can be modified easily and quickly by changing the toolpath when the part shape changes [8]. Therefore, ISF possesses a high degree of flexibility. Additionally, the formability in ISF is higher than conventional processes due

to the incremental and localised nature of ISF [9]. The relatively small contact zone and incremental step size also leads to small forming forces.

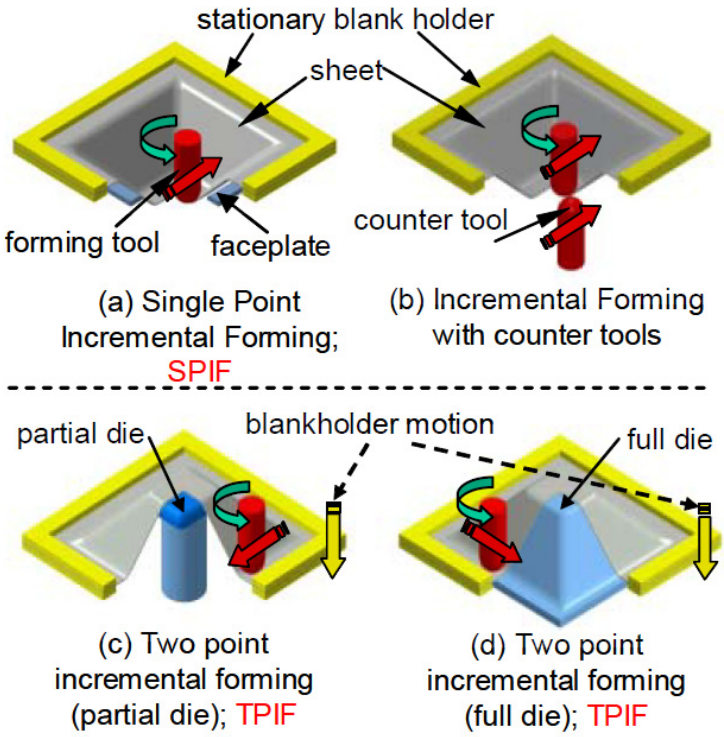

Figure 1-1 Different variants of ISF [9].

Three common variants of ISF are shown in Figure 1-1: Single Point Incremental Forming (SPIF) (Figure 1-1a), Two Point Incremental Forming (TPIF) (Figure 1-1c, d), and incremental forming with counter tools (Figure 1-1b). SPIF is a truly dieless forming process because it does not use any positive or negative dies except a simple backing plate, namely the faceplate in Figure 1-1a. In SPIF, there is theoretically only one simple tool that is in contact with the sheet blank for deformation, as shown in Figure 1-1a. TPIF needs a simple fixed die to support the deformation and it can be classified into two types, namely TPIF with a full die and TPIF with a partial die, as illustrated in Figure 1-1c, d. Similarly, incremental forming with counter tools, also referred as Double-sided Incremental Forming (DSIF) [10, 11], utilises a moving counter tool to provide flexible support in the local forming area.

As a flexible forming technology, ISF is able to shape metal sheets into a wide range of shapes with the use of simple and cheap tooling. It has great potential in cost-effective production of small-batch or customised sheet parts in various fields, including automotive, aviation, architectural, and medical industries. Some example parts formed by ISF are shown in Figure 1-2. Figure 1-3 shows the potential application fields of this forming technology in terms of small-batch production.

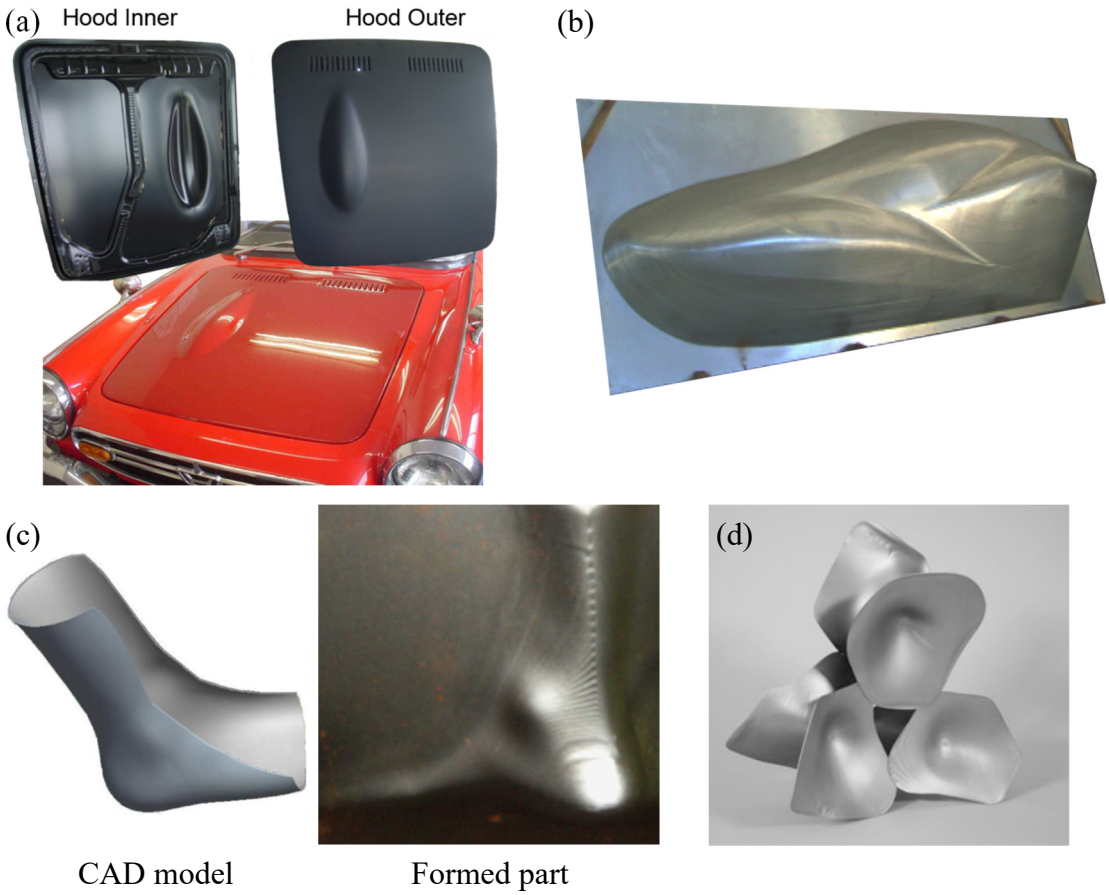

Figure 1-2 Example parts formed by ISF: (a) Hood of Honda S800 formed by AMINO Corporation [1]; (b) Bullet train nose (scale model) (Amino North America Corporation website); (c) Customised ankle support [12]; (d) Architectural Skin parts [13].

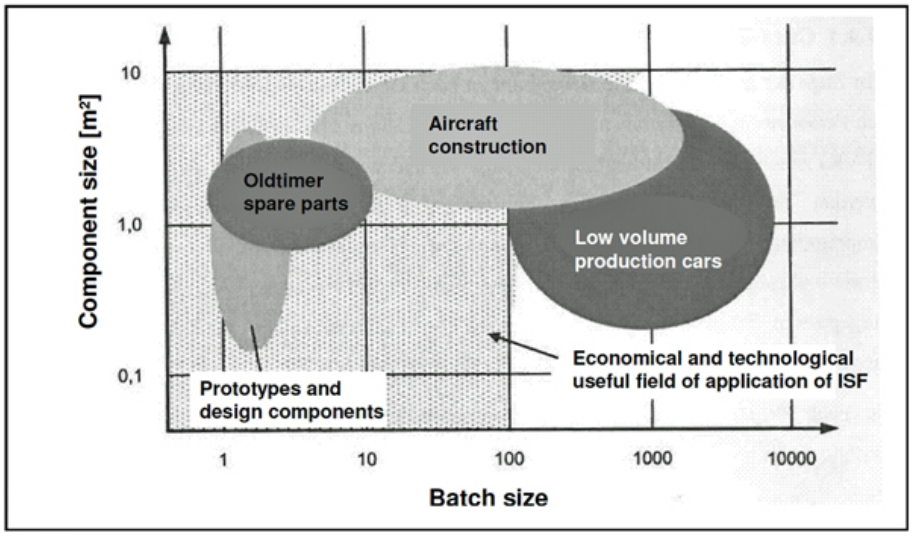

Figure 1-3 Potential application fields of ISF [14].

1.1.1 Advantages of ISF

As an innovative sheet forming technology, ISF has great potential in the sheet forming field in terms of small batch or customised production. The advantages of ISF over conventional sheet forming technologies are summarised as follows,

- High flexibility: ISF is able to form sheets into a wide range of shapes with the use of the same simple tooling. It can deal with products in different sizes from different fields. When the product changes or the part shape is upgraded, all it takes for the fabrication of the new part is to change the toolpath based on the shape design, which is quick and easy. Additionally, the ISF process can be conducted on the forming platform of a wide range of CNC-controlled three-axis machines or industrial robots through some simple modifications of the platform, such as replacing the forming tool and adding some simple clamping devices [9].

- Low tooling cost and short lead time: With no need of dedicated dies and/or tooling, ISF uses simple tool sets for fabricating different sheet parts. The forming and supporting tools used in ISF processes are quite simple and not expensive. Tools with different sizes and head shapes are shown in Figure 1-1. The simple dies used in TPIF processes are generally made of cheap materials like timber or resin [15] so that the cost in the fabrication and storage of dies is greatly saved. At the same time, the time cost for fabricating dies in ISF is also not large while it takes quite a long time (8-25weeks) for the prototyping in conventional sheet forming processes due to the iterative cycle in tooling design and fabrication [2]. Therefore, the lead time for the products can be greatly shortened by using ISF [16].

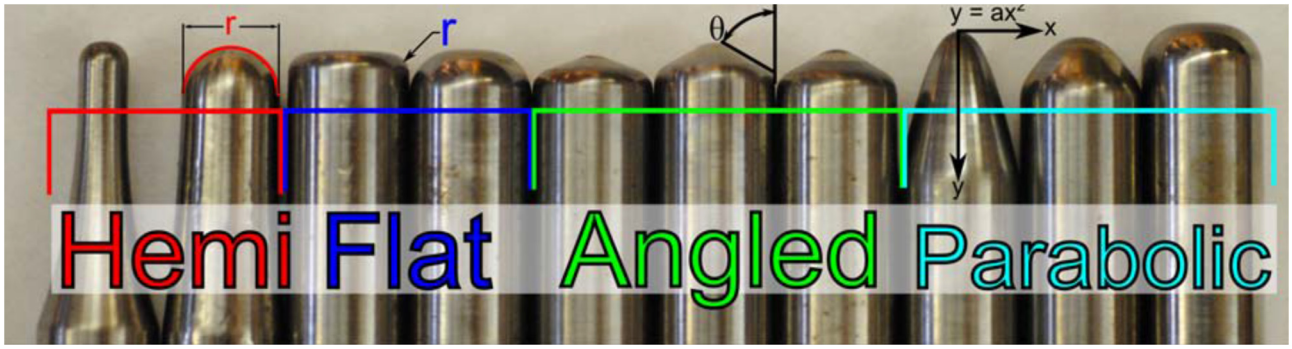

Figure 1-4 Different forming tools: Hemispherical, Flat, Angled and Parabolic. [17]

- Small forming forces: During the ISF process, plastic deformation is highly localized around the tool end when the forming tool deforms the clamped metal sheet following a predefined toolpath.

The forming zone is generally small and the incremental step size of the tool movement is small as well. Therefore, the forming forces are smaller than the forming forces in conventional sheet forming processes. That is also the reason why dies made of wood or resin can be used to support the metal sheets. What's more, the forming forces do not increase with the size of a product because they are determined by several process parameters involved with the local deformation conditions (tool shape, tool size, sheet material, sheet thickness, and step depth size, etc.). [18]

- Improved formability: The formability in ISF is higher than the conventional forming processes since much higher strains can be achieved in ISF [9], as shown in Figure 1-5. The forming limit curve (FLC) of ISF, a straight line in the positive region of minor strain, is above the one of conventional sheet forming processes (e.g., stamping/deep drawing) [19].

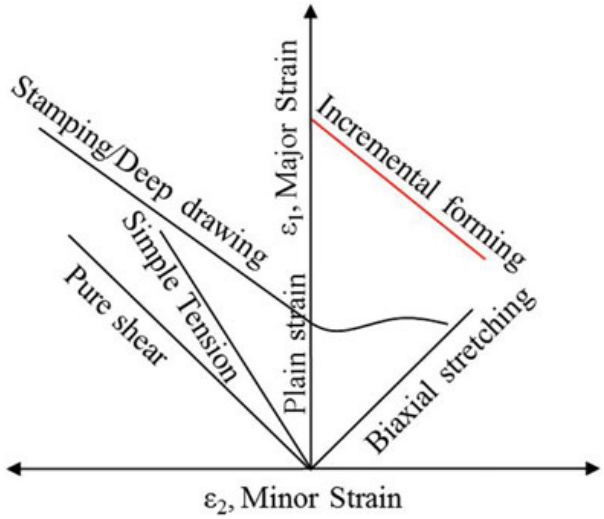

Figure 1-5 Forming limit curve (FLC) in SPIF against conventional forming [19].

1.2.2 Limitations of ISF

The above merits of ISF would make ISF a promising sheet forming technology in terms of small batch production. However, ISF still suffers from certain limitations that greatly limit its application and take-up in the forming industry. The major limitations of ISF are:

- Low geometric accuracy: The major disadvantage of ISF is that the geometric accuracy obtained currently cannot reliably reach suitable levels specified by industrial users. Specifically, geometric tolerances in most industrial applications are less than ±1 mm over the whole part surface and some significant part types require the accuracy level within ±0.2mm. Reported geometric inaccuracy levels in ISF usually exceed these limits [20]. The geometric inaccuracies

are mainly caused by the sheet bending effect, continuous local springback around the tool, and global springback that occurs after the tool and clamping devices are released [19].

- Long processing time: Due to the point-to-point forming nature [21], the processing time in ISF is generally longer than conventional sheet forming processes. This makes ISF only suitable for small batch production.

- Excessive sheet thinning: Excessive sheet thinning and even fracture can occur in ISF when the wall angles of the part are large (e.g. 70° or more). It is nearly impossible to form a part with a very large wall angle in a single pass [22]. Consequently, the ability of ISF to form a wide range of shapes is weakened by excessive sheet thinning.

- Rough surface finish: Surface finish quality is a weakness of the products formed via ISF. The wavy tool marks on the forming surface of the part and the "orange peel" phenomenon on the other side of the part are the main causes of rough surface quality [23]. Several process parameters, including tool diameter, step depth size, scallop height, sheet material, and thickness, have direct effects on the part surface quality.

The limitations listed above have limited the development and industrial applications of ISF in the past two decades. On the other hand, extensive research work on addressing the major limitations of ISF is motivated to enhance the applications in the forming industry.

1.2 Scope and Objectives of this Thesis

This thesis aims to develop feedback control algorithms for toolpath control/correction in ISF to improve the part accuracy via in-process correction of the springback, the major type of SPIF geometric errors. More specifically, the toolpath control/correction strategies are developed based on Model Predictive Control (MPC). This thesis will focus on three aspects in ISF: process investigation, toolpath control/correction in SPIF and toolpath control/correction in TPIF. The objectives of this thesis are:

Objective 1. Develop and verify a model predictive control algorithm to optimise a single toolpath parameter (step depth) for geometric accuracy improvement in SPIF.

(a) Investigate the influence of step depth on the part accuracy, surface finish and formability;

(b) Based on shape feedback, develop a simplified MPC control algorithm to optimise step depth for in-process toolpath correction in SPIF;

(c) Verify the developed MPC algorithm in SPIF by experimentally forming two typical test shapes.

Objective 2. Develop and verify a two-directional MPC control algorithm with the optimisation of two critical toolpath parameters for the SPIF process.

(a) Further develop the MPC control algorithm developed in **Objective** 1 to optimise two critical toolpath parameters, namely the step depth and the horizontal step increment, for toolpath correction in the vertical and horizontal directions in SPIF.

(b) Experimentally verify the MPC algorithm for two-directional toolpath correction in SPIF using two case studies.

Objective 3. Develop an enhanced MPC control algorithm for TPIF to improve geometric accuracy via two-directional toolpath correction and experimentally verify it.

(a) Develop an enhanced MPC control algorithm for TPIF with a partial die to correct the toolpath by optimising the two critical toolpath parameters.

(b) Experimentally verify the TPIF MPC algorithm in the experiment by forming a non-axisymmetric shape.

1.3 Thesis Outline

To achieve the aims of the research, this thesis consists of 5 chapters in total. This chapter, **Chapter 1,** provides a brief introduction of the background, merits and limitations of ISF as well as the objectives of the research work. The subsequent chapters of this thesis are organised in the following manner.

Chapter 2 reviews the state-of-the-art research work involved with ISF. It provides an overview of the ISF processes and summarises the current studies on part accuracy improvement in ISF, with a particular focus on strategies for toolpath correction/optimisation and control of ISF. Besides this, control techniques used in contemporary industry, especially MPC, are also introduced. A summary at the end of this chapter outlines the current gaps in the geometric accuracy improvement in ISF.

Chapter 3 details the methodology, including the design and modelling methods and validation experiments, to fulfil the proposed aims of this thesis.

Chapter 4 presents the research results with a comprehensive illustration about how the research progresses were made step by step and how the research findings contribute to the development of the ISF technology. This chapter also provides a summary of published/submitted papers that were all completed during the PhD studies of the candidature, either as the first author or a co-author. All the papers are appended to the main body of this thesis.

Chapter 5 summarises this thesis and describes the expected contributions of the research to the ISF field and the process control in the manufacturing field. At the same time, this chapter also suggests some potential research topics to further explore the ISF technology in the future.

Chapter 2 Literature Review

This chapter presents a detailed literature review of the current research related to the general development of ISF technology and geometric accuracy improvement in ISF processes. First of all, a brief research development of ISF is introduced to understand the development of ISF research, followed by a discussion on the part accuracy in ISF. Subsequently, various strategies, presented in the published literature, for part accuracy improvement are reviewed and summarised. In particular, toolpath correction/optimisation strategies based on feedback control technologies are summarised and discussed in a separate section. Finally, an overall summary of this chapter is provided to identify the limitations and opportunities in the ISF field in terms of geometric accuracy improvement.

2.1 Research development of ISF

The conceptual ideas of ISF were patented about four decades ago by Roux (1960) [24] and Leszak (1967) [25]. However, academic research in ISF only began in the early 1990s, mainly due to the development of the CNC machines [26]. Recently, global attention has been increasingly paid to this flexible forming approach. In 2003, Park and Kim [27] conducted a fundamental study on the ISF technique. They demonstrated the higher formability of ISF, compared with conventional sheet forming techniques, under several different forming conditions and formed some shapes that are difficult to form. Later, Allwood et al. [20] explored the applications and potential of ISF based on economic and technical data. This study provided useful indicators about future development and applications of ISF that are mainly involved with the low-volume high-value products.

Two comprehensive reviews of research and development of ISF are provided by Jeswiet et al. (2005) [9] and Echrif et al. (2011) [6], respectively. Jeswiet et al. [9] focused on the a wide variety of fundamental aspects and the "makeability" of products in the widest sense. More specifically, the authors summarised the definition, common types, process advantages and disadvantages of ISF processes. Besides this, they reviewed the tooling and the equipment used for ISF processes, and a wide range of process parameters and aspects including formability, forming limits, surface roughness, forming forces, thinning, toolpath generation, process mechanics and FEA, and process accuracy. Additionally, this study also reviewed some applications of ISF in the previous literature and discussed the potential business applications for ISF, the potential research aspects, and challenges in the ISF field. In 2011, Echrif et al. [6] used a new classification of the process variables to review the research and progress in ISF. Previous studies were reviewed by several aspects: forming methods, sheet materials, toolpath strategies, forming limits, simulation work, and forming tools. The authors provided the distribution and trend of reported studies in these aspects from 2004

to 2010. They also summarised some potential research areas that could be improved to enhance the capability of current ISF processes. This review work provided a helpful guideline for the research studies in the ISF field in terms of different process variables.

In 2012, Hirt and Bambach wrote a separate chapter (chapter 13) to introduce the ISF technology in a published book [28] on sheet metal forming processes and applications. They presented various parts formed by ISF using different metal materials in the introduction part. This chapter summarised the significant aspects of ISF, including current ISF variations, the ISF machines and process parameters, the process limits, multi-stage forming strategies, finite element (FE) simulation, and hybrid ISF processes: ISF with stretch forming and laser-assisted ISF. Then, Nimbalkar and Nandedkar (2013) [29] summarised the research status of ISF in a review paper, covering process types, ISF equipment and tooling, toolpath generation, material process parameters, deformation mechanism, the forming of lightweight materials via ISF, and numerical simulation. In 2014, Reddy et al. [19] presented an significant overview of ISF processes. The authors discussed the advantages of ISF over conventional sheet forming technologies, its basic features and various ISF configurations, especially the DSIF process. They also summarised previous literature on formability, thinning, part accuracy, surface finish, and toolpath planning. At the same year, Ishikawa et al. [1] introduced the basic aspects of ISF and its industrial applications from AMINO Corporation. In particular, this study introduced the development of ISF technology and machines in AMINO Corporation and presented several example applications of ISF in the fabrication of automotive panel parts and frame parts with thick/high-strength materials.

In the past two decades, there are various forming machines that have been developed for the ISF processes since ISF can theoretically be conducted using all the three-axis CNC machines [9], or industrial robots. The size of the forming platform directly determines the maximum size of parts that can be formed. Some ISF machines from different research institutes or companies are shown in Figure 2-1. An ISF machine, used in the early years of the development of this technology, was developed by adding a moveable blank holder to a conventional milling machine [9] (Figure 2-1a). In 2002, a dedicated commercial ISF machine (Figure 2-1b) was designed and developed by AMINO Corporation based on the work by Amino et al. [30] and Matsubara [31] as well as a technology patented by Aoyama and Amino et al [32]. The commercial ISF machine has an electro-pneumatically controlled clamping platform and it can form parts via ISF at high feed rates [9]. Additionally, some researchers also developed self-designed forming systems for ISF, such as an ISF machine by Allwood et al. [33] (Figure 2-1c) and a DSIF machine by Cao et al. [10, 34] (Figure 2-1d). Besides these, ISF processes can also be performed using industrial robots, as seen in Figure 2-1e and f.

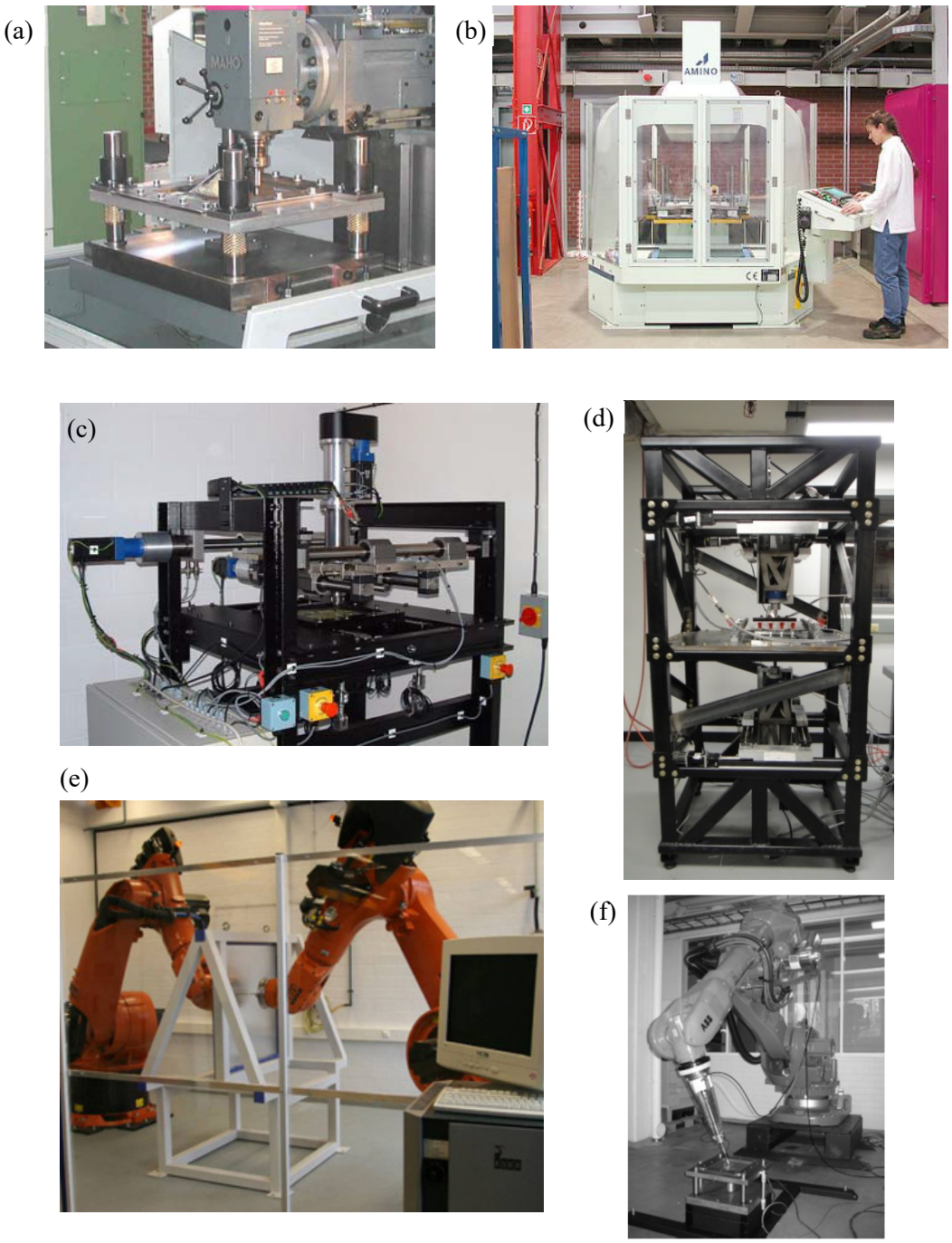

Figure 2-1 ISF forming platforms: (a) Modification of a conventional milling machine [9]; (b) Dedicated ISF machine from AMINO Corporation [35]; (c) A self-designed ISF machine at the University of Cambridge [33]; (d) A self-designed DSIF machine at Northwestern University [11]; (e) A DSIF systems using two industrial robots [36]; (f) An ISF system based on an industrial robot [37].

2.2 ISF Geometric Accuracy

In the forming industry, fabricated part accuracy is one of the most significant aspects for all the forming techniques. Specifically, the importance of geometric accuracy to incremental forming processes is clearly illustrated in [20]. However, low geometric accuracy is still one of the major

limitations of ISF which greatly limits its industrial applications. The geometric accuracy obtained in current ISF processes cannot reliably meet the geometric specifications in most applications in the aircraft and automotive industries. Specifically, geometric tolerances in most industrial applications are less than ± *1mm* over the whole part surface and some significant part types would require around ± *0.2mm* while reported accuracy levels in ISF usually exceed these limits [20]. The geometric inaccuracies in ISF are mainly caused by the sheet bending effect, sheet thinning, continuous local springback around the tool, and global springback that occurs after the tool and clamping devices are released [19, 38]. Allwood et al. [39] explained the ISF part accuracy in three different stages during the part fabrication process: (a) clamped accuracy, (b) unclamped accuracy, and (c) final accuracy. Reported research studies were mainly focused on the improvement of the clamped accuracy. Micari et al. [40] illustrated that the measurable differences between the formed shapes before and after unclamping are small based on some preliminary tests on Alloy 1050-O sheets. Micari et al. [40] also claimed that the changes of part accuracy resulted by the unclamping, and trimming procedures are strongly influenced by the part shape, sheet material, and sheet thickness so that these changes of part accuracy should be carefully investigated case by case.

In [40], Micari et al. defined the geometrical errors in ISF as the distance between the designed profile and the formed one. There are mainly three types of geometrical inaccuracies associated with SPIF after releasing the forming tool (Figure 2-2):

- Sheet bending near the clamped sheet edges;
- Springback, the major type of ISF defects, which results from the sudden decrease of stress as the deformation load from the tool is released. It causes a smaller final depth than the designed depth;
- The “pillow effect” that is the unwanted curvature at the flat base of the final product.

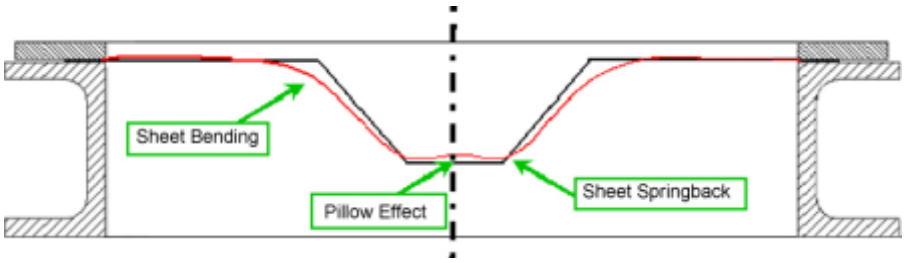

Figure 2-2 Typical geometrical errors in ISF [40]

Ambrogio et al. [41] comprehensively summarised the parameters that affect ISF accuracy, into different categories based on previous studies, which are collected in Table 1:

Table 1 ISF parameters related to part accuracy

Parameter type	Parameters
Process parameters	tool diameter
	toolpath (step depth, etc.)
	tool feed speed
	spindle speed
	use of lubricant
Parameters related to component being fabricated	sheet thickness
	geometry (forming depth, forming wall angle)
Material parameters	strain hardening, normal anisotropy, Young modulus

2.3 Strategies for part accuracy improvement

Low geometric accuracy has been the major limitation of ISF processes in the past few decades. To improve the geometric accuracy in ISF, various approaches have been reported in existing literature. These approaches can generally be categorised into several categories: (a) ISF variation development; (b) Multistage strategies; (c) Toolpath correction/optimisation; (d) Feedback control in ISF; (e) Some alternative strategies. These are reviewed in the following sections.

2.3.1 Development of ISF variations

In the process development of the ISF technology, SPIF and TPIF are the two most common types of ISF. In 1989, the modern ISF process was developed by Iseki et al. [42]. Later, Matsubara developed TPIF using a positive die in [31]. In both of these processes, the shell parts are deformed by a simple forming tool following the specified toolpath with the sheet clamped on a blank holder during the whole process. The major distinction between them is that there is a partial or a full die for support in TPIF while no support tooling is needed in SPIF. Although this can make SPIF more flexible, it adversely influences the part accuracy. It has been shown in a comparative study [43] that the use of a supporting die leads to better geometric accuracy, but further improvements are required [44]. Besides the two most commonly-used ISF processes, several ISF variations have been developed and studied for reducing part inaccuracies.

2.3.1.1 Double-sided incremental forming (DSIF)

As the third typical ISF process (Figure 1-1b), DSIF recently has drawn much attention in the ISF field for its improved geometric accuracy and enhanced formability [19, 45]. In 2007, Meier et al. [36, 45] developed a DSIF machine using two moving tools mounted on two industrial robots (KUKA KR360), as shown in Figure 2-3. During the DSIF process, a forming tool is used to form one side of the metal sheet, which is similar to SPIF and TPIF, while a moving supporting tool is added to provide

flexible support on the backside of the sheet. The two tools move in a synchronous manner with a predefined gap between them, as shown in Figure 2-3b.

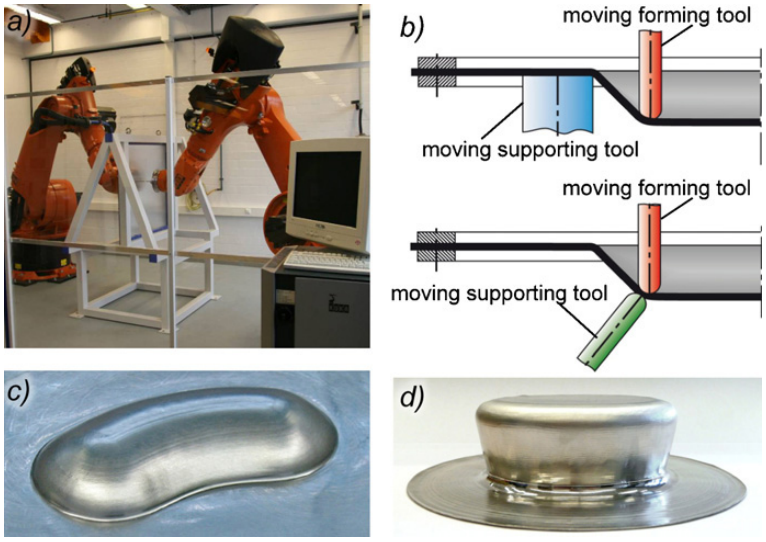

Figure 2-3: (a) Robot-based DISF setup; (b) Forming principles in DSIF; (c) A free-form shape; (d) A cylinder with undercut [36].

In 2008, Wang and Cao [46] developed a simple DSIF facility by using two moving tools mounted on a lathe to form parts by locally squeezing the metal sheet between the forming tool and the supporting tool. They demonstrated that the gap between the tools, the tool diameter and the feed rate could influence the geometric accuracy and the surface finish quality of the formed parts. Cao [34] and Wang [47] also developed another simple DSIF system with two moving tools connected on a rigid C-frame to improve geometric accuracy. The results of their work showed that geometric accuracy of the formed part was improved with the use of a larger amount of squeezing on the sheet by the tools. However, the main shortcoming of this DSIF system was that it was only able to form parts with the wall angle in a certain range due to the structure of the C-frame.

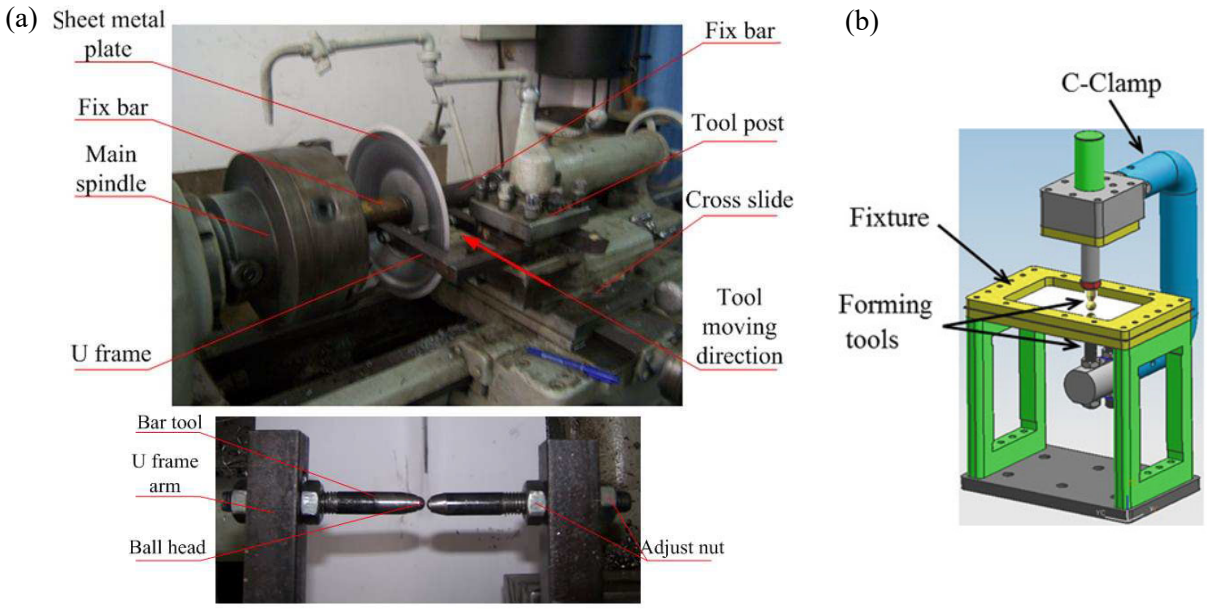

Figure 2-4 Two simple DSIF systems: (a) two tools mounted on a C-clamp [46]; (b) two tools mounted on a C-clamp [34, 47].

Later, an enhanced DSIF machine, as shown in Figure 2-5a, was presented by Malhotra and Cao et al. [10, 11]. Figure 2-5b schematically illustrates the DSIF process, in which the two tools on either side of the sheet were independently controlled during the forming process. It was pointed out that the gap between the tools should be smaller than the thickness of contact area to achieve improved geometric accuracy. Otherwise, this technique will suffer from the loss of contact between the sheet and the lower tool, which would degrade the DPIF process into the SPIF process.

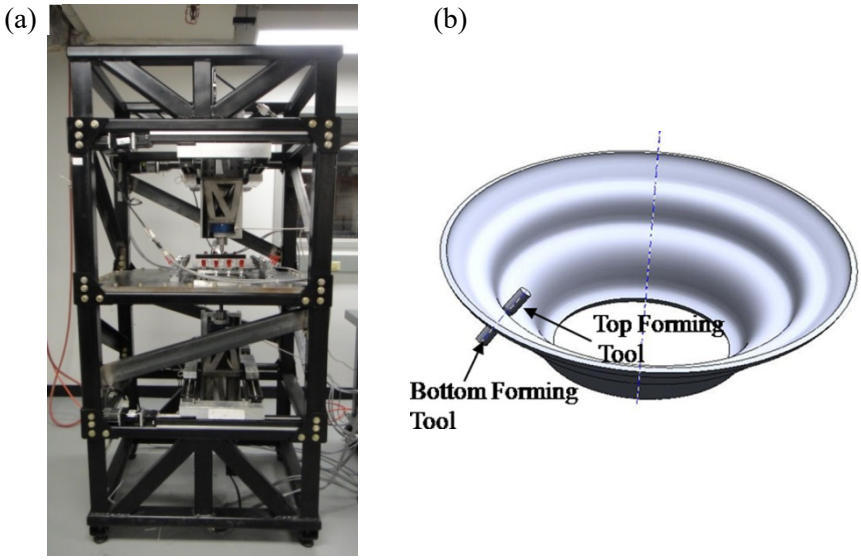

Figure 2-5: (a) A enhanced DSIF machine at Northwestern University [11]; (b) Schematic illustration of DSIF [10].

2.3.1.2 Hybrid ISF

To solve major limitations of ISF, especially the geometric accuracy improvement, some hybrid ISF variations were reported in the previous studies, including a combination of ISF with stretch forming, laser assisted ISF, and electric hot ISF.

In 2009, Taleb et al. [48, 49] put forward a hybrid ISF process by combining TPIF with stretch forming (Figure 2-6) to address the ISF limitations. As shown in Figure 2-6, a stretch forming process was used to get a preform shape in the first step before the normal TPIF process with a full die. The detailed features were not formed in the stretch forming process, but would be detailed in the normal TPIF process. In particular, the proposed hybrid ISF process was conducted on an AMINO DNLC-RB ISF machine. To implement the stretch forming process, four screws jacks driven by a servo motor were used to replace the original hydraulically controlled clamping frame. The screws jacks could provide large downward forces (up to 50 kN) to preform relatively soft metal materials, such as aluminium alloys, in the stretch forming step. The results in [48] showed that the hybrid ISF process led to more uniform sheet thinning and less forming time than the typical TPIF process. Taleb et al. also mentioned that, the tensile stresses resulting from stretch forming could reduce the residual stresses caused by the cyclic bending and unbending on the sheet in ISF [48].

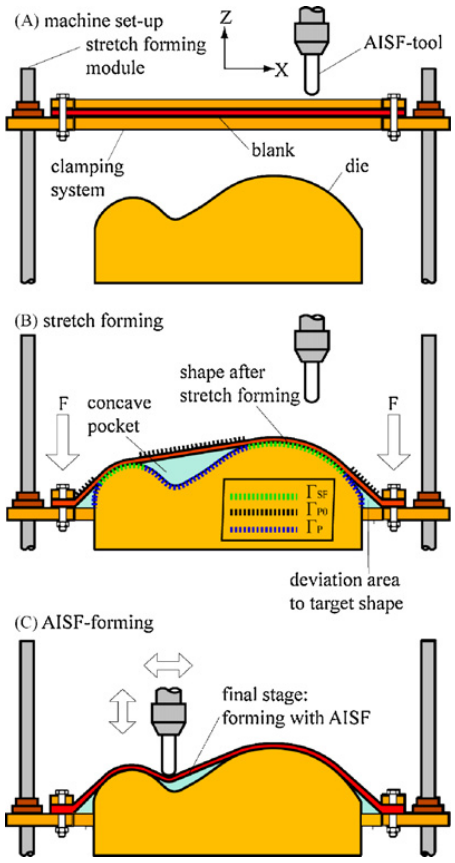

Figure 2-6 Principle of the hybrid ISF process [48].

In [49], Taleb et al. reported a new forming machine for the combination of stretch forming and ISF. The new forming machine for hybrid ISF was built based on a 5-axis portal milling machine and used four independent modules with two independently controlled axes for stretch forming, as seen in Figure 2-7. The results of the experimental test, in which an AIRBUS A320 door panel was formed using mild steel (DC04), showed that the maximum error was reduced from 3.34mm in pure ISF to 1.26mm in the hybrid ISF.

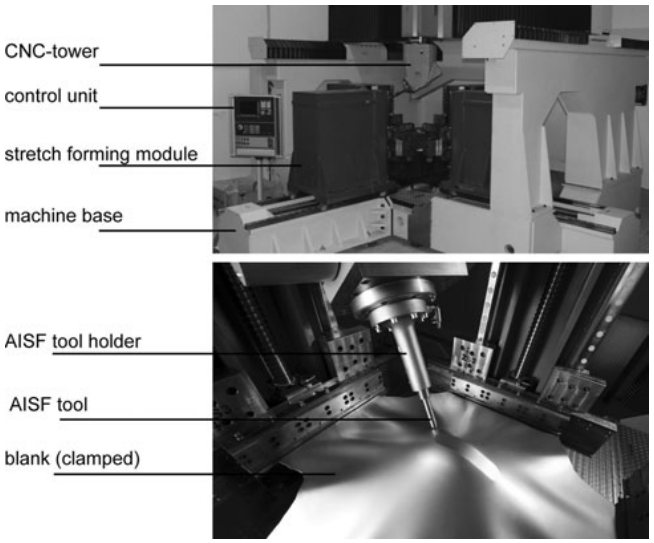

Figure 2-7 A new machine for hybrid ISF at the Institute of Metal Forming (IBF) [49].

In 2011, Taleb et al. [49] also reported another hybrid forming process: the laser assisted ISF process. Taleb et al. [49] developed a different setup, as shown in Figure 2-8, with the forming tool and the laser on the forming side of the metal sheet. The laser was used to locally heat the unformed area that was going to be formed by the forming tool. They mentioned that this approach could realise both laser assisted SPIF and laser assisted TPIF. From their results, the laser assisted ISF was able to improve the formability of magnesium and titanium alloys, which are hard to form in ISF.

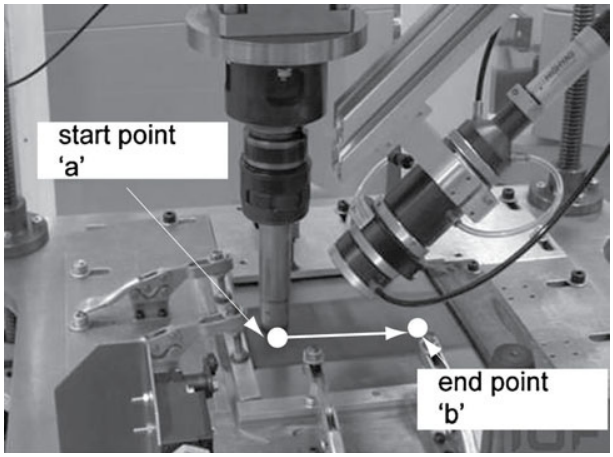

Figure 2-8 The setup of laser assisted ISF at IBF [49].

In 2007, Duflou et al. [50] developed a forming machine for laser assisted SPIF (Figure 2-9) for formability and accuracy improvement. The forming machine used on a 6-axis robot to hold the forming tool, and a laser, located on the backside of the metal sheet, as the local heating device. Their results showed that the use of a laser for local and dynamic heating was able to reduce the forming force in ISF. Also, the final dimensional accuracy from laser assisted SPIF was improved, as seen in Figure 2-10, since the local heating helped to reduce the residual stresses and the springback effect. Their results also demonstrated that the increased formability was achieved in the hybrid SPIF process compared with the typical SPIF process.

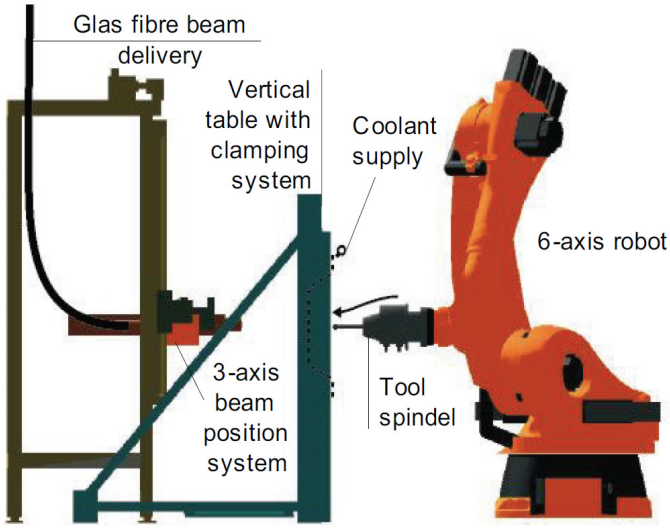

Figure 2-9 The laser assisted SPIF machine structure [50].

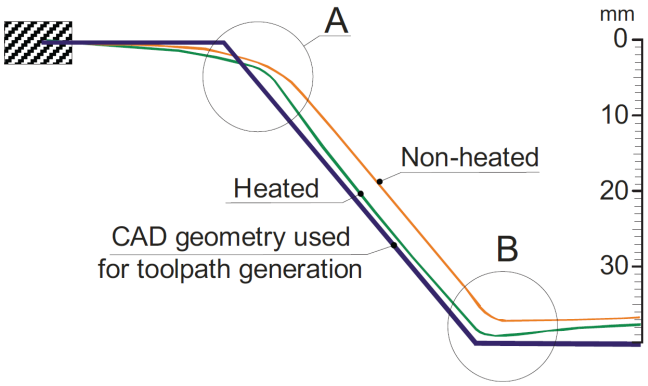

Figure 2-10 Comparison of geometric accuracy in typical SPIF and laser assisted SPIF processes [50].

Another hybrid ISF variant with a local heating system was the electric hot incremental forming reported by Fan and Gao et al. [51]. With a closed circuit comprising a DC power source, cables, a tool and metal sheet, the heat was generated locally in the contact zone by high-current density when the current flowed from the tool to the sheet, as shown in Figure 2-11. The generated heat raised the temperature in the tool-sheet contact zone, which enhanced the ductility of the material at that area and the material formability. This hot ISF enabled the incremental forming of hard-to-form materials,

like magnesium and titanium alloys. The results showed that more geometric distortion occurred on the asymmetric parts (e.g., a truncated pyramid) than the axisymmetric parts (e.g., a truncated cone) after the hot ISF process. A strategy with the use of small tool diameter, small pitch, and low feed rate in the early forming stage could reduce the geometric distortion of the parts formed in electric hot ISF.

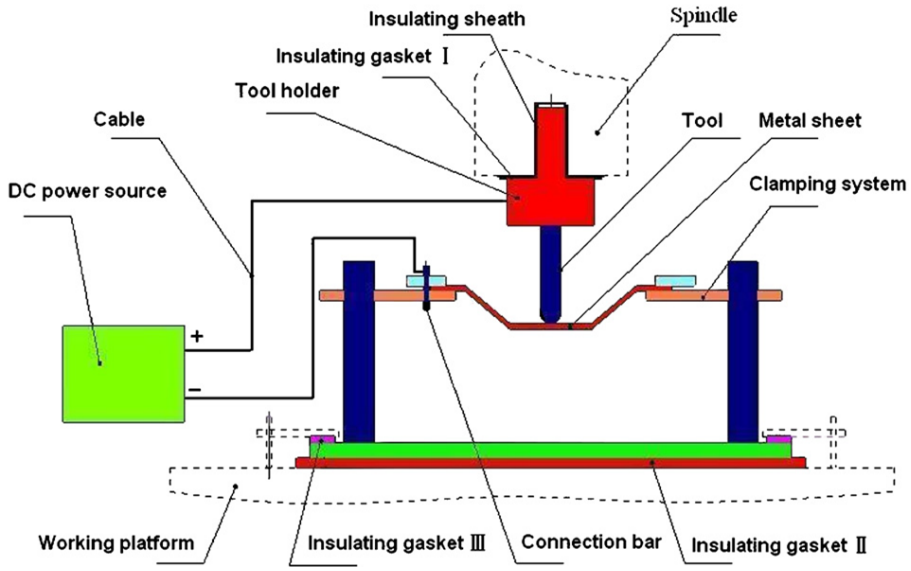

Figure 2-11 The principle of electric hot ISF [51].

Using the same electric hot ISF system in [51], Shi and Gao et al. [52] reported a study on accuracy improvement in electric hot forming of low carbon steel sheets. They investigated the influence of the current on the "pillow effect", an unwanted curvature at the flat base of the part formed in SPIF, by using 4 different current values (0, 200A, 300A, 400A) in the experimental test. From the test results, it was demonstrated that the "pillow effect" was reduced with the use of higher current values in electric hot ISF. More specifically, the pillow height at the flat base decreased with the increase of the current value. The pillow height of a formed pyramid was reduced from 1.2 mm (non-heated ISF) to 0.26 mm with the current value as 400A in the electric hot ISF process. Based on the results of another test for forming a pyramid with two different wall angles, they concluded that the electric hot ISF process could improve the geometric accuracy in terms of the reduction of sheet bending caused by the change of the wall angle.

In 2012, Ambrogio et al. [53] developed a similar hot ISF equipment using DC power to study the improved formability of hot ISF using three light weight alloys. In that work, they also investigated the microstructural changes and surface roughness in the hot ISF process.

In 2015, Xu et al. [23] reported a customised electrically-assisted DSIF (E-DSIF) system [54], in which the closed circuit Mode I was adopted to avoid the possible overheating in Mode II, as shown in Figure 2-12. In [23], the authors investigated the geometric accuracy and the surface finish and in E-DSIF in a series of tests, in which the test shape was a truncated cone and the 1.4mm thick sheet was made of AZ31B magnesium alloy. The results showed that E-DSIF helped to reduce geometric errors but they were still large. Then, a modified toolpath strategy, in which the supporting tool acted as a flexible backing plate at the early forming stage, was demonstrated as able to reduce sheet bending near the clamped sheet edges. Additionally, a strategy with the use of lower backing pressure from the air cylinder at the early stage could further reduce the geometric errors caused by the sheet bending. They also analysed the geometric accuracy in different strategies in terms of clamped, unclamped, and trimmed accuracy. They concluded that E-DSIF could help to decrease the part springback in the unclamping and trimming procedures. On the other hand, the authors also mentioned that the materials with larger electrical resistance were favourable in the E-DSIF process because it would be energy-consuming to form materials with low electrical resistance, such as aluminium alloys, in this hybrid DSIF process due to the need of larger current for local heating.

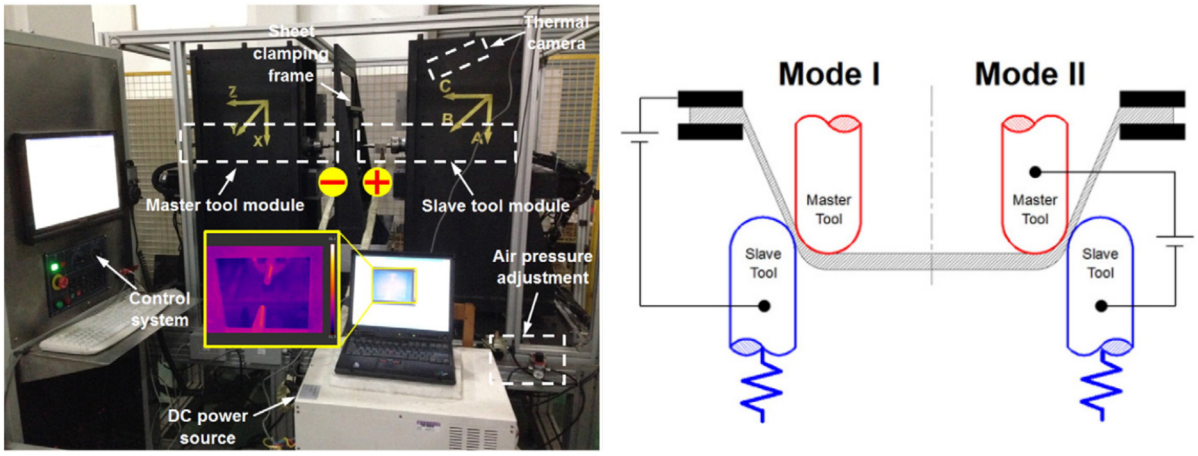

Figure 2-12 Illustration of the E-DSIF setup [23].

Several different variations of ISF have been reviewed in this section in terms of geometric accuracy improvement in ISF. These new variations of ISF have identified new directions of the development of the ISF process. Some of them are still under investigation since the geometric errors generated are still considerably large although part accuracy and formability have been improved. These techniques also require further research efforts to realise the industrial applications of ISF processes. Nevertheless, the development of these ISF variations provides great potential in addressing ISF limitations, especially low geometric accuracy.

2.3.2 Multistage strategies

Inspired by the forming strategies used in other sheet forming processes, such as sheet metal spinning, multistage forming strategies were recently developed in ISF to improve the geometric accuracy and increase the formability of ISF [55].

In the typical ISF process, a part is generally formed in a single forming stage by using a single-stage forming toolpath. More specifically, the part is deformed sequentially level by level in only one stage, in which the tool moves following a toolpath that is identical to the final target shape. In multi-stage ISF, a pre-form shape is firstly formed. After that, the sheet will be deformed into intermediate shapes in several following forming stages and the final shape is obtained in the last stage. Actually, each forming stage can be considered as an independent single-stage forming process in which the toolpath is generated from a definite intermediate shape in that stage. Figure 2-13 shows a multi-stage strategy [56] for forming a cup with a vertical wall, which cannot be successfully produced in single-stage ISF.

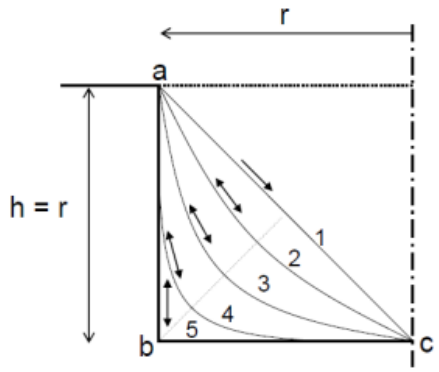

Figure 2-13 Five stage strategy for forming a cup with a vertical wall [56].

Early attempts of multistage ISF were firstly presented by Kitazawa et al. [57, 58]. In particular, a two-stage ISF process was adopted to produce hemi-ellipsoidal axisymmetric parts [58]. An intermediate conical shape was deformed prior to fabricating the final part in the second stage. Kim and Yang [59] proposed a double-pass forming method to get a more uniform thickness distribution in the products, which gives improved formability and higher mechanical strength. Similarly, Young and Jeswiet [60] used a double-stage forming method to improve the final thickness distribution by reducing thinning in the zones where the material fracture could occur in the single-stage ISF, thereby improving the formability of ISF. This enables successful fabrication of parts with steep walls that cannot be achieved via the conventional SPIF technique.

Referring to the multistage forming strategies for axisymmetric components in [61], Hirt et al [62] extended the multi-stage strategy to TPIF, as shown in Figure 2-14, for producing non-axisymmetric parts. In this method, a preform with a shallow wall angle is produced by using a typical TPIF with a partial die in the preforming stage (Figure 2-14a). Then, the forming direction alternates from upward

(Figure 2-14b) to downward (Figure 2-14c) in the following stages until the part is finished. Each intermediate shape is generally designed with an increase in wall angle of 3° or 5° from that of the last stage. A four-sided pyramid with rectangular side walls (Figure 2-15) was successfully formed using this strategy. It is also suggested that decreasing the number of intermediate stages could avoid surface wear and greatly save forming time but may lead to wrinkling on the part.

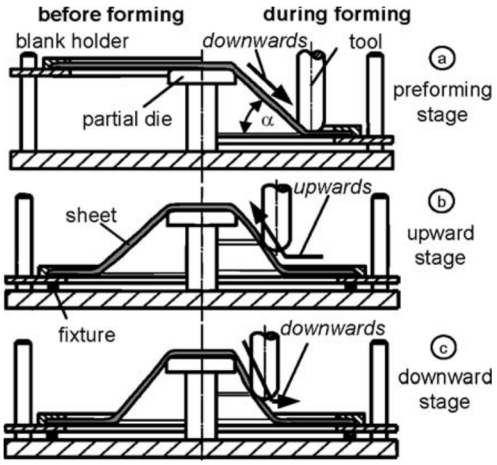

Figure 2-14 Multistage forming strategy [62].

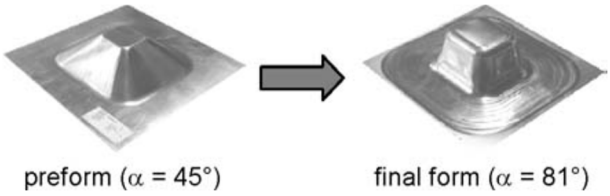

Figure 2-15 Preform and four-sided pyramid with a = 81° [62].

Recently, Skjoedt et al. [56] and Verbert et al. [63] developed different multistage forming strategies for SPIF, with which cylindrical parts with vertical walls was successfully formed in multiple forming stages. Duflou et al. [16] experimentally demonstrated that the multi-stage strategy has the ability of obtaining part geometries exceeding conventional single-step forming limits through a number of case studies.

Bambach et al. [15] proposed a method by combining multi-stage forming with a stress-relief annealing process to improve the final accuracy of formed and trimmed parts. Using the proposed multi-stage approach, a pyramidal benchmark part and a fender section were fabricated and the geometric accuracy obtained was improved compared with single-stage forming (Figure 2-16). However, the enhanced geometric accuracy obtained in multi-stage forming is lost after trimming the formed fender section due to the residual stresses generated in the forming process. Then, an additional stress-relief annealing process after multi-stage forming annealing was adopted to reduce

the final deviations, which has given improved part accuracy, although the maximum error (4.9 mm) was still large.

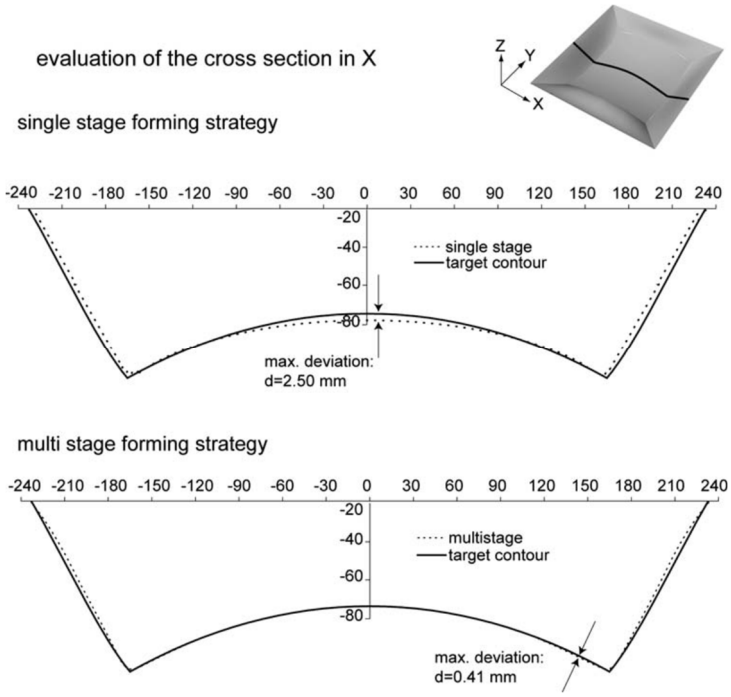

Figure 2-16 Comparison of geometry accuracy between single-stage and multi-stage forming (before trimming) [15].

Interestingly, Ambrogio et al. [41] proposed a novel two-stage approach by adding an additional back-drawing incremental forming step (Figure 2-17b) after the conventional ISF deformation (Figure 2-17a). The tool deforms the formed sheet on the other side during the back-drawing step to correct the shape errors in the traditional ISF step. To further understand the effect of this strategy, they also increased the number of back-drawing steps to two (double back-drawing incremental forming) and compared it with simple back-drawing ISF and conventional ISF. According to the presented results, the geometric accuracy was significantly improved, with both the maximum and the average geometric errors reduced by 50% compared with that of normal ISF. Moreover, there is no big difference between simple back-drawing and double back-drawing ISF strategies.

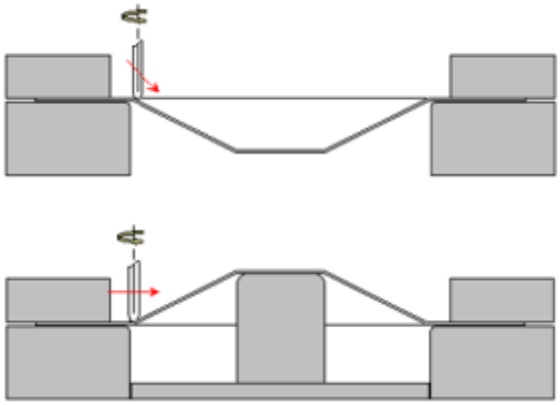

Figure 2-17 Two-stage Backdrawing ISF [41].

Later, Skjoedt et al. [22] established the forming limits of multi-stage SPIF by adopting experimentally determined fracture forming-limit curves (FFLCs) and utilized an enhanced multi-stage strategy for forming cylindrical cups with flat bottom vertical walls (Figure 2-18). Liu et al. [64] proposed and compared three different multistage strategies for SPIF to achieve better sheet thickness distribution and to successfully form cylindrical cups. Later, Liu et al. [65] developed a multi-stage ISF strategy using analytical models to optimise the design of the intermediate forming stages in TPIF with a full die. The developed strategy was validated in finite element analysis (FEA) and experiments. The results showed that the optimised design of intermediate stages was able to prevent material failure and led to improved thickness distribution.

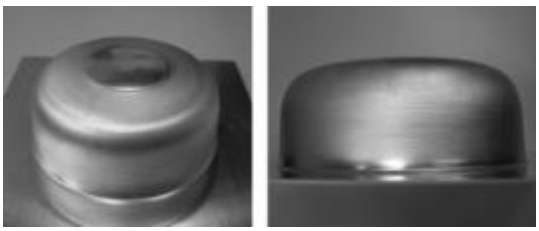

Figure 2-18 Cylindrical cup obtained via the multi-stage SPIF strategy [22].

Malhotra et al. [66] developed a multi-stage approach using a combination of in-to-out and out-to-in toolpaths for forming each intermediate shape so as to reduce the final geometric errors. The authors proposed analytical formulations to predict and compensate for the rigid body motion during the forming process. Based on this, they then developed a multi-stage strategy and experimentally demonstrated its effectiveness in eliminating the stepped features on the cylinder base which was originally raised and discussed in [16].

Very recently, Li et al. [67] presented a feature-based multi-stage approach. To get better thickness distribution and avoid part fracture, the intermediate stages were designed based on the types of part

features in terms of the forming depth. In their work, a car taillight bracket (Figure 2-19), was successfully formed with no obvious part fracture while cracks and wrinkles were detected in the two critical regions in traditional multi-stage forming.

Figure 2-19 The processed taillight bracket: (a) fabricated part via ISF (b) laser trimmed part [67].

Overall, studies above have indicated that multi-stage forming can be an effective alternative for improving the geometric accuracy and part formability in ISF. Nonetheless, a drawback of this strategy is that reprocessing the sheet blank can greatly increase the forming time and may lead to worse final surface quality in some areas of the part. More importantly, current multi-stage strategies lack validation via fundamental models and are only practical for certain circumstances. Most of them are based on intuition, experience or trial-and-error [15]. Further understanding of sheet springback and bending in ISF still need to be achieved for the development of more efficient multi-stage forming strategies. However, the strategy of multi-stage forming is a good approach to improve material formability and the part accuracy of ISF. The integration of the multi-stage strategies with other strategies, such as toolpath correction, would be a promising approach for geometric accuracy improvement in ISF.

2.3.3 Toolpath optimisation/correction

Besides the use of the multi-stage forming strategy, toolpath optimisation/correction for part accuracy improvement in ISF has attracted extensive attention recently [62, 68, 69]. The toolpath can directly affect the final part accuracy since the shape is formed by a simple forming tool following the designed toolpath. Toolpath optimisation/correction is an important aspect of ISF to improve geometric accuracy as it can be combined with the aforementioned approaches for further improvement of geometric accuracy.

The most commonly-used toolpath type is a contour toolpath (Figure 2-20) generated in the milling module of the commercial CAM software and consists of a series of z-level contours that are parallel to the horizontal plane [70, 71]. However, this method normally fails to fabricate parts with good

geometric accuracy. Many studies on toolpath optimisation/correction have been carried out to improve the geometric accuracy of the formed part and to overcome other limitations of ISF.

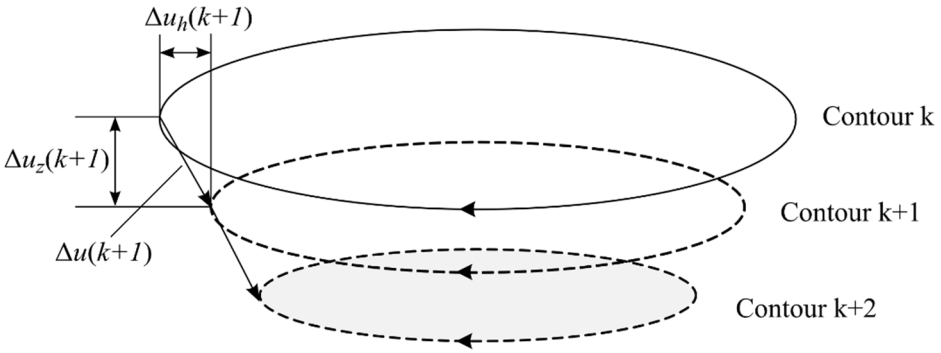

Figure 2-20 The contour toolpath in ISF [71].

Hirt et al. [62] developed a toolpath optimisation strategy based on a iterative correction algorithm to enhance the geometric accuracy, illustrated in Figure 2-21a. In the correction module, a trial component is produced using regular ISF. Then, this preliminary shape is measured and compared with the ideal one. Based on this, the trial points of the new path (Figure 2-21b) will be calculated to compensate the error obtained. If necessary, several correction processes can be repeated until the geometric accuracy reaches the required level. Their result (Figure 2-22) shows that the strategy with one correction loop leads to reduced geometric deviation in comparison with the regular process.

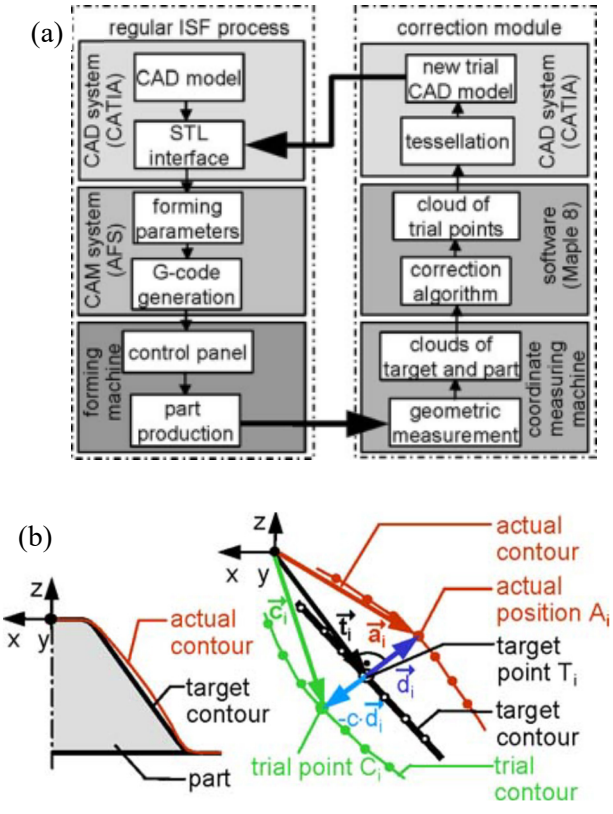

Figure 2-21: (a) ISF process with correction module; (b) Determination of corrected points [62].

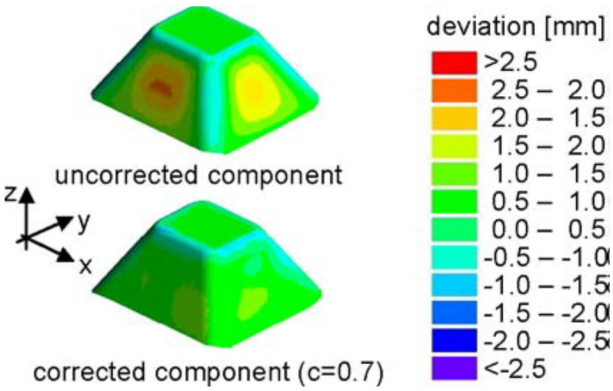

Figure 2-22 Geometric deviations of uncorrected and corrected components [62].

Behera et al. [72] proposed another toolpath compensation strategy to enhance the geometric accuracy in SPIF by using multivariate adaptive regression splines (MARS) for the prediction of the formed shape. Based on the detection of the category of feature and interaction between features in the shape design, the formed profile is firstly predicted in the proposed model. To offset the deviations between the predicted and ideal profiles, a compensated single stage toolpath can be generated by translating the points in the STL (STereoLithography) model. In a number of test cases, it has been demonstrated that the compensated toolpaths can reduce the average dimensional errors to within ±0.4 mm. Nevertheless, the MARS method has a significant weakness in forming parts with features close to failure because there are some zones with wall angles greater in the compensated model than the designed one. These angles may exceed the forming limits for material fracture.

Ceretti et al. showed in [73] that a spiral toolpath leads to a better result than the conventional one with parallel contours. To compensate the elastic springback, Ambrogio et al. [74] modified the toolpath by using a steeper slope (Figure 2-23) for forming the part to the first half depth. This method was further developed to form correct shapes using vitiated trajectories, i.e., it actually uses an incorrect toolpath to form accurate parts by error compensation [12]. Later, Ambrogio et al. [75] proposed another toolpath optimisation strategy to reduce geometric errors in SPIF. This work used a measuring system, composed of a digital inspector and a CNC open program, to measure the geometry data and modify the position of the tool. At each loop during the forming process, the open program modified the position of the tool (a specified point) of next loop based on the feedback of the error between a specified point on the formed shape profile and the corresponding point on the ideal shape profile. This simple approach could improve the geometric accuracy in SPIF. This approach is very simple and could be extended to achieve good accuracy improvement since it only used a single point on the sectional profile of the formed shape to represent the whole shape and the toolpath modification was performed based on the modification of the coordinates of a single point, namely the tool position at each loop.

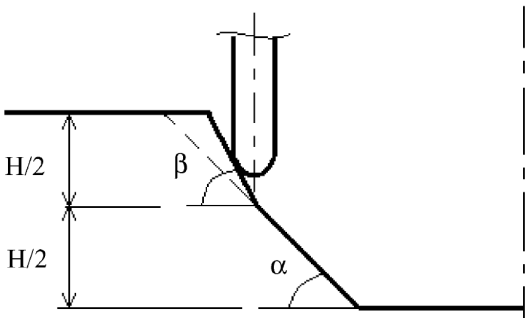

Figure 2-23 The modified toolpath [74].

Attanasio and his co-workers [44, 76] reported their study on experimental toolpath optimisation in TPIF. They investigated the effects of two path generation methods (Figure 2-24) on surface quality, dimensional accuracy and thickness distribution with step depth and scallop height set as constant, respectively. They optimised the two parameters in a series of tests and concluded that the toolpath type with constant scallop height and variable step depth, contributes to good results with regard to surface finish quality, geometric accuracy and sheet thinning. Additionally, scallop height and maximum step depth should be set at low values in toolpath design if they do not exceed the tolerance range.

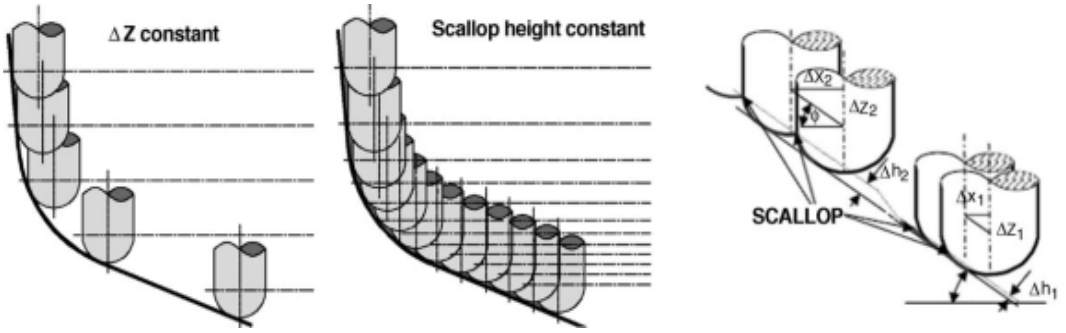

Figure 2-24 The two toolpath types and the illustration of scallop height parameter [77].

Interestingly, Verbert et al. [78] proposed a feature-based toolpath optimisation method in SPIF. Based on feature detection, the workpiece is divided into zones with different feature types, such as planes, edges, freeform surfaces and others. The toolpath for forming each zone is optimised specially in terms of the forming characteristics of its feature type. The optimised toolpath enables the fabrication of parts with better accuracy compared to the conventional one.

To compensate the errors caused by the springback, Zettler et al. [79] developed an iterative toolpath correction approach for ISF with a incremental die. This approach needed several iterations, which can be conducted in the FE simulation or experimental trials, to form serveral full parts to achieve improved geometric accuracy. In each iteration, a new toolpath was generated using the new CAD

shape after compensating for the springback measured in the last iteration in their model. They applied this method in TPIF with a partial die to form a benchmark shape and the overall geometric errors were reduced to less than 1mm after 4 iterations. They mentioned that the major drawback of their procedure for springback compensation was that the finial shape would be wavy in terms of the overall error distribution and distortions might occur in the part areas with a large wall angle.

These studies above used commerial CAM software for toolpath generation while other researchers have presented different toolpath generation techniques for toolpath optimisation. Malhotra et al. [70] developed an automatic spiral toolpath generation method for SPIF. In their methodology, parallel z-level contours are firstly obtained by adaptive slicing of the surface of a CAD model. Then, a spiral path is generated by linear interpolation between points on the two successive parallel contours with constraints on both scallop height and volumetric errors. The geometric accuracy obtained is similar or better and the processing time is reduced when compared with methods using commercial CAM toolpaths. Zhu et al. [80] proposed a new method for generating the spiral toolpath with a constant scallop height by using a customized special software system based on a triangular mesh model. Continuous and smooth spiral toolpaths can be obtained in their software, which makes the ISF process even and continuous and impoves the surface quality. However, the effectiveness of the proposed method still needs to be validated in experimental work.

Moreover, another feature-based toolpath generation approach was introduced by Lu et al. [81]. In the algorithm, the key edges on the part are initially defined and contours are calculated based on the proper gradients between neighbouring contours and a specified scallop height. Then, the toolpath for forming the part is generated from the obtained contours. The results of some test cases (Figure 2-25) showed that the proposed feature-based method is advantageous over the conventional z-level based algorithm with improved geometric accuracy and surface quality as well as reduced forming time.

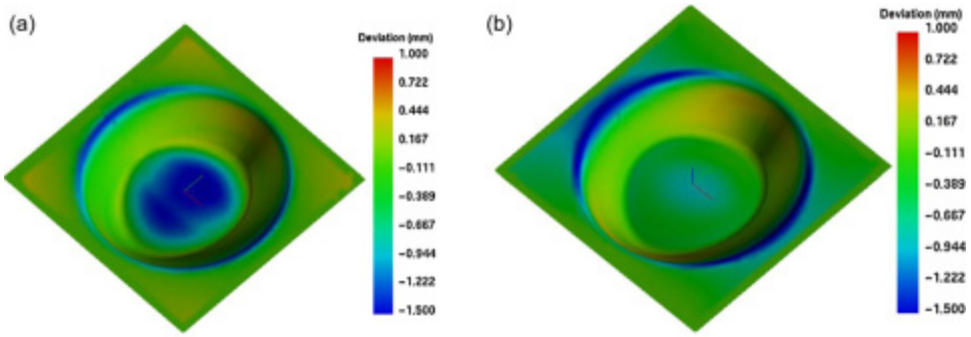

Figure 2-25 Comparison of geometric accuracy: (a) z-height based slicing algorithm and (b) feature-based algorithm [81].

In summary, the toolpath optimisation strategies presented above have made contributions to part accuracy improvement in ISF and play a vital role in boosting the development of ISF. To optimise the toolpath, many methods are based on the compensation of errors measured on previously formed parts. Consequently, multiple parts need to be fabricated to achieve the ideal part accuracy. The improvement of part accuracy by toolpath optimisation requires deeper research in the future.

2.3.4 Some alternative strategies

Control strategies in ISF, reported in previous literature, for geometric accuracy improvement are directly related to this thesis and they will be reviewed in a separate section, (see **Section 2.4**). In this section, some other strategies related to part accuracy improvement will be reviewed.

Allwood et al. [82] proposed the use of partially cut-out blanks in which tabs or holes were created at the perimeter of the target part. The aim of this method was to reduce geometric deviations by localising deformation to the area where the tool travels. The results indicated that cut-outs did not contribute to large improvement in part accuracy. They also concluded that the idea of localising the deformation area around the tool earlier has great significance in the fabrication of more accurate parts via ISF. Ambrogio [83] conducted a parameter investigation to study the ISF parameters in terms of part accuracy improvement.

2.4 Control in ISF

Although extensive studies on improving ISF geometric accuracy have been conducted, not too much attention has been given to the feedback control aspect of this technology, which is an important approach to improve the part accuracy and quality of formed parts. This section mainly discusses the current research status of control in ISF. Firstly, several control technologies commonly used in the industry will be generally introduced. Then, previous research on the control of ISF will be reviewed. To be more specific, previous research into the control of the ISF process has been categorized into several approaches: control with force feedback and control with shape feedback. The advantages and limitations of these methods are discussed and summarised in this section.

2.4.1 Control techniques

There are many different control techniques used for process control in the manufacturing industry. Major control techniques used are Proportional-Integral-Derivative (PID) control, robust control, fuzzy logic control, optimal control, neural network control and MPC.

- PID control: PID control is a generic control loop feedback mechanism widely used in industrial control systems since this control technology is simple to be implemented and can offer a satisfactory performance in a wide variety of industrial processes. On the other hand, PID has low robust ability and the use of the PID algorithm for control that the closed loop system is optimal or stable [84].

- Robust control: Robust control is a branch of control theory that explicitly deals with uncertainty in its approach to controller design. In contrast with adaptive control in which the controller must adapt to the controlled process with varying or uncertain parameters [85], a robust control policy is static. Rather than adapting to measurements of variations, the controller is designed to work assuming that certain variables will be unknown but, for example, bounded. This combined approach is systematic and very general [86, 87].

- Fuzzy logic control: Fuzzy logic control, which mathematically emulates human reasoning, provides an intuitive way to design function blocks for intelligent control systems, advanced fault detection and other complex applications. It deals with uncertainty in engineering by attaching degrees of certainty to the answer to a logical question. Nonetheless, fuzzy logic is not the answer to all control problems, but has been found to be useful for control problems where simplicity and speed of implementation is important. Tuning and retuning of the controllers might be time-consuming, especially in large industrial applications, since the controller needs to be re-tuned even in similar industrial cases. [88-90].

- Optimal control: Optimal control aims to maximize or minimize one or more of the process specifications while keeping all others within their constraints. It deals with the problem of finding an optimal control law for a given system such that a prescribed optimality criterion is achieved. However, optimal control methods are typically only tractable for restrictive classes of system models, such as linear systems. It is difficult to build proper control models for complex systems in optimal control [91, 92].

- Neural network control: Neural network (NN) control includes learning unknown nonlinear dynamics and compensating for structured/unstructured uncertainties existing in the dynamic model. Neural networks are built based on biological neuronal structures of interconnected nodes. NN control is developed as a natural extension of adaptive control approaches to deal with learning systems that may not be linearly parameterised [93].

- Model predictive control: Model predictive control is an advanced model-based control technology for its ability to explicitly handle complex system constraints using linear system

models. Unlike the optimal control techniques, MPC can use a wide range of models for process control [94-96]. Detailed information of MPC will be introduced subsequently, as the focus of this thesis.

2.4.1.1 Model Predictive Control (MPC)

MPC was first proposed in the 1960s [97], however its development was slow with early industrial implementation emerging in the late 1970s, before reaching a level of maturity in the late 1990's [98]. MPC was proposed for this work due to its flexibility in the type of model used in the controller compared to optimal control.

Generally, MPC (Figure 2-26) uses the receding horizon paradigm: implemented by solving a finite-horizon optimal control problem at each sampling instant and applying the first input only to the system under control. That is, at a certain sampling time k, it solves an open-loop optimal control problem over a finite future horizon then applies only the first optimal move to the process. At the next sampling time k+1, based on new measured feedback, a finite horizon optimization problem is solved, and again, only the first optimal move is applied to the process under control. The actions of measurement, solving the finite horizon optimization problem, then applying the first input to the system under control is repeated until the process is completed. This receding horizon manner of optimisation is the unique feature that distinguishes MPC from other control techniques.

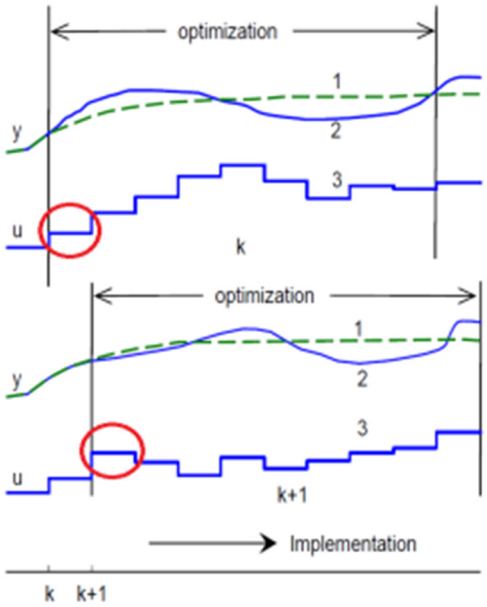

Figure 2-26 MPC control process (1 - target trajectory; 2 - optimal predicted output; 3- optimal control move) [95].

MPC uses a predictive model of the process for output prediction in the optimisation process. Unlike the optimal and robust control techniques reviewed above, which have strict requirements on the model structure, MPC can directly utilise a wide range of models for prediction, including traditional models (state-space equation and transfer function) non-parametric models (e.g., impulse response and step response) and other models or systems with available information for prediction. In complex industrial processes, model-plant mismatch, time-varying behaviour and disturbances are inevitable and they will cause uncertainties that can greatly reduce the effectiveness of traditional control actions. MPC is a receding horizon optimisation process, during which the optimisation for the future is always based on the real-time measurements and references at each sampling instant and only the first optimal move is applied so that the receding finite-horizon optimisation can be more powerful and adaptable to plant uncertainties than the global one-time optimisation (open-loop optimal control) [95]. Therefore, MPC is an effective control strategy in complex industrial processes with uncertainties. MPC can be used to deal with inputs and state constraints for large-scale multivariable plants and to handle coupled variables and robustness to run uncertainties. These advantages offer MPC the ability to be applied in the complex industrial processes, such as in oil-refineries, chemical, metallurgical, and machinery producing industries [97, 99].

Even though academic research on ISF has been conducted for decades, there is still no accurate mathematical model to model this process. The ability of MPC to use simple prediction models and handle the uncertainty using feedback is a promising alternative for the development of a feedback control strategy to improve ISF part accuracy. Studies on MPC of SPIF has been reported by Wang et al. [68, 100]. It has been demonstrated that MPC has good capacity to control and optimise toolpath for improving geometric accuracy. A detailed introduction and review of this work will be provided subsequently. In general, it can be concluded that MPC has great potential in reducing ISF part inaccuracy through toolpath control and optimisation.

2.4.2 ISF Control with force feedback

Several researchers proposed control methods with force feedback in their research work. Petek et al. [101] proposed an autonomous on-line system for fracture identification in ISF using a dynamometer for force measurement. The forming force in the z-direction was considered as an indicator in identifying the material fracture. Specifically, an unexpected sudden drop of the reaction force in the z-direction occurs when the workpiece fractures. Strictly speaking, this system is not a control system because it cannot make any adjustments before part fracture occurs and can only be used for fracture identification. Even so, the system is a versatile tool for the identification of the location and time of the occurrence of the fracture.

An on-line control strategy for failure prevention in SPIF was presented by Filice et al. [102]. The on-line control model was based on a failure prevention algorithm proposed in one of their previous studies [103]. It used the force gradient after the contact force peak as a critical criterion to predict the occurrence of failure and defined the threshold value in order to predict the initiation of failure. During the forming process, if the measured value of the force gradient increased to the threshold value, the process had to be considered as unsafe. Then, some critical process parameters (step depth, tool diameter), whose influence on the force trend have been previously investigated, would be changed automatically to avoid the material failure. Simple parts could be safely formed using the control strategy, without which part fracture occurred. Nevertheless, this control method was based on prediction models which need quite a large number of experiments for validation. The number of experiments required for parameter investigation would grow rapidly with the number of input parameters in the fabrication of complex shapes.

Interestingly, Fiorentino [104] proposed a real-time force-based failure criterion and tested its effectiveness on several materials (steel, aluminium, and titanium alloys). It has great potential in fracture prevention through an online control method. Li et al. developed [105, 106] analytical models for force prediction in ISF, which would provide significant information for building control models based on force feedback to prevent material failure and improve part accuracy.

The common feature of a force feedback control system is that a precise force measurement device is required during the ISF process. Duflou et al. [107] used a table type force dynamometer with an incremental forming fixture mounted on top to measure three components of force throughout the forming process. The force measuring systems utilised by Filice [102], Petek [101], and Duflou [107] are illustrated in Figure 2-27a, b and c, respectively.

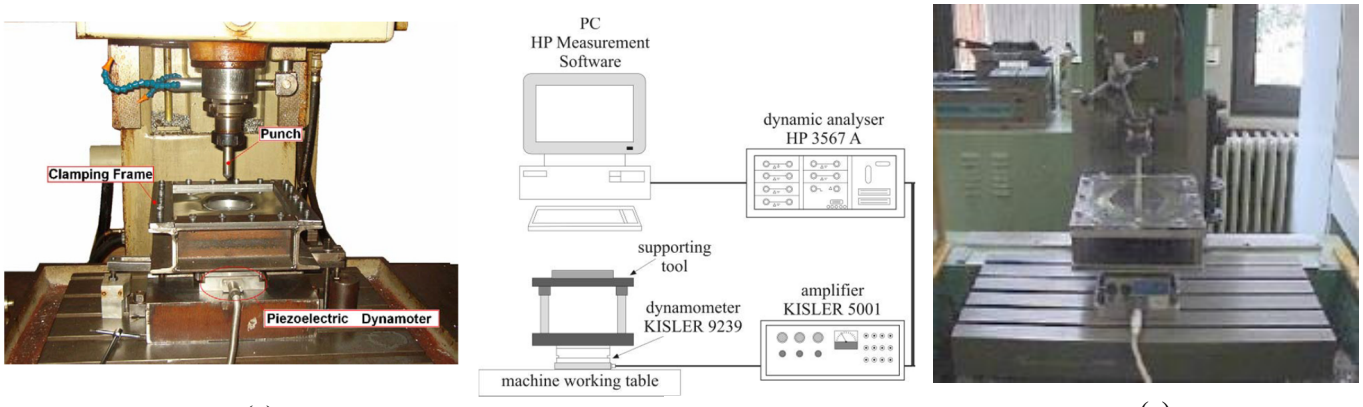

(a) (b) (c)

Figure 2-27 The devices for force measurement in ISF [101, 102, 107].

2.4.3 ISF Control with shape feedback

Besides force feedback, shape feedback also has been used for feedback control of ISF in the past few years. In 2009, a closed-loop feedback control system, using spatial impulse responses to control part geometry, was presented by Allwood et al. [108]. This paper presented an online feedback control model formed from a set of spatial impulse responses found by linearisation around a pre-planned toolpath, with shape feedback provided by a Vialux Z-Snapper stereo-vision camera, as shown in Figure 2-28a. In their work, a set of experiments were conducted in a simplified single-point incremental forming process as illustrated in Figure 2-28a to evaluate their approach. In the results, the final dimensional deviation was within ±0.2 mm using feedback control compared to the deviation of 2-3 mm without feedback control. They mentioned, in the discussion, that the proposed control approach would be difficult to conduct in terms of freeform parts since the impulse responses must rely on the current curvature of the toolpath. Also, multiple workpieces in trial fabrication were required to predict the spatial impulses of a toolpath.

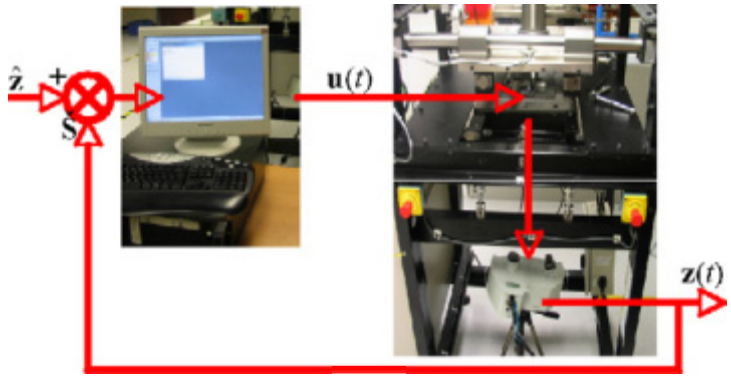

(a)

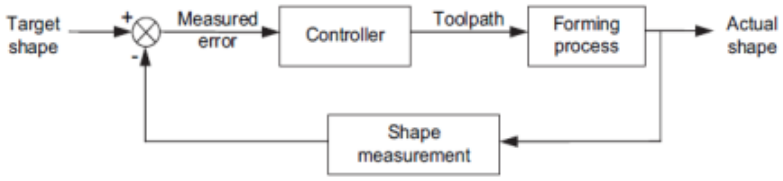

(b)

Figure 2-28 Control system setup and representation: (a) process setup with feedback control; (b) control system representation [108].

Using the ISF Machine in Allwood's research group at Cambridge University, Wang et al. [68, 100] used a closed loop MPC control scheme to optimise the tool trajectory of an ISF process. Based on the shape feedback, a simplified linear forming process model was firstly derived and then modified to tackle the "tool contact" issue and after that a full MPC formulation was established. In a contour

following toolpath, the tool movement between two consecutive layers can be illustrated in Figure 2-29. The vertical inputs (u_k), namely step depth, are constant for all layers. In their control strategy, the inputs (u_k) are varying and optimised in a constrained MPC model to get a better geometric accuracy, with the radial input set as constant. Two types of shapes (Truncated Cone and Truncated Square Pyramid) were produced, which showed that the final geometrical errors could be reduced compared to a standard contour following approach, as shown in Figure 2-29.

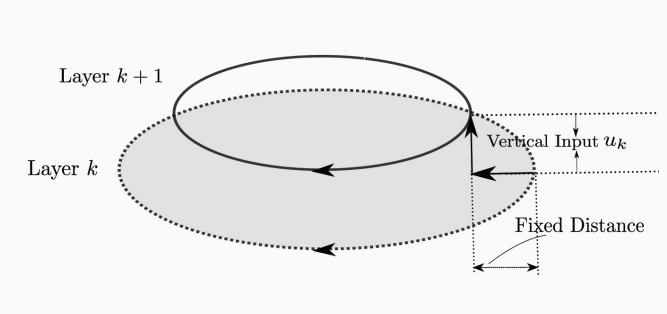

Figure 2-29 Consecutive layers of the contour toolpath for a cone: [68].

Both Allwood's and Wang's control methods could lead to great accuracy improvement at the base of the formed shapes while the errors in the wall areas of the test shape were still relatively large. What's more, the error distribution map of the whole part, a significant indicator for fully evaluating the accuracy of the whole part, was not reported in these studies [68, 100, 108].

Similarly, Han et al. [109] developed a closed loop control model, shown in Figure 2-30, to compensate for springback and enhance the work piece precision. A closed loop algorithm of the trajectory profile for incremental sheet forming based on the wavelet transform combined with fast Fourier transform was constructed and a finite element method (FEM) was developed to simulate and correct the springback of incremental sheet forming. The proposed algorithm could predict a desirable processing path and minimize the springback error to improve workpiece dimensional accuracy in numerical simulation. Later, this study was further expanded in [110]. To verify the correction algorithm, a truncated pyramid was formed using the corrected toolpath after three iterations based on simulation and the results showed relative high accuracy in geometry. However, at each iteration step, it requires the part shape measured from the previous iteration to correct the toolpath in the next forming process until the geometric accuracy reaches the specified level. This iterative control method would take several iterations to obtain improved geometric accuracy, which would be time-consuming, especially using the FEM method for toolpath correction in this work.

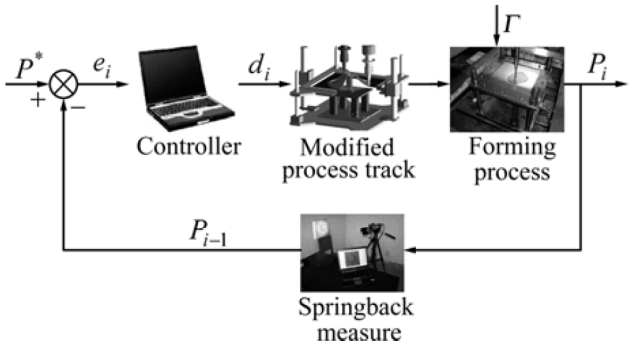

Figure 2-30 Feedback control model for ISF **[109]**.

Rauch et al. [111, 112] proposed a new method for the generation and in-process control of an Intelligent CAM (ICAM) toolpath. During the control process, as shown in Figure 2-31, process data (tool loads or probing) are firstly evaluated directly from CNC data. Based on this, CNC controllers are used to adjust the initial CAM toolpath in real time. In particular, they have carried out two types of ICAM applications, based on tool load evaluation and probing, respectively. Notwithstanding being able to online optimise the toolpath, this approach is limited to accuracy improvement in the final part depth and the surface roughness.

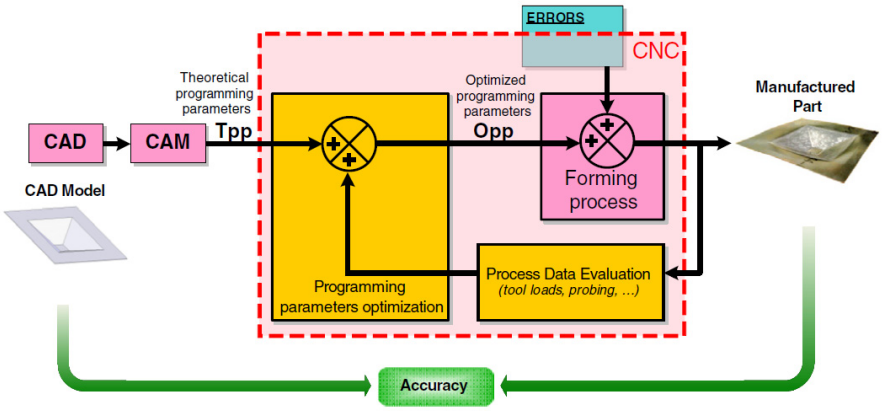

Figure 2-31 ICAM approach for toolpath control [112].

Recently, Fiorentino et al. [113, 114] reported an artificial cognitive system based on the Iterative Learning Control (ILC) for part accuracy improvement via toolpath correction, as shown in Figure 2-32. More specifically, their work was an iterative toolpath correction approach so that there were a number of iterations. In each iteration, after a whole part was fabricated and measured, the correction algorithm would correct the intermediate part shape to be produced in the next iteration, other than directly correct the toolpath to compensate the geometric errors. The algorithm was developed into a self-developed software and was experimentally verified using two different shapes. They mentioned that it took only a few iterations to reduce the geometric deviations of the formed shape to the

reasonable level. Therefore, multiple parts would be formed to obtain the final part with improved accuracy.

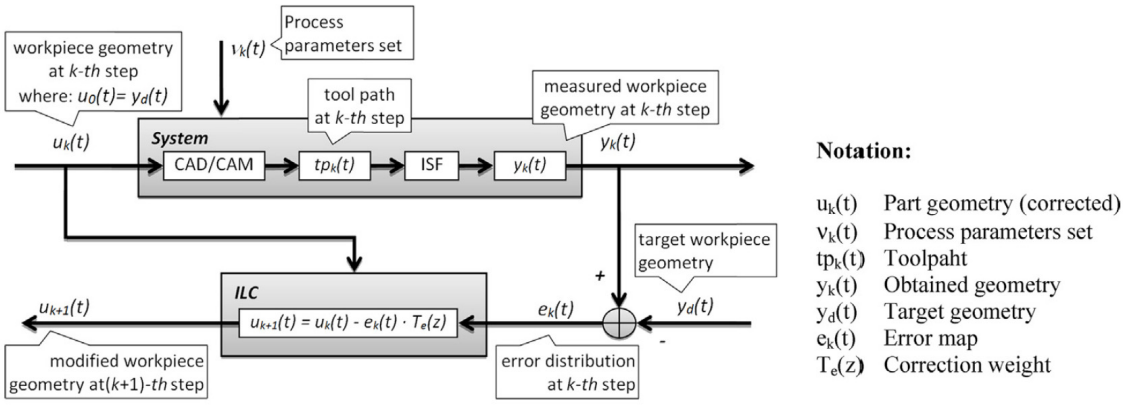

Figure 2-32 The application of ILC in ISF[114].

According to the studies above, the ISF control strategy with shape feedback has great potential in accuracy improvement via feedback control since it directly deals with the correction and compensation of shape errors during the forming process.

2.4.4 Shape measurement in ISF

To measure the formed geometry in ISF, various camera systems have been developed for shape measurement in ISF. Sasso et al. [115] developed a system, which consists of a projector and four fixed cameras, to measure the final formed shape through the fringe projection and phase shift techniques. Orteu et al. [116] developed a multiple-camera system (more than two cameras), as shown in Figure 2-33c, to measure the shape variations and the 3D displacement field of a sheet metal part during a SPIF operation. Setti et al. presented a trinocular system, as illustrated in Figure 2-33a, for shape measurement in ISF by using three cameras and random pattern projection in [117]. In our lab, a non-contact 3D laser scanner (VIVID 9i) was used to measure the formed shape, as seen in **Section 3.5.2**. Paniti et al. [118] used a Hall-effect sensor integrated into the forming tool for precise real-time thickness measurements in the ISF processes.

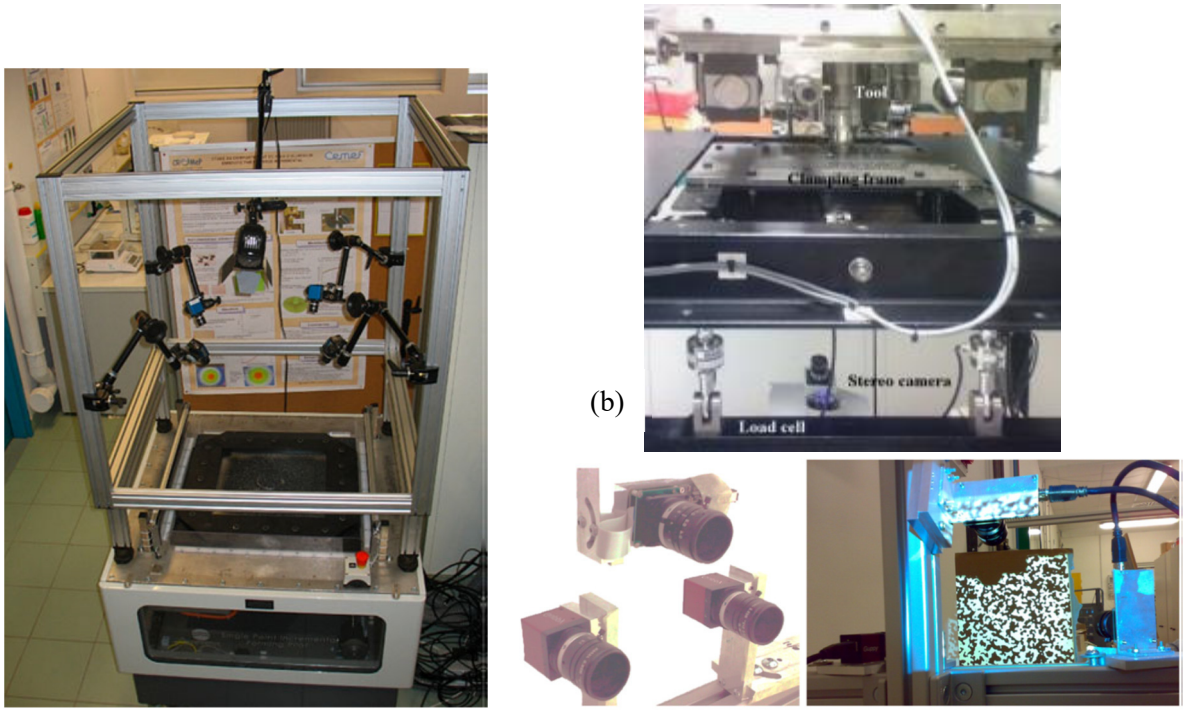

(a) (b) (c)

Figure 2-33 Shape measurement systems developed for ISF.

Various camera systems have been developed for shape measurement in ISF. In this thesis, shape feedback is adopted as the main feedback for MPC control in ISF.

2.5 Summary

The goal of this chapter was to provide an overview of previous research on part accuracy improvement in ISF, especially those studies considering control strategies. Firstly, the early research development of ISF was briefly introduced. Then, various strategies, presented in published literature so far, for the part accuracy improvement were reviewed and summarised. These strategies can be categorized into several types: ISF variation development, multistage strategies, toolpath optimisation/correction and feedback control in ISF. The review of research on the first three types offer useful information in understanding the ISF forming process, limitations and factors that affect the part accuracy. These works also provide significant guidance in many areas of future research.

The previously reported studies on control in ISF were reviewed in detail as a separate section (**Section 2.4**) as a focus of this thesis. Several typical control techniques were firstly reviewed in this section. In the control strategies for ISF, some researchers proposed control models using force feedback while others used shape feedback in their control strategies. Most previous control strategies could improve the final geometrical accuracy to a higher level but had some limitations. Some of them were complex and time-consuming because quite a large number of experiments were required for prediction models or trial fabrication while the control algorithms used in others were only suitable

for simplified ISF processes. Additionally, the final geometric accuracy obtained still could not meet the requirements in most industrial applications.

Although a simple ISF control strategy based on MPC has been successfully achieved by Wang et al. [68, 100], the control model used in that work was empirically built based on the information obtained from the uncontrolled forming process and only dealt with the optimisation of step depth in control process in simple SPIF cases. The results showed that final geometric errors were reduced at the base of the formed shapes using the control strategy while the errors in the wall areas of the test shape are still relatively large. What's more, the error distribution map of the whole part was not reported in these studies.

This thesis builds upon and addresses the limitations of the previous research on a simple MPC control strategy for ISF [68, 100]. The MPC control algorithm for ISF have been developed and enhanced step by step in this PhD project. The developed MPC algorithms use analytical models, which are developed based on the incremental nature of the ISF deformation, for shape state predictions so that control actions can be directly performed in the forming process. Two-directional control algorithm is developed to control and correct the toolpath in both the vertical and horizontal directions. Two key toolpath parameters, horizontal step increment and step depth, are optimised for in-process toolpath correction. The MPC algorithms have been developed for SPIF and TPIF processes and also have been experimentally verified for forming different test shapes. The review of previously reported studies will motivate this PhD project in which the unsolved low part accuracy in ISF will be improved through in-process toolpath correction using MPC feedback control algorithms.

Chapter 3 Methodologies

This chapter summarises the methodologies of the major research work in this thesis to achieve the objectives listed in Chapter 1. Firstly, Section 3.1 introduces the critical toolpath parameters in ISF and the methodology used for ISF process investigation. Section 3.2 illustrates the methodology for the design and the experimental validation of a MPC algorithm for toolpath correction in SPIF. Section 3.3 provides the introduction of a toolpath correction strategy developed for TPIF with a partial die as well as the experimental validation of this strategy. Further details about the methodologies are provided in the **Appended papers**.

3.1 Parameter investigation (Objective 1a)

This section briefly introduces the methodology of investigation of step depth in SPIF. More details of the methodology can be found in **Papers 1** in **Chapter 4**.

3.1.1 Critical toolpath parameters

In ISF, sheet parts are generally formed by a smooth-end tool in a stepwise way. The simple tool moves over the surface of the clamped metal sheet along a toolpath generated from a definite 3D shape design. Figure 3-1 schematically illustrates the SPIF process. The vertical distance between two neighbouring z-level steps is the step depth (Δu_z), also referred to as the step down in some literature [44, 50, 81, 119], which determines the downward displacement of the tool between the z-level planes of two neighbouring forming steps.

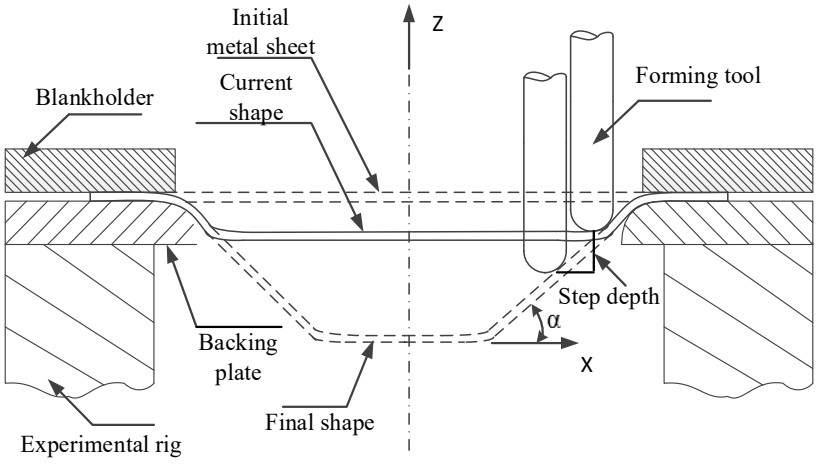

Figure 3-1 The principle of the SPIF process.

Currently, there are no specialised modules for generating an ISF toolpath in commercial CAM software. The most commonly-used toolpath type in ISF is the parallel contour toolpath generated in the milling module of CAM software [70]. It consists of a sequence of z-level contours that are parallel to each other. To determine the toolpath for a given shape, the horizontal step increment (Δu_h) and the step depth (Δu_z) are the critical toolpath parameters in ISF, shown in Figure 3-2.

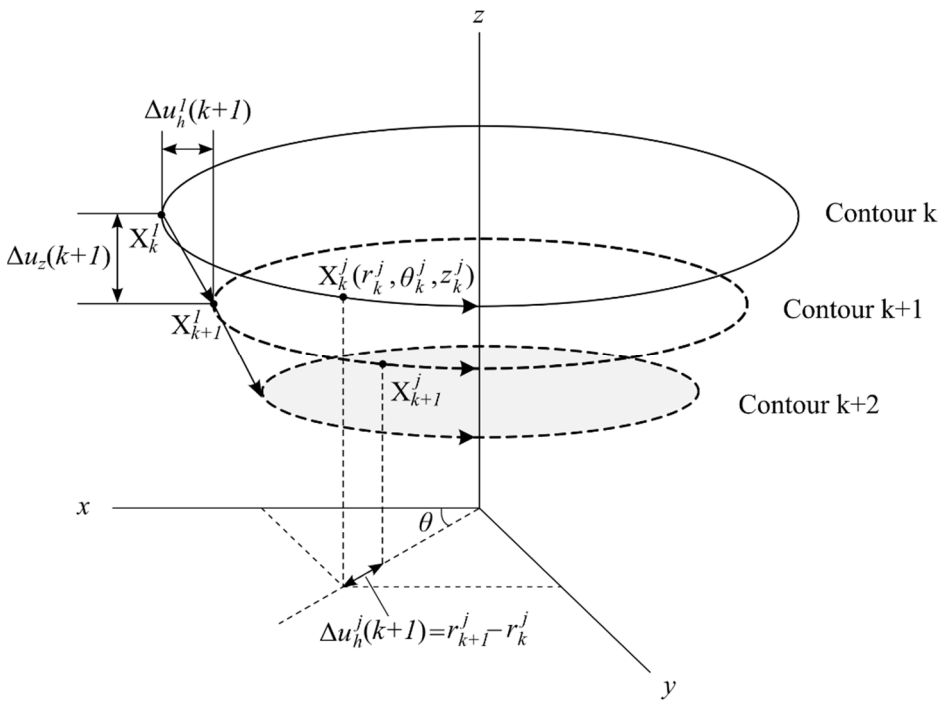

Figure 3-2 Two critical parameters of the typical ISF toolpath for an example shape (a truncated cone).

There are a number of contour points on each single contour and their coordinates are defined in a cylindrical coordinate system. $X_k^j(r_k^j,\theta_k^j,z_k^j)$ is the *j*th contour point on contour *k*. At a single step, e.g., step *k+1*, all the points of a single contour are on the same z-level plane so that $\Delta u_z(k+1)$ is taken as a scalar. It can be expressed as,

$$\Delta u_z(k+1)=z_{k+1}-z_k, \tag{1}$$

where z_{k+1} and z_k are the *z* coordinates of X_k^j and X_{k+1}^j, respectively. Δu_h is a vector that captures the radial distances between points of interest on two successive contours. Δu_h of step *k+1* can be expressed by the following equation,

$$\Delta u_h(k+1)=\left[\Delta u_h^1(k+1),\Delta u_h^2(k+1),\ldots,\Delta u_h^j(k+1),\ldots,\Delta u_h^m(k+1)\right], \tag{2}$$

where m is the number of points on a single contour and $\Delta u_{h\,k+1}^{\,j}$ is the radial distance between the jth pair of points (X_k^j and X_{k+1}^j) on two neighbouring contours, as shown in Figure 3-2. The value of Δu_z is typically defined by the user. The values of Δu_h are computed, according to the Δu_z value and the part design, in the CAM software.

3.1.2 Experimental investigation of step depth

Currently, the initial contour toolpath generated by the CAM software fails to reliably fabricate parts with good geometric accuracy. Toolpath correction/control is one of the most promising approaches to improve the geometric accuracy in ISF. The step depth is of significance in the generation, correction/control of the ISF toolpath since the step depth is a critical toolpath parameter defined by the user in the generation of the ISF toolpath using the CAM software. Therefore, the investigation of step depth can provide helpful information to understand the influences of this parameter on the geometric accuracy, surface finish, and formability in ISF.

Two sets of tests with varying Δu_z values were performed in SPIF to study this parameter. CAD models of truncated cones with two different wall angles were designed in SOLIDWORKS. Dimensional accuracy, surface morphology and material formability of the formed parts were compared and analysed. The parameter settings of the experimental tests are illustrated in detail in Table 2.

Table 2 Parameter settings of experiments on step depth

Parameter	**Geometric accuracy and surface quality test**	**Formability test**
Shape design	Truncated cone	Truncated Cone
Wall angle (°)	50	60
Feed rate (mm/min)	4000	4000
Sheet thickness (mm)	1.6	1.6
Tool diameter (mm)	30	30
Step depth/ Δu_z (mm)	0.1, 0.6, 1.1	0.1, 0.2, 0.3, 0.4, 0.5, 0.7, 1.0

In summary, two critical toolpath parameters in ISF are discussed and they have direct effects on the forming process and formed geometric accuracy. The parameter investigation work focuses on the investigation of step depth, which is directly defined by the user in toolpath generation. This would

provide useful information for building models for toolpath control and correction in ISF. The results of this methodology are provided in **Section 4.1.**

3.2 SPIF toolpath correction using a simplified MPC algorithm (Objective 1b and 1c)

This section briefly introduces a simplified MPC algorithm for single-directional toolpath correction in SPIF. More details about the development of this MPC algorithm can be found in **Papers 2** of the **Appended Papers**.

3.2.1 Simplified MPC algorithm

MPC [94] is a control strategy that uses a predictive model of the system under control to choose inputs that optimise a system performance index, such as minimising geometric errors in ISF, while ensuring system constraints are satisfied over a prediction horizon. To achieve **Objective 1** of this thesis, as described in **Section 1.3**, a simplified MPC algorithm was developed for vertical toolpath correction in SPIF. To improve the poor geometric accuracy of the SPIF process, the toolpath is corrected by optimising the step depth (Δu_z) in a receding fashion during the forming process with feedback control while the horizontal increment (Δu_h) is the same as that of the initial toolpath. The structure of MPC application in ISF is shown in Figure 3-3.

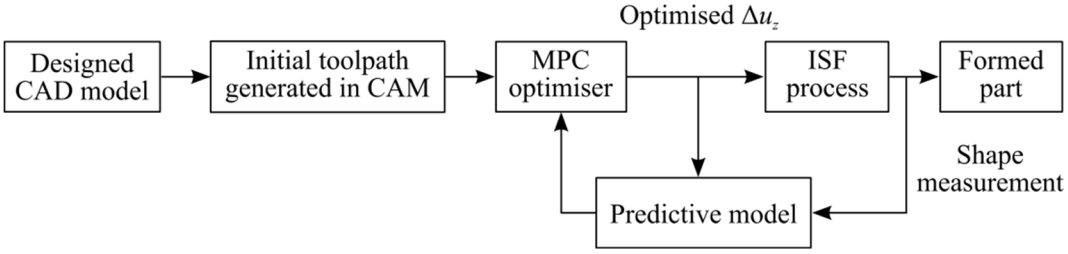

Figure 3-3 Structure of a simplified MPC algorithm for ISF.

In this simplified MPC algorithm, Δu_z is defined as the input to the ISF process. The forming of a single contour is taken as a "time" step. The number of steps taken to form the shape depends on the designed depth of the shape and the initial Δu_z value. At each step, the MPC optimiser optimises a sequence of Δu_z values over a predefined prediction horizon by solving a finite-horizon optimisation problem, in which the optimiser is aimed to drive the predicted shape states to be close to the target shape states with the inputs within the constraints. However, only the first optimal move, namely the

optimal Δu_z of the next single step, will be applied to form the next single contour. This control process will be repeated at each subsequent step until the shape is formed.

During the forming process, the cross-sectional profile, obtained by sectioning the scanned 3D shape of the formed part through a predefined section plane, is taken as the shape state at each step (Figure 3-4). At the beginning of step *k+1*, the profile state of last step is measured as $y_z(k) \in R^n$,

$$y_z(k) = \left[y_z^1(k), y_z^2(k), \ldots, y_z^i(k), \ldots, y_z^n(k) \right]^T, \tag{3}$$

where *n* is the number of profile state points. $y_z^i(k)$ is the *z*-coordinate of the *i*th point on the profile.

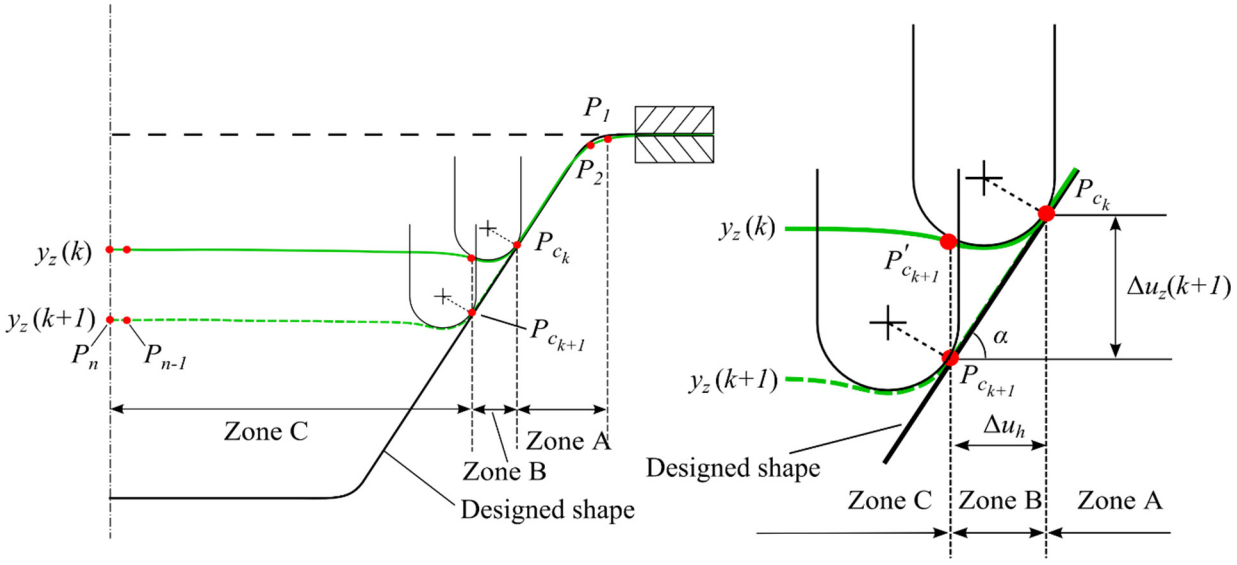

Figure 3-4 Incremental deformation of the metal blank between two neighbouring steps.

The shape state of the next step is $y(k+1)$, which is expressed as,

$$y(k+1) = f(y(k), \Delta u_{k+1}), \tag{4}$$

where *f* is the process model of SPIF that determines how the shape state changes with the step depth. It is difficult to find an accurate mathematical model (f) to formulate the future shape states in ISF since the part is formed by a single tool and the sheet material undergoes deformation caused by bending, stretching, shearing and the springback effect. In the previous literature [100, 108], simplified linear models were empirically built based on experimental forming data to estimate the process model (f). Besides this, MPC control is also known for its ability to use linear models to achieve good control of constrained nonlinear systems in various industries [68, 120]. Based on the

incremental nature of ISF, the shape is formed incrementally step by step and the size of Δu_z typically is small. Therefore, the amounts of springback in two neighbouring steps are very close to each other and can be considered to be approximately equal to each other for building a linear model for MPC control, as expressed in the following equation.

$$\hat{y}_z(k+1|k) = y_z(k) + B_z(k+1)\Delta u_z(k+1) \tag{5}$$

Similarly, at step k, the predicted profile states along the prediction horizon are given in the following equation,

$$\begin{aligned}
&\hat{y}_z(k+1|k) = y_z(k) + B_z(k+1)\Delta u_z(k+1)\\
&\hat{y}_z(k+2|k) = \hat{y}_z(k+1|k) + B_z(k+2)\Delta u_z(k+2)\\
&\qquad = y_z(k) + B_z(k+1)\Delta u_z(k+1) + B_z(k+2)\Delta u_z(k+2)\\
&\quad \vdots\\
&\hat{y}_z(k+N_p|k) = y_z(k) + B_z(k+1)\Delta u_z(k+1) + B_z(k+2)\Delta u_z(k+2) + \ldots +\\
&\qquad B_z(k+N_p)\Delta u_z(k+N_p)
\end{aligned}, \tag{6}$$

where $B_z(k+j) = \left[b_z^1(k+j), b_z^2(k+j), \ldots, b_z^n(k+j)\right]^T$, $j = 1, 2, \ldots, N_p$, N_p is the prediction horizon, which stands for the next N_p steps. Note that all predictions in the future are formulated in terms of currently measured state $y_z(k)$ and the future control move $\Delta u_z(k+j)$, where $j = 1, 2, \ldots, N_p$.

Equations (5) and (6) can be collected together into a compact matrix form as,

$$\hat{Y}_z(k) = Y_z(k) + B_z \Delta U_z(k), \tag{7}$$

where $\hat{Y}_z(k) = \left[\hat{y}_z(k+1|k), \hat{y}_z(k+2|k), \ldots, \hat{y}_z(k+N_p|k)\right]^T$ are the predictions along the prediction horizon, $Y_z(k) = [y_z(k), y_z(k), y_z(k), \ldots, y_z(k)]^T$ and $Y_z(k)$ can be written as,

$$Y_z(k) = I_{N_p \times 1} \otimes y_z(k), \tag{8}$$

where $\otimes$ is the Kronecker product, an operation to calculate the product of two matrices with arbitrary sizes [121]. $\Delta U_z(k) = \left[\Delta u_z(k+1), \Delta u_z(k+2), \ldots, \Delta u_z(k+N_p)\right]^T$, and B_z is the coefficient matrix to predict how future inputs influence the changes of the vertical profile state in the linear model. B_z is expressed as,

$$B_z = \begin{bmatrix} B_z(k+1) & 0 & 0 & \cdots & 0 \\ B_z(k+1) & B_z(k+2) & 0 & \cdots & 0 \\ B_z(k+1) & B_z(k+2) & B_z(k+3) & \cdots & 0 \\ \vdots & \vdots & \vdots & \ddots & 0 \\ B_z(k+1) & B_z(k+2) & B_z(k+3) & \cdots & B_z(k+N_p) \end{bmatrix}. \quad (9)$$

Actually, the coefficient matrix determines how the profile state changes when the tool is driven by future input moves. Figure 3-4 shows how the vertical cross-sectional profile varies with the vertical input between two consecutive steps in an example case. This approach can be generalised to general shapes that can be produced via ISF. The green lines are the formed profiles $y_z(k)$ and $y_z(k+1)$ and the black one represents the target profile in design. P_1 and P_n are the first point and the last point on the formed profile, respectively. P_{c_k} and $P_{c_{k+1}}$ are denoted as the point of tangency, where the tool is tangential to the wall, at step *k* and step *k+1* and they are detected based on the local geometry. $P'_{c_{k+1}}$ is the projection of $P_{c_{k+1}}$ onto profile $y_z(k)$. The profile $y_z(k+1)$ can be divided into three zones, namely Zone A ($P_1 \sim P_{c_k}$), Zone B ($P_{c_k} \sim P_{c_{k+1}}$), and Zone C ($P_{c_{k+1}} \sim P_n$).

In the linear model, as the tool moves down from contour *k* to contour *k+1*, the material in Zone C will be pushed down by approximately the step depth size (Δu_z). Since Zone A is a formed region and will not be directly formed by the tool in the future, the small deformation of material in this region can be ignored in this model. The metal blank in Zone B will be pushed down and stretched by the single tool following the predefined slope in the forming step. Therefore, in this linear model, the $B_z(k+1)$ coefficients within Zone A can be estimated as 0 while those values of points within Zone C can be estimated as 1. Regarding Zone B, the $B_z(k+1)$ values at point P_{i_k} and $P_{i_{k+1}}$ are 0 and 1, respectively. All the other $B_z(k+1)$ values are obtained in a linear interpolation, as illustrated in Equation(10). Generally, Zone B contains only a few points. Therefore, all the elements in $B_z(k+1) = \left[b^1_z(k+1), b^2_z(k+1), \ldots, b^n_z(k+1) \right]^T$ can be computed in the following equation,

$$b^i_z(k+1) = \begin{cases} 0, & 1 \le i < c_k \quad (\text{Zone A}) \\ \dfrac{i - c_k}{i - c_{k+1}}, & c_k \le i < c_{k+1} \quad (\text{Zone B}) \\ 1, & c_{k+1} \le i \le n \quad (\text{Zone C}) \end{cases}, \quad (10)$$

where i is the index number of the profile points, and c_k and c_{k+1} are the index number of points P_{c_k} and $P_{c_{k+1}}$, respectively.

Consequently, all $B_z(k+j)=\left[b^1_z(k+j),b^2_z(k+j),\ldots,b^n_z(k+j)\right]^T$, $j=1,2,\ldots,N_p$, of the next N_p steps can be obtained similarly.

At each step (e.g., step *k*), the optimisation problem can be posed as,

$$\min\ J_z=\left\|\hat{Y}_z-W_z\right\|^2+\lambda_z\Delta U_z{}^T\Delta U_z, \tag{11}$$

$$\text{subject to } \hat{y}_z\left(k+j\,|\,k\right)=y_z(k)+\sum_{i=1}^{j}B_z(k+i)\Delta u_z(k+i),\ j=1,2,\ldots,N_p$$

$$\Delta u_{z\,\min}\le\Delta u_z(k+j)\le\Delta u_{z\,\max},\ j=1,2,\ldots,N_p$$

where J_z is the cost function, $\Delta U_z(k)=\left[\Delta u_z(k+1),\Delta u_z(k+2),\ldots,\Delta u_z(k+N_p)\right]^T, k=1,2,\ldots,N$ is the inputs, *N* is the number of total steps, W_z is the target profile states, The second item of J_z is added to conduct penalties on large oscillation of the control inputs, and λ_z is a non-negative weighting factor and is set as 0.2 after tuning.

3.2.2 Quadratic Programming for MPC solution

In the MPC algorithm, the optimisation problem at each step, see Equation(11), can be transformed into Quadratic Programming (QP) problems. The QP problem involves optimising a quadratic objective function subject to equality and inequality constraints. It is a special type of convex optimisation problem. The standard quadratic programming problem can be formulated in the following form [122],

$$\min\ \frac{1}{2}x^TPx+q^Tx+r, \tag{12}$$

$$\text{subject to } Gx\preceq h \text{ (inequality constraints)}$$
$$Bx=c \text{ (equality constraints)}$$

where *P*, *q*, *r*, *G*, *h*, *B* and *c* are compatible matrices or vectors. It is required that *P* should be symmetric and positive semidefinite to ensure that the objective is convex quadratic.

Therefore, the above QP problem is solved to obtain the optimal input $\Delta U_z(k)$ for the receding optimisation problem in constrained MPC of ISF. At step *k*, the cost function can be expressed as,

$$J_z = \left\| \hat{Y}_z - W_z \right\|^2 + \lambda_z \Delta U_z{}^T \Delta U_z . \tag{13}$$

By putting(7), (12) and (13) together, the cost function can be defined as,

$$\begin{aligned} J_z &= \| Y_z + B_z \Delta U_z - W_z \|^2 + \lambda \Delta U_z{}^T \Delta U_z \\ &= U_z{}^T (B_z{}^T B_z + \lambda I) \Delta U_z + 2(Y_z - W_z)^T B_z \Delta U_z + (W_z - Y_z)^T (W_z - Y_z), \\ &= \frac{1}{2} \Delta U_z{}^T P \Delta U_z + q^T \Delta U_z + r \end{aligned} \tag{14}$$

where $P = 2(B_z{}^T B_z + \lambda I), q^T = 2(Y_z - W_z)^T B_z, r = (W_z - Y_z)^T (W_z - Y_z)$. The cost function in Equation (14) is solved in a script programmed in Python to obtain the optimal input values.

3.2.3 Case studies

To verify the developed closed-loop feedback control strategy, a truncated cone and a truncated pyramid, two commonly used shapes in the validation of ISF processes, were chosen as benchmark shapes for the experiments. CAD models of the test shapes were designed in SOLIDWORKS. The parameter settings of experiments are summarised in Table 3. The designed depth is consistent with previous approaches [68, 100].

Table 3 Experimental parameter settings

ISF Parameters	**Truncated cone (Case 1); Truncated pyramid (Case 2)**
Wall angle (°)	50
Designed depth (mm)	30
Feed rate (mm/min)	4000
Initial sheet thickness (mm)	1.6
Tool diameter (mm)	30
Step depth / Δu_z (mm)	2 (uncontrolled); varying (controlled)

In this work, the initial toolpath used for feedback control is generated using the CAD/CAM software, Unigraphix NX7.5 (UG NX7.5) from Siemens. Figure 3-5 illustrates the initial toolpaths of test shapes. Both of them are parallel contour toolpaths with a constant step depth.

To evaluate the geometric accuracy of the formed part, the 3D geometry of formed parts can be measured using a non-contact 3D Digitiser (VIVID 9i), which will be introduced in detail in **Section 3.5.2**. GEOMAGIC Qualify is used to produce 3D geometry data of the scanned shape and analyse the dimensional error between deformed test parts and designed CAD models. Specifically, both produced and designed profiles are given in large sets of points in the same Cartesian coordinate system. In particular, the cross-sectional profile along a defined section plane is used to evaluate the geometric accuracy since test shapes are symmetric. A system plane (plane XOZ) across the symmetric axis of the test shape is set as the section plane. The deviation in Z direction between the designed and fabricated profiles is calculated as the geometric error in the cross-sectional comparison.

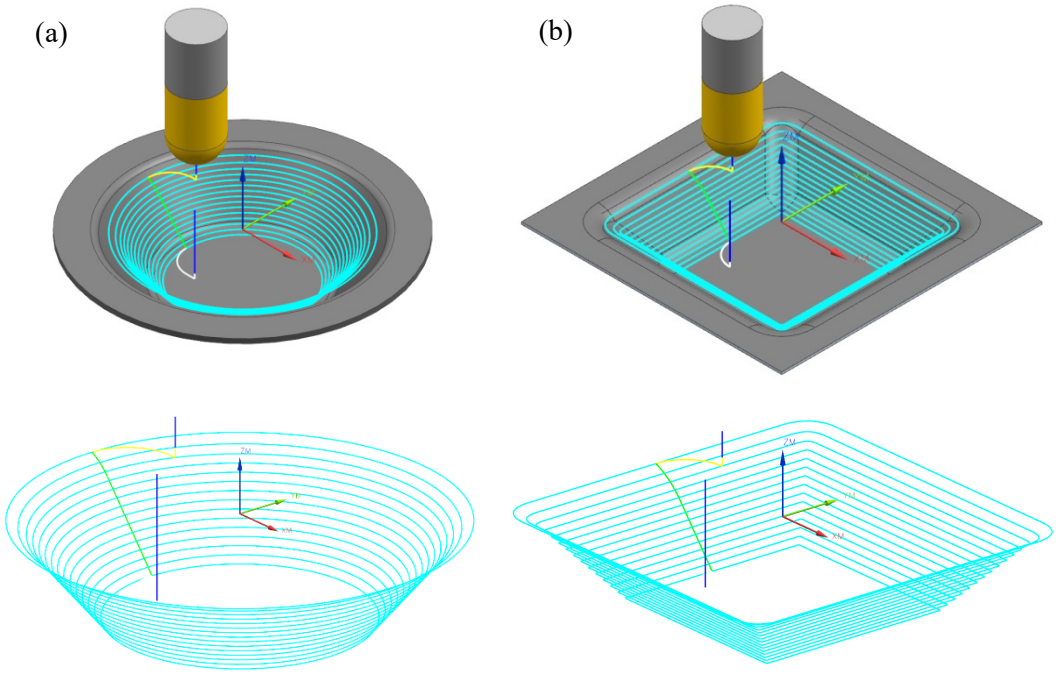

Figure 3-5 Illustration of initial toolpaths of test shapes: (a) Truncated cone; (b) Truncated Pyramid.

3.3 SPIF toolpath correction using a two-directional MPC algorithm (Objective 2)

This section briefly introduces a two-directional MPC algorithm for toolpath correction in the vertical and horizontal directions in SPIF. More details about the development and implementation of this MPC algorithm can be found in **Papers 3** in **Chapter 4.**

3.3.1 Two-directional MPC algorithm for SPIF

To correct the geometric errors of the formed part in the horizontal and vertical directions (Figure 3-6), a two-directional MPC algorithm was developed by augmenting the simplified MPC algorithm above with a new control module for horizontal toolpath correction. There are two separate MPC modules that are used to optimise Δu_h and Δu_z (Figure 3-6). As similar to the simplified MPC algorithm discussed above, each MPC "time" step is also taken to be the forming of a single contour and the number of steps taken to form the shape depends on the designed depth of the shape and the initial Δu_z value. The forming of a single contour depends on the values of Δu_z and Δu_h computed in the control strategy. The ISF process with two-directional MPC control is shown in Figure 3-6.

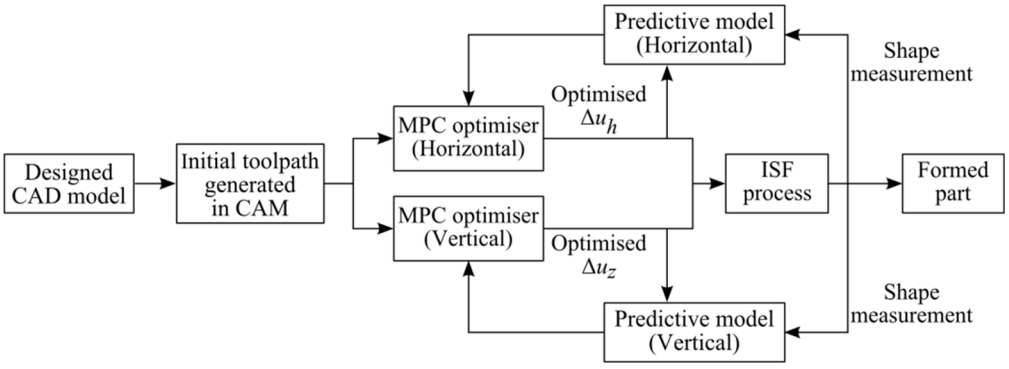

Figure 3-6 Structure of an enhanced MPC algorithm for ISF.

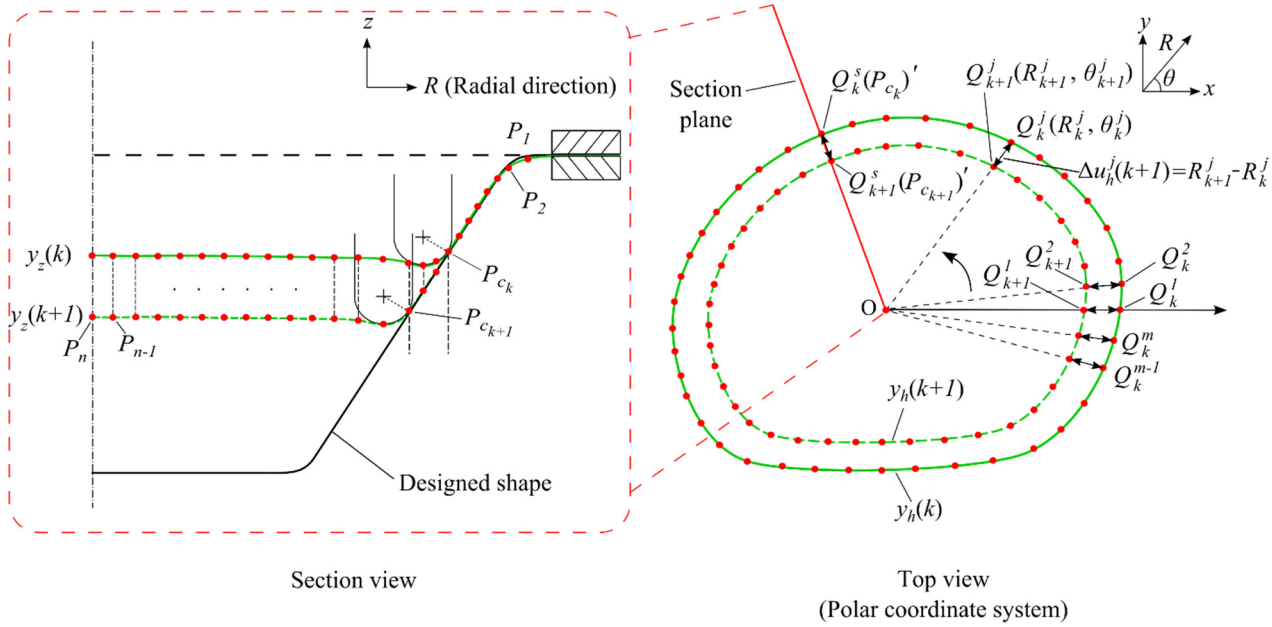

Figure 3-7 Incremental deformation in the two directions.

Figure 3-7 illustrates the incremental deformation between two neighbouring steps in terms of the vertical and horizontal sections of the shape. In the top view of Figure 3-7, the vertical cross-sectional

profile $y_z(k)$ is obtained in a vertical section through points Q_k^s and Q_{k+1}^s, which are the contact points P_{c_k} and $P_{c_{k+1}}$ in the section view, respectively. Meanwhile, the horizontal cross-sectional profile $y_h(k)$ is on the horizontal section plane through the contact point (P_{c_k}).

3.3.1.1 Vertical control module

To correct the toolpath in the vertical direction, the MPC algorithm in this control module is identical to the algorithm described in **Section 3.2.1**. Therefore, the optimisation problem of step *k* is summarised as,

$$\min\ J_z = \left\| \hat{Y}_z - W_z \right\|^2 + \lambda_z \Delta U_z{}^T \Delta U_z , \tag{15}$$

$$\text{subject to } \hat{y}_z\left(k+j \mid k\right) = y_z(k) + \sum_{i=1}^{j} B_z(k+i)\Delta u_z(k+i),\ j = 1,2,\ldots,N_p$$

$$\Delta u_{z\,\min} \le \Delta u_z(k+j) \le \Delta u_{z\,\max},\ j = 1,2,\ldots,N_p$$

where $\Delta U_z(k) = \left[\Delta u_z(k+1), \Delta u_z(k+2), \ldots, \Delta u_z(k+N_p)\right]^T, k = 1,2,\ldots,N$. The solution of Equation (15) can be found using the quadratic programming (QP) described in **Section 3.2.2**.

3.3.1.2 Horizontal control module

In the two-directional MPC algorithm for SPIF, a new horizontal MPC module is added for toolpath correction in the horizontal direction with the aim to reduce geometric errors in the wall area of the parts. In the horizontal control module, the horizontal cross-sectional profile is represented by a number of profile points for optimisation, as shown in Figure 3-7. Q_k^j and Q_{k+1}^j is the *j*th pair of points on $y_h(k)$ and $y_h(k+1)$, respectively. At step *k*, the radial coordinate (R_k^j) of each profile point (Q_k^j) is the profile state of this point. Therefore, the horizontal profile state at step *k* is measured as $y_h(k)$ expressed as follows,

$$y_h(k) = \left[y_h^1(k), y_h^2(k), \ldots, y_h^j(k), \ldots, y_h^m(k) \right], \tag{16}$$

where $y_h^j(k) = R_k^j$, *m* is the number of profile points on the profile.

However, in this horizontal module, not all *m* profile points will be directly measured and used for error correction in the horizontal direction. Only several profile points in the predefined radial

directions, which is selected using a feature-based method, would be directly measured and used to correct the horizontal geometric errors. The profile point states and the horizontal errors in the other radial directions will be calculated with the use of two different models for estimating the horizontal springback distribution along the horizontal profile. More details will be discussed in the case studies (**Section 3.3.2**).

In SPIF, the part is formed incrementally step by step with the sizes of Δu_h and Δu_z typically being small. Consequently, the amounts of vertical and horizontal springback in two neighbouring steps are very close to each other and can be taken to be equal to each other. Therefore, a linear model was built in this module based on the incremental deformation nature of SPIF for MPC control. That is the horizontal distance between Q_k^j and Q_{k+1}^j is taken to be the horizontal input $\Delta u_h^j(k+1)$. At step *k*, the state of a point on the profile of next step can be predicted by,

$$\hat{y}_h^j(k+1) = y_h^j(k) + \Delta u_h^j(k+1). \tag{17}$$

Consequently, the profile state of step *k+1* can be predicted by,

$$\hat{y}_h(k+1 \mid k) = y_h(k) + \Delta u_h(k+1), \tag{18}$$

where $\hat{y}_h(k+1) = \left[\hat{y}_h^1(k+1), \hat{y}_h^2(k+1), \ldots, \hat{y}_h^j(k+1), \ldots, \hat{y}_h^m(k+1)\right]$ is the predicted profile state of step *k+1*, and $\Delta u_h(k+1) = \left[\Delta u_h^1(k+1), \Delta u_h^2(k+1), \ldots, \Delta u_h^j(k+1), \ldots, \Delta u_h^m(k+1)\right]$ is the horizontal step increment of step *k+1*.

Also, the profile predictions along the prediction horizon can be expressed as,

$$\begin{aligned}
&\hat{y}_h(k+1 \mid k) = y_h(k) + \Delta u_h(k+1) \\
&\hat{y}_h(k+2 \mid k) = \hat{y}_h(k+1 \mid k) + \Delta u_h(k+2) \\
&\qquad\qquad = y_h(k) + \Delta u_h(k+1) + \Delta u_h(k+2) \\
&\quad \vdots \\
&\hat{y}_h(k+N_p \mid k) = y_h(k) + \Delta u_h(k+1) + \Delta u_h(k+2) + \ldots + \Delta u_h(k+N_p)
\end{aligned} \quad . \tag{19}$$

Equation (19) can also be written as,

$$\hat{Y}_h(k) = Y_h(k) + L_h \Delta U_h(k), \tag{20}$$

where $\hat{Y}_h(k)=\left[\hat{y}_h(k+1|k),\hat{y}_h(k+2|k),\ldots,\hat{y}_h\left(k+N_p|k\right)\right]$ is the collection of predicted profile states of next N_p steps, $Y_h(k)=[y_h(k),y_h(k),y_h(k),\ldots,y_h(k)]^T$ is the measured profile state at step k and can be written as $Y_h(k)=I_{N_p\times 1}\otimes y_h(k)$, $\Delta U_h(k)=\left[\Delta u_h(k+1),\Delta u_h(k+2),\ldots,\Delta u_h(k+N_p)\right]$, L_h is the coefficient matrix to determine how the horizontal profile state varies with the horizontal input in the next N_p steps. L_h is expressed in the matrix-vector form in Equation(21).

$$L_h=\begin{bmatrix} I_{m\times m} & 0 & 0 & 0 \\ I_{m\times m} & I_{m\times m} & 0 & 0 \\ \vdots & \vdots & \ddots & 0 \\ I_{m\times m} & I_{m\times m} & I_{m\times m} & I_{m\times m} \end{bmatrix} \tag{21}$$

At each step, the optimisation problem for the horizontal control module can also be summarised as a finite-horizon optimisation problem:

$$\min\ J_h=\left\|\hat{Y}_h-W_h\right\|^2+\lambda_h\left\|\Delta U_h-\Delta U_{h0}\right\|^2, \tag{22}$$

$$\text{subject to } \left|\Delta u_h(k+i)-\Delta u_{h\,0}(k+i)\right|\le e, i=1,2,\ldots,N_p$$

$$\hat{y}_h(k+i|k)=y_h(k)+\sum_{i=1}^{j}\Delta u_h(k+1),\ j=1,2,\ldots,N_p$$

where J_h represents the cost function, W_h is the horizontal profile state in design, the last item of J_h is to limit the variation range of the control inputs around the initial inputs, λ_h is the non-negative weighting factor. In this work, $\lambda_h=0.7$ has been adopted after tuning, $\Delta u_{h\,0}(k+i)$ is the initial horizontal step increment in the initial toolpath, e is the inequality constraints of the horizontal inputs and is set as 0.5. The optimisation problem given in Equation (22) can be transformed into the form of a quadratic programming (QP) problem and can be solved using the method described in **Section 3.2.2**.

3.3.2 Case studies

The proposed two-directional MPC algorithm was experimentally verified in SPIF using two forming case studies. In the first case study (a truncated pyramid), two control approaches with different assumptions for the horizontal springback distribution along the horizontal cross-sectional profile were tested and compared. Then, the developed MPC control algorithm was applied to form a more

complex asymmetric shape. The detailed parameter settings of the experiments and the MPC controllers are illustrated in Table 4.

Table 4 Parameter settings in experiment

Parameters	Truncated pyramid	Asymmetric Cone
Tool diameter (mm)	30	20
Raw thickness (mm)	1.6	1.6
Feed rate (mm/min)	4000	4000
Total depth (mm)	35	35
Wall angle (°)	40	Varying at different radial directions
Prediction Horizon (N_p)	6	6

3.3.2.1 Case Study 1

In this case study, the developed control algorithm is verified by forming a truncated pyramid (Figure 3-8), which is a typical test shape in ISF because it has flat wall areas as well as relatively sharp corners where the shape bends significantly. The yellow area is the concerned region.

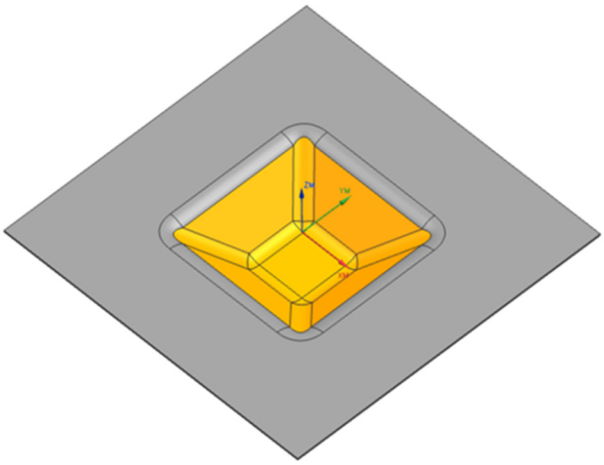

Figure 3-8 Test shape in case study 1.

To optimise Δu_z, the vertical cross-sectional profile is obtained in a section through the corner of the pyramid, as shown in Figure 3-9. The optimisation of Δu_h will only consider one eighth of the shape due to its symmetry. Two models with different assumptions of the horizontal springback distribution were utilised to simplify the optimisation problem in the control process. The first model assumes that the horizontal component of springback is uniformly distributed along the horizontal cross-sectional profile at each step. The second model assumes that the horizontal springback linearly varies with the radial coordinate of the point on the horizontal cross-sectional profile. The use of a simplified

model allows the entire horizontal contour to be adjusted based upon the optimised Δu_h values of only a few profile points rather than all the profile points.

Uniform horizontal springback

In the first model, under the assumption of uniform horizontal springback, the correction of this springback is taken to be uniformly distributed along the cross-sectional profile, as shown in Figure 3-9. That is, the optimised contour is assumed to be obtained by slightly enlarging or shrinking the initial contour by a constant scale factor. Therefore, this scale factor can be calculated using a profile point in any radial direction. In Figure 3-9, $X_k^j(r_k^j,\theta_k^j)$ is the point on the initial contour k and $Q_k^j(R_k^j,\theta_k^j)$ is the point on the profile $y_h(k)$.

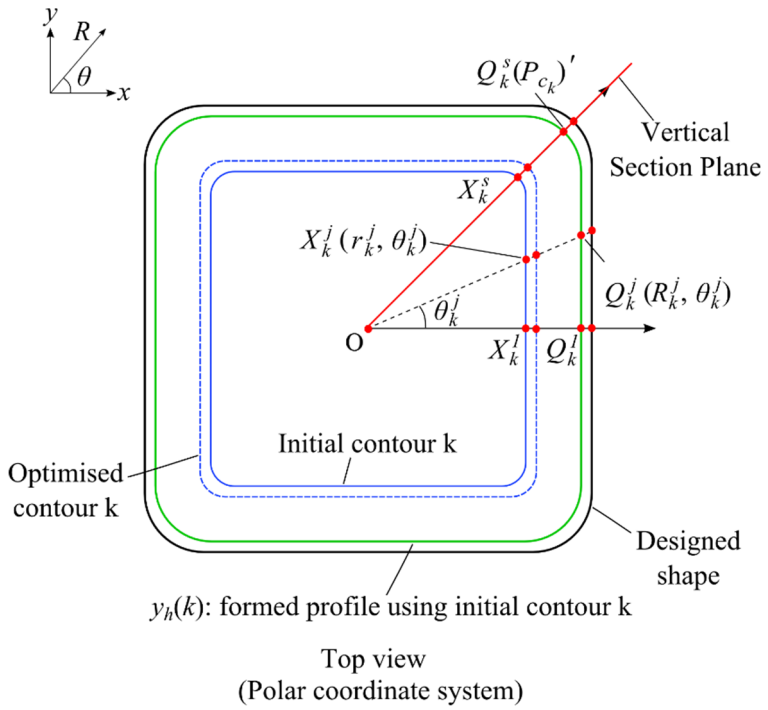

Figure 3-9 Optimisation of contour in the horizontal direction.

The scale factor can be calculated in the following equation,

$$\beta_k = r^{*j}_k / r^j_k = \left[r^j_k + (\Delta u^{*j}_h(k) - \Delta u^j_h(k)) \right] / r^j_k = 1 + (\Delta u^{*j}_h(k) - \Delta u^j_h(k)) / r^j_k , \qquad (23)$$

where β_k is the scale factor, r_k^j is the radial coordinate of point X_k^j on the initial contour k, r^{*j}_k is the radial coordinate of point X^{*j}_k on the optimised contour. $\Delta u_h^j(k)$ and $\Delta u^{*j}_h(k)$ are respectively the initial horizontal input and the optimised input in the direction of $\theta = \theta_k^j$.

In this case, the profile point at the corner, namely point Q_k^s ($R_k^s, \theta_k^s = 45°$), is chosen for calculating the scale factor. Q_k^s is also where the shape is vertically sectioned to get the vertical profile. Therefore, β_k is calculated as,

$$\beta_k = 1 + (\Delta u^{*s}_h(k) - \Delta u^s_h(k)) / r^s_k, \tag{24}$$

where $\Delta u^s_h(k)$ and $\Delta u^{*s}_h(k)$ are respectively the initial horizontal input and the optimised input in the direction of $\theta = \theta^s_k$. The horizontal input in any direction can be obtained by combining Equations (23) and (24),

$$\Delta u^{*j}_h(k) = \Delta u^j_h(k) + r^j_k(\Delta u^{*s}_h(k) - \Delta u^s_h(k)) / r^s_k,\ j = 1, 2, \ldots, m\,. \tag{25}$$

Therefore, the optimisation of $\Delta u^*{}_h(k) = \left[\Delta u^{*1}_h(k), \Delta u^{*2}_h(k), \ldots, \Delta u^{*j}_h(k), \ldots, \Delta u^{*m}_h(k)\right]$ shrinks to an optimal problem requiring the optimisation of $\Delta u^{*s}_h(k)$ with the use of the horizontal MPC module.

Interpolated horizontal springback

From the experimental results of the simplified MPC algorithm described in **Section 3.2.1** [71], it appeared that while there was significant error at the corner of the pyramid, the use of the MPC module for vertical toolpath correction was able to reduce errors in the middle of the wall to be fairly low, as shown in Figure 3-10. This suggests that the horizontal springback is not uniformly distributed along the horizontal profile, which is consistent with other sheet forming processes, such as air bending [123]. A model with varying horizontal springback is developed to correct the horizontal errors. More specifically, the horizontal springback distribution is assumed to vary linearly between the springback of point Q_k^1 ($R_k^1, \theta_k^1 = 0°$) and point Q_k^s ($R_k^s, \theta_k^s = 45°$) based on the radial coordinates of the points, as shown in Figure 3-10.

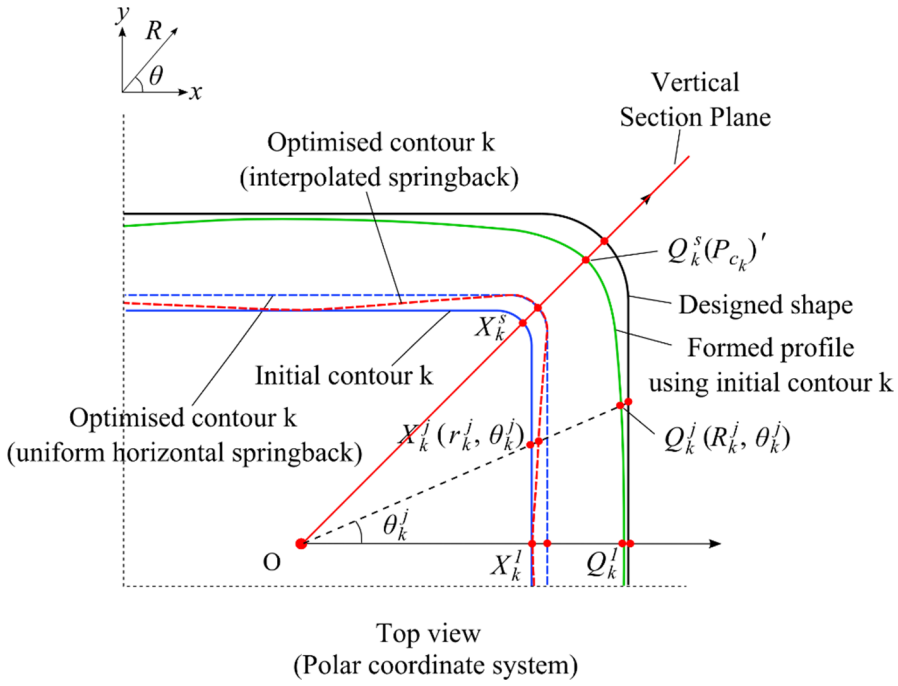

Figure 3-10 Optimisation of contour at step *k* (enhanced model).

To control this springback effect, the contour is adjusted based on the model with varying springback distribution. Consequently, the scale factor β_k for adjusting the initial contour varies at different radial directions and can be expressed as,

$$\beta_k = \left[\beta_k^1, \beta_k^2, \ldots, \beta_k^j, \ldots, \beta_k^m\right]. \tag{26}$$

For the linearly interpolated horizontal springback model, only springback at the two radial directions ($\theta = \theta_k^1$ and $\theta = \theta_k^s$) will be detected and the springback at any radial direction ($\theta = \theta_k^j$) is estimated by a linear interpolation based on the radial coordinates. Therefore, the scale factor value β_k^j can be obtained using the following equation,

$$\beta_k^j = \beta_k^1 + (\beta_k^s - \beta_k^1)(r_k^j - r_k^1)/(r_k^s - r_k^1). \tag{27}$$

Also, β_k^j can be expressed in a generalisation of Equation(24),

$$\beta_k^j = 1 + (\Delta u^{*j}_h(k) - \Delta u_h^j(k))/r_k^j. \tag{28}$$

Similarly, β_k^s is expressed as,

$$\beta_k^s = 1 + (\Delta u^{*s}_h(k) - \Delta u_h^s(k))/r_k^s. \tag{29}$$

With the use of the simplified MPC algorithm described in **Section 3.2.1**, geometric accuracy in the middle of four pyramid walls was greatly improved to the desirable level (± 0.3 mm) when only Δu_z is optimised and Δu_h is kept unchanged from the initial CAD toolpath [71]. The radial direction $\theta = \theta_k^1$ corresponds to the middle of the pyramid wall. Therefore, β_k^1 is taken to be 1. It means that the position of the contour point in this direction will not be adjusted while optimising the contour.

By combining Equations (27), (28) and (29) together, the optimal input at any radial direction can be obtained using the linear interpolation,

$$\Delta u^{*j}_h(k) = \Delta u^j_h(k) + (\Delta u^{*s}_h(k) - \Delta u^s_h(k)) \frac{r^j_k (r^j_k - r^1_k)}{r^s_k (r^s_k - r^1_k)},\ j = 1, 2, \ldots, m. \qquad (30)$$

Once again, the optimisation of $\Delta u^*_h(k) = \left[\Delta u^{*1}_h(k), \Delta u^{*2}_h(k), \ldots, \Delta u^{*j}_h(k), \ldots, \Delta u^{*m}_h(k) \right]$ shrinks to an optimal problem for optimising $\Delta u^{*s}_h(k)$. After $\Delta u^{*s}_h(k)$ is calculated in the horizontal MPC module at each step, the optimised contour can be obtained for springback correction. Hence, the computational complexity for using either of the two springback models is identical.

3.3.2.2 Case Study 2

To further verify the developed MPC control algorithm, another case study was performed using a more complex asymmetric shape. The test shape is an asymmetric truncated cone, as shown in Figure 3-11, with the wall angle varying at different radial directions from the centre.

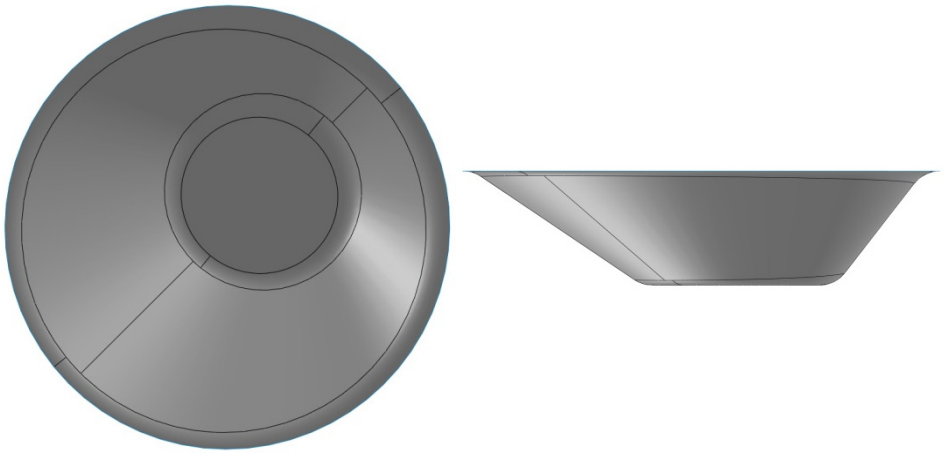

Top view Side view

Figure 3-11 Test shape in case study 2.

In the vertical optimisation, the formed shape is sectioned through point Q_k^s ($R_k^s, \theta_k^s = 45°$), as shown in Figure 3-12, to obtain the vertical cross-sectional profiles. As for the horizontal optimisation, the model with interpolated horizontal springback distribution was used to estimate the horizontal errors. The optimised Δu_h values in five selected radial directions ($\theta = 0°, 45°, 90°, 180°, 270°$), which are marked by arrow lines in Figure 3-12, are computed directly in the horizontal MPC optimiser. The optimised Δu_h values in other radial directions are calculated using linear interpolation between the sample points, that is, using an appropriate modification to Equation (30) for each inter-sample segment.

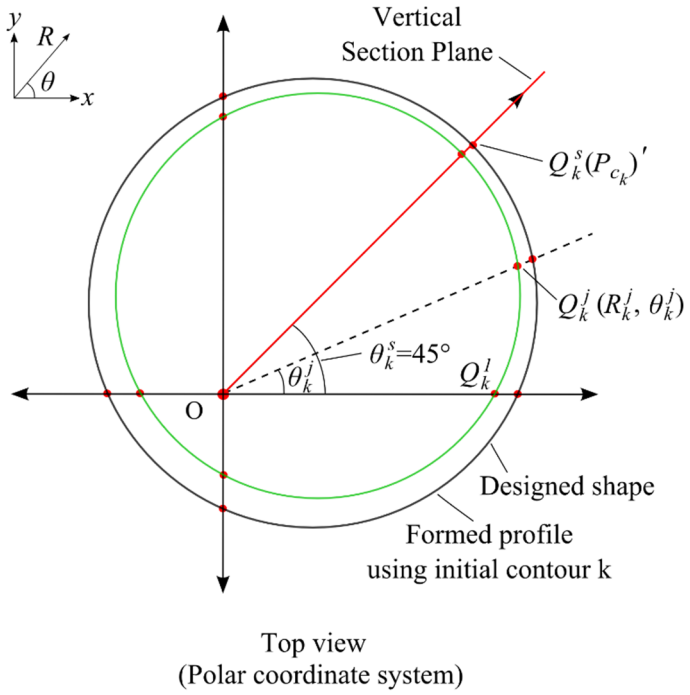

Figure 3-12 Application of the horizontal model with interpolated springback.

3.4 TPIF toolpath correction using an enhanced MPC algorithm (Objective 3)

This section briefly introduces the methodology for a two-directional toolpath correction strategy developed for TPIF. More details about the development and experimental validation of this control algorithm can be found in **Papers 4** in **Chapter 4**.

Currently, there are not many studies that have been reported on in-process toolpath correction in TPIF. In TPIF with a single full die, it is difficult to correct the geometric errors by freely adjusting the toolpath because the tool movement is greatly limited by the full die with a definite shape as shown in Figure 3-13b. A possible way for toolpath correction in TPIF with a full die is to use

different full dies with modified shapes at the intermediate stages of the forming process. It would be time-consuming to fabricate multiple full dies for forming a part. On the contrary, TPIF with a partial die (Figure 3-13c) is more flexible and the toolpath can be more freely adjusted in a wide range to improve the geometric accuracy of the formed part. The toolpath correction was performed through properly adjusting the toolpath in two directions based on the optimised toolpath parameters at each step.

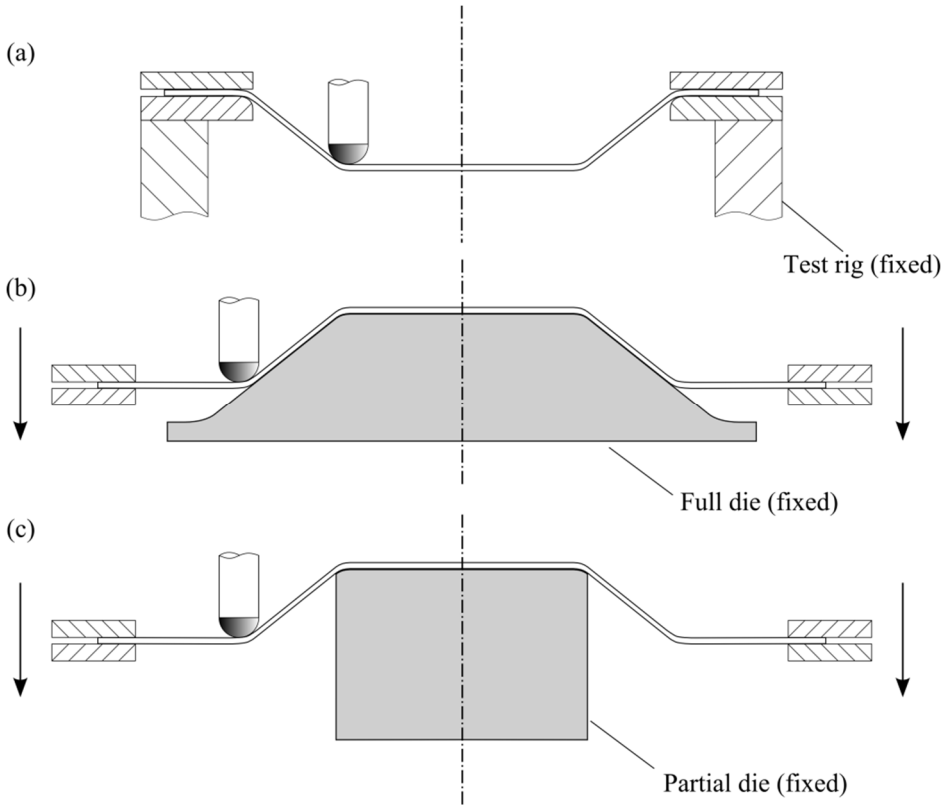

Figure 3-13 SPIF and TPIF processes.

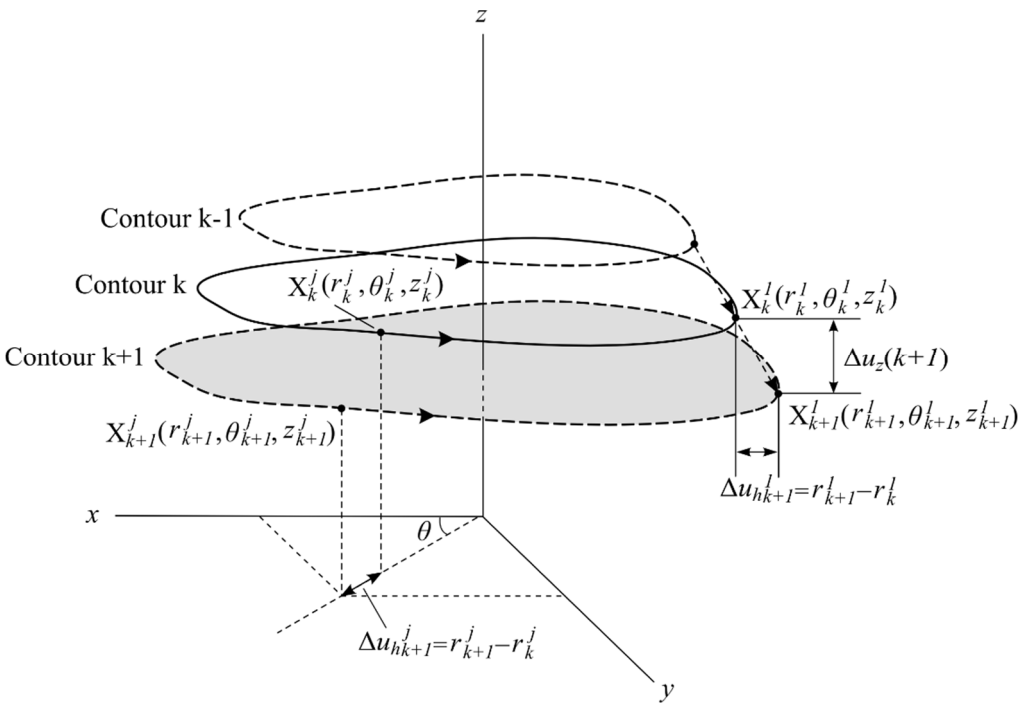

Figure 3-14 Parameters of contour toolpath in TPIF.

3.4.1 Enhanced MPC algorithm for TPIF with a partial die

In this section, an enhanced MPC algorithm has been developed specially for TPIF with a partial die to correct the toolpath in the vertical and horizontal directions. Based on the deformation nature of TPIF with a partial die, the vertical predictive model used in the TPIF MPC algorithm is slightly different from the model used in SPIF, see **Section 3.2.1**. Besides this, an enhanced horizontal control module in this MPC algorithm was modelled by further developing the interpolated springback model in the horizontal control module for SPIF. In the horizontal control module, dense profile points in the evenly distributed radial directions of the horizontal section were used to estimate the horizontal error distribution along the horizontal sectional profile during the forming process, which provide an achievable method to estimate the horizontal error distribution in forming general shapes.

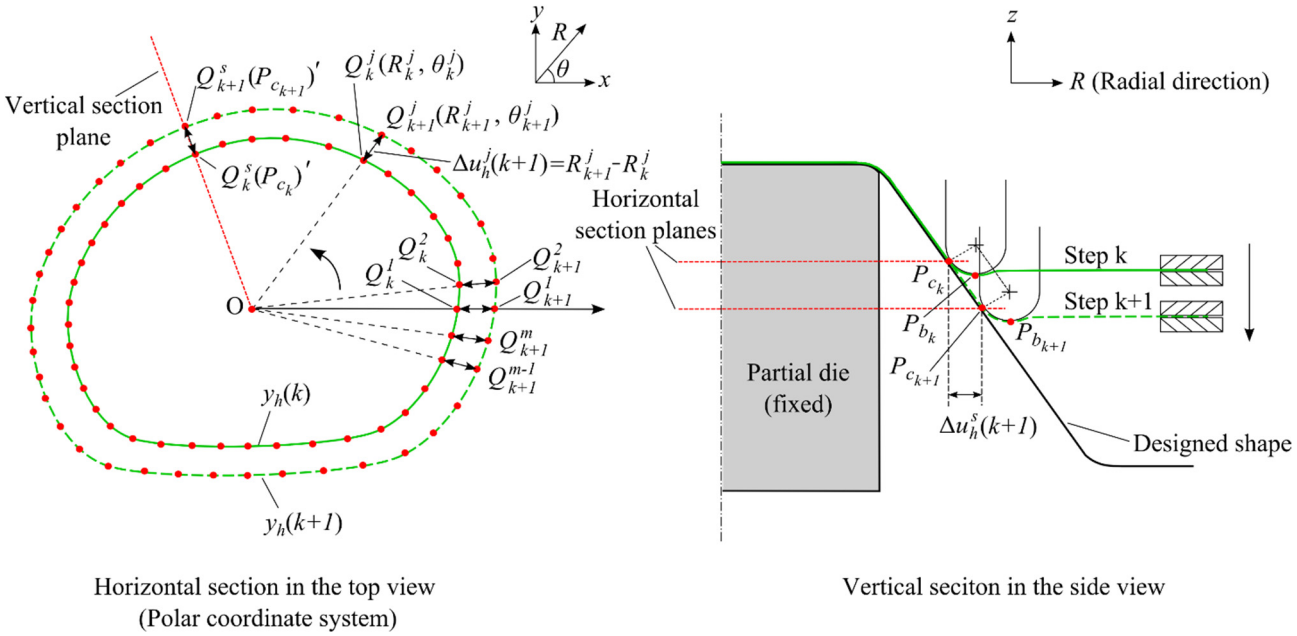

Figure 3-15 Cross-sectional profiles of formed shapes during TPIF.

Figure 3-15 shows the cross-sectional profiles of the formed shape in two directions during the forming process of TPIF. At each step, the formed shape is scanned and sectioned horizontally and vertically to get the cross-sectional profiles in the horizontal and vertical directions, respectively. The cross-sectional profiles in the two directions are taken as the shape states for optimisation in the control modules. Each vertical sectional profile is obtained in a vertical section plane through each radial direction $\theta^s_k = \theta^j_k (j = 1, 2, \cdots, m)$. In the side view of Figure 3-15, the vertical cross-sectional profile at each step is a curve that also can be represented by a number of points. At step k, P_{c_k} is the contact point where the flat local wall is tangential to the hemispherical end of the tool, while P_{b_k} is the point where the bottom point of the ball end touches the metal blank. On the vertical sectional profiles, contact points P_{c_k} and $P_{c_{k+1}}$ in the side view are the points Q^s_k and Q^s_{k+1} in the top view, respectively. The top view of Figure 3-15 illustrates the horizontal sections, which corresponds to the horizontal section planes in the side view, at two neighbouring steps.

3.4.1.1 Horizontal control module

Compared with the interpolated springback model in **Section 3.3.1.2**, which only uses a few profile points in the selected radial directions for horizontal springback estimation, this horizontal control module for TPIF uses dense profile points in the evenly distributed radial directions of the horizontal section, as shown in the top view of Figure 3-15, to estimate the horizontal error distribution along the horizontal sectional profile. As a matter of the resolution for representing a curve, more profile

points can give more accurate estimation of the formed sectional profiles. To guarantee enough accuracy in representing the formed profiles and the horizontal error distribution, the horizontal sectional profile at each step is sampled in 360 uniformly distributed radial directions in this study. That is, the number of profile points is set as m=360.

The structure of this horizontal control module is similar to the one used in the two-directional MPC algorithm for SPIF (**Section 3.3.1.2**). Therefore, at step k, $Q_k^j(R_k^j, \theta_k^j)$ is the jth profile point of horizontal profile $y_h(k)$ and its radial coordinate (R_k^j), is taken as the profile state of this point. The horizontal profile state of step k is defined in Equation(16).

Similarly, at step k, the control problem in the horizontal module can be summarised as an optimisation problem to optimise the horizontal toolpath inputs through minimising the difference between the predicted profile states and target profile states in the prediction horizon, as expressed in Equation(22). In particular, the values of e and λ_h are set as the same as the values used in the two-directional MPC algorithm for SPIF (**Section 3.3.1.2**).

3.4.1.2 Vertical control module

To optimise Δu_z for toolpath correction in the vertical direction, the vertical MPC module is developed using a similar control structure as the horizontal control module in **Section 3.4.1.1**. The vertical cross-sectional profile at each step is represented by a number of points, as seen in the side view of Figure 3-15. Due to the springback, the formed depth of the shape is generally smaller than the target depth. This control module is aimed to drive the metal blank to the target depth by using the optimised Δu_z. That is, the vertical control module aims to drive the bottom point on the cross-sectional profile to the target position. Considering the vertical sectional profiles in all the radial directions ($\theta_k = \theta_k^1, \theta_k^2 \cdots, \theta_k^j, \cdots, \theta_k^m$) in the top view of Figure 3-15, the z coordinates of the bottom points of these vertical sectional profiles are taken as the shape state in the vertical direction. The vertical shape state at step k can be expressed as,

$$y_z(k) = \left[y_z^1(k), y_z^2(k), \ldots, y_z^j(k), \ldots, y_z^m(k) \right] . \tag{31}$$

In TPIF, the shape is formed incrementally contour by contour and the size of Δu_z typically is small. Therefore, the amounts of vertical springback in two neighbouring contours are very close to each other and can be considered to be equal to each other for building a linear model for MPC control. Under this simplification that the vertical springback amounts at step k and step $k+1$ are equal, the

vertical distance between P_{b_k} and $P_{b_{k+1}}$ in the radial direction $\theta = \theta_k^s$ can be taken as $\Delta u_z^s(k+1)$ when the vertical springback is taken into consideration in the model. $\Delta u_z^s(k+1)$ can be expressed in the following equation,

$$\Delta u_z^s(k+1) = \hat{y}_z^s\left(k+1 \mid k\right) - y_z^s(k). \tag{32}$$

In the contour toolpath, the contours are parallel to each other. The contour points of each contour are on the same z-level plane, which is consistent with the way they are defined in the initial contour toolpath. Therefore, the $\Delta u_z(k+1)$ values in all the radial directions are the same. That is, $\Delta u_z(k+1) = \left[\Delta u_z^1(k+1), \Delta u_z^2(k+1), \ldots, \Delta u_z^j(k+1), \ldots, \Delta u_z^m(k+1)\right]$ can be expressed as,

$$\Delta u_z(k+1) = \Delta u_z^s(k+1)\, I_{1\times m}. \tag{33}$$

Based on this, the optimised $\Delta u_z(k+1)$ can be obtained in the optimisation of just one element, namely $\Delta u_z^s(k+1)$, in a selected radial direction. In this work, the radial direction through the middle of one of the curved fillets ($\theta_k^s = 45°$) was used for optimising $\Delta u_z(k+1)$ in the vertical control module.

Consequently, only one element of $y_z(k) = \left[y_z^1(k), y_z^2(k), \ldots, y_z^j(k), \ldots, y_z^m(k)\right]$, namely $y_z^s(k)$, is investigated in the vertical control module. The vertical shape state at each step can be simplified as,

$$y_z(k) = y_z^s(k), \tag{34}$$

where $y_z^s(k)$ can be obtained in the cross-sectional profile in the selected radial direction ($\theta_k^s = 45°$) after measuring the formed shape at step *k*. The vertical state of next step can be predicted as,

$$\begin{aligned} \hat{y}_z\left(k+1 \mid k\right) &= y_z(k) + \Delta u_z^s(k+1) \\ &= y_z^s(k) + \Delta u_z^s(k+1) \end{aligned}, \tag{35}$$

where $\hat{y}_z(k+1)$ is the predicted profile state of next step. Similarly, the vertical shape states over the prediction horizon can be obtained by,

$$
\begin{aligned}
\hat{y}_z(k+1\,|\,k) &= y_z^s(k) + \Delta u_z^s(k+1) \\
\hat{y}_z(k+2\,|\,k) &= \hat{y}_z(k+1\,|\,k) + \Delta u_z^s(k+2) \\
&= y_z^s(k) + \Delta u_z^s(k+1) + \Delta u_z^s(k+2) \\
&\vdots \\
\hat{y}_z(k+N_p\,|\,k) &= y_z^s(k) + \Delta u_z^s(k+1) + \Delta u_z^s(k+2) + \Delta u_z^s(k+N_p)
\end{aligned} \quad . \tag{36}
$$

Equation (36) can be gathered into the matrix-vector form,

$$
\hat{Y}_z(k) = Y_z(k) + L_z \Delta U_z(k), \tag{37}
$$

where $\hat{Y}_z(k) = \left[\hat{y}_z(k+1\,|\,k), \hat{y}_z(k+2\,|\,k), \ldots, \hat{y}_z(k+N_p\,|\,k)\right]^T$ collects the state predictions of future N_p steps, $Y_z(k) = [y_z^s(k), y_z^s(k), \ldots, y_z^s(k)]^T$ is the measured shape state at step k and can be written as $Y_z(k) = I_{N_p \times 1} \otimes y_z^s(k)$, $\Delta U_z(k) = \left[\Delta u_z^s(k+1), \Delta u_z^s(k+2), \ldots, \Delta u_z^s(k+N_p)\right]^T$ is the vertical toolpath inputs, L_z is a matrix obtained by collecting Equation (36) together and is expressed as,

$$
L_z = \begin{bmatrix} 1 & 0 & 0 & 0 \\ 1 & 1 & 0 & 0 \\ \vdots & \vdots & \ddots & 0 \\ 1 & 1 & \cdots & 1 \end{bmatrix}. \tag{38}
$$

To the drive the formed depth as close as possible to the target depth at each step, the control problem in the vertical control module at step k can also be summarised as an optimisation problem in Equation(39). The second item is used to limit the size of vertical toolpath inputs that are negative at all steps. λ_z is set as 0.2, which is the same as in [71].

$$
\min\ J_z = \left\| \hat{Y}_z - W_z \right\|^2 + \lambda_z \Delta U_z{}^T \Delta U_z \tag{39}
$$

$$
\text{subject to } \Delta U_z(k) = \left[\Delta u_z^s(k+1), \Delta u_z^s(k+2), \ldots, \Delta u_z^s(k+N_p)\right]^T, k = 1, 2, \ldots, N
$$

$$
\hat{y}_z(k+j\,|\,k) = y_z^s(k) + \sum_{i=1}^{j} \Delta u_z^s(k+i),\ j = 1, 2, \ldots, N_p,\ \Delta u_{z\,\min} \le \Delta u_z(k+j) \le \Delta u_{z\,\max},\ j = 1, 2, \ldots, N_p
$$

where J_z is the cost function and W_z is the target vertical states.

In summary of **Section 3.4.1**, two separate MPC control modules have been developed to provide the optimal Δu_h and Δu_z for in-process toolpath correction at each step. To solve the optimisation

problems in the two control modules, the cost functions can be transformed into typical quadratic programming (QP) problems and would be solved using the method described in **Section 3.2.2**. After solving the optimisation problems, ΔU_z^* and ΔU_h^*, the optimised toolpath inputs over the next N_p steps will be obtained. Only the first optimal move, namely the optimised toolpath inputs in the next one step, will be applied to form the contour in the next single step. Control actions will be conducted using the two-directional MPC control algorithm at each subsequent step until the shape is finally formed.

3.4.2 Case studies

A case study for forming a non-axisymmetric shape was conducted to experimentally verify the developed toolpath correction strategy. The test shape used for the experiments was a non-axisymmetric shape, which contains both flat and curved walls (Figure 3-16). The wall angle was 40° and the total depth was 35mm. There are a number of z-level contours in the initial toolpath, as shown in Figure 3-16. The initial step depth was set as 1mm. Consequently, the number of steps in the forming process was calculated as 35. The metal sheet used for tests was made of aluminium (AA 7075-O) and the raw thickness was 1.6 mm. The unformed blank size was 300 mm × 300 mm. A ball-ended tool with a 20 mm diameter was used in the experiments. The feed rate in the forming process was 4000 mm/min. Based on the test shape, a partial die (Figure 3-17) made of timber was fabricated for the TPIF forming process in the test.

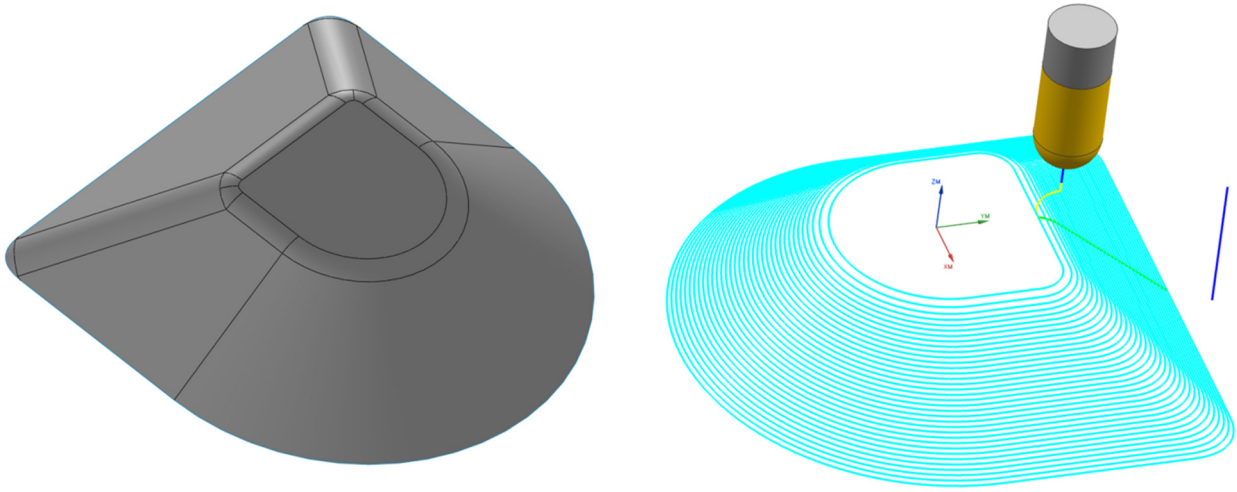

Figure 3-16 Test shape and the initial toolpath from CAM software.

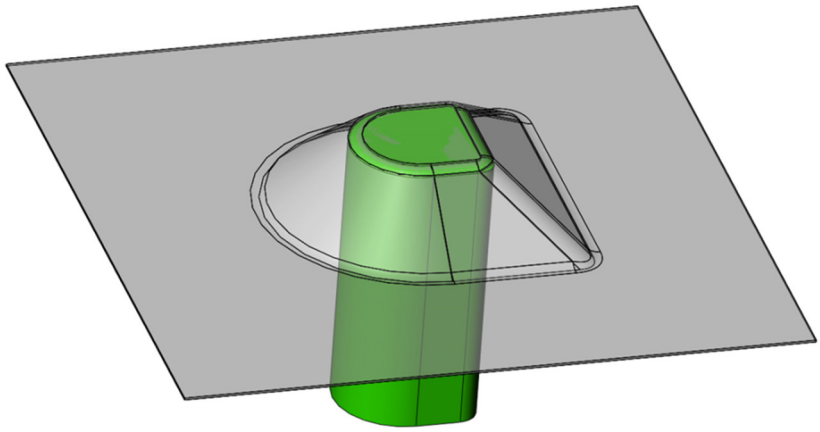

Figure 3-17 The partial die used in the TPIF process.

3.5 Experimental setup

3.5.1 AMINO ISF machine

Experiments were carried out on an AMINO® DLNC-PC ISF machine equipped with a 3D laser scanner (Figure 3-18). The machine has a large forming platform controlled by a FANUC controller and an electro-pneumatically controlled clamping platform. The maximum size of the part that can be formed using this ISF machine can reach 2100 mm×1450 mm×550 mm. The moving speed of the X and Y axes can reach a maximum value of 60 m/min with a repeatability of ± 0.05 mm, which enables the part fabrication at high feed rates. The *Z* axis is driven by an AC servo motor with the power of 1 kW that allows a maximum forming force of 3 kN. Hemispherical tools with the diameters ranging from 10 mm to 30 mm are equipped with this machine.

The sheet blank is clamped between a blank holder and a steel backing plate to limit the movement of the blank edges during the forming process. The metal blank, with 1.6 mm in thickness and 300 mm × 300 mm in size, is made of aluminium (AA 7075-O), which is a commonly-used metal material in aviation and automotive industries. A 30 mm diameter cylindrical steel tool with a hemispherical end was used to deform the blank; the tip of the tool is tungsten carbide and the body is made of K110 steel which was hardened and tempered to HRC60. Lubricant (oil-Shell Tellus Oil 68) was used to reduce the wear of the tool and friction between the tool and the blank.

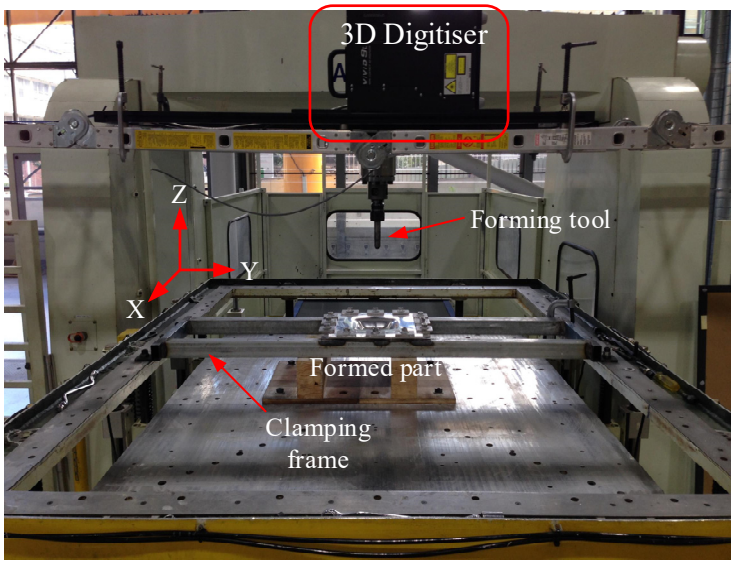

Figure 3-18 The AMINO® DLNC-PC ISF Machine equipped with a 3D Digitiser.

3.5.2 Geometry measurement

To measure the geometric accuracy, the 3D geometry of formed parts can be measured using a laser scanner, a non-contact 3D Digitizer (VIVID 9i), mounted on the top of the forming platform, as shown in Figure 3-18. The VIVID 9i digitizer uses the light-stripe method to emit a horizontal stripe light through a cylindrical lens to the object. The reflected light from the object is received by the CCD, and then converted by triangulation into distance information. This process is repeated by scanning the stripe light vertically on the object surface using a Galvano mirror, to obtain 3D dimensional data of the test part. The scanning accuracy is within ±0.05mm, which is sufficiently accurate for the shape measurement in ISF. It takes about 2.5 seconds for a single scan of a formed shape. GEOMAGIC Qualify is used to produce 3D data of the scanned shape and analyse the dimensional error between deformed test parts and designed CAD models.

3.5.3 ISF manufacturing system with feedback control

To experimentally implement the developed control algorithms, an ISF manufacturing system with feedback control has been developed based on the AMINO® DLNC-PC ISF machine in the lab, as shown in Figure 3-19. After the forming of a certain step was finished, currently formed shape was measured by the 3D digitiser. The shape states of current shape used for feedback control were generated by sectioning the scanned geometry. The shape states then were imported into the MPC control module where toolpath parameters were optimised in the well-defined optimisers. As a result, the metal blank was deformed by the tool following a corrected toolpath in the next step. As the tool

formed down step by step, the toolpath was continuously corrected based on the shape feedback to get improved geometric accuracy in the final part.

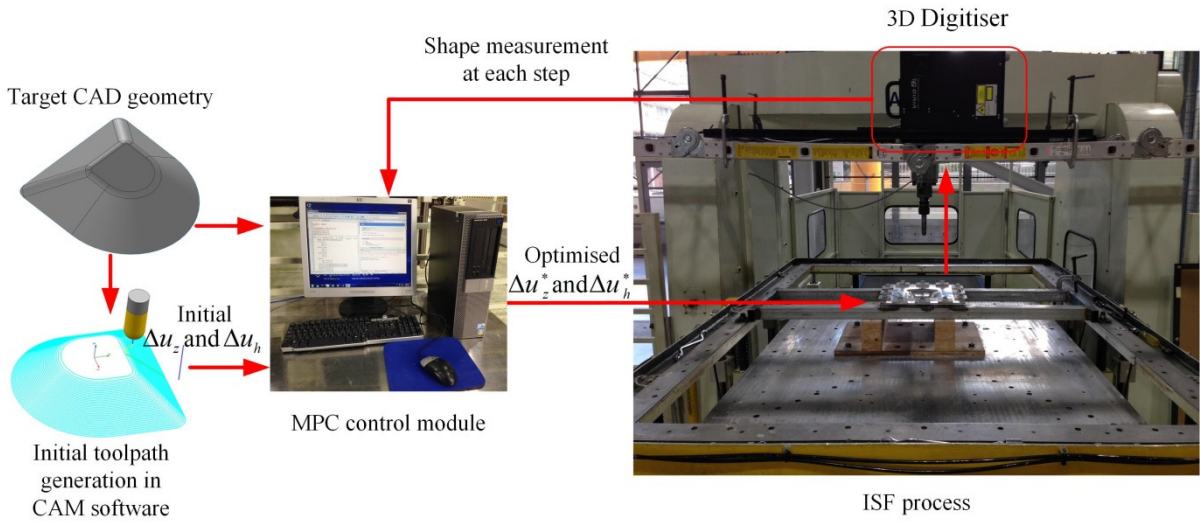

Figure 3-19 Structure of the closed-loop control system for ISF.

Figure 3-20 illustrates the flow chart of the implementation of the developed MPC algorithms in the ISF processes. The system inputs include the target shape states (W_z and/or W_h) and toolpath contours generated from CAM software. After forming contour *k*, the formed shape is measured and the measured profile state is then used by the predictive models to predict the shape states of next several steps in terms of vertical and horizontal directions. Then, the MPC optimisers will determine a sequence of control inputs that minimise the difference between the target shape states and the predicted shape states. Optimised inputs of the next N_p steps, namely $\Delta U_z^*(k)$ and $\Delta U_h^*(k)$, will be obtained by solving the optimisation problems in the control modules. For each direction, only the first element of the optimised parameters will be used to correct the toolpath in the following single step. The entire control process is then repeated at each subsequent step (forming contour) until the shape is formed.

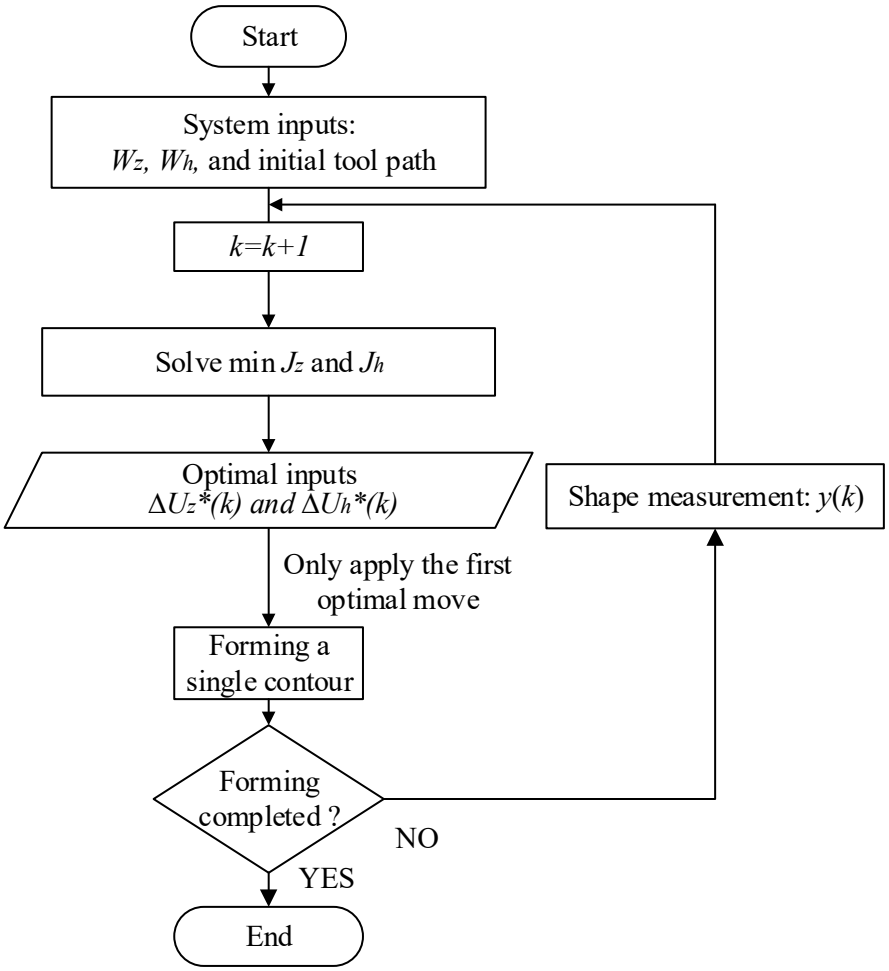

Figure 3-20 Flow chart for MPC application to ISF.

The results of these methodologies are provided in the subsequent chapter.

Chapter 4 Results

This chapter presents the main results that have been achieved for this PhD project. Much of the results are the summary of some key sections of the published/submitted papers during the PhD studies, as attached in **Appended Papers**. The published/submitted papers are briefly summarised at the end of this chapter.

4.1 Results of parameter investigation (Objective 1a)

To achieve **Objective 1a** of this thesis**,** the influence of step depth on the part accuracy, surface finish and formability was firstly investigated (**Paper 1**). This section presents the experimental results obtained in tests to analyse the influence of step depth in the SPIF process.

In this study, two sets of experiments were conducted in a typical SPIF process (no toolpath control) to investigate this toolpath parameter defined by the user in generating the toolpath in CAM software. A test was performed to analyse the geometric accuracy and surface morphology of formed parts using three different step depth sizes (0.1, 0.6, 1.1mm). A formability test was conducted to analyse the material formability in SPIF in the form of the total depth of the formed parts using a series of varying step depth sizes (0.1, 0.2, 0.3, 0.4, 0.5, 0.7, 1.0mm).

The test shape used for the experiments was a truncated cone. In the geometric accuracy test, the wall angles was 50° and the total target depth was 35mm. In the formability test, the wall angle was 60° and the total target depth was 75mm. The sheet blank was clamped between a blank holder and a steel backing plate to prevent any movement of the blank during forming process. The metal blank, with 1.6 mm in thickness and 300 mm × 300 mm in size, is made of aluminium (AA 7075-O). A 30 mm diameter cylindrical steel tool with a hemispherical end was used to deform the blank. The feed rate in the forming process was set as 4000 mm/min. Lubricant (oil-Shell Tellus Oil 68) was used to reduce the wear of the tool and friction between the tool and the blank.

4.1.1 Geometric accuracy

GEOMAGIC Qualify was used to produce 3D geometry data of the scanned shape (the truncated cones) and analyse the dimensional error between deformed test parts and designed CAD models. In this work, cross-sectional comparison along a defined section plane was used to evaluate the geometric accuracy since the truncated cone is symmetric. A system plane (plane XOZ) across the symmetry axis of the cone was set as the section plane. The deviation in the *Z* direction between the designed and fabricated profiles was calculated as the geometric error in cross-sectional comparison.

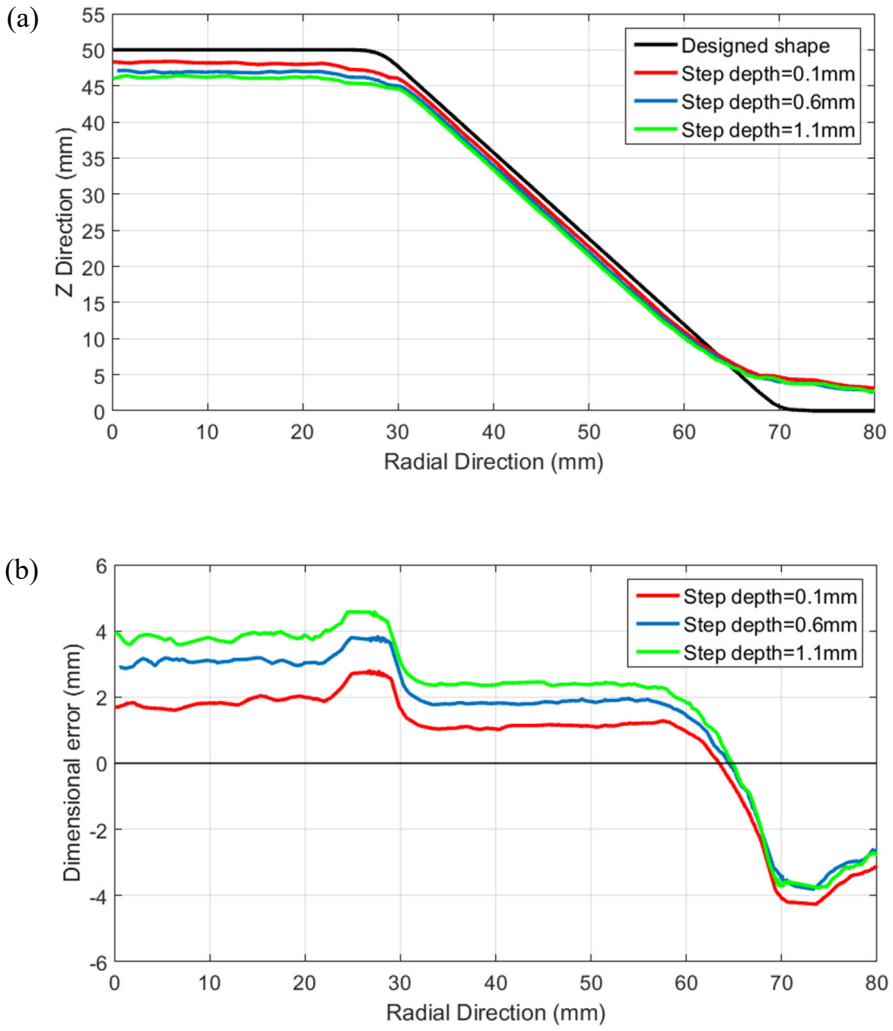

Figure 4-1 (a) Cross-sectional comparison among deformed profiles and the target profile; (b) Error distribution of deformed parts.

The comparison among profiles of formed parts and the designed shape in the geometric accuracy test is illustrated in Figure 4-1a, while detailed error distributions are correspondingly shown in Figure 4-1b. According to the curves in Figure 4-1, the profile with a 0.1 mm step depth has the best dimensional accuracy in the test compared with the target profile. Therefore, step depth can significantly affect the geometric accuracy. Specifically, the geometric accuracy increases when decreasing the step depth size. This observation can be due to the fact that the generated forming contours are denser when setting step depth at a small value. With the use of a smaller step depth, the movement of the forming tool would be smaller between two adjacent parallel contours, providing more homogeneous material distribution and deformation as well as the reduction of the spring-back effect.

4.1.2 Surface morphology

Surface morphology of inner faces, namely the machined faces, of deformed cones was shown in Figure 4-3. Obviously, in the comparison of surface waviness among three produced parts, step depth has a great influence on the surface finish quality. As can be seen in Figure 4-3a and Figure 4-3b, there are obvious wavy tool marks left on the machined surfaces when using large step depth sizes (0.6mm and 1.1mm). The distance between two adjacent tool marks on the formed surface, *d*, illustrated in Figure 4-2, increases with the increase of step depth value. The relationship between *d* and Δu_z, coincides with the sine law, as shown in the following equation,

$$d = \Delta u_z / sin\alpha , \tag{40}$$

where α is the wall angle of the truncated cone.

Due to the geometric error, the measured *d* values (1.406mm and 0.751mm with Δu_z at 1.1mm and 0.6mm, respectively) are a little smaller than calculated ones (1.436mm and 0.783mm). On the contrary, as for small step depth (0.1mm), the formed surface shown in Figure 4-3c is much smoother than the two surfaces above, with no visible tool marks on the surface. Thus, it can be concluded that the surface quality can be improved by choosing small step depth in the ISF process in this case.

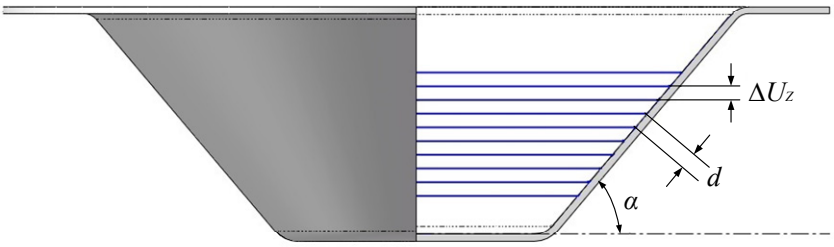

Figure 4-2 Diagram of tool marks on the inner part face.

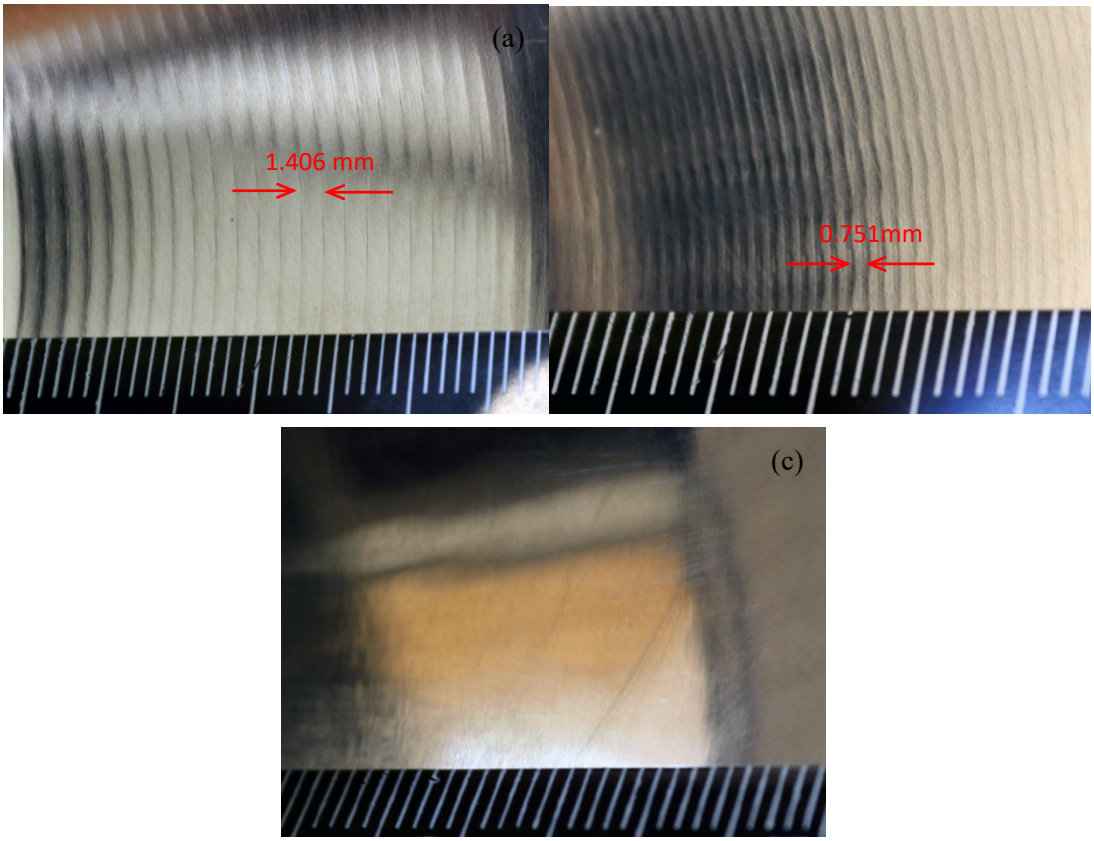

Figure 4-3 Surface morphology of deformed parts in surface quality test: (a) Δu_z =1.1mm; (b) Δu_z =0.6mm; (c) Δu_z=0.1mm.

4.1.3 Fracture analysis

Based on the analysis above, smaller step depth contributes to better geometric accuracy and part surface quality but lower efficiency due to the increase of forming time. More importantly, small step depth also adversely affects the forming process in terms of material formability, especially when the forming wall angle gets close to the forming wall angle limit. In the formability test, a truncated cone with a 60° wall angle (close to the wall angle limit) was used to evaluate the formability at different step depth sizes, with Δu_z ranging from 0.1 to 1.0 mm. The sheet fractured during the forming process with small step depth below 0.5 mm while only the parts with Δu_z over 0.7mm were successfully produced. Figure 4-4a shows the material fracture of a deformed cone with Δu_z being 0.1mm. Furthermore, the material fracture occurs at a smaller forming depth in the Z direction when the step depth is smaller, which is illustrated in Figure 4-4b. This can be due to the fact that a smaller step depth size means a smaller tool contour distance between two neighbouring contours. Thus, more intensive contact between the sheet material and the tool end will happen in the ISF process, during which material in the contact zone of the metal sheet is pressed and hardened by the tool end in each forming contour. More already hardened material would be deformed again by the tool in the

following several contours when using a tool path with smaller step depth. This leads to a great increase in the contact stress required to reach the target deformation. Consequently, sheet formability will be reduced due to a higher stress state induced in the material. Therefore, too small step depth values should be avoided in consideration of material failure. In this case, 0.7 mm step depth was suggested to be the optimum value for the forming of the truncated cone with a 60° wall angle.

(a)

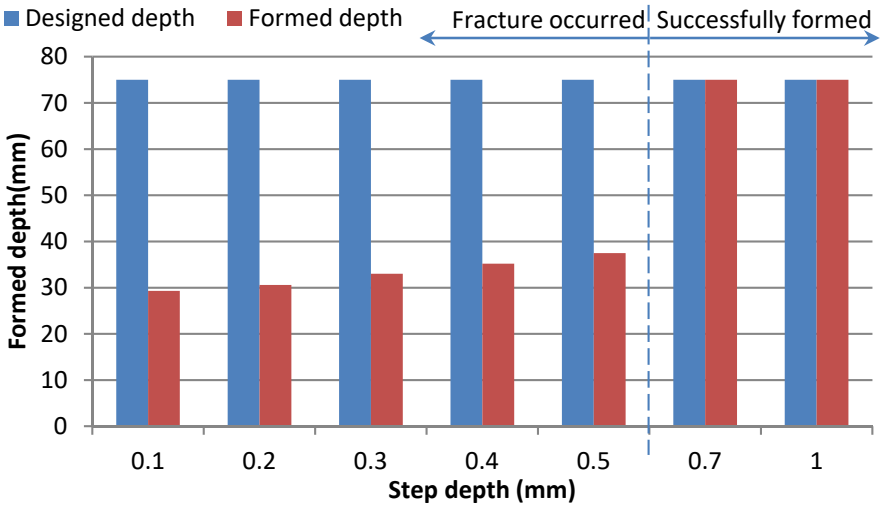

(b)

Figure 4-4: (a) Part fracture in formability test (Δu_z=0.1mm); (b) Formed depth of parts in formability test.

4.2 Results of SPIF toolpath correction using a simplified MPC algorithm (Objective 1b and 1c)

To achieve **Objective 1b and 1c** of this thesis**,** a simplified MPC control algorithm has been developed and experimentally verified for geometric accuracy improvement in SPIF via in-process toolpath correction (**Paper 2**). This section presents the experimental results of this work.

The geometry of the deformed components is measured at each step. To demonstrate the feedback control strategy is effective, the formed shape at each step is compared with the one formed in

uncontrolled ISF (fixed Δu_z) and the target one via cross-sectional profile comparison. Specifically, dimensional errors of the whole shape in both ISF with and without control are analysed by using contour graphs. In addition, history of the average depth at the bottom and its error along the steps are compared to provide the evolution of the control action and its effectiveness.

The test shapes for the two case studies were a truncated cone and a truncated pyramid, with the wall angles as 50° and the designed depth as 30mm. The initial step depth value was set as 2mm in the uncontrolled process. The sheet blank was clamped between a blank holder and a steel backing plate. The backing plate can provide a rigid support for the undeformed areas of the blank. This helps to reduce geometric inaccuracies caused by the sheet bending effect. The metal blank, with 1.6 mm in thickness and 300 mm × 300 mm in size, is made of aluminium (AA 7075-O). A 30 mm diameter cylindrical steel tool with a hemispherical end was used to deform the blank. The feed rate in the forming process was set as 4000 mm/min. Lubricant (oil-Shell Tellus Oil 68) was used.

4.2.1 Case study 1: Truncated Cone

The test shape in **Case study 1** is a truncated cone. The results are shown in the figures from Figure 4-5 to Figure 4-9. In the first two steps of the forming process, dramatic springback was observed when the tool is released due to a large proportion of elastic deformation in the early forming stage. The formed shape is nearly flat and the formed depth is much shallower than the target depth by over 2mm. This makes it difficult to capture the shape features for the comparison work. The first three steps are formed in an uncontrolled fashion. Then, closed-loop control is conducted from the end of the third step after measuring the formed shape at this step.

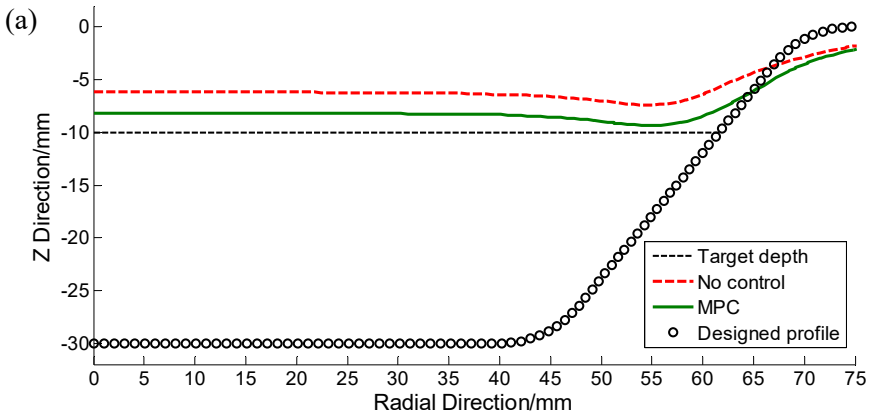

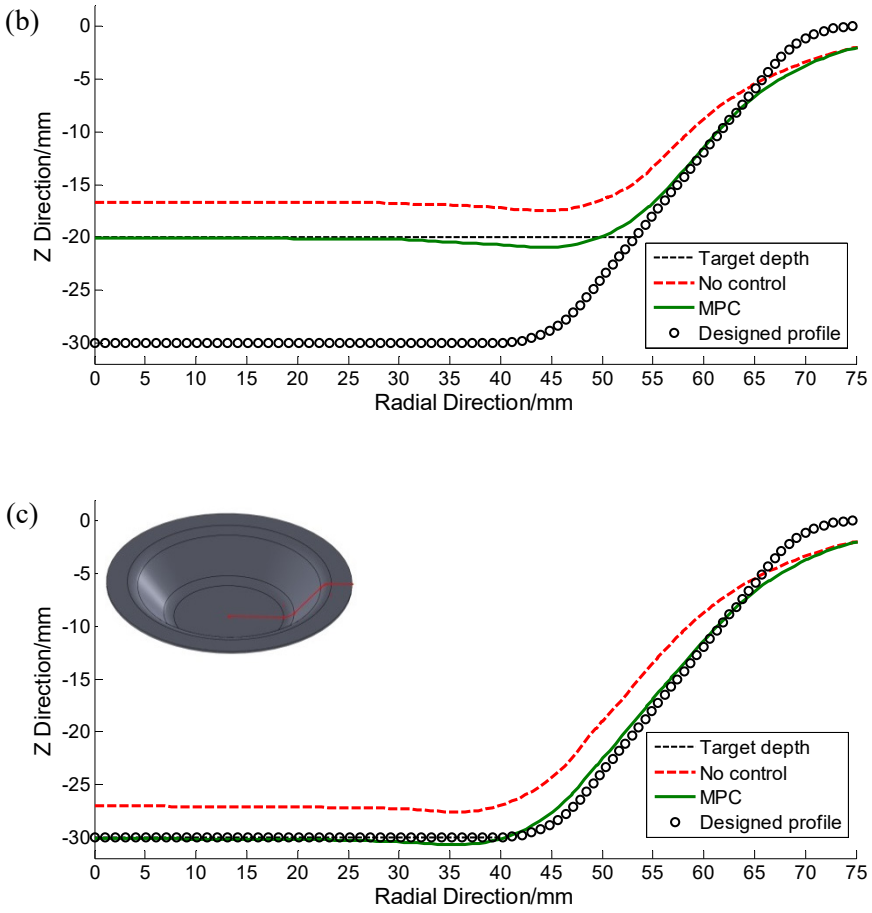

Figure 4-5 Cross-sectional comparison at three steps: (a) Step 5; (b) Step 10; (c) Final Step.

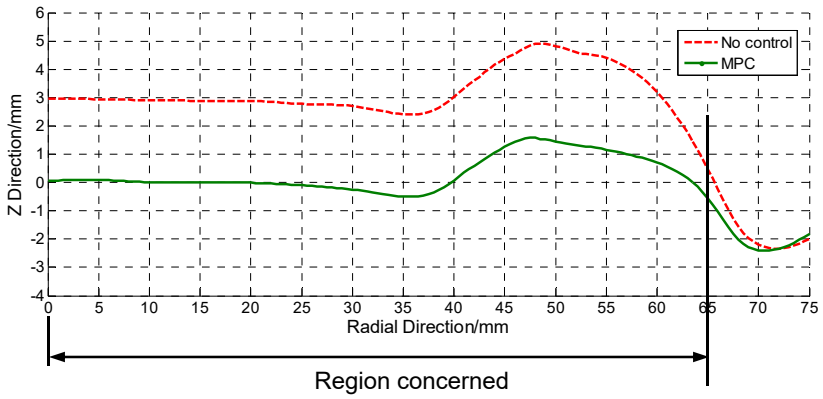

Figure 4-6 Error distribution of truncated cone finally formed.

In Figure 4-5, formed shapes in ISF with MPC control and without control are compared together with the designed shape by using cross-sectional profiles at three different steps. For the validation of the developed MPC feedback control strategy, the number of steps is set as 15. In this work, we only present the profile comparison at the 5th, 10th and final steps that represent the early stage, the middle and the end of the control process, respectively. Figure 4-5(a) shows that in the early stage of the MPC control process, the errors between the formed profile and the target profile are reduced but

still need to be improved. This is also shown in Figure 4-7, which illustrates the values of the average depth at the bottom and the corresponding errors along the steps. Figure 4-5(b) and (c) illustrate that the dimensional accuracy has been improved compared with that in uncontrolled ISF. The error distributions of the final profiles are shown in Figure 4-6. The final formed shape and the designed one are well-matched in the region concerned (the bottom area and the wall area). The geometric errors at the bottom have been greatly reduced from ±3 mm to ±0.25 mm while the geometric errors in the wall areas have been reduced but are still relatively large. The geometric errors in the region near the clamped edges (Figure 4-5 and Figure 4-6) are caused by the bending effect. This type of geometric errors can be greatly reduced in DSIF with a flexible supporting tool [19, 23] or by using a proper backing plate underneath the metal blank in SPIF. In this study, a steel backing plate was used to reduce the bending effect. Nevertheless, the bending effect is still difficult to control in SPIF [100]. The work of this thesis mainly deals with the in-process correction of the springback, which accounts for the majority of SPIF defects, for geometric accuracy improvement in ISF. The accuracy in the area affected by the bending effect will not be fully studied in this work.

To provide an overview of the effectiveness of the developed feedback control strategy, the average depth of the part bottom, is analysed along the steps, as shown in Figure 4-7. More specifically, the average depth is the average of the formed depth of points at the bottom plane.

Step depth, is optimised from the third forming step to the end. From step 3 to step 7, the formed depth is getting closer to the target one at each step. From then on, the error between the formed depth and the designed one is greatly reduced (within ±0.2mm). Optimised inputs at different steps are varying while the inputs are set as constant at 2mm in uncontrolled ISF, as illustrated in Figure 4-8.

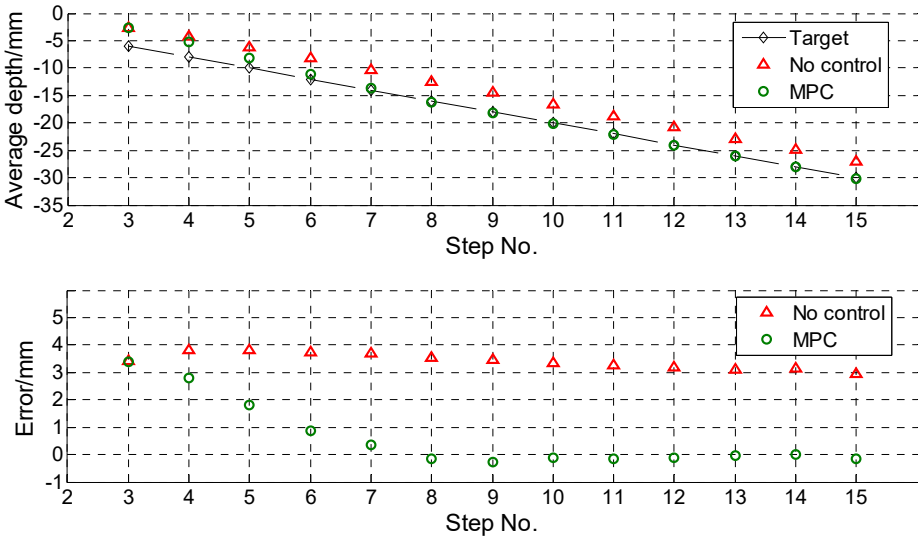

Figure 4-7 History of average depth of the part bottom and its error along the steps.

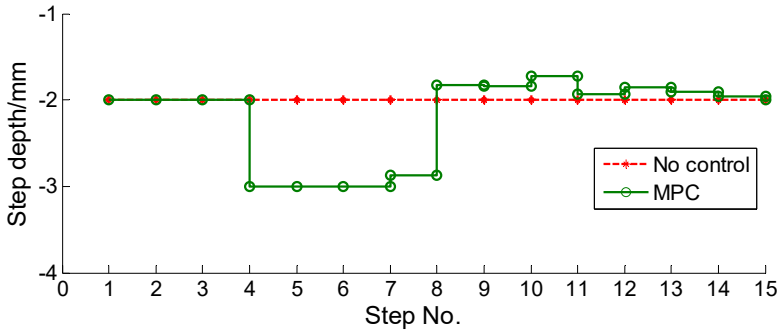

Figure 4-8 Inputs along the steps.

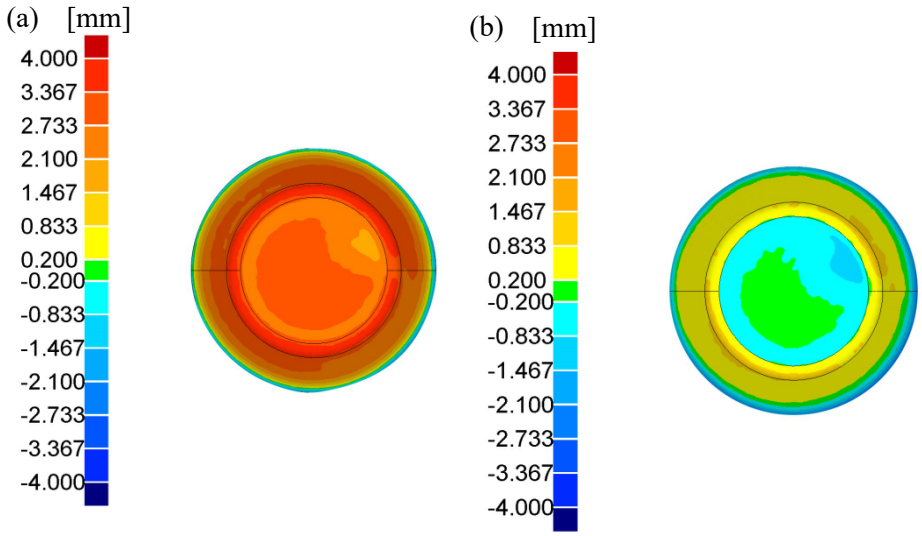

Figure 4-9 Top view of accuracy colour plots: (a) Formed cone in uncontrolled ISF; (b) Formed cone in ISF with MPC control.

To examine the global geometric accuracy, parts formed in both uncontrolled and controlled ISF are compared with the nominal model through colour contour plots. The scanned point cluster can be directly compared with the CAD file in 3D comparison module of Geomagic Qualify. Figure 4-9 shows the global dimensional accuracy in the normal direction in these two processes. Results in the figures indicate that the geometric deviations in ISF with MPC control has been significantly reduced compared to uncontrolled ISF. More specifically, the geometric error in the bottom area has been reduced from ±3.0mm to ±0.25mm. Improved geometric accuracy also has been observed in the wall area but does not reach the accuracy level of the bottom area. This lack of improvement is due to horizontal increment values being kept the same as those used in the uncontrolled ISF process and only the step depth values are optimised during the forming process with control.

Figure 4-5 and Figure 4-9 also show that changes of step depth values have direct influence on the deformation of the wall area. In a single step with the horizontal increment set as unchanged, the wall

area will be stretched down further by the tool as current step depth increases, and vice versa. Similarly, the wall area of formed shape can be driven closer to the target one through adjusting the horizontal increment values. The geometric accuracy of the wall area could be further improved by optimising the horizontal increment and step depth at the same time.

4.2.2 Case study 2: Truncated pyramid

The results for the truncated pyramid are shown in Figure 4-10 to Figure 4-17. Like Case study 1, the control actions were also conducted after measuring the formed part at the third step. The cross-sectional comparison of formed profiles at three steps is shown in Figure 4-10. Figure 4-10(a) illustrates that geometric errors are reduced in the early stage of the feedback control process but are still relatively large. This is also shown in Figure 4-12 that shows the history of the average depth and its error during the ISF processes. Figure 4-10(b) and (c) represent the stable stages of the control process. Figure 4-11 shows corresponding error distributions of the final profiles in Figure 4-10(c). The dimensional accuracy has been greatly enhanced compared with that in uncontrolled ISF. The final formed shape and the designed one are well-matched at the bottom.

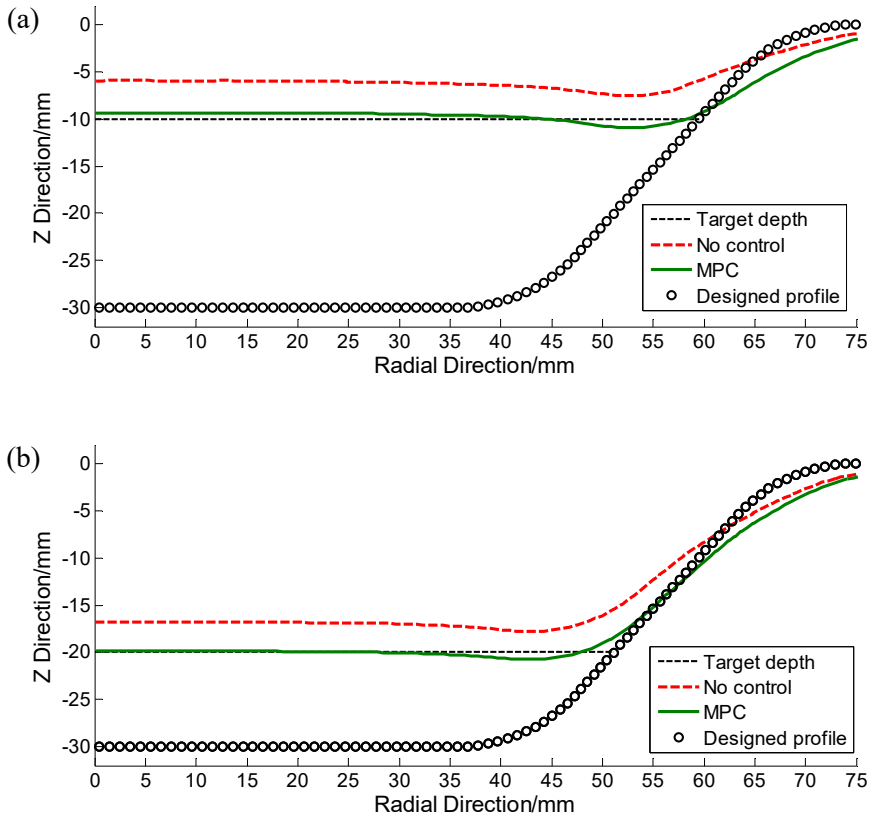

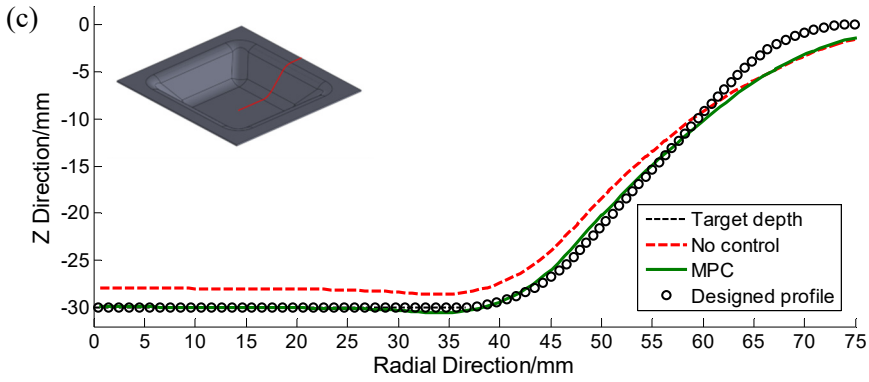

Figure 4-10 Cross-sectional comparisons at three steps: (a) Step 5; (b) Step 10; (c) Final Step.

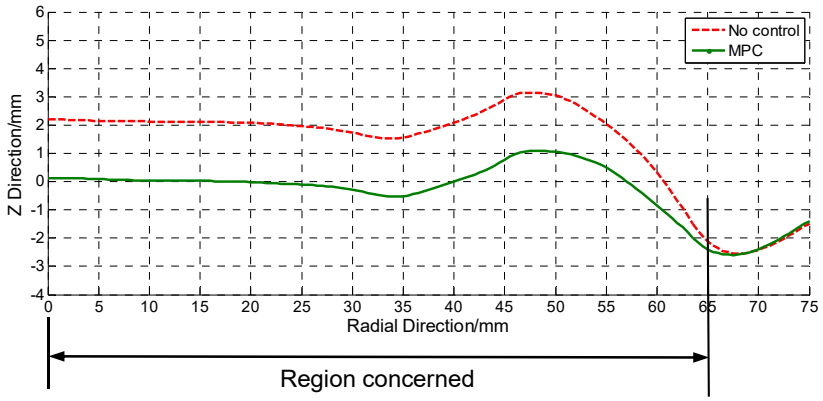

Figure 4-11 Error distribution of truncated pyramid finally formed.

Figure 4-12 illustrates the average depth of the bottom along the steps. This demonstrates the effectiveness of developed feedback control strategy. The input, namely step depth, is optimised from the third step to the end. From step 3 to step 7, the formed depth is getting closer to the target one at each step. From then on, the error between the formed depth and the designed one is greatly reduced (within ±0.2mm). Optimised inputs at different steps are varying while the inputs are set as constant at 2mm in uncontrolled ISF, as illustrated in Figure 4-13.

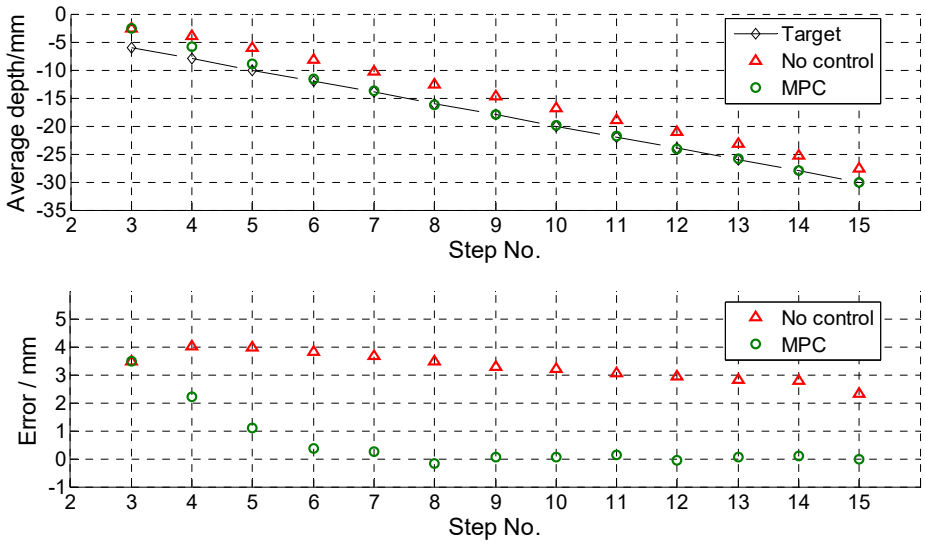

Figure 4-12 History of average depth of the part bottom and its error along the steps.

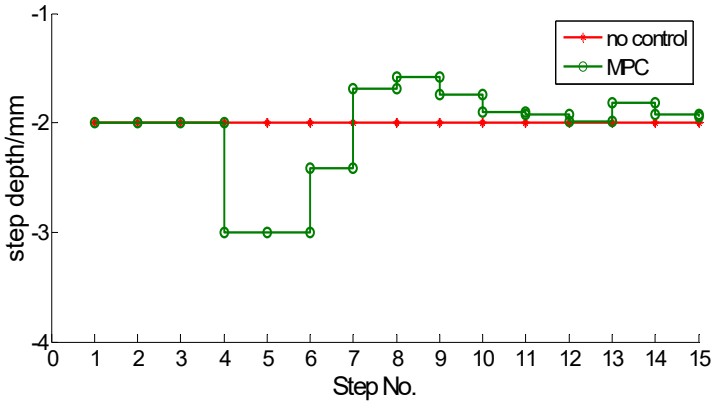

Figure 4-13 Inputs along the steps.

In Figure 4-14, the global geometric accuracy of the formed pyramid is evaluated by comparing parts formed in both uncontrolled and controlled ISF with the designed one. The colour contour plots show the distribution of geometric deviations. The geometric accuracy in the bottom area has been significantly improved via feedback control of ISF. The accuracy level at the bottom can reach ±0.3 mm compared with that in uncontrolled ISF (±3.0mm) while the geometric errors in the wall areas have been reduced but are still relatively large. As discussed in **Section 4.2.1**, the accuracy in the area affected by the bending effect near clamped edges will not be fully studied in this work due to fact the bending effect is still difficult to control in SPIF after using a steel backing plate underneath the metal blank.

The MPC control strategy can also help to reduce the geometric errors in the wall areas excluding the four corners from ±3.0mm to ±1.0mm. That is, the wall area of the part obtained in controlled ISF is less accurate than its bottom area. This is due to the fact that only the step depth is optimised during

the forming process with control. Larger geometric errors can be observed in the four corners of the formed pyramid in Figure 4-14(a). These errors are reduced in controlled ISF but still are relatively large, as shown in Figure 4-14(b). Further improvement of the inaccuracy in the wall area will be investigated in the subsequent sections in which the horizontal increment will be optimised. As for the nonaxisymmetric shapes, some key features, such as the corners of the truncated pyramid, will be taken into consideration in the module of horizontal increment optimisation.

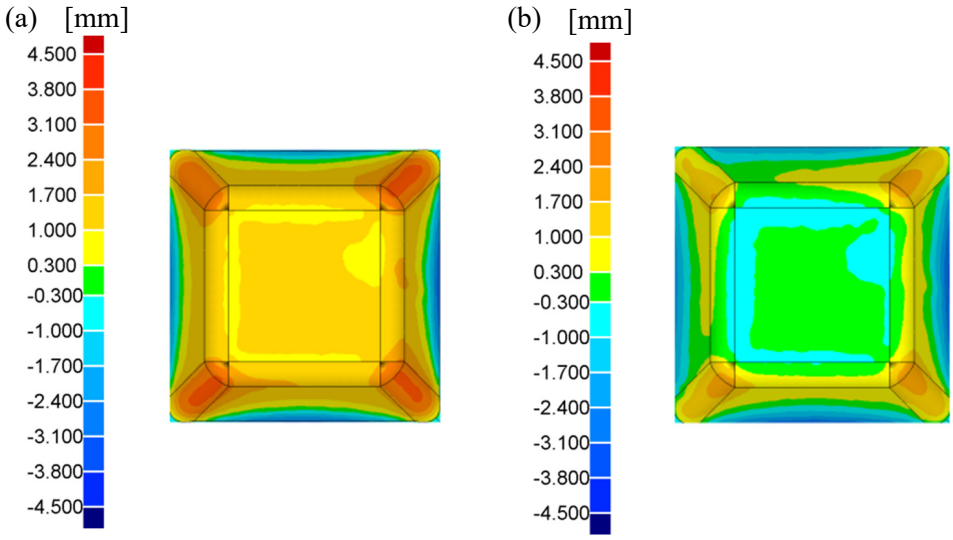

Figure 4-14 Top view of accuracy colour plots: (a) uncontrolled ISF; (b) ISF with MPC control.

Overall, these indicate that the average geometric deviation in ISF with MPC control has been greatly reduced in comparison with that in uncontrolled ISF. The formed cone and pyramid in ISF with feedback control are shown in Figure 4-15 (a) and (b), respectively.

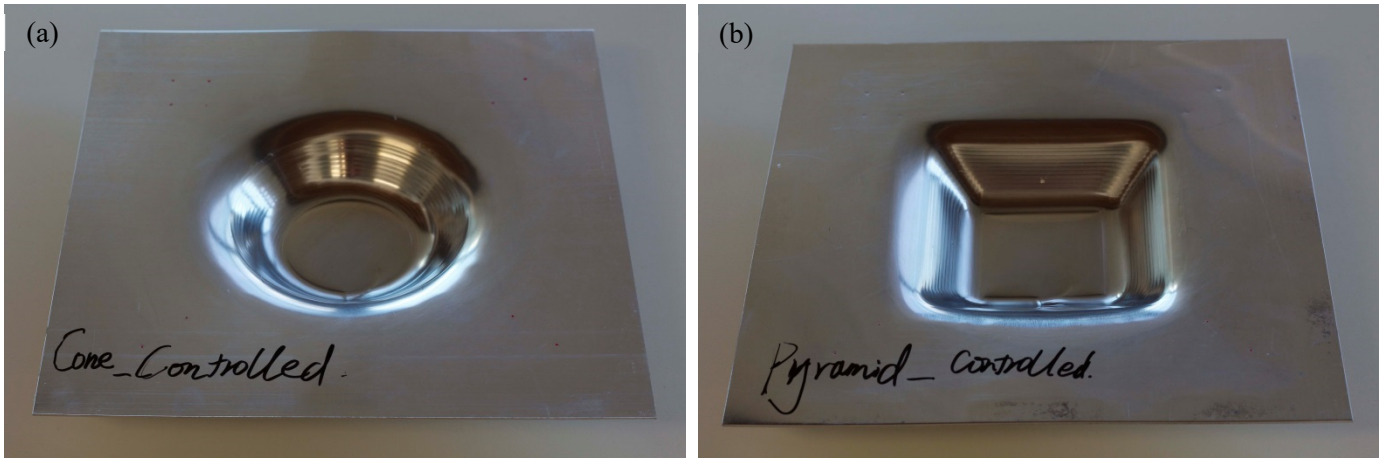

Figure 4-15 Formed parts in ISF with feedback control.

4.3 Results of SPIF toolpath correction using a two-directional MPC algorithm (Objective 2)

To achieve **Objective 2** of this thesis**,** an enhanced MPC control algorithm has been developed and experimentally verified for two-directional toolpath correction in SPIF (**Paper 3**). This section presents the experimental results of this work.

Two case studies was performed to verify the developed control algorithm. In the first case study, the test shape was a truncated pyramid with the wall angles as 50° and the designed depth as 35mm. In the second case study, the test shape was an asymmetric cone, with the designed depth as 35mm and the wall angle varying at different radial directions from the centre. In the SPIF process, a 3 mm thick steel backing plate and clamping blocks were used to clamp the sheet blank. Besides this, the backing plate can also provide a rigid support for the undeformed areas of the blank. This helps to reduce geometric inaccuracies caused by the sheet bending effect. The test material is aluminium (AA 7075-O). The initial blank is a 300 mm × 300 mm square and the thickness is 1.6 mm. A ball-ended tool with a 30 mm diameter was used in the experiments. The feed rate in the forming process was set as 4000 mm/min. Lubricating oil was used for lubrication during the forming process.

4.3.1 Justification of the predictive model

To model the forming process for MPC control, simplifications were made to predict the formed vertical profiles during the control process. Before analysing the results of MPC control strategies, the simplified model (Figure 3-7) used for vertical profile predictions was experimentally justified in forming the test shape in Case study 1. In the uncontrolled ISF process, the formed shape of each step was measured during the forming process. To verify this model, the predicted profile of the next step was compared with the formed profile of the next step (Figure 4-16a). The predicted profile of the next step was obtained in the predictive model based on the formed profile of the current step. The comparisons from two example steps show that the majority of the predicted profile of the next step matches well with the formed one while the prediction error near the position where the tool touches the blank, namely Zone B in Figure 3-7, is relatively large. However, there are only a few profile points within this region so that it will not significantly affect the optimisation in the control strategy.

Figure 4-16b illustrates how the prediction error changes along the steps in terms of the centre point in Figure 4-16a. The prediction error is defined as the difference between the predicted z-coordinate of the centre point and the formed one at each step. In the first three steps of the forming process, the metal blank is formed without control and the MPC control modules are turned on when the forming of third step is finished, since the formed shape at the early stage is too shallow to accurately capture

the formed features. The control strategy in the vertical direction was applied after the first three steps so that the prediction of the profile begins from the 4th step. The prediction error is relatively large at the early stage of the forming process, which is due to the fact that the springback is relatively large in the first few steps. As the formed depth increases, the prediction error begins to fluctuate in a small range (-0.05~+0.12mm) from about the 10th step. This result illustrates that the prediction error will not accumulate due to the feedback of measured shape state at each step. The prediction errors cannot be ignored, especially in the first few steps, but the influence of the prediction errors can be partially compensated in the MPC optimiser by updating the feedback of the measured shape state and control actions at each step. Therefore, the simplifications in the model can be considered as reasonable for in-process feedback control of ISF in this case.

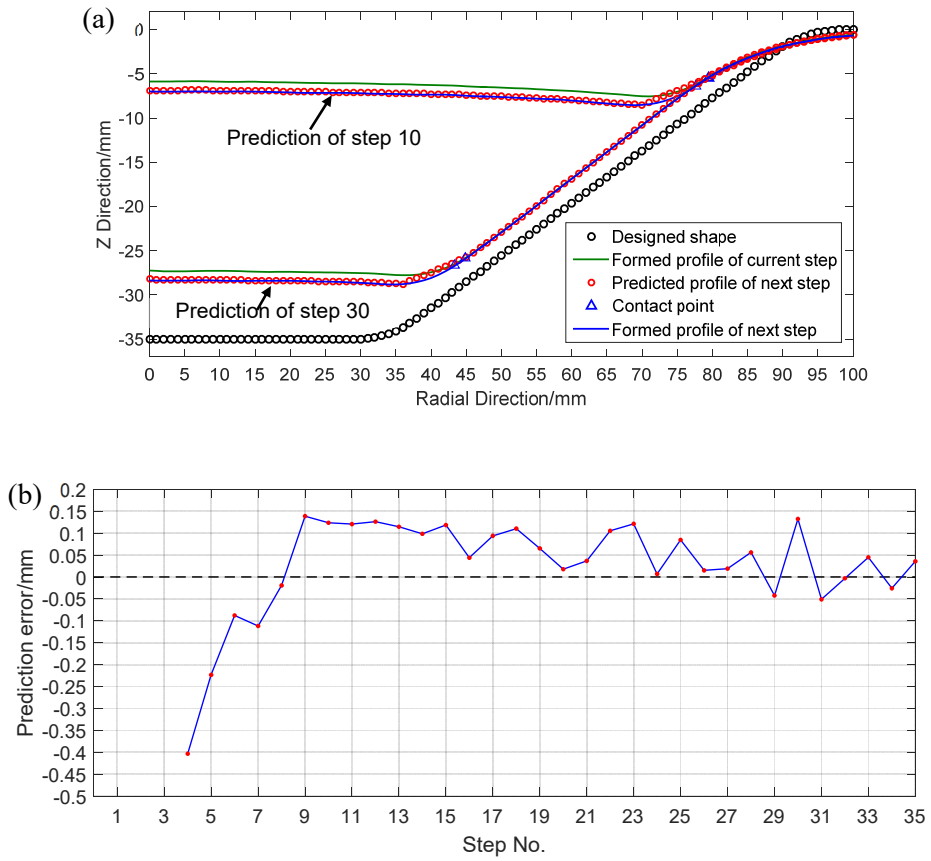

Figure 4-16 Experimental justification of the predictive model in typical ISF (no control):

(a) Comparison of the predicted profile and formed file at two example steps;

(b) Prediction errors at the centre point of the cross-sectional profile at different steps.

4.3.2 Case study 1

To verify the developed control algorithm, the test shape is formed in four tests using different strategies (Table 5). Control strategy MPC-0 is the one reported in our previous work [71] and in

Section 4.2. It only deals with the optimisation of Δu_z. In the two-directional MPC strategy, two parameters will be optimised at the same time. To determine Δu_h at each step, strategy MPC-1 uses a simplified model with uniform horizontal springback while an enhanced model with interpolated horizontal springback is used in strategy MPC-2. In the experimental verification of the MPC strategy, the cross-sectional profile through the centre axis and two corners is chosen as the shape state for feedback control. The profile provides the vertical states of all the points for vertical optimisation. Control actions are conducted after the measured state and the target state are compared and computed in the MPC optimisers.

Table 5 Different strategies

Strategies	Δu_z	Δu_h
No control (typical ISF)	from CAM (1mm)	from CAM
MPC-0 (previous work [71])	MPC-vertical	from CAM
MPC-1	MPC-vertical	MPC-horizontal (uniform horizontal springback)
MPC-2	MPC-vertical	MPC-horizontal (interpolated horizontal springback)

After experimental justification of the predictive model, the results obtained from the four strategies are analysed and compared in several aspects. Figure 4-17a shows the comparison of profiles from cross-sections through the corners and the corresponding error distributions. The deviations in z direction are regarded as the geometric errors. The results show that errors formed from the uncontrolled ISF process are quite large and those in the wall area reach about 3mm. In Strategy MPC-0, errors at the bottom are greatly reduced to ± 0.3 mm while those on the wall are also reduced, compared with those in uncontrolled ISF, and are still relatively large (± 1 mm). With the addition of the horizontal MPC module, significant accuracy improvement (within ± 0.3 mm) is achieved in both the bottom and wall areas in MPC-1 and MPC-2. As discussed in **Section 4.2.1**, a steel backing plate was used to reduce the bending effect in this study but the bending effect is still difficult to control in SPIF [100]. The errors in the sheet bending region (Figure 4-17 and Figure 4-18) are caused by the bending effect and will not be fully studied in this work.

However, in MPC-1, the model with an assumption of uniform horizontal springback fails to obtain high-level accuracy on the wall in terms of the cross-section through the centre and the middle of the wall. Figure 4-18a and b show that the accuracy of the wall area gets worse in MPC-1 compared with MPC-0. In MPC-1, each contour was horizontally enlarged in a constant scale based on the horizontal error of cross-sectional profile through the corners. This leads to too much deformation on the planar

walls of the pyramid shape because the horizontal springback values on the planar walls are less than those at the curved corners where there are larger residual stresses. Using an enhanced model that better accounts for the spatial variance of horizontal springback, MPC-2 helps to address the issue in MPC-1 and greatly reduces the error on the planar walls, as shown in Figure 4-18b. In all three controlled processes, accuracy at the bottom have been improved to the range of ± 0.3 mm. Figure 4-19a illustrates the vertical inputs along all the steps and Figure 4-19b and Figure 4-19c show how the horizontal input differs from the initial one at each step at the radial directions through the corner and the wall middle, respectively.

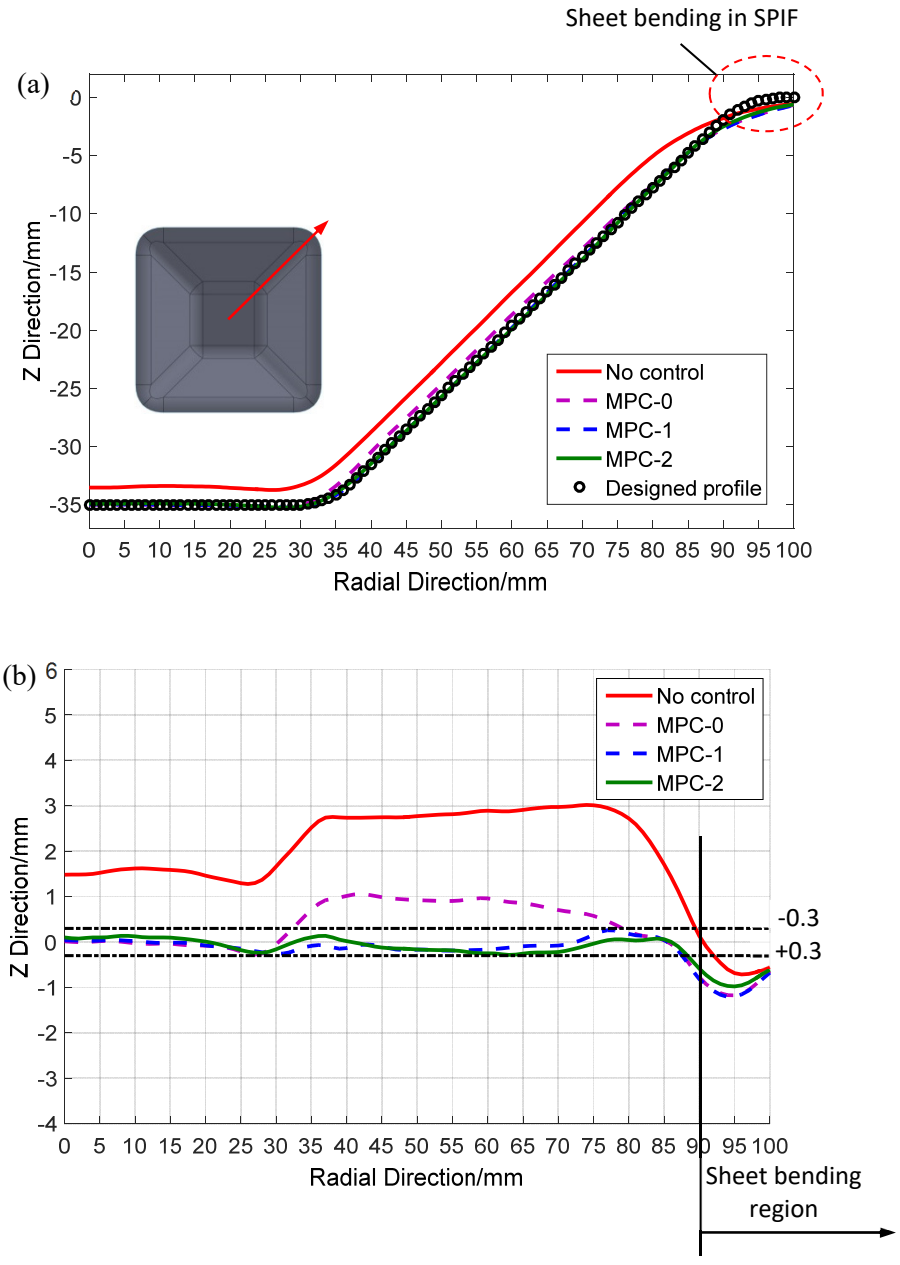

Figure 4-17 : (a) Cross-sectional profiles through the corners; (b) Corresponding error distribution.

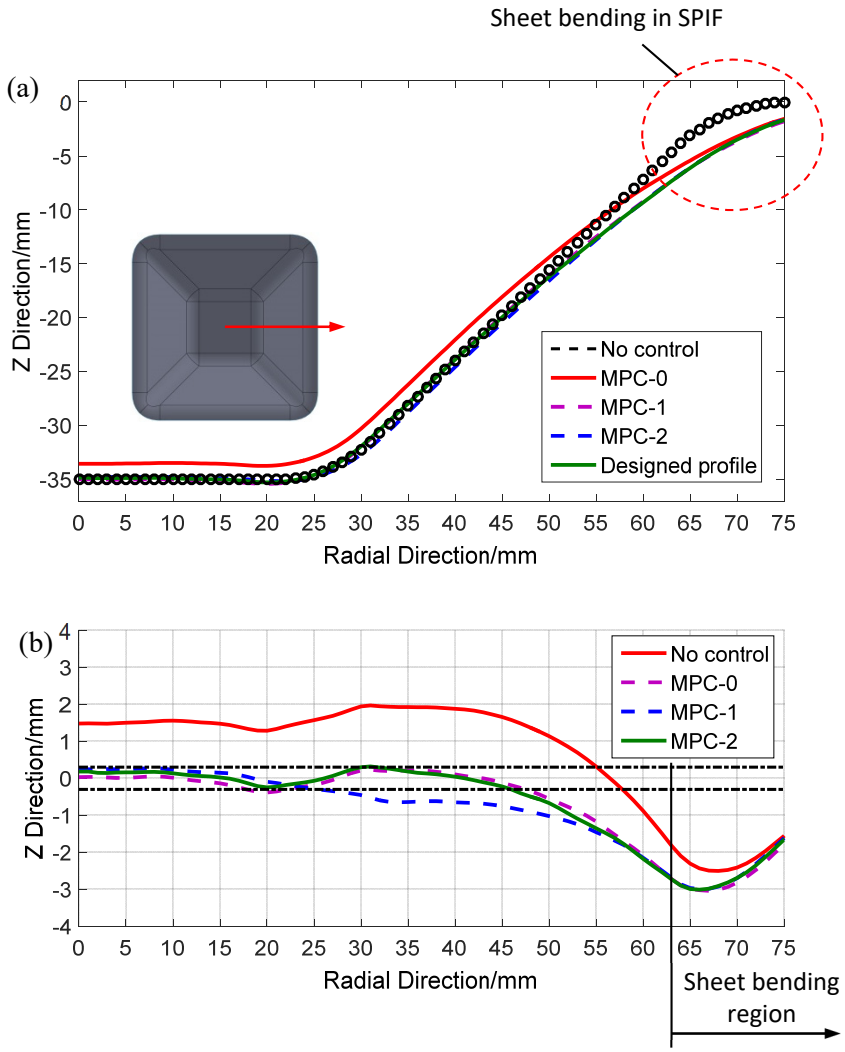

Figure 4-18: (a) Cross-sectional profiles through the middle of walls; (b) Corresponding error distribution.

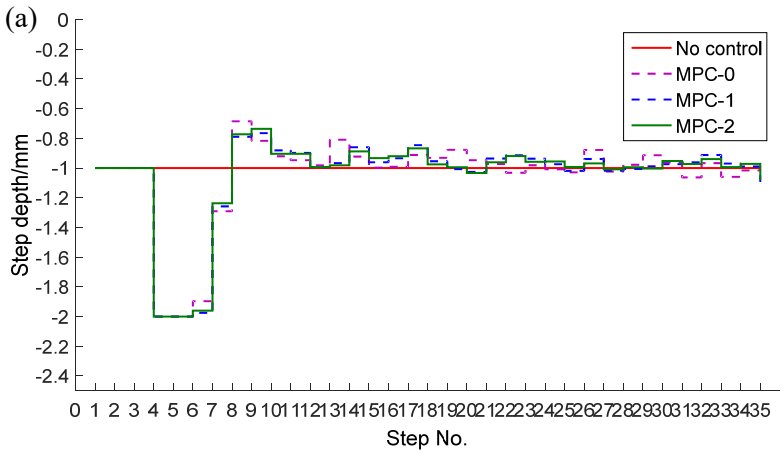

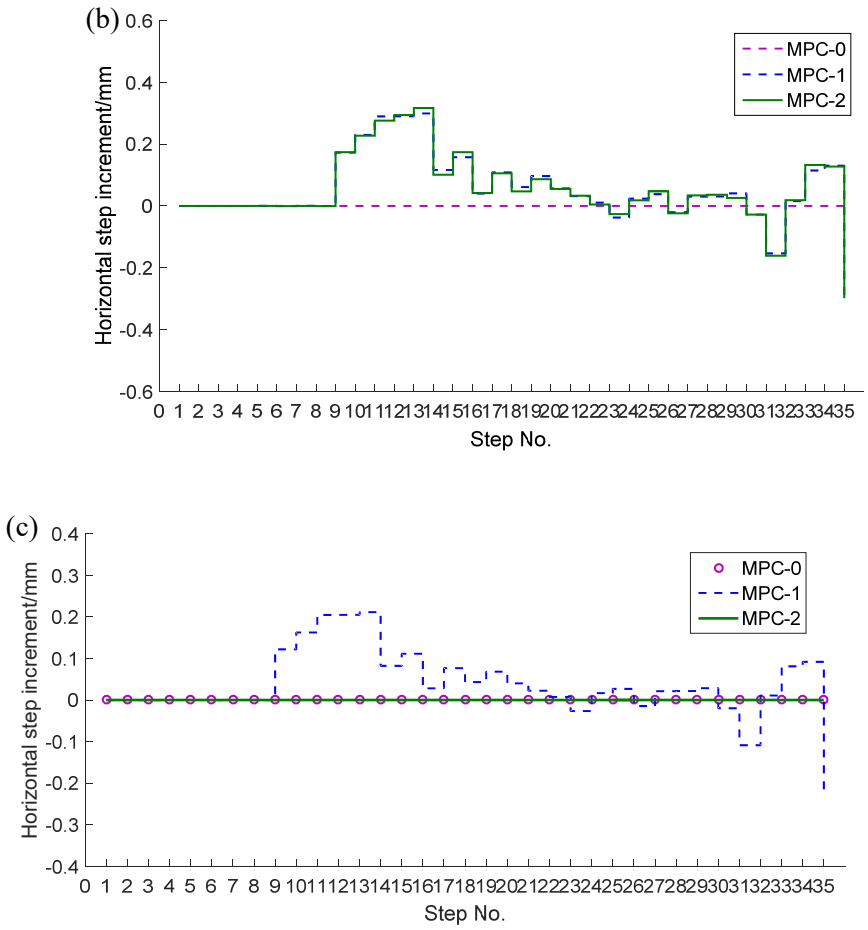

Figure 4-19 Inputs along the steps: (a) Step depth;

(b) Horizontal step increment through the corner (deviations from initial inputs);

(c) Horizontal step increment through the wall middle (deviations from initial inputs).

To fully evaluate the geometric accuracy from different strategies, error maps of the formed parts, in the clamped condition, are presented in Figure 4-20. The scanned shape and the CAD file are compared in the 3D comparison module of Geomagic Qualify. In additional to these maps, horizontal sections were made through a horizontal plane with the depth of 25mm to quantify the horizontal error distribution more clearly. Horizontal cross-sectional profiles along a section trajectory (from A to B in Figure 4-20 b, c, and d) and the corresponding error distributions are compared in terms of strategy MPC-0, strategy MPC-1, and strategy MPC-2, as shown in Figure 4-21.

Compared with uncontrolled ISF with no toolpath control (Figure 4-20a), large accuracy improvements have been observed at the bottom area and part of wall areas in strategy MPC-0 while errors around the corners have been reduced to some extent and still need to be further reduced (Figure 4-20b). Figure 4-21 shows that most of the wall areas have high accuracy (+0.3mm) but errors around the corners have reached the level of +1.5mm.

In strategy MPC-1, a horizontal optimisation module was added to improve the poor accuracy in the horizontal direction. Figure 4-20c shows that errors around corners are significantly lessened and the accuracy at the bottom area remains similar to MPC-0. This indicates that the horizontal module in strategy MPC-1 helps to increase the geometric accuracy around the corners and it does not have significant influence on the vertical optimisation. This means the varying of Δu_h in a range at one step does not substantially influence the formed depth of bottom areas. Figure 4-21 shows that a new problem occurred associated with MPC-1. The errors of main wall areas have increased to a higher level (-1.0 mm) from strategy MPC-0 as these areas were over-deformed beyond the walls of the part design. Figure 4-21 also shows that the horizontal errors are not uniformly distributed along the section trajectory at a certain z-level, which demonstrates that the springback is not uniformly distributed in the horizontal direction.

With the use of strategy MPC-2, the bottom area and most parts of the wall areas have high accuracy ($\pm$0.3 mm) while a small part of the wall areas near the corner is less accurate but still has improved accuracy ($\pm$0.5 mm), as illustrated in Figure 4-20d and Figure 4-21. This can be due to the fact that the estimation of the distribution of springback effect along the horizontal profile is not perfect. This limitation might be solved when more sample points on the horizontal profile are considered for the estimation of horizontal errors in various radial directions. Overall, these show that strategy MPC-2 with an interpolated springback model can give better evaluation of the horizontal springback distribution than MPC-1 with a uniform springback model. Compared with uncontrolled ISF and the previous work described in **Section 4.2**, the dimensional accuracy of the formed part has been greatly improved in the concerned areas.

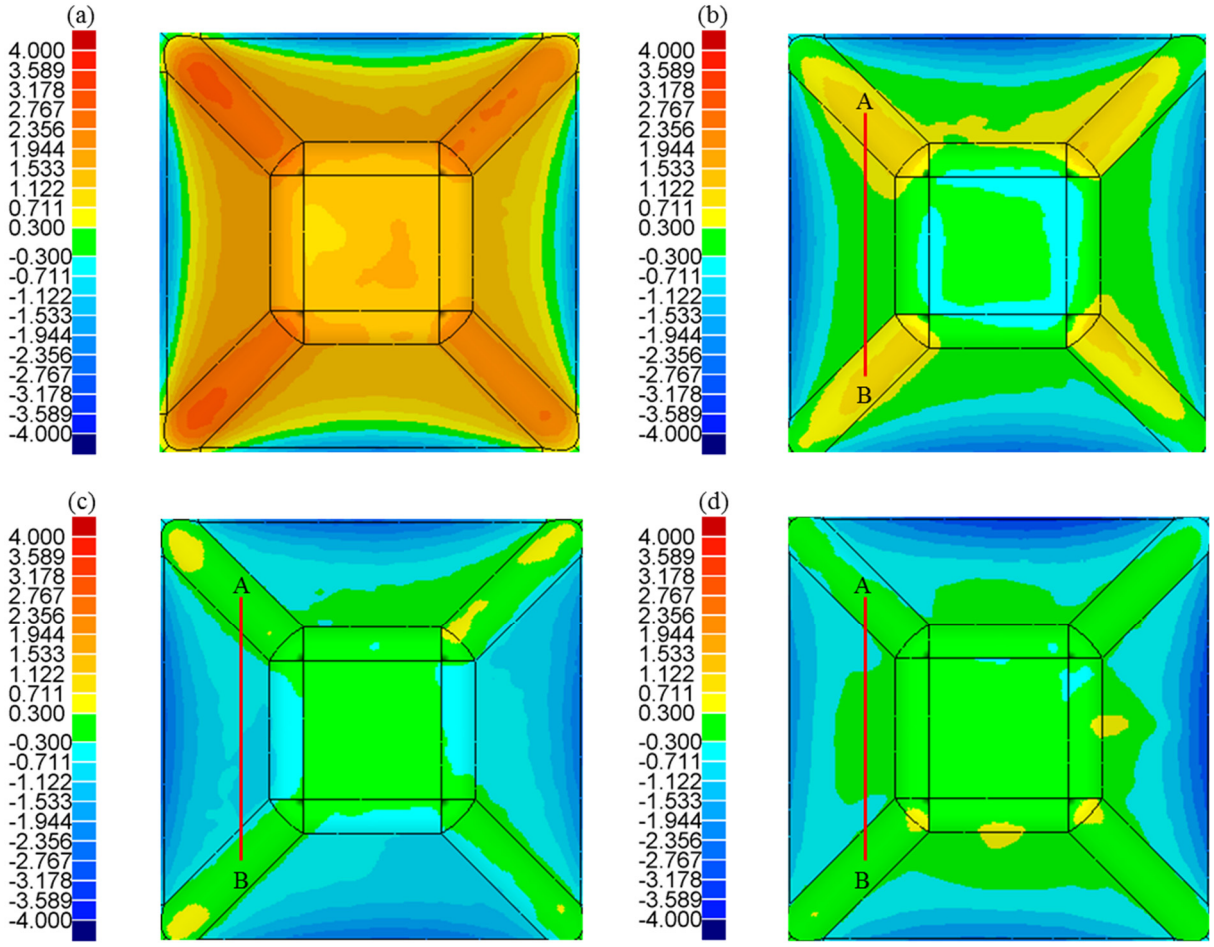

Figure 4-20 Geometric error maps of the formed parts: (a) No control; (b) MPC-0; (c) MPC-1; (d) MPC-2.

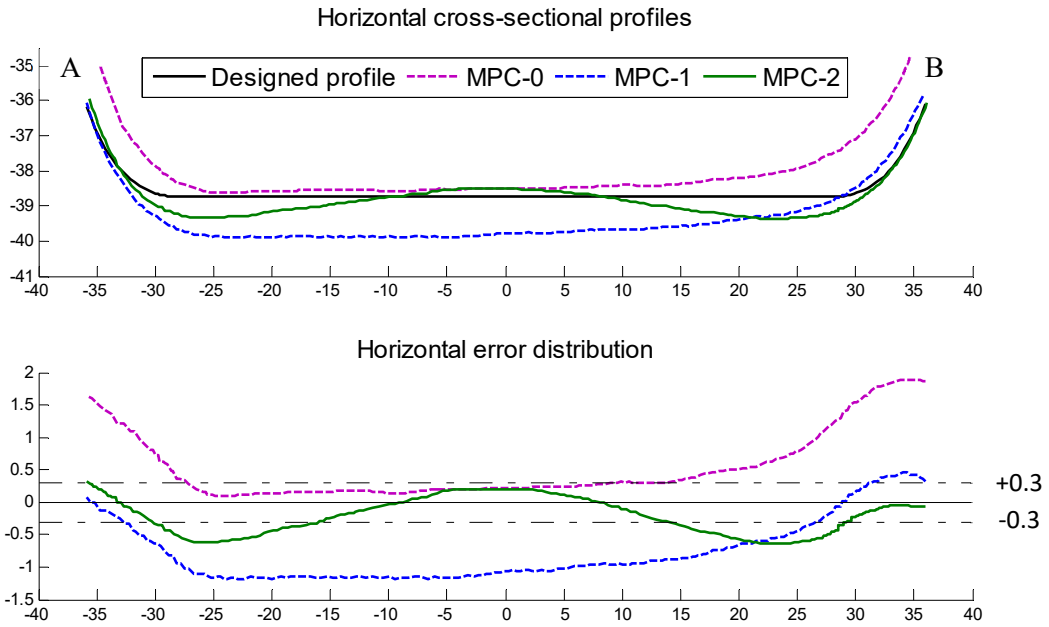

Figure 4-21 Comparison of horizontal cross-sectional profiles and the corresponding error distributions.

4.3.3 Case study 2

The developed MPC control algorithm was applied to form an asymmetric cone to demonstrate the applicability of the developed control strategy to asymmetric shapes. More specifically, strategy MPC-2 using the model with interpolated horizontal springback was used in this case study. To compare uncontrolled ISF and controlled ISF, the geometric accuracy of formed shapes in the unclamped condition were analysed in terms of the geometric error maps. At the same time, the influence of the release of clamping plates on the formed shapes was analysed.

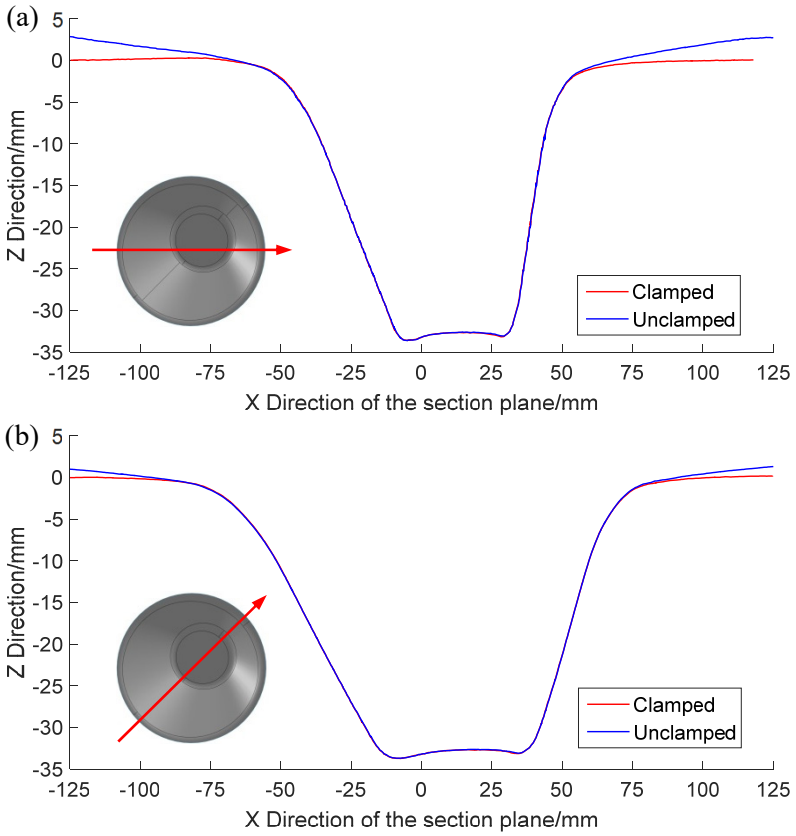

Figure 4-22 Comparison of the formed shapes in clamped and unclamped conditions: (a) Section through plane XOZ ($\theta = 0°$); (b) Section through the radial direction $\theta = 45°$.

Figure 4-22 shows that there is large springback at the clamped edges of the metal blank after the removal of clamping plates, which is caused by the residual stress around the clamped areas. In contrast, the release of clamping plates nearly has no influence on the concerned region of the formed part. These results indicate that the formed region should not be too close to the clamped edges when choosing the size of the metal blank for part fabrication.

The error distributions of the whole parts are shown in Figure 4-23. In the base and most wall areas of the formed part, the geometric accuracy is greatly improved from ±3 mm to ±0.3 mm (a 90% decrease) with the use of the MPC control strategy.

In Figure 4-23b, an annulus zone in light blue colour can be observed at the bottom, which is the "pillow effect" that occurs at the flat base of the part formed in SPIF (Figure 2-2). This area is where the tool travels at the final step and it is lower than the centre area of the bottom due to the residual stress. The "pillow effect" can also be observed in Figure 4-22 and Figure 4-23a. This work focused on reducing the geometric errors caused by springback so that the errors caused by "pillow effect" will not be studied here. In the region near the clamped edges, which can be identified in dark blue colour in Figure 4-23, the geometric error level in the controlled forming process is similar to the error level before control and remains to be large. As discussed in **Section 4.2.1**, the errors in this region are caused by the bending effect. A steel backing plate was used to reduce the bending effect in this study but the bending effect is still difficult to control in SPIF [100]. The bending effect will not be fully studied in this work.

In some very small areas of the wall, the geometric errors have been reduced but remain slightly larger than the desirable level. These can be due to fact that current model with interpolated horizontal springback does not fully capture how the horizontal springback is actually distributed along the horizontal profiles. Nevertheless, the developed two-directional control algorithm leads to an order of magnitude overall improvement in geometric accuracy compared to ISF without toolpath control.

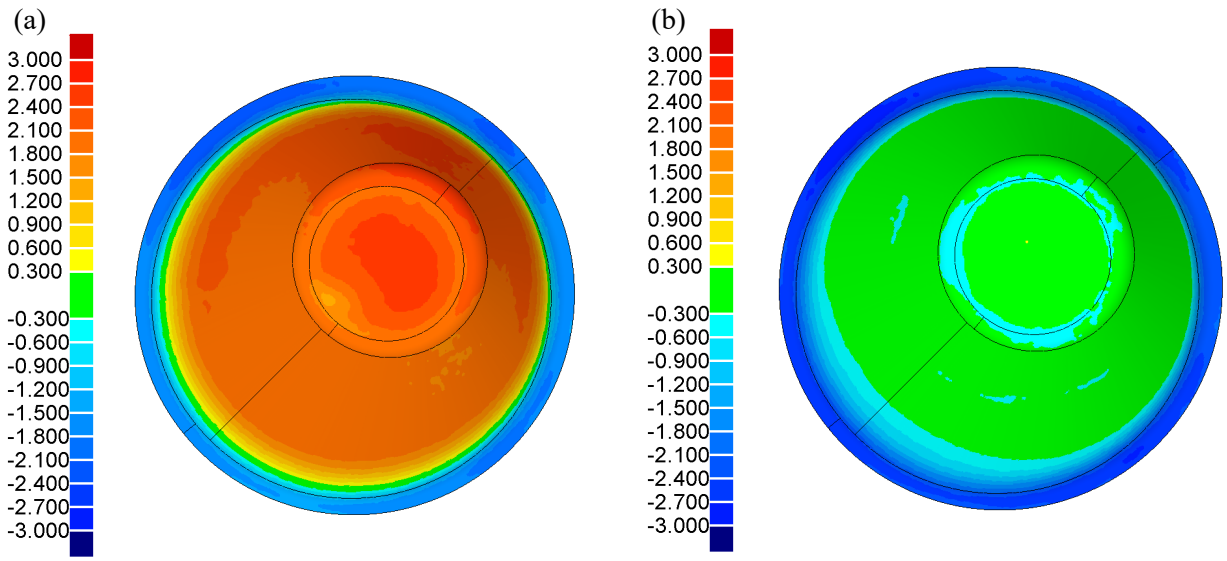

Figure 4-23 Comparison of the formed parts in terms of the geometric error map: (a) No control; (b) Control strategy MPC-2.

In the toolpath control/correction work for SPIF presented by Wang et al. [68], the geometric errors in the major areas were reduced from ±1.2 mm to ±0.3 mm, with a 75% decrease, in the experimental test for forming a truncated pyramid. However, only the comparisons of cross-sectional profiles obtained from two sectional planes of the formed part were presented in the results while the error distribution map of the whole part, a significant indicator for fully evaluating the accuracy of the whole part, was not reported. Recently, Fiorentino et al. [113] reported the geometric errors in the major areas of the formed part were reduced from ±1.34 mm to ±0.3mm (a 77.61 % decrease) with the use of iterative toolpath correction strategy in SPIF. In comparison, the geometric accuracy in the major part areas was improved from ±3 mm to ±0.3 mm (a 90% decrease) with the use of the two-directional MPC control strategy in SPIF in this work. Overall, this is only a rough comparison due to the fact that the previous studies in the literature and the work in this thesis may use different test shapes, sheet material types, sheet thickness, forming tools, forming machines and etc. Each of these parameters might have influences on the formed geometric accuracy.

4.4 Results of TPIF toolpath correction using an enhanced MPC algorithm (Objective 3)

To achieve **Objective 3** of this thesis**,** an enhanced MPC control algorithm has been developed for TPIF with a partial die to correct the toolpath for geometric accuracy improvement. The developed algorithm has been experimentally verified in a case study for forming a non-axisymmetric shape (**Paper 4**). This section presents the experimental results of this work. In particular, the developed control strategy for TPIF with a partial die was experimentally verified in forming a non-axisymmetric shape. The experiment results from uncontrolled and controlled TPIF processes were compared and analysed in terms of the geometric accuracy.

In the case study, the test shape used for the experiments was a non-axisymmetric shape, which contains both flat and curved walls. The wall angle was 40° and the total depth was 35mm. The initial step depth value was set as 1mm. The metal sheet used for tests was made of aluminium (AA 7075-O) and the raw thickness was 1.6 mm. The unformed blank size was 300 mm × 300 mm. A ball-ended tool with a 20 mm diameter was used in the experiments. The feed rate in the forming process was 4000 mm/min. Lubricating oil was used for lubrication during the forming process.

4.4.1 Case study results

In this section, the results of toolpath correction in TPIF are firstly illustrated by the comparison of initial toolpath and the corrected toolpath. Figure 4-24 shows the contours of the corrected toolpath

and initial toolpath in terms of three sample steps (10th, 20th, and 30th). The initial depth of the contours at the three steps are z = -10, -20, -30mm, respectively, since the initial step depth was set as 1mm. From the comparison in the isometric view and the top view, it can be observed that the toolpath is corrected in the horizontal and vertical directions. This is achieved based on the optimised Δu_z and Δu_h at each step during the forming process.

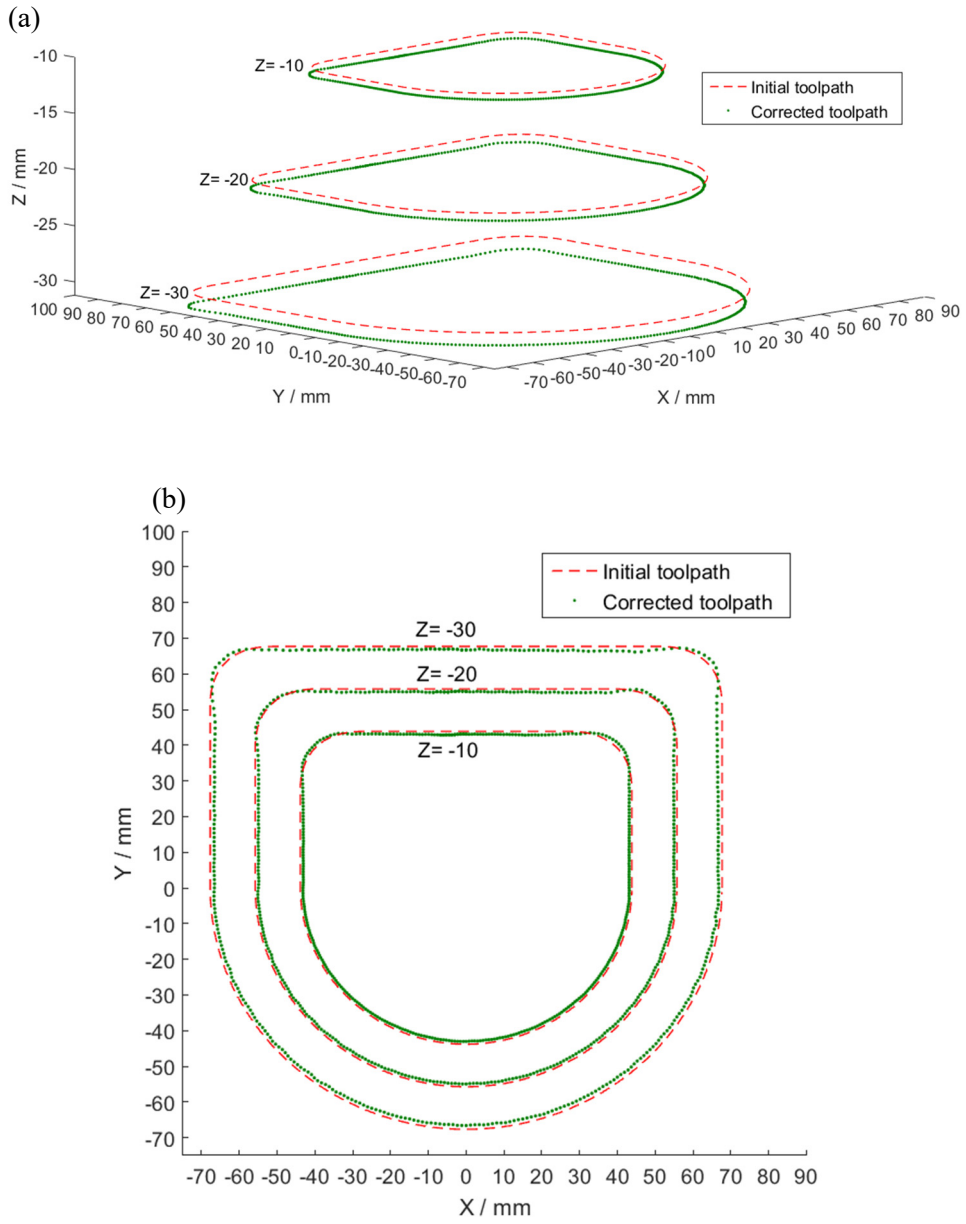

Figure 4-24 Contours of the corrected toolpath and the initial toolpath at three sample steps: (a) Isometric view; (b) Top view.

To analyse the geometric accuracy of uncontrolled and controlled TPIF processes, formed parts in the unclamped condition are compared using horizontal sectional profiles (Figure 4-25) and error

distribution colour maps from the top view (Figure 4-26). The sectional profiles in Figure 4-25 were obtained in the horizontal sections at three *z* levels (*z* = -10, -20, -30mm).

In the TPIF process without toolpath control, the formed part has low geometric accuracy in the wall areas and the errors reach as large as 3 mm near the outside (bottom) edges, as shown in Figure 4-25 and Figure 4-26a. This is mainly caused by the sheet springback. However, from the top view (Figure 4-26), the inside base area (top) supported by the partial die is of high accuracy (±0.3 mm) in both controlled and uncontrolled TPIF processes. Also, there is no notable "pillow effect", which occurs in the flat base of the formed part in SPIF, observed in the base areas in the TPIF processes.

Compared with the part formed in uncontrolled TPIF, the part formed with MPC control has improved accuracy in most areas, as shown in Figure 4-26b. This can also be demonstrated by the comparison of the sectional profiles (Figure 4-25). In particular, there is significant improvement (from ±3 mm to ±0.3 mm) on the geometric accuracy in the wall areas. Nevertheless, the accuracy in certain areas of the corner fillets is still out of the desirable range and is slightly worse than the result from TPIF without toolpath control. In the areas of corner fillets, the local curvature of the shape changes sharply in a relatively small distance since the fillet radius equals the tool radius in the shape design. This could cause sudden changes of the strain when the tool deforms this area. As a result, the springback in the corner fillet areas varies rapidly so that the springback would be more complex and more difficult to capture. The springback of these areas was not well compensated in the current control model, which is the primary limitation of the current work.

Figure 4-27 shows the comparison of deviation distributions (percentage) between TPIF processes with and without control. More specifically, the formed shape was scanned into a large number of scatter points. This figure illustrates how dimensional deviations of all the points are distributed in different deviation ranges in the form of percentage distribution. The percentage of deviations ranging from +0.6 mm to +3.0 mm is greatly reduced from 78% to 8.5% by using the MPC control algorithm. The percentage of deviations in the range ±0.3 mm significantly increases from 19.5% to 70%. Compared with uncontrolled TPIF, the deviations of the points are more intensively distributed near the desirable range in terms of the TPIF with toolpath control.

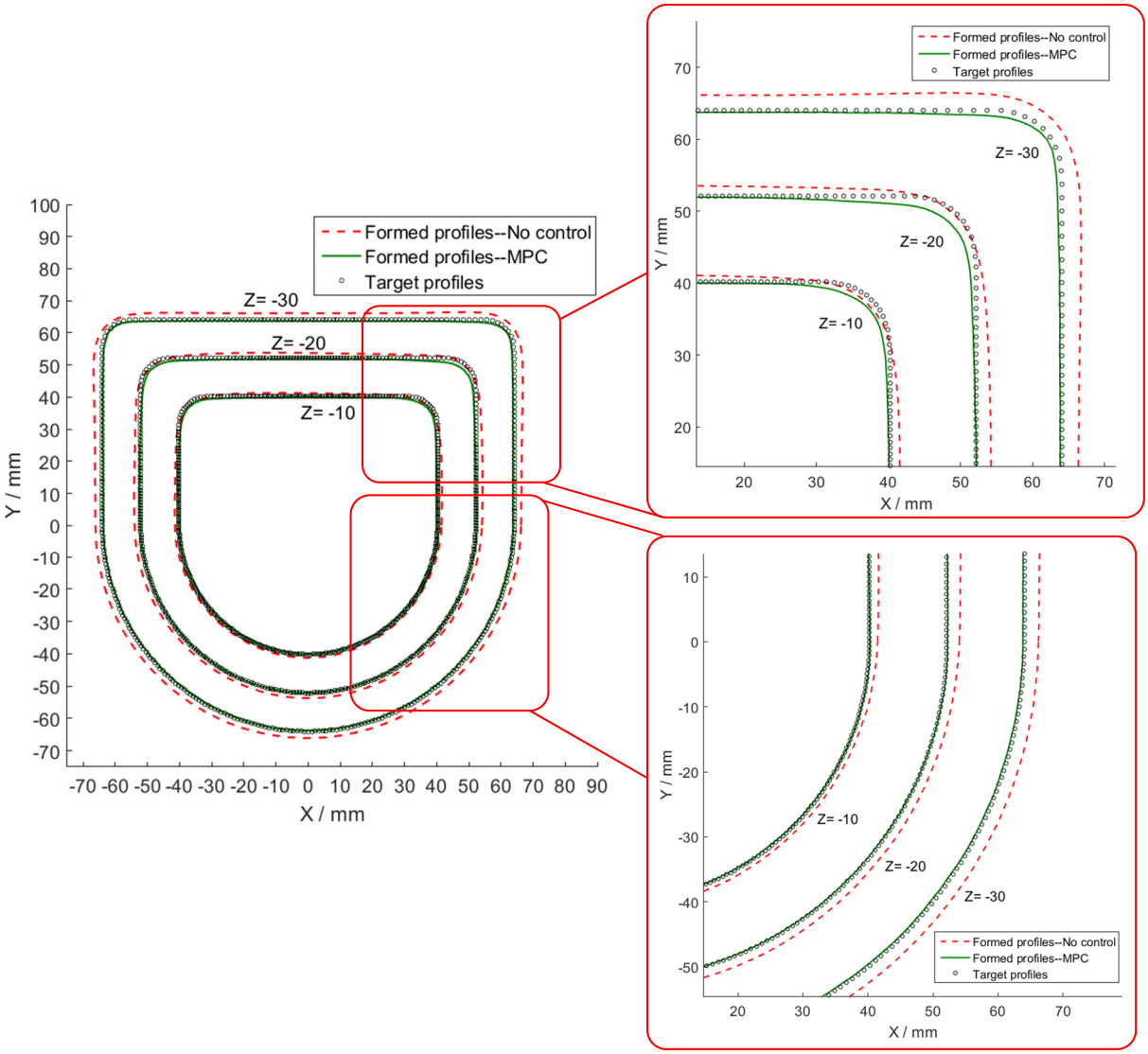

Figure 4-25 Comparison of sectional profiles from three horizontal sections.

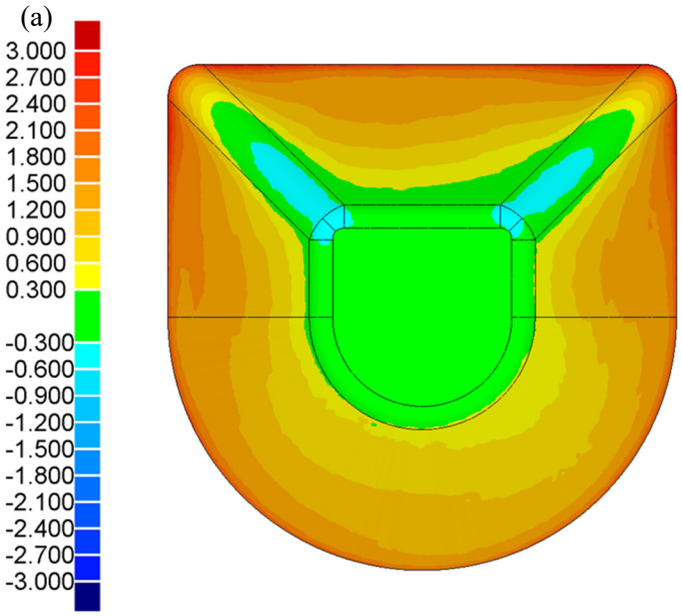

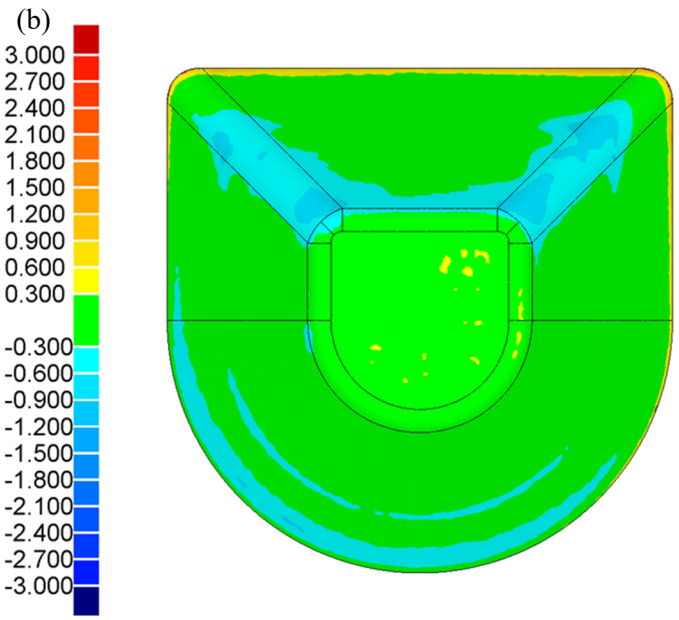

Figure 4-26 Geometric accuracy colour maps: (a) No control; (b) MPC control.

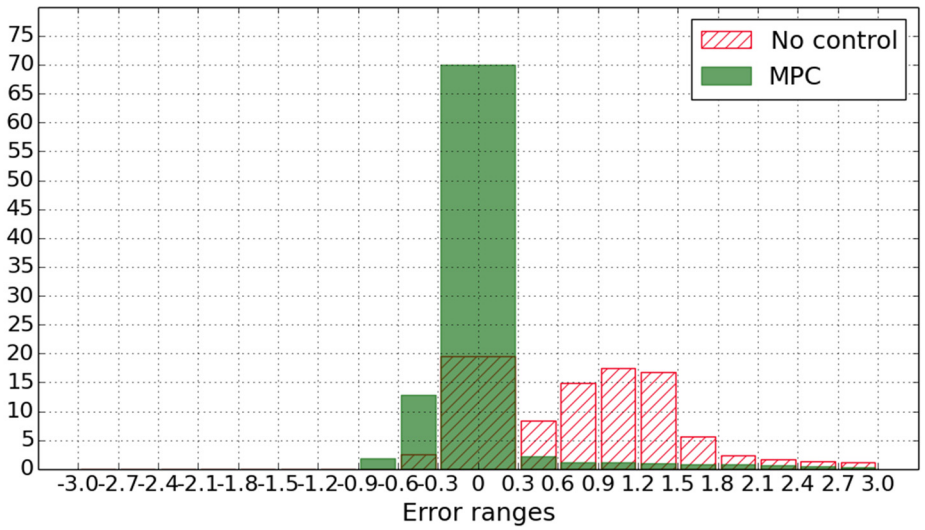

Figure 4-27 Deviation distributions (percentage) of different error ranges in the colour maps.

4.5 Summary of papers

This section summarises all the published papers during the PhD studies.

Paper 1 (*Lu, H. B.*, *Li, Y. L., Liu, Z. B., Liu, S., & Meehan, P. A. (2014). Study on step depth for part accuracy improvement in incremental sheet forming process. Advanced Materials Research, 939, 274-280*): This paper presented a study on step depth, a critical parameter in ISF, for improving the geometric accuracy, surface quality and formability. Two sets of experiments were conducted to investigate the influence of step depth on part quality. Dimensional accuracy, surface morphology and material fracture of deformed parts were compared and analysed. An optimum value of step depth was suggested for forming a truncated cone. The reported work provided significant fundamental information for the development of toolpath control/correction strategies for ISF.

Paper 2 (*Lu, H.*, *Kearney, M., Li, Y., Liu, S., Daniel, W. J., & Meehan, P. A. (2015). Model predictive control of incremental sheet forming for geometric accuracy improvement. The International Journal of Advanced Manufacturing Technology, 82(9-12), 1781-1794*): This paper presented a feedback control strategy using Model Predictive Control (MPC) to obtain improved geometric accuracy in ISF. Based on the incremental deformation mechanism of ISF, a novel model for shape state prediction has been proposed. The step depth of the toolpath was optimised based on shape state feedback during the forming process. Two different cases were studied for experimental validation of the developed control strategy. Comparisons between formed parts in both controlled and uncontrolled ISF processes were implemented in terms of cross-sectional profiles, formed depth at the bottom area and global deviation distribution. Results showed that the geometric accuracy in ISF with feedback control had been greatly improved at the bottom area of the formed parts compared with a standard ISF approach without control. Improved geometric accuracy had been achieved on the wall of the parts as well.

Paper 3 (*Lu, H.*, *Kearney, M, Liu, S., Daniel, W. J., & Meehan, P. A (2016). Two-directional toolpath correction in single point incremental forming using Model predictive control. The International Journal of Advanced Manufacturing Technology, 1-16*): This paper reported a toolpath correction approach to enhance ISF forming accuracy using a two-directional Model Predictive Control (MPC) algorithm. A toolpath optimisation method for vertical toolpath correction had been verified in **Paper 2** [71], and it helped to reduce errors in the base of the test shapes to a suitable level while its major limitation was that horizontal geometric errors were relatively large. This paper extended the work in **Paper 2** [71] by augmenting the vertical control module with a new control module for horizontal toolpath correction. The proposed control algorithm was experimentally verified in single point

incremental sheet forming (SPIF) using two forming case studies. In the first case study (a truncated pyramid), two control approaches with different assumptions for the horizontal springback distribution along the horizontal cross-sectional profile were tested and compared. Then, the developed MPC control algorithm was applied to form a more complex asymmetric shape. Results showed that the developed strategy was able to reduce the forming errors in the wall of the formed shape compared to the existing works. The ISF process with MPC control led to significant accuracy improvement in comparison with the uncontrolled ISF process.

Paper 4 (*Lu, H., Kearney, M, Wang C., Liu, S., & Meehan, P. A (2017), Part accuracy improvement in two point incremental forming with a partial die using a model predictive control algorithm. Precision Engineering, 49, 179-188*)**:** This paper reported an enhanced MPC algorithm specially developed for TPIF with a partial die. The enhanced control algorithm was developed based on a simple deformation model for TPIF with a partial die and was able to correct the toolpath in both the vertical and horizontal directions. In the newly-added horizontal control module, dense profile points in the evenly distributed radial directions of the horizontal section were used to estimate the horizontal error distribution along the horizontal sectional profile during the forming process. The toolpath correction was performed through properly adjusting the toolpath in two directions based on the optimised toolpath parameters at each step. A case study for forming a non-axisymmetric shape was conducted to experimentally verify the developed toolpath correction strategy. Experiment results indicated that the two-directional toolpath correction approach contributes to part accuracy improvement in TPIF compared with the typical TPIF process that is without toolpath correction.

Paper 5 (*Li, Y., **Lu, H.**, Daniel, W. J., & Meehan, P. A. (2015). Investigation and optimisation of deformation energy and geometric accuracy in the incremental sheet forming process using response surface methodology. The International Journal of Advanced Manufacturing Technology, 79(9-12), 2041-2055*)**:** This paper was aimed to study the optimal parameter settings in ISF to achieve higher geometric accuracy with lower consumed energy through a comprehensive investigation of the influences of different process parameters on the consumed energy during the forming process, and the geometric accuracy of the formed parts. Using the Box-Behnken method for the multi-objective optimisation, a large set of experimental tests with 27 samples were performed by using varying values of four parameters, including step down, sheet thickness, tool diameter and wall angle. The test shape was a truncated pyramid. In each test, the forming forces were measured and used to calculate the consumed energy. The results showed that the sheet thickness had a significant influence on the deformation energy since higher plastic energy was required with the increase of the sheet thickness. Besides this, the deformation energy consumed was lower with the increase of step-down size within a limited range or the decrease of the wall angle. Moreover, it was summarised that the

quadratic effect of wall angle, the linear effect of sheet thickness and the interaction effect of thickness and step down could significantly affect the geometric quality. The optimal parameter setting of the pyramid-forming process were provided with the aim of minimising the deformation energy and geometric errors simultaneously.

Paper 6 (*Li, Y., Liu, Z.,* ***Lu, H.****, Daniel, W. B., Liu, S., & Meehan, P. A. (2014). Efficient force prediction for incremental sheet forming and experimental validation. The International Journal of Advanced Manufacturing Technology, 73(1-4), 571-587***):** This work presented an efficient analytical model for tangential force prediction. The forming forces in the cone-forming process were measured in a set of tests with varying step-down sizes and different wall angles. Different force trends were analysed by using different deformation mechanisms. Based on the energy method, an efficient model was developed to study the deformation zone in the ISF process for forming a truncated cone. The effects of deformation modes from shear, bending and stretching were independently considered in two sub-models. The comparison of the predicted tangential forces with the experimentally measured ones showed that an average error of 6 and 11 % in respect to the variation of step-down size and wall angle in the explored limits, respectively. The proposed model would greatly improve the prediction efficiency of forming force and benefit both the design and forming process.

Paper 7 (*Li, Y., Daniel, W. J., Liu, Z.,* ***Lu, H.****, & Meehan, P. A. (2015). Deformation mechanics and efficient force prediction in single point incremental forming. Journal of Materials Processing Technology, 221, 100-111***):** This paper reported a comprehensive finite element (FE) model with fine solid elements for ISF. An analytical model, based on the integration of three deformation modes including stretching, bending, and shearing, for tangential force prediction was developed to understand the deformation mechanism of the ISF process. The change of process parameters would affect the ratio and contribution of each deformation mode in the proposed model. Using two test shapes (truncated cone and pyramid), the proposed model was verified in different tests where varying values of parameters (step down, wall angle, tool radius, and sheet thickness) were used. The results showed that the predicted forces had a good match with the experimentally measured ones. Then, the proposed model was further developed and verified in a test for forming an ellipsoidal cup. The results showed that the trend of tangential force could be properly predicted with the change of the local curvature.

Paper 8 (*Li, Y. L., Liu, Z. B.,* ***Lu, H.****, Daniel, W. J. T., & Meehan, P. A. (2014). Experimental study and efficient prediction on forming forces in incremental sheet forming. Advanced Materials Research, 939, 313-321***):** This paper was aimed to study the forming forces under different forming conditions, and to develop an efficient model for force prediction in ISF. In this study, forming forces

were measured in the cone-forming process using varying step down sizes and wall angles. Based on bending and strain hardening mechanics, different force trends were observed and analysed. Influences of different parameters on the formability were also studied. With the use of an upper-bound approach, an efficient model was developed for force prediction in a case study. The results showed that the predicted tangential forces matched with the experimentally measured ones well.

Paper 9 (*Wang, C, Daniel, W. J. T.,* ***Lu, H.****, Liu, S., & Meehan, P. A. (2017). An experimental and numerical study on forming force, fracture behaviour, and strain states in two point incremental forming process. Key Engineering Materials, 725, 586-591***):** This paper investigated the forming force evolution, material fracture, and strain states in the single-pass TPIF process. This study was performed in experiments and numerical simulation using a hemisphere shape. It was concluded that both the peak force and fracture depth increased with the tool diameter and the step depth size in TPIF. The deformation mechanism or the failure mechanism was strongly dependent on particular forming conditions based on a failure parts morphology observation. FEM simulation results indicated that the major plastic strain was positive while the minor plastic strain was negative in the TPIF process to form a hemisphere shape. The strain increment and total equivalent plastic strain was affected by both the tool diameter and the step depth size.

Chapter 5 Conclusions and Future Work

This chapter summarises the research work performed in this PhD project, which mainly focuses on two aspects: MPC control in the SPIF process and that in the TPIF process. The contributions to the advanced manufacturing field are listed, followed by some potential future work related to this thesis.

Before developing the MPC algorithms for toolpath correction/control in ISF, the parameter investigation (**Objective 1a**) was performed to study the step depth, a critical toolpath parameter defined by the user in the toolpath generation, and to demonstrate the significance of this parameter in the generation and control of toolpath. Compared with previous studies on step depth [124, 125], which only focused on only one or two aspects of the formed part quality, this work investigated its influence on three aspects of the formed parts, including geometric accuracy, surface morphology and formability, in two sets of experiments, using a typical test shape (a truncated cone). The results show that a smaller step depth leads to better geometric accuracy and part surface quality in the ISF process while too small a step depth value should be avoided with regard to the material fracture, especially when producing parts with large wall angles. Also, the forming time increases as the step depth decreases. Even so, smaller step depth should be used within a reasonable range in toolpath control and optimisation. A trade-off between geometric accuracy, material failure, part surface quality, and forming time should be made in the design and control of toolpaths and the first two aspects should be considered as priorities.

To address the limitation of poor geometric accuracy in ISF processes, reported attempts for accuracy improvement have concentrated on toolpath optimisation/correction. A simple MPC algorithm has been developed for in-process toolpath control/correction in SPIF since MPC has the ability to use linear models to achieve good control of constrained nonlinear systems in various industries [68, 120]. Compared with the simple MPC control strategy for SPIF reported by Wang et al. [68, 100], in which the control model was empirically built based on the information obtained from the uncontrolled forming process, our work utilised an analytical control model built based on the incremental deformation mechanism of SPIF. Hence, the control strategy can be directly applied to the forming process without forming trial parts in the uncontrolled ISF process to build the control model. Besides this, the formed part geometric accuracy was fully analysed with the use of the error distribution map of the whole part, which was not presented in previous work [68, 100]. In our work on a simple MPC algorithm, step depth of the toolpath was optimised at each forming step by solving a receding optimal problem, based on shape state feedback during the forming process. Two different shapes were formed in experiments to verify the developed control method. Results show that the geometric accuracy in ISF with feedback control has been greatly improved compared with the ISF

process without feedback control. As for the bottom areas, the geometric errors of the truncated cone and pyramid have been reduced from ±3.0mm to ±0.25mm and ±0.3mm, respectively. Enhanced geometric accuracy in the wall areas of the formed parts has also been achieved although not as much as the bottom areas. Overall, the developed MPC algorithm for the ISF process could contribute to the improvement of geometric accuracy in SPIF.

In the simple MPC algorithm, only step depth (Δu_z) is optimised during the forming process, which leads to significant accuracy improvement in the vertical direction (bottom area) while the geometric accuracy of the wall area also has been improved but needs further improvement. Therefore, a two-directional MPC control algorithm for SPIF has been developed to correct the toolpath in the horizontal and vertical directions. With two separate MPC modules in vertical and horizontal directions, the toolpath was corrected by optimising Δu_z and Δu_h at each step during the forming process. The developed two-directional MPC algorithm was experimentally verified in two case studies for forming two different shapes. In the first case study, two different simplifying models for the horizontal optimisation were tested in strategy MPC-1 and strategy MPC-2, respectively. Results show that the previous simplified control algorithm (MPC-0), described above, leads to significant error reduction in the bottom area from ± 3 mm (No control) to ± 0.3mm while one of its limitations is that errors around the pyramid corners are relatively large (+1.5 mm). The two-directional strategy MPC-1 can help to improve the geometric accuracy around the corners while the wall areas were excessively formed. Strategy MPC-2 contributes to addressing the major limitation of strategy MPC-0 as well as the shortcoming of MPC-1. Control strategy MPC-2 was further verified in case study 2 for forming an asymmetric cone. The geometric errors in the base and most wall areas have been reduced from ± 3 mm (No control) to ± 0.3 mm (MPC-2). The two-directional control strategy provides a useful feedback control method to improve the accuracy via toolpath correction in SPIF. What's more, the ISF process with MPC control offers a good attempt for accurate manufacturing via in-process control and/or optimisation.

Finally, an enhanced MPC algorithm has been specially developed for TPIF with a partial die to conduct in-process toolpath correction in TPIF processes. The analytical predictive models used in the algorithm were developed based on the deformation nature of TPIF with a partial die, and the structure of the MPC algorithm for SPIF. The enhanced control algorithm is able to deal with toolpath correction in the horizontal and vertical directions through optimising two toolpath parameters (Δu_h and Δu_z) in two separate control modules. This toolpath correction strategy was experimentally tested to form a non-axisymmetric shape. Compared with the typical TPIF process that has no

toolpath correction, fairly good improvement in geometric accuracy (from ±3 mm to ±0.3 mm) was achieved with the use of the toolpath correction strategy in TPIF with a partial die while the geometric accuracy in the partial fillet areas requires further improvement. This work provides a helpful approach to achieve in-process toolpath control/correction in TPIF for geometric accuracy improvement.

5.1 Thesis contributions

The development of MPC control of the SPIF and TPIF processes offers a good approach for in-process control and/or optimisation in the ISF field as well as the accurate manufacturing field. The following results from this thesis are believed to be novel contributions to the existing literature:

- The parameter investigation work (**Objective 1a**)

  This work is fundamental to understanding the influences of step depth, a critical toolpath parameter defined by the user, on the part quality of the formed parts, which provides basic guidelines for the generation and correction/control of ISF toolpath to achieve improved forming abilities of the ISF technology. Compared with previous studies on step depth [124, 125], which only focused on only one or two aspects of the formed part quality, this work investigated its influence on three aspects of the formed parts, including geometric accuracy, surface morphology and formability, in two sets of experiments, using a typical test shape (a truncated cone).

- The development of the simplified MPC algorithm for SPIF (**Objective 1b and 1c**)

  Compared with previously reported control models for ISF [68, 100, 108] that were built based the measured process information from the forming process with no feedback control, the simplified MPC algorithm for SPIF uses an analytical predictive model built based on the incremental deformation nature of the SPIF process and can be directly applied for in-process toolpath control/correction. The experimental verification of the simplified MPC algorithm for SPIF provides experimental data for the toolpath control/correction in ISF.

- The development of the two-directional MPC algorithm for SPIF (**Objective 2**)

  The two-directional MPC algorithm for SPIF is the first reported two-directional MPC algorithm for optimising the step depth and horizontal increment to improve geometric accuracy in SPIF. The MPC algorithm for SPIF used analytical predictive models, which were built based on the SPIF deformation mechanism in the vertical and horizontal directions, to build two separate MPC modules for toolpath correction in two directions. The development and experimental verification

of the two-directional MPC algorithm provides a helpful approach and experimental data for the development of toolpath control/correction strategies in ISF.

- The development of an enhanced MPC control algorithm for TPIF with a partial die (**Objective 3**)

  The control algorithm for TPIF with a partial die is believed to be the first reported attempt to improve the geometric accuracy in the TPIF process through in-process toolpath correction by optimising the step depth and horizontal increment during the forming process. The MPC algorithm for TPIF used analytical predictive models built based on the TPIF deformation mechanism in the two directions. In particular, in the horizontal control module, dense profile points in the evenly distributed radial directions of the horizontal section were used to estimate the horizontal error distribution along the horizontal sectional profile. The development and experimental verification of the MPC algorithm for TPIF provides a helpful approach and experimental data for the work on toolpath control/correction and geometric accuracy improvement in ISF.

5.2 Suggested future work

Although this PhD project has made some progress in understanding and promoting the ISF technology towards its industrial application, the research also raises a number of questions and issues which remain unsolved and further studies are needed. They are summarised as follows:

- The parameter investigation work could be extended to further study the step depth and other ISF parameters (e.g., sheet thickness, sheet material type, tool diameter, tool feed speed, scallop height, forming forces, clamping and supporting devices, forming pressure of the clamping frame in TPIF and etc.) with the aim to obtain comprehensive information and understanding of the forming processes and how to reduce the part inaccuracies (springback, the bending effect, and the "pillow" effect) in ISF.

- As for the predictive models in the MPC algorithms, more complex analytical models for modelling the forming process could be developed to deal with the fabrication of complex shapes in ISF processes with MPC control.

- The developed MPC algorithms for SPIF and TPIF processes could be further developed to more accurately estimate and compensate the springback in ISF, especially in the areas with sharply curved features of the test shape. For instance, the step depth (Δu_z) values in different radial

directions at each step might need to be optimised differently in each radial direction since the step depth (Δu_z) value was taken as constant in all radial directions in current MPC algorithms. Besides this, the coupling of the two toolpath parameters, the step depth and the horizontal step increment, might be considered in the further development of the developed MPC algorithms.

- The developed MPC algorithm could be applied to optimise the toolpath parameters of some other toolpath types for ISF, such as the spiral toolpath, to improve the low geometric accuracy in ISF.

- The developed MPC algorithm with shape feedback might be combined with the control strategy with force feedback to prevent material failure and improve the geometric accuracy in the forming of complex shapes via ISF.

- The integration of the developed MPC control strategy and the multi-stage strategy in ISF might offer a means of reducing geometric errors in the part region that has already been formed to obtain the accurate parts with improved accuracy in all areas. Also, this might enable the accurate manufacturing of complex parts with large wall angles that cannot be successfully produced in the single-stage ISF process.

- After the further development, the MPC control strategy might be generalised and verified for the fabrication of sheet parts with various sheet materials, sheet thickness values and part sizes.

References

1. Ishikawa, T., et al., *11th International Conference on Technology of Plasticity, ICTP 2014, 19-24 October 2014, Nagoya Congress Center, Nagoya, JapanCurrent Status of "Dieless" Amino's Incremental Forming.* Procedia Engineering, 2014. **81**: p. 54-62.

2. Cao, J., et al., *A Hybrid Forming System: Electrical-Assisted Double Side Incremental Forming (EADSIF) Process for Enhanced Formability and Geometrical Flexibility*. 2012. p. Medium: ED; Size: 7.3MB.

3. Filice, L., L. Fratini, and F. Micari, *Analysis of Material Formability in Incremental Forming.* CIRP Annals - Manufacturing Technology, 2002. **51**(1): p. 199-202.

4. Kim, Y.H. and J.J. Park, *Effect of process parameters on formability in incremental forming of sheet metal.* Journal of Materials Processing Technology, 2002. **130–131**(0): p. 42-46.

5. Hagan, E. and J. Jeswiet, *A review of conventional and modern single-point sheet metal forming methods.* Proceedings of the Institution of Mechanical Engineers, Part B: Journal of Engineering Manufacture, 2003. **217**(2): p. 213-225.

6. Echrif, S.B.M. and M. Hrairi, *Research and Progress in Incremental Sheet Forming Processes.* Materials and Manufacturing Processes, 2011. **26**(11): p. 1404-1414.

7. Bahloul, R., H. Arfa, and H. BelHadjSalah, *A study on optimal design of process parameters in single point incremental forming of sheet metal by combining Box–Behnken design of experiments, response surface methods and genetic algorithms.* The International Journal of Advanced Manufacturing Technology, 2014. **74**(1-4): p. 163-185.

8. Filice, L., G. Ambrogio, and M. Gaudioso, *Optimised tool-path design to reduce thinning in incremental sheet forming process.* International Journal of Material Forming, 2013. **6**(1): p. 173-178.

9. Jeswiet, J., et al., *Asymmetric single point incremental forming of sheet metal.* Cirp Annals-Manufacturing Technology, 2005. **54**(2): p. 623-649.

10. Malhotra, R., et al., *Improvement of Geometric Accuracy in Incremental Forming by Using a Squeezing Toolpath Strategy With Two Forming Tools.* Journal of Manufacturing Science and Engineering, 2011. **133**(6): p. 061019-061019.

11. Malhotra, R., et al., *Accumulative-DSIF strategy for enhancing process capabilities in incremental forming.* CIRP Annals - Manufacturing Technology, 2012. **61**(1): p. 251-254.

12. Ambrogio, G., et al., *Application of Incremental Forming process for high customised medical product manufacturing.* Journal of Materials Processing Technology, 2005. **162–163**(0): p. 156-162.

13. Kalo, A. and M.J. Newsum, *An Investigation of Robotic Incremental Sheet Metal Forming as a Method for Prototyping Parametric Architectural Skins*, in *Robotic Fabrication in Architecture, Art and Design 2014*, W. McGee and M. Ponce de Leon, Editors. 2014, Springer International Publishing: Cham. p. 33-49.

14. Ames, J.P., *Systematische Untersuchung der Beeinflussung des Werkstoffflusses bei der inkrementellen Blechumformung mit CNC-Werkzeugmaschinen*. 2008: Shaker.

15. Bambach, M., B. Taleb Araghi, and G. Hirt, *Strategies to improve the geometric accuracy in asymmetric single point incremental forming.* Production Engineering, 2009. **3**(2): p. 145-156.

16. Duflou, J.R., et al., *Process window enhancement for single point incremental forming through multi-step toolpaths.* Cirp Annals-Manufacturing Technology, 2008. **57**(1): p. 253-256.

17. Adams, D.W., *Improvements on single point incremental forming through electrically assisted forming, contact area prediction and tool development*. 2014, ProQuest, UMI Dissertations Publishing.

18. Singh, A. and A. Agrawal, *Comparison of deforming forces, residual stresses and geometrical accuracy of deformation machining with conventional bending and forming.* Journal of Materials Processing Technology, 2016. **234**: p. 259-271.

19. Reddy, N.V., R. Lingam, and J. Cao, *Incremental Metal Forming Processes in Manufacturing*, in *Handbook of Manufacturing Engineering and Technology*, A.Y.C. Nee, Editor. 2014, Springer London. p. 411-452.

20. Allwood, J.M., G.P.F. King, and J. Duflou, *A structured search for applications of the incremental sheet-forming process by product segmentation.* Proceedings of the Institution of Mechanical Engineers, Part B: Journal of Engineering Manufacture, 2005. **219**(2): p. 239-244.

21. Ambrogio, G., L. Filice, and F. Gagliardi, *Improving industrial suitability of incremental sheet forming process.* The International Journal of Advanced Manufacturing Technology, 2012. **58**(9-12): p. 941-947.

22. Skjoedt, M., et al., *Strategies and limits in multi-stage single-point incremental forming.* The Journal of Strain Analysis for Engineering Design, 2010. **45**(1): p. 33-44.

23. Xu, D.K., et al., *Enhancement of process capabilities in electrically-assisted double sided incremental forming.* Materials & Design, 2016. **92**: p. 268-280.

24. Rous, P., *Machines for shaping sheet metal*. 1960, Google Patents.

25. Leszak, E., *Apparatus and process for incremental dieless forming*. 1967, Google Patents.

26. Henrard, C., *Numerical simulations of the single point incremental forming process.* 2009.

27. Park, J.-J. and Y.-H. Kim, *Fundamental studies on the incremental sheet metal forming technique.* Journal of Materials Processing Technology, 2003. **140**(1–3): p. 447-453.

28. Altan, T. and A.E. Tekkaya, *Sheet Metal Forming - Processes and Applications*. 2012, ASM International.

29. Nimbalkar, D. and V. Nandedkar, *Review of Incremental Forming of Sheet Metal Components.* 2013.

30. Amino, H., et al. *Dieless NC forming, prototype of automotive service parts*. in *Proceedings of the 2nd International Conference on Rapid Prototyping and Manufacturing (ICRPM), Beijing*. 2002.

31. Matsubara, S., *Incremental Backward Bulge Forming of a Sheet Metal with a Hemispherical Head Tool-A Study of a Numerical Control Forming System II.* JOURNAL-JAPAN SOCIETY FOR TECHNOLOGY OF PLASTICITY, 1994. **35**: p. 1311-1311.

32. Aoyama, S., et al., *Apparatus for dieless forming plate materials.* Europäisches Brevet EP0970764, 2000.

33. Allwood, J., N. Houghton, and K. Jackson. *The design of an incremental sheet forming machine*. in *Advanced Materials Research*. 2005. Trans Tech Publ.

34. Cao, J., et al. *Incremental sheet metal forming: advances and challenges*. in *Proceedings of International Conference on Technology of Plasticity (ICTP 2008), Gyeongju, Korea*. 2008.

35. Hirt, G. *Tools and Equipment used in Incremental Forming*. in *1st Incremental Forming Workshop, University of Saarbrucken*. 2004.

36. Meier, H., et al., *Increasing the part accuracy in dieless robot-based incremental sheet metal forming.* CIRP Annals - Manufacturing Technology, 2009. **58**(1): p. 233-238.

37. Vihtonen, L., A. Puzik, and T. Katajarinne, *Comparing two robot assisted incremental forming methods: incremental forming by pressing and incremental hammering.* International Journal of Material Forming, 2008. **1**(1): p. 1207-1210.

38. Essa, K. and P. Hartley, *An assessment of various process strategies for improving precision in single point incremental forming.* International Journal of Material Forming, 2011. **4**(4): p. 401-412.

39. Allwood, J.M., D. Braun, and O. Music, *The effect of partially cut-out blanks on geometric accuracy in incremental sheet forming.* Journal of Materials Processing Tech, 2010. **210**(11): p. 1501-1510.

40. Micari, F., G. Ambrogio, and L. Filice, *Shape and dimensional accuracy in Single Point Incremental Forming: State of the art and future trends.* Journal of Materials Processing Technology, 2007. **191**(1-3): p. 390-395.

41. Ambrogio, G., L. Napoli, and L. Filice, *A novel approach based on multiple back-drawing incremental forming to reduce geometry deviation.* International Journal of Material Forming, 2009. **2**(1): p. 9-12.

42. Iseki, H., K. Kato, and S. Sakamoto, *Flexible and incremental sheet metal forming using a spherical roller.* Journal of Process Technology, 1989: p. 41-44.

43. Attanasio, A., et al., *Use of TPIF or SPIF for Prototype Productions: an Actual Case.* AIP Conference Proceedings, 2007. **907**(1): p. 163-168.

44. Attanasio, A., et al., *Asymmetric two points incremental forming: Improving surface quality and geometric accuracy by tool path optimization.* Journal of Materials Processing Technology, 2008. **197**(1-3): p. 59-67.

45. Meier, H., et al. *Two point incremental forming with two moving forming tools*. in *Key Engineering Materials*. 2007. Trans Tech Publ.

46. Wang, Y., et al. *Experimental and Numerical Analysis of Double Sided Incremental Forming*. in *ASME 2009 International Manufacturing Science and Engineering Conference*. 2009. American Society of Mechanical Engineers.

47. Wang, Y., et al. *Experimental study on a new method of double side incremental forming*. in *ASME 2008 International Manufacturing Science and Engineering Conference collocated with the 3rd JSME/ASME International Conference on Materials and Processing*. 2008. American Society of Mechanical Engineers.

48. Araghi, B.T., et al., *Investigation into a new hybrid forming process: Incremental sheet forming combined with stretch forming.* Cirp Annals-Manufacturing Technology, 2009. **58**(1): p. 225-228.

49. Taleb Araghi, B., et al., *Review on the development of a hybrid incremental sheet forming system for small batch sizes and individualized production.* Production Engineering, 2011. **5**(4): p. 393-404.

50. Duflou, J.R., et al., *Laser Assisted Incremental Forming: Formability and Accuracy Improvement.* CIRP Annals - Manufacturing Technology, 2007. **56**(1): p. 273-276.

51. Fan, G., et al., *Electric hot incremental forming: A novel technique.* International Journal of Machine Tools and Manufacture, 2008. **48**(15): p. 1688-1692.

52. Shi, X., et al., *Electric hot incremental forming of low carbon steel sheet: accuracy improvement.* The International Journal of Advanced Manufacturing Technology, 2013. **68**(1): p. 241-247.

53. Ambrogio, G., L. Filice, and F. Gagliardi, *Formability of lightweight alloys by hot incremental sheet forming.* Materials & Design, 2012. **34**: p. 501-508.

54. Cao, J., et al., *A Hybrid Forming System: Electrical-Assisted Double Side Incremental Forming (EADSIF) Process for Enhanced Formability and Geometrical Flexibility.* Northwestern University, Document ID: DE-EE0003460, 2012.

55. Altan, T. and A.E. Tekkaya, *Sheet Metal Forming - Processes and Applications*. ASM International.

56. Skjoedt, M., et al., *Multi Stage Strategies for Single Point Incremental Forming of a Cup.* International Journal of Material Forming, 2008. **1**(1): p. 1199-1202.

57. Kitazawa, K., et al., *Metal-flow phenomena in computerized numerically controlled incremental stretch-expanding of aluminum sheets.* Journal of Japan Institute of Light Metals, 1996. **46**(2): p. 65-70.

58. Kitazawa, K. and M. Nakane, *Hemi-ellipsoidal stretch-expanding of aluminum sheet by CNC incremental forming process with two path method.* JOURNAL-JAPAN INSTITUTE OF LIGHT METALS, 1997. **47**: p. 440-445.

59. Kim, T.J. and D.Y. Yang, *Improvement of formability for the incremental sheet metal forming process.* International Journal of Mechanical Sciences, 2000. **42**(7): p. 1271-1286.

60. Young, D. and J. Jeswiet, *Wall thickness variations in single-point incremental forming.* Proceedings of the Institution of Mechanical Engineers, Part B: Journal of Engineering Manufacture, 2004. **218**(11): p. 1453-1459.

61. Kitazawa, K. and A. Nakajima. *Cylindrical incremental drawing of sheet metals by CNC incremental forming process*. in *6th international conference on advanced technologies of plasticity. Nürnberg*. 1999.

62. Hirt, G., et al., *Forming strategies and Process Modelling for CNC Incremental Sheet Forming.* CIRP Annals - Manufacturing Technology, 2004. **53**(1): p. 203-206.

63. Verbert, J., et al., *Multi-Step toolpath approach to overcome forming limitations in single point incremental forming.* International Journal of Material Forming, 2008. **1**: p. 1203-1206.

64. Liu, Z.B., Y.L. Li, and P.A. Meehan, *Vertical Wall Formation and Material Flow Control for Incremental Sheet Forming by Revisiting Multistage Deformation Path Strategies.* Materials and Manufacturing Processes, 2013. **28**(5): p. 562-571.

65. Liu, Z.B., et al., *Multi-pass deformation design for incremental sheet forming: Analytical modeling, finite element analysis and experimental validation.* Journal of Materials Processing Technology, 2014. **214**(3): p. 620-634.

66. Malhotra, R., et al., *A new methodology for multi-pass single point incremental forming with mixed toolpaths.* CIRP Annals - Manufacturing Technology, 2011. **60**(1): p. 323-326.

67. Junchao, L., S. Junjian, and W. Bin, *A multipass incremental sheet forming strategy of a car taillight bracket.* The International Journal of Advanced Manufacturing Technology, 2013: p. 1-8.

68. Wang, H. and S. Duncan. *Constrained model predictive control of an incremental sheet forming process*. in *Control Applications (CCA), 2011 IEEE International Conference on*. 2011.

69. Behera, A.K., B. Lauwers, and J.R. Duflou, *Tool path generation for single point incremental forming using intelligent sequencing and multi-step mesh morphing techniques.* International Journal of Material Forming, 2014. **8**(4): p. 517-532.

70. Malhotra, R., N.V. Reddy, and J.A. Cao, *Automatic 3D Spiral Toolpath Generation for Single Point Incremental Forming.* Journal of Manufacturing Science and Engineering-Transactions of the Asme, 2010. **132**(6).

71. Lu, H., et al., *Model predictive control of incremental sheet forming for geometric accuracy improvement.* The International Journal of Advanced Manufacturing Technology, 2015: p. 1-14.

72. Behera, A.K., et al., *Tool path compensation strategies for single point incremental sheet forming using multivariate adaptive regression splines.* Computer-Aided Design, 2013. **45**(3): p. 575-590.

73. Ceretti, E., C. Giardini, and A. Attanasio, *Experimental and simulative results in sheet incremental forming on CNC machines.* Journal of Materials Processing Technology, 2004. **152**(2): p. 176-184.

74. Ambrogio, G., et al., *Influence of some relevant process parameters on the dimensional accuracy in incremental forming: a numerical and experimental investigation.* Journal of Materials Processing Technology, 2004. **153–154**(0): p. 501-507.

75. Ambrogio, G., et al., *A simple approach for reducing profile diverting in a single point incremental forming process.* Proceedings of the Institution of Mechanical Engineers, Part B: Journal of Engineering Manufacture, 2005. **219**(11): p. 823-830.

76. Attanasio, A., E. Ceretti, and C. Giardini, *Optimization of tool path in two points incremental forming.* Journal of Materials Processing Technology, 2006. **177**(1-3): p. 409-412.

77. Attanasio, A., E. Ceretti, and C. Giardini, *Optimization of tool path in two points incremental forming.* Journal of Materials Processing Technology, 2006. **177**(1–3): p. 409-412.

78. Verbert, J., J.R. Duflou, and B. Lauwers. *Feature based approach for increasing the accuracy of the SPIF process*. in *Key Engineering Materials*. 2007. Trans Tech Publ.

79. Zettler, J., H. Rezai, and G. Hirt. *Springback Compensation for Incremental Sheet Metal Forming Applications*. in *7th LS-Dyna Forum, Bamberg, Germany, September*. 2008.

80. Zhu, H., Z.J. Liu, and J.H. Fu, *Spiral tool-path generation with constant scallop height for sheet metal CNC incremental forming.* International Journal of Advanced Manufacturing Technology, 2011. **54**(9-12): p. 911-919.

81. Lu, B., et al., *Feature-based tool path generation approach for incremental sheet forming process.* Journal of Materials Processing Technology, 2013. **213**(7): p. 1221-1233.

82. Allwood, J.M., D. Braun, and O. Music, *The effect of partially cut-out blanks on geometric accuracy in incremental sheet forming.* Journal of Materials Processing Technology, 2010. **210**(11): p. 1501-1510.

83. Ambrogio, G., L. Filice, and F. Gagliardi, *Improving industrial suitability of incremental sheet forming process.* The International Journal of Advanced Manufacturing Technology, 2011. **58**(9-12): p. 941-947.

84. Visioli, A., *Practical PID control*. 2006: Springer.

85. Åström, K.J. and B. Wittenmark, *Adaptive control*. 2013: Courier Corporation.

86. Dullerud, G.E. and F. Paganini, *A course in robust control theory*. Vol. 6. 2000: Springer New York.

87. Bhattacharyya, S.P., H. Chapellat, and L.H. Keel, *Robust control*. 1995: Prentice-Hall Upper Saddle River, New Jersey.

88. Ashbaugh, B. and J. Boitano, *Advantages and Disadvantages of Controller Designs Using Fuzzy Logic.*

89. Mendel, J.M., *Fuzzy logic systems for engineering: a tutorial.* Proceedings of the IEEE, 1995. **83**(3): p. 345-377.

90. Albertos, P. and A. Sala. *Fuzzy logic controllers. Advantages and drawbacks*. in *VIII International Congress of Automatic Control*. 1998.

91. Evans, L.C., *An introduction to mathematical optimal control theory version 0.2.* Lecture notes available at http://math. berkeley. edu/~ evans/control. course. pdf, 1983.

92. Fikar, M. and K. Kostur. *Optimal process control*. in *Carpathian Control Conference (ICCC), 2012 13th International*. 2012.

93. Lewis, F. and S.S. Ge, *Neural networks in feedback control systems.* Mechanical Engineer's Handbook, 2005.

94. Camacho, E.F. and C.B. Alba, *Model predictive control*. 2013: Springer Science & Business Media.

95. Bao-Cang, D. and D. Baocang, *Modern predictive control*. 2010: CRC press.

96. Wang, L., *Model predictive control system design and implementation using MATLAB®*. 2009: springer.

97. Morari, M. and J. H. Lee, *Model predictive control: past, present and future.* Computers & Chemical Engineering, 1999. **23**(4–5): p. 667-682.

98. Qin, S.J. and T.A. Badgwell, *A survey of industrial model predictive control technology.* Control Engineering Practice, 2003. **11**(7): p. 733-764.

99. Maciejowski, J. and M. Huzmezan, *Predictive control*, in *Robust Flight Control*, J.-F. Magni, S. Bennani, and J. Terlouw, Editors. 1997, Springer Berlin Heidelberg. p. 125-134.

100. Wang, H. and S. Duncan. *Optimization of tool trajectory for Incremental Sheet Forming using closed loop control*. in *Automation Science and Engineering (CASE), 2011 IEEE Conference on*. 2011.

101. Petek, A., K. Kuzman, and B. Suhač, *Autonomous on-line system for fracture identification at incremental sheet forming.* CIRP Annals - Manufacturing Technology, 2009. **58**(1): p. 283-286.

102. Filice, L., G. Ambrogio, and F. Micari, *On-Line Control of Single Point Incremental Forming Operations through Punch Force Monitoring.* CIRP Annals - Manufacturing Technology, 2006. **55**(1): p. 245-248.

103. Ambrogio, G., L. Filice, and F. Micari, *A force measuring based strategy for failure prevention in incremental forming.* Journal of Materials Processing Technology, 2006. **177**(1-3): p. 413-416.

104. Fiorentino, A., *Force-based failure criterion in incremental sheet forming.* The International Journal of Advanced Manufacturing Technology, 2013. **68**(1-4): p. 557-563.

105. Li, Y., et al., *Deformation mechanics and efficient force prediction in single point incremental forming.* Journal of Materials Processing Technology, 2015. **221**: p. 100-111.

106. Li, Y., et al., *Efficient force prediction for incremental sheet forming and experimental validation.* The International Journal of Advanced Manufacturing Technology, 2014. **73**(1-4): p. 571-587.

107. Duflou, J., et al., *Experimental study on force measurements for single point incremental forming.* Journal of Materials Processing Technology, 2007. **189**(1–3): p. 65-72.

108. Allwood, J.M., et al., *Closed-loop feedback control of product properties in flexible metal forming processes with mobile tools.* CIRP Annals - Manufacturing Technology, 2009. **58**(1): p. 287-290.

109. Han, F., et al., *Method of closed loop springback compensation for incremental sheet forming process.* Journal of Central South University of Technology, 2011. **18**(5): p. 1509-1517.

110. Fu, Z., et al., *Tool path correction algorithm for single-point incremental forming of sheet metal.* The International Journal of Advanced Manufacturing Technology, 2012. **64**(9-12): p. 1239-1248.

111. Rauch, M., et al., *A new approach for toolpath programming in Incremental Sheet Forming.* International Journal of Material Forming, 2008. **1**(1): p. 1191-1194.

112. Rauch, M., et al., *Tool path programming optimization for incremental sheet forming applications.* Computer-Aided Design, 2009. **41**(12): p. 877-885.

113. Fiorentino, A., C. Giardini, and E. Ceretti, *Application of artificial cognitive system to incremental sheet forming machine tools for part precision improvement.* Precision Engineering, 2015. **39**(0): p. 167-172.

114. Fiorentino, A., et al., *Part precision improvement in incremental sheet forming of not axisymmetric parts using an artificial cognitive system.* Journal of Manufacturing Systems, 2015. **35**(0): p. 215-222.

115. Sasso, M., M. Callegari, and D. Amodio, *Incremental forming: an integrated robotized cell for production and quality control.* Meccanica, 2008. **43**(2): p. 153-163.

116. Orteu, J.J., et al., *Multiple-Camera Instrumentation of a Single Point Incremental Forming Process Pilot for Shape and 3D Displacement Measurements: Methodology and Results.* Experimental Mechanics, 2011. **51**(4): p. 625-639.

117. Setti, F., et al., *Shape measurement system for single point incremental forming (SPIF) manufacts by using trinocular vision and random pattern.* Measurement Science and Technology, 2012. **23**(11): p. 115402.

118. Paniti, I. and A. Paroczi. *Design and modeling of integrated Hall-effect sensor based on-line thickness measurement device for incremental sheet forming processes*. in *Advanced Intelligent Mechatronics (AIM), 2011 IEEE/ASME International Conference on*. 2011.

119. Liu, Z.B., Y.L. Li, and P.A. Meehan, *Experimental Investigation of Mechanical Properties, Formability and Force Measurement for AA7075-O Aluminum Alloy Sheets Formed by Incremental Forming.* International Journal of Precision Engineering and Manufacturing, 2013. **14**(11): p. 1891-1899.

120. Camacho, E.F., et al., *Model predictive control*. Vol. 2. 2004: Springer London.

121. Brewer, J., *Kronecker products and matrix calculus in system theory.* IEEE Transactions on circuits and systems, 1978. **25**(9): p. 772-781.

122. Boyd, S. and L. Vandenberghe, *Convex optimization*. 2009: Cambridge university press.

123. Yilamu, K., et al., *Air bending and springback of stainless steel clad aluminum sheet.* Journal of Materials Processing Technology, 2010. **210**(2): p. 272-278.

124. Radu, C., *Effects of Process Parameters on the Quality of Parts Processed by Single Point Incremental Forming.* Int. J. Mod. Manuf. Technol, 2011. **3**(2): p. 91-96.

125. Attanasio, A., et al., *Asymmetric two points incremental forming: Improving surface quality and geometric accuracy by tool path optimization.* Journal of Materials Processing Technology, 2008. **197**(1–3): p. 59-67.

Appended Papers

Paper 1

Study on Step Depth for Part Accuracy Improvement in Incremental Sheet Forming Process

Lu, H.B., **Li, Y.L.**, Liu, Z.B., Liu, S. and Meehan, P. A.

Advanced Materials Research

2014, Volume: 939, Pages: 274-280.

Study on step depth for part accuracy improvement in incremental sheet forming process

Haibo Lu[1, a], Yanle Li[1,b], Zhaobing Liu[1,c], Sheng Liu[1,d] and Paul A. Meehan[1,e]

[1]School of Mechanical & Mining Engineering, University of Queensland, St Lucia, Brisbane, QLD 4072, Australia

[a]h.lu2@uq.edu.au, [b]yanle.li@uq.edu.au, [c]z.liu7@uq.edu.au, [d]s.liu3@uq.edu.au, [e]meehan@uq.edu.au

Keywords: incremental sheet forming, step depth, part accuracy

Abstract. Incremental Sheet Forming (ISF) is a new-emerging sheet forming process well suited for small batch production or prototyping because it does not need any dedicated dies or punches. In this forming process, sheet metal parts are formed by a smooth-end tool in a stepwise way, during which plastic deformation is highly localized around the tool end. The part geometric accuracy obtained in the current ISF process, however, has not met the industry specification for precise part fabrication. This paper deals with a study on step depth, a critical parameter in ISF, for improving the geometric accuracy, surface quality and formability. Two sets of experiments were conducted to investigate the influence of step depth on part quality. Dimensional accuracy, surface morphology and material fracture of deformed parts were compared and analysed. An optimum value of step depth was suggested for forming a truncated cone. The present work provided significant fundamental information for the development of an advanced ISF control system on tool path control and optimization.

Introduction

Sheet metal forming is a widely used manufacturing process and plays a significant role in industry. There is a wide range of sheet metal forming processes, including stamping, pressing, etc. These require dedicated dies and punches to manufacture sheet-metal components with complex shapes. Due to the high cost in realizing such process and the lack of flexibility, conventional manufacturing methods are efficient for large scale production but less competitive for small scale fabrication of customised parts [1]. As market demand in the sheet forming area is becoming increasingly customer-oriented and sophisticated, more flexible manufacturing technologies for custom parts fabrication are demanded to be introduced and developed [2]. Incremental sheet forming (ISF) is a flexible process well suited for small batch production or prototyping because expensive dies and tools are not required, which makes it a promising alternative to meet the new market requests [3, 4].

In ISF, sheet metal parts are formed by a smooth-end tool, generally mounted on a three-axis CNC milling machine, in a stepwise way. Fig. 1 schematically illustrates the single point incremental forming (SPIF) process. The simple tool moves over the surface of the clamped metal sheet along a tool path directly generated from a 3D CAD file, during which plastic deformation is highly localized around the tool end. ISF is a dieless forming process and possesses a high degree of flexibility because specialised tooling is not required. The product design can be modified or changed easily and quickly. Additionally, the formability in ISF is higher than conventional processes due to the small plastic zone and incremental nature of the process, making it easier to deform sheet metal with low formability [5]. The small contact zone and incremental step size also contributes to small forces within the material. Therefore, the lead-time and cost of tooling in ISF can be greatly minimized. This forming technique makes rapid prototypes or small serial production of sheet metal parts relatively fast and economical [6].

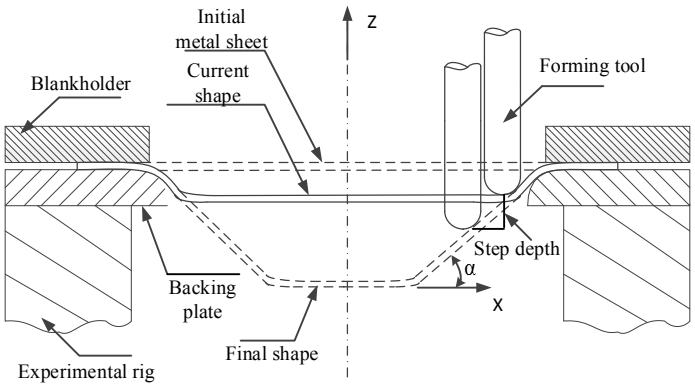

Fig.1 Process principle of SPIF: step depth (ΔZ) is the vertical distance between two neighbouring contours.

Nevertheless, the major limitation of ISF is that the geometric accuracy obtained currently is lower compared with conventional forming processes and cannot reliably reach suitable levels specified by industrial users. Hence, the ISF process is still in the embryonic stage with no widespread industrial applications although rapid advances have been achieved recently. Additionally, the forming process is slow due to its point-to-point forming nature.

Recently, the improvement of part accuracy and process optimization in ISF has been a key issue for researchers. During the ISF process, the tool path directly affects the forming accuracy since the shape is formed by a simple tool following a designed tool path. Regarding the generation of tool path, the most common method is a contour parallel method by which the tool path is generated in commercial CAM software and consists of a series of contours, with the step depth constant, parallel to the sheet plane. However, this method fails to fabricate complex parts with high precision. Many studies on the design, optimization and control of forming tool path have been carried out to overcome the limitations. Hirt et al. [7] proposed a tool path optimization method based on experiments and the modification of the tool path by a correction algorithm in the second run. Attanasio et al. [8] conducted a study on tool path optimization in TPIF and concluded that tool path with a small scallop height and variable step depth sizes contribute to better part quality. As reported in [9], a closed loop control scheme was used to modify the step depth during the forming process for tool trajectory control. Malhotra et al. [10] presented an automatic spiral tool path generation algorithm for SPIF, in which the incremental depth is controlled by the geometrical error between CAD model and formed parts.

According to the previous research, step depth has been considered as a critical parameter in the design, optimization and control of tool paths. At present, comprehensive research work on step depth is required to further study the relationship between step depth and part quality, especially for improving part accuracy via tool path control and optimization. This paper focuses on the investigation of step depth to fully understand its influence on the formability and part quality, including geometric accuracy and surface finish. This would be of great significance for ISF tool path control and optimization to address the limitation of low geometric accuracy.

Experiments

Experiments were carried out on an AMINO® DLNC-PC ISF machine (Fig. 2). The sheet blank is clamped between a blank holder and a steel backing plate to prevent any movement of the blank during forming process. The metal blank, with 1.6 mm in thickness and 300 mm × 300 mm in size, is made of aluminium (7075-O), commonly utilized for forming automotive and aviation components. A 30 mm diameter cylindrical steel tool with a hemispherical end was used to deform

the blank; the tip of the tool is tungsten carbide and the body is made of K110 steel which was hardened and tempered to HRC60. Lubricant (oil-Shell Tellus Oil 68) was used to reduce the wear of the tool and friction between the tool and the blank.

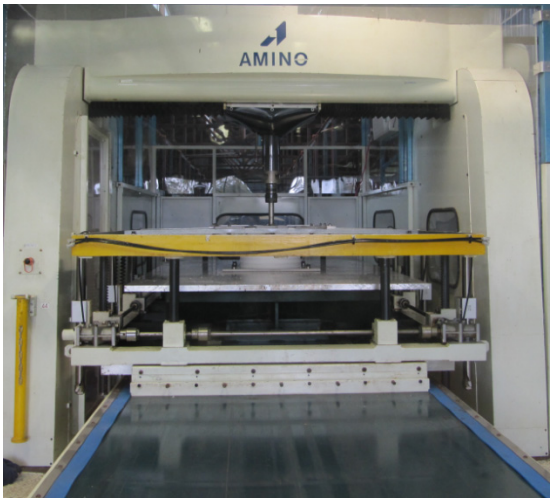

Fig. 2 AMINO® DLNC-PC ISF Machine

Two sets of tests were performed by varying the ΔZ values to study this parameter, focusing on geometric accuracy and surface quality and on material formability, respectively. CAD models of truncated cones with two different wall angles were designed in SOLIDWORKS. A laser scanner (Non-contact 3D Digitizer VIVID 9i) was used to measure the geometry of the deformed components. Surface morphology of machined faces on produced truncated cones was analysed as well. The parameter settings of experiments are shown in Tables 1, as follows.

Table 1 Parameter settings of experiments on step depth

Parameter	**Geometric accuracy and surface quality test**	**Formability test**
Shape design	Truncated cone	Truncated Cone
Wall angle (˚)	50	60
Feed rate (mm/min)	4000	4000
Sheet thickness (mm)	1.6	1.6
Tool diameter (mm)	30	30
Step depth/ΔZ (mm)	0.1, 0.6, 1.1	0.1, 0.2, 0.3, 0.4, 0.5, 0.7, 1.0

Results and Discussion

This section presents experimental results obtained in the tests to analyse the influence of step depth in ISF process in terms of geometric accuracy, surface morphology and material fracture.

Geometric accuracy. GEOMAGIC Qualify was used to produce 3D geometry data of the scanned shape and analyse the dimensional error between deformed test parts and designed CAD models. Specifically, both produced and designed profiles were given in large sets of points in the same Cartesian coordinate system. In this work, cross-sectional comparison along a defined section plane was used to evaluate the geometric accuracy since the truncated cone is symmetric. A system plane (plane XOZ) across the symmetry axis of the cone was set as the section plane. The deviation in Z

direction between the designed and fabricated profiles was calculated as the geometric error in cross-sectional comparison.

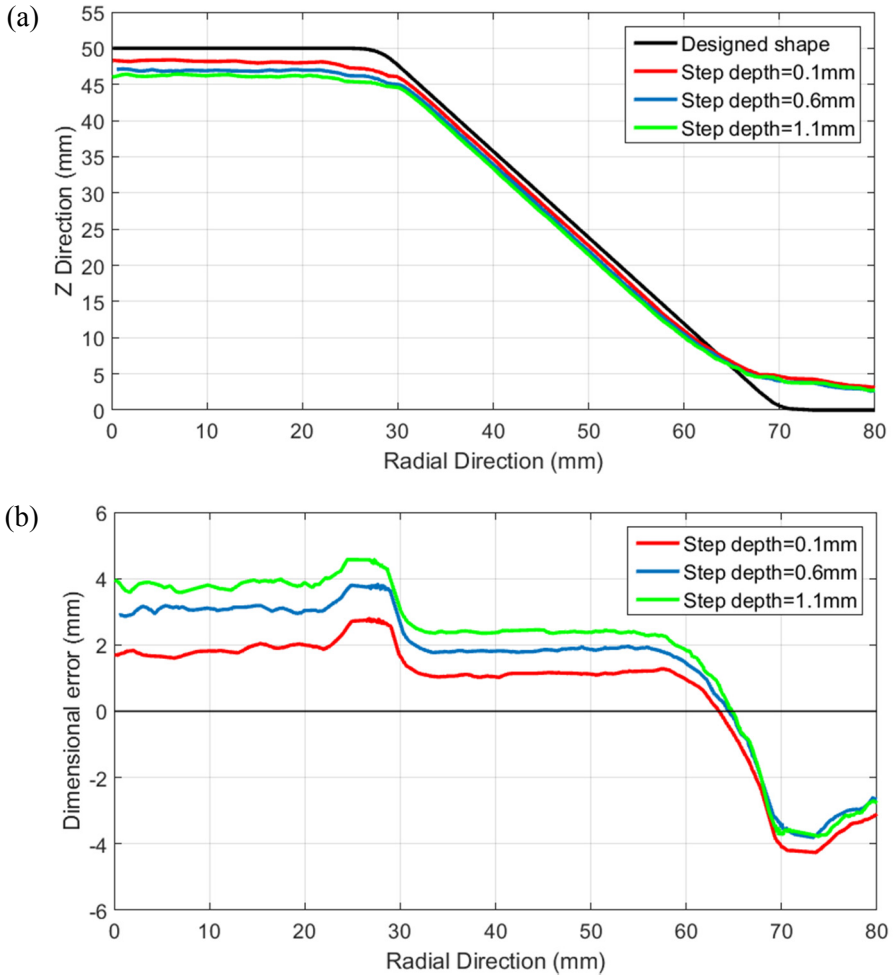

Fig.3: (a) Cross-sectional comparison among deformed profiles and the target profile; (b) Error distribution of deformed parts

The comparison among profiles of formed parts and the designed shape in geometric accuracy test is illustrated in the Fig. 3a), while detailed error distributions are correspondingly shown in Fig. 3b). According to the curves in Fig. 3, the profile with 0.1 mm step depth has the best dimensional accuracy in the test compared with the target profile. Therefore, step depth can significantly affect the geometric accuracy. Specifically, the geometric accuracy increases when decreasing the step depth size. This can be due to the fact that the generated forming contours are more intensive when setting step depth at a small value. Consequently, the movement of the forming tool would be smaller between two adjacent parallel contours, providing more homogeneous material distribution and deformation as well as the reduction of the spring-back effect.

Surface morphology. Surface morphology of inner faces, namely the machined faces, of deformed cones was shown in Fig. 5. Obviously, in the comparison of surface waviness among three produced parts, step depth has a great influence on the surface finish quality. As can be seen in Fig. 5a) and 5b), there are obvious tool marks left on the machined surfaces when using large step depth sizes (0.6mm and 1.1mm). The distance between two adjacent tool marks on the formed surface, d, illustrated in Fig. 4, increases with the increase of step depth value. The relationship between d and ΔZ coincides with the sine law, as shown in Equation 1.

$$d = \Delta Z / sin\alpha \ . \tag{1}$$

Where α is the wall angle of the truncated cone.

Due to the geometric error, the measured d values (1.406mm and 0.751mm with ΔZ at 1.1mm and 0.6mm, respectively) are a little smaller than calculated ones (1.436mm and 0.783mm). On the contrary, as for small step depth (0.1mm), the formed surface shown in Fig. 5c) is much smoother than the two surfaces above, with no visible tool marks on the surface. Thus, it can be concluded that the surface quality can be improved by choosing small step depth in the ISF process.

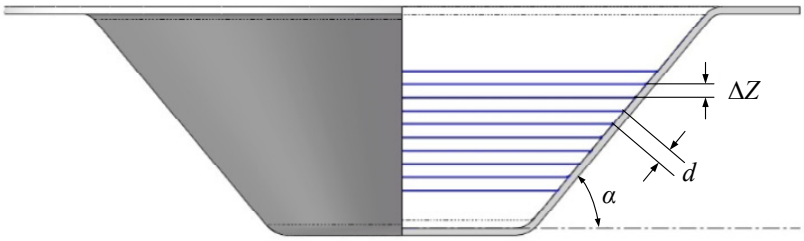

Fig. 4 Diagram of tool marks on the inner part face

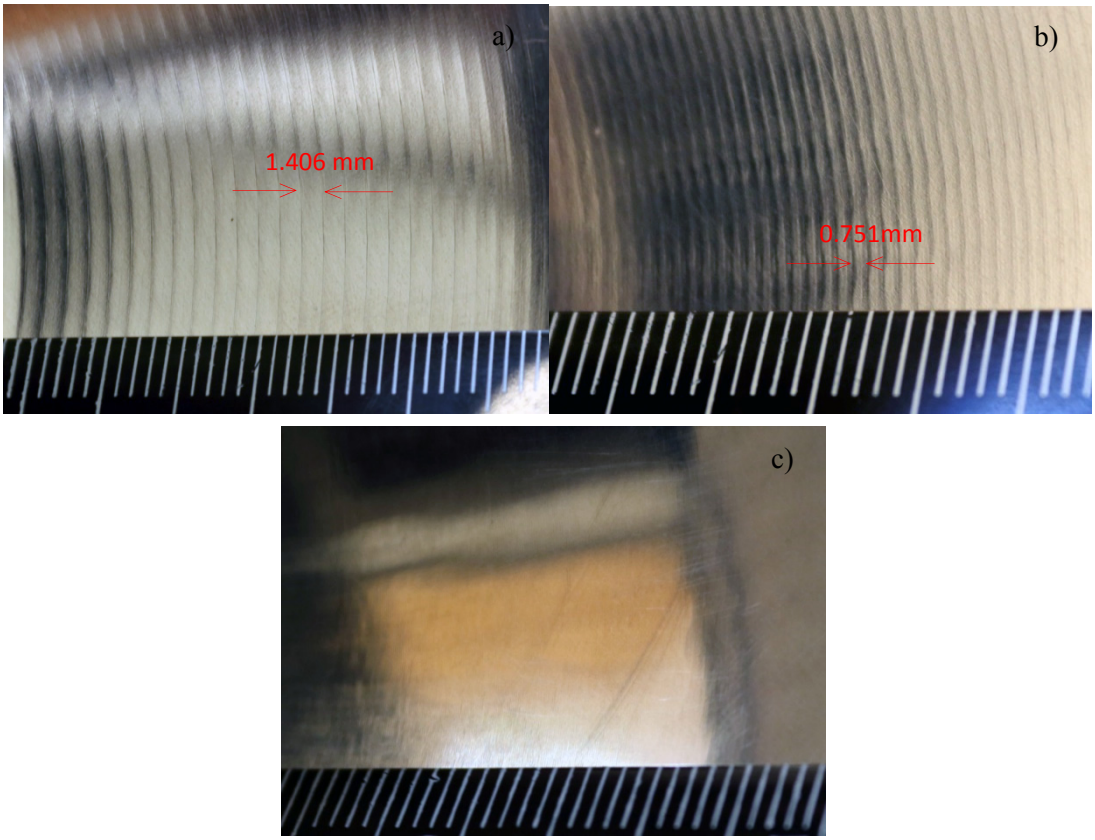

Fig. 5 Surface morphology of deformed parts in surface quality test: (a) ΔZ=1.1mm; (b) ΔZ=0.6mm; (c) ΔZ=0.1mm

Fracture analysis. Based on the analysis above, smaller step depth contributes to better geometric accuracy and part surface quality but lower efficiency due to the increase of forming time. More importantly, small step depth also adversely affects the forming process in terms of material formability, especially when the forming wall angle gets close to the forming wall angle limit. In the formability test, a truncated cone with a 60° wall angle (close to the wall angle limit) was used to evaluate the formability at different step depth sizes, with ΔZ ranging from 0.1 to 1.0 mm. The sheet fractured during the forming process with small step depth below 0.5 mm while only the parts with ΔZ over 0.7mm were successfully produced. Fig. 6a) shows the material fracture of a deformed cone with ΔZ being 0.1mm. Furthermore, the material facture occurs at smaller forming depth in Z direction when the step depth is smaller, which is illustrated in Fig. 6b). This can be due to the fact

that a smaller step depth size means a smaller tool contour distance between two neighbouring contours. Thus, more intensive contact between sheet material and tool end will happen in the ISF process, during which material in the contact zone of the metal sheet is pressed and hardened by the tool end in each forming contour. More already hardened material would be deformed again by the tool in the following several contours when using a tool path with smaller step depth. This leads to a great increase in the contact stress required to reach the target deformation. Consequently, sheet formability will be reduced due to higher stress state induced in the material. Therefore, too small step depth values should be avoided in consideration of material failure. In this case, 0.7 mm step depth was suggested to be the optimum value for the forming of the truncated cone with 60° wall angle.

(a)

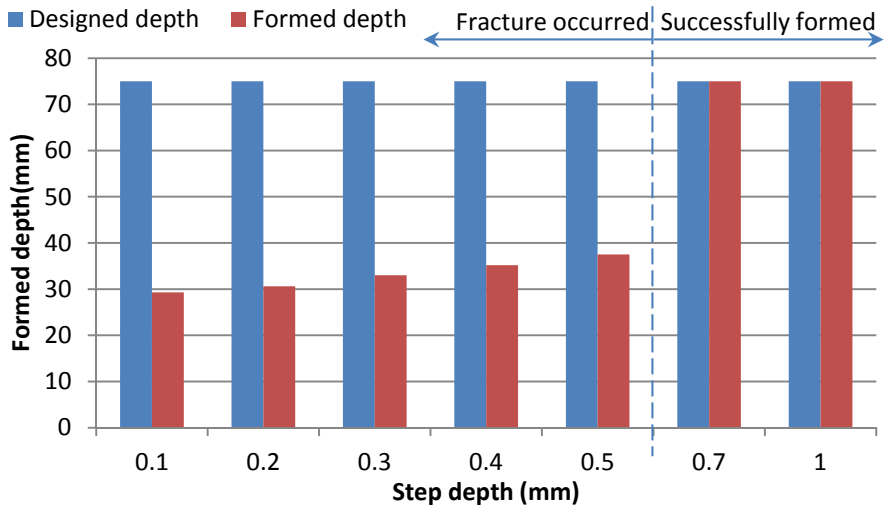

Fig. 6: (a) Part fracture in formability test (ΔZ=0.1mm); (b) Formed depth of parts in formability test

Conclusion and future work

This research aimed to provide a comprehensive investigation on step depth, as a critical process variable in ISF process, and to demonstrate that this variable is of great importance in design and control of tool path. Several experiments were conducted to investigate its influence on the part quality of the formed parts, including geometric accuracy, part surface quality and material formability. According to the results, smaller step depth leads to better geometric accuracy and part surface quality in ISF process. Parts deformed with large step depth cannot reach the required level both in geometric accuracy and surface quality but too small a step depth value should also be avoided with regard to the material fracture, especially when producing parts with large wall angles. Also, the forming time will increase as the step depth decreases. Even so, smaller step depth should be used within a reasonable range in tool path control and optimization. A trade-off among

geometric accuracy, part surface quality, material failure and forming time should be made in the design and control of tool paths and the first two aspects should be considered as priorities. It is clearly suggested that there is an optimum value of step depth in the ISF path design; for instance 0.7mm in the case presented. Further research on the optimization of step depth should be included in the design of an advanced ISF control system. The presented work is a foundation, which offers significant information for tool path control and optimization, and needs to be developed to further determine the constraints in tool path control system. The inaccuracy of parts is still obvious in using contour tool paths with constant step depth. For the future, control of tool path will be developed for part accuracy improvement and to reduce design time for new parts in the ISF process.

Acknowledgements The present work was supported by CSC scholarship.

References

[1] L. Filice, L. Fratini, F. Micari, Analysis of material formability in incremental forming, CIRP Ann. Manuf. Technol. 51 (2002) 199-202.

[2] Y. H. Kim, J. J. Park, Effect of process parameters on formability in incremental forming of sheet metal, J. Mater. Process. Technol. 130 (2002) 42-46.

[3] E. Hagan, J. Jeswiet, A review of conventional and modern single-point sheet metal forming methods, Proc. Inst. Mech. Eng. Pt. B J. Eng. Manufact. 217 (2003) 213-225.

[4] S. B. M. Echrif, M. Hrairi, Research and Progress in Incremental Sheet Forming Processes, Mater. Manuf. Processes 26 (2011) 1404-1414.

[5] J. Jeswiet, F. Micari, G. Hirt, A. Bramley, J. Duflou, J. Allwood, Asymmetric single point incremental forming of sheet metal, CIRP Ann. Manuf. Technol. 54 (2005) 88-114.

[6] J.R. Duflou, J. Verbert, B. Belkassem, J. Gub, H. Sol, C.A.M Henrard, A.M. Habraken, Process window enhancement for single point incremental forming through multi-step toolpaths, CIRP Ann. Manuf. Technol. 57 (2008) 253-256.

[7] G. Hirt, J. Ames, M. Bambach, R. Kopp, Forming strategies and process modelling for CNC incremental sheet forming, CIRP Ann. Manuf. Technol. 53 (2004) 203-206.

[8] A. Attanasio, E. Ceretti, C. Giardini, L. Mazzoni, Asymmetric two points incremental forming: improving surface quality and geometric accuracy by tool path optimization, J. Mater. Process. Technol. 197 (2008) 59-67.

[9] W. Hao, S. Duncan, Optimization of tool trajectory for Incremental Sheet Forming using closed loop control, In CASE, IEEE Int Conf, (2011) 779-784.

[10] R. Malhotra, N.V. Reddy, J. Cao, Automatic 3D spiral toolpath generation for single point incremental forming, J. Manuf. Sci. Eng. 132 (2010).

Paper 2

Model predictive control of incremental sheet forming for geometric accuracy improvement

Lu, H., Kearney, M., Li, Y., Liu, S., Daniel, W. J., & Meehan, P. A.

The International Journal of Advanced Manufacturing Technology

2015, Volume: 82, Pages: 1781-1794.

Model predictive control of incremental sheet forming for geometric accuracy improvement

Haibo Lu [a], Michael Kearney [a], Yanle Li [a], Sheng Liu [a], William J.T. Daniel [a] and Paul A. Meehan [a]

[a] School of Mechanical & Mining Engineering, University of Queensland, St Lucia, Brisbane, QLD 4072, Australia

Keywords: Incremental sheet forming; Model predictive control; Geometric accuracy

Abstract

Incremental Sheet Forming (ISF) is a highly flexible sheet forming process, but it suffers from poor geometric accuracy. This paper presents a feedback control strategy using Model Predictive Control (MPC) to obtain improved geometric accuracy in ISF. Based on the incremental deformation mechanism of ISF, a novel model for shape state prediction has been proposed. The step depth of the toolpath was optimised based on shape state feedback during the forming process. Two different cases were studied for experimental validation of the developed control strategy. Comparisons between formed parts in both controlled and uncontrolled ISF processes were implemented in terms of cross-sectional profiles, formed depth at the bottom area and global deviation distribution. Results show that the geometric accuracy in ISF with feedback control has been greatly improved at the bottom area of the formed parts compared with a standard ISF approach without control. Improved geometric accuracy has been achieved on the wall of the parts as well.

1. Introduction

Incremental sheet forming (ISF) is a flexible sheet forming process in which sheet parts are formed by a single tool with a smooth end following a predefined toolpath. Compared with traditional metal sheet forming processes, such as stamping and deep drawing, ISF has no need of dedicated tooling or specialised dies so that various shapes can be fabricated using the same tooling [1]. The product design can be modified easily and quickly by changing the toolpath when the part shape changes [2]. Additionally, this technology possesses higher formability than conventional ones due to the localised deformation and incremental nature of the process [3]. In small batch production or rapid prototyping, ISF has been considered as a promising alternative to traditional sheet forming techniques that suffer from high cost in fabricating and maintaining dies as well as the lack of flexibility. Besides this, the time cost for the design, test and fabrication of dedicated dies and/or punches, which accounts for a large portion of the product prototyping time, can be saved in ISF. ISF has great potential to meet the new trend in the sheet metal forming industry that the life-cycle of pre-series and final products is becoming greatly shortened and product demand is becoming increasingly costumer-oriented [4].

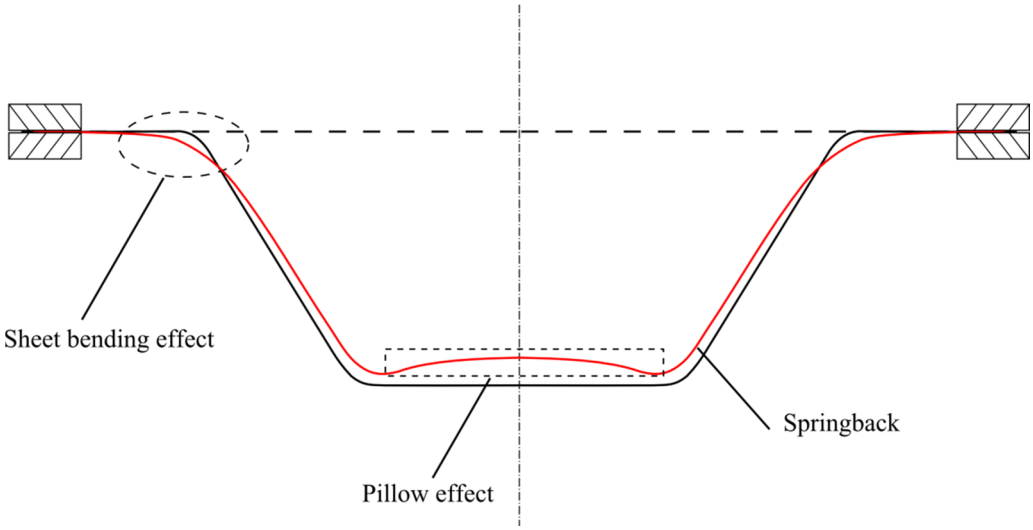

Figure 1 Geometric inaccuracy in ISF.

The geometric accuracy of the final parts is one of the most significant aspects in forming industries. However, poor geometric accuracy has been the major limitation of ISF in its development ever since its early conceptions were proposed in [5, 6]. There are three types of geometric inaccuracies detected in ISF processes [7], as shown in Figure 1. At the end of the forming process, the formed blank will move backwards slightly both at the wall area and the bottom area after the tool is released. This phenomenon is called 'springback' and is common in the sheet metal forming industry. Generally, springback is caused by the reduction of stress when the removal of the deformation load takes place. Sheet springback is the major type of ISF defects. Secondly, another kind of error, the so called 'pillow' effect, can be observed at the undeformed bottom area. It is due to the bulging of sheet blank during the forming process [8]. Besides this, dimensional errors can also be detected around the clamped edges of the metal sheet. This type of inaccuracy is caused by the sheet bending effect [7]. It is uncontrollable in single point incremental forming (SPIF) [9]. Therefore, this kind of dimensional error is not considered in the control of ISF in this work.

Since low geometric accuracy has greatly limited the industry take-up of ISF, the improvement of accuracy has become a key research aspect involved with ISF. In previous literature, different attempts have been conducted to enhance geometric accuracy in ISF. Attanasio et al. [4, 10] investigated the effects of two path generation methods on surface quality, dimensional accuracy and thickness distribution and optimised the two parameters in a series of tests. They concluded that the toolpath type with small scallop height and variable step depth contributes to good accuracy. Allwood et al. [11] proposed the use of partially cut-out blanks in which tabs or holes were created at the perimeter of the target part. The aim of this method was to reduce geometric deviations by localising deformation to the area where the tool travels. The results indicated that cut-outs did not contribute to large improvement in part accuracy. They also concluded that the idea of localising the deformation area around the tool earlier has great significance in the fabrication of more accurate parts via ISF. Bambach et al. [12] proposed a method by combining multi-stage forming with a stress-relief annealing process to improve the final accuracy of formed and trimmed parts. Using the proposed multi-stage approach, a pyramidal benchmark part and a fender section were fabricated and the geometric accuracy obtained was improved compared with single-stage forming. Then, an additional stress-relief annealing process after multi-stage forming annealing was adopted to reduce the final deviations, which has provided improved part accuracy although the maximum error (4.9

mm) is still large. Interestingly, Ambrogio et al. [13] used a novel two-stage approach by adding an additional back-drawing incremental forming step after the conventional ISF deformation to reduce geometric errors.

In ISF processes, the toolpath is essential and has direct influence on the geometric accuracy. Therefore, toolpath optimisation and correction is one of the most promising approaches for improving geometric accuracy. Ambrogio et al. [14] proposed a preliminary toolpath modification strategy by using a steeper slope in the first half depth of the part. Hirt et al. [15] developed a toolpath correction algorithm to enhance the geometric accuracy. After analysing dimensional deviations between the trial part produced using a regular toolpath and the ideal part, the points of the new toolpath were calculated by mirroring the corresponding points on the formed part along the designed part. Several correction processes could be repeated until the geometrical accuracy reaches the required level. Behera et al. [16] proposed another toolpath compensation strategy in SPIF by using multivariate adaptive regression splines (MARS) for the prediction of the formed shape. Based on the detection of the category of feature and interaction between features in the shape design, the formed profile is firstly predicted in the proposed model. To offset the deviations between the predicted and ideal profiles, a compensated single stage toolpath can be generated by translating the points in the STL model. Their result showed that the compensated toolpaths can reduce the average dimensional errors to within ±0.4 mm. Fu et al. [17] developed an iterative algorithm to correct toolpath in SPIF based on Fast Fourier and wavelet transforms. The iterative correction of tool path in the algorithm was conducted in Finite Element (FE) simulation. A truncated pyramid-shaped workpiece with improved geometric accuracy was fabricated using the corrected toolpath after three iterations in simulation. This method can suffer from the time consuming nature of FE method and its complexity.

Also, some studies on the control of the ISF process to correct the toolpath have been performed to achieve better geometric accuracy. Allwood et al. [18] presented an online feedback control model formed from a set of spatial impulse responses found by linearisation around a pre-planned toolpath. In the results, the final dimensional deviation was reduced using feedback control. However, their model requires the trial fabrication of workpieces to obtain the spatial impulses of a toolpath before forming the part in ISF with feedback control. Their discussion also indicated that the proposed control approach would be difficult to conduct for freeform parts. Wang et al. [9, 19] used a closed loop MPC control scheme to optimise the tool trajectory of an ISF process. The results in their work showed that the final geometrical errors were reduced, compared with a standard contour following approach. Nevertheless, the predictive model is also based on the trial fabrication of parts in open loop ISF. Also, the global geometric accuracy of the parts was not presented in their studies in which only the geometric errors between cross-sectional profiles of parts were analysed.

The corrected/optimised toolpath will lead to more accurate shapes. This idea has been widely accepted for ISF toolpath control and/or optimisation in previous work discussed above. This work proposes a novel MPC control strategy for ISF to improve geometric accuracy through toolpath control and optimisation. In this strategy, the predictive control model is based on the incremental deformation mechanism of ISF. Control actions can be conducted directly without forming a trial part in open loop ISF previously. Step depth, a critical toolpath parameter, is optimised by solving a finite-horizon optimal control problem at each forming step in a receding manner. Experiments, in

which two different shapes were formed, were performed in single point incremental forming (SPIF) to validate the proposed control strategy. Geometric accuracy of clamped parts obtained in controlled and uncontrolled ISF processes are compared by analysing the cross-sectional profiles, formed depth along the steps and the global dimensional deviation distribution of the parts.

2. Methodology

2.1 Toolpath parameters

During the ISF process, the toolpath directly affects the forming accuracy since the shape is formed by a simple tool following a designed toolpath. Therefore, toolpath control and optimisation has great potential in improving part accuracy in ISF. As for toolpath generation in ISF processes, the most commonly used method is the parallel contour strategy. The contour toolpath is usually generated in commercial CAM software using a surface milling module. It consists of a certain number of z-level contours that are parallel to each other, as shown in Figure 2. Two critical parameters of the contour toolpath are step depth (Δu_z) and horizontal step increment (Δu_h). In the parallel contour strategy, Δu_z is generally defined by the user. After that, the value of Δu_h will be calculated by the CAM software based on the designed shape and the Δu_z value. However, this method fails to fabricate parts with accurate geometry due to springback and other effects. To improve the part accuracy, a MPC strategy is utilised to control and optimise the toolpath. During the forming process, Δu_z is optimised to achieve a final shape with better geometric accuracy, while Δu_h is the same as that of the initial toolpath generated in the CAM software and it does not need to be constant.

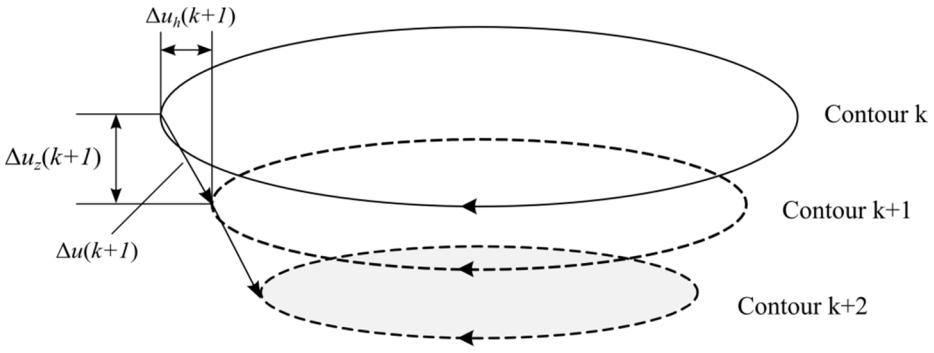

Figure 2 Two critical parameters of the contour toolpath.

2.2 Model Predictive Control algorithm

A MPC algorithm based on shape feedback has been developed for feedback control of ISF processes. In this MPC algorithm, control actions are implemented by solving a finite-horizon optimal control problem at each forming step which contains a single contour. At each step, the MPC optimiser optimises the step depth (Δu_z) in a predefined horizon by analysing the difference between the target shape state and the predicted one. Only the first optimal move (optimised parameters) will be applied in the next forming step. The structure of MPC application in ISF is shown in Figure 3.

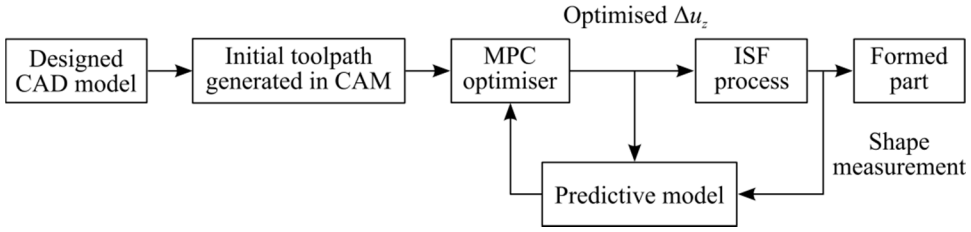

Figure 3 Structure of MPC application in ISF.

To improve the poor geometric accuracy of the ISF process, this MPC control strategy optimises $\triangle u_z$ in a receding horizon fashion at each forming step while horizontal increment $\triangle u_h$ keeps unchanged from the initial toolpath. $\triangle u_z$ is defined as the input (Δu) in this MPC model. The controller is to drive the formed shape state to be as close as to the target one at each step. As a result, errors between the final shape and the ideal one can be reduced greatly through receding horizon control. Therefore, the predictive controller can be characterised as the following optimisation problem at each step *k*:

$$\min\ J = \| \hat{Y} - W \|^2 + \lambda \Delta U^T \Delta U \tag{1}$$

$$\text{subject to}\ \ \Delta U(k) = \left[\Delta u_{k+1}, \Delta u_{k+2}, \Delta u_{k+3}, \ldots, \Delta u_{k+N_p} \right]^T, k = 1, 2, \ldots, N$$

$$\Delta u_{min} \le \Delta u_{k+i} \le \Delta u_{max}, i = 1, 2, \ldots, \mathrm{N}_p$$

where J is the cost function; N is the number of steps; N_p is the prediction horizon; ΔU is the input; $\hat{Y}$ is the predicted geometry state; W is the target geometry state; The second item of the cost function J is to conduct penalties on large oscillation of the control inputs; λ is the weighting coefficient and is a non-negative scalar. In this work, an optimal λ value, 0.2, is adopted after tuning.

In this paper, a truncated cone and a truncated pyramid are formed to test the developed feedback control model. For these two shapes, cross-sectional profiles through the centre are chosen to capture the dimensional features [16, 18, 19]. Therefore, cross-sectional profile states are used to represent the shape state in the control process.

At the beginning of step k+1, the profile state of last step is measured as $y(k) \in R^n$, which can be written as,

$$y(k) = \left[y_k^1, y_k^2, y_k^3, \ldots, y_k^{n-1}, y_k^n \right]^T \tag{2}$$

where n is the number of profile state points.

The state of next step is $y(k+1)$, which is expressed as,

$$y(k+1) = f(y(k), \Delta u_{k+1}) \tag{3}$$

Although studies on ISF have been conducted for decades, there is still no accurate mathematical model that can be used to formulise this forming process in terms of geometry state. In the ISF

process, the part is formed by a single tool and the sheet material undergoes deformation caused by bending, shearing and the springback effect, which makes the forming mechanism quite complex. Hence, it is impossible to build such a perfect model (f) to predict the future profile state. In previous literature, linear simplifications have been made to estimate the function f. Allwood et al. [18] used a linear impulse response model to characterise the shape states during the forming process. Wang et al. [9] made a linearisation around the contour trajectory based on shape states measured in open loop forming. In this paper, we estimate the profile state of the next step by assuming that future profile state is the linear combination of currently formed profile state and the deformation under the effect of the future input. This is based on the incremental nature of ISF. Therefore, the prediction of profile state in next step can be obtained in Equation (4).

$$\hat{y}\left(k+1\,|\,k\right)=y(k)+B_{k+1}\Delta u_{k+1} \tag{4}$$

Similarly, at step k, the predicted profile states along the prediction horizon are given in the following equation,

$$\begin{aligned}\hat{y}\left(k+2\,|\,k\right)&=\hat{y}\left(k+1\,|\,k\right)+B_{k+2}\Delta u_{k+2}\\&=y(k)+B_{k+1}\Delta u_{k+1}+B_{k+2}\Delta u_{k+2}\\&\vdots\\\hat{y}(k+N_p\,|\,k)&=y(k)+B_{k+1}\Delta u_{k+1}+B_{k+2}\Delta u_{k+2}+\ldots+B_{k+N_p}\Delta u_{k+N_p}\end{aligned} \tag{5}$$

where $B_{k+j}=\left[b_{k+j}^{1},b_{k+j}^{2},\ldots,b_{k+j}^{n-1},b_{k+j}^{n}\right]^{T}$, $j=1,2,\ldots,N_p$.

Note that all predictions in the future are formulated in terms of currently measured state $y(k)$ and the future control move Δu_{k+j},where $j=1,2,\ldots,N_p$.

Equations (4) and (5) can be collected together into a compact matrix form as,

$$\hat{Y}\left(k\right)=Y\left(k\right)+B\Delta U\left(k\right) \tag{6}$$

where $\hat{Y}\left(k\right)=\left[\hat{y}\left(k+1\,|\,k\right),\hat{y}\left(k+2\,|\,k\right),\ldots,\hat{y}\left(k+N_p\,|\,k\right)\right]^{T}$ are the predictions along the prediction horizon; $Y(k)=[y(k),y(k),y(k),\ldots,y(k)]^{T}$; $\Delta U(k)=\left[\Delta u_{k+1},\Delta u_{k+2},\ldots,\Delta u_{k+N_p}\right]^{T}$; B is the coefficient matrix and can be expressed as,

$$B=\begin{bmatrix}B_{k+1}&0&0&\cdots&0\\B_{k+1}&B_{k+2}&0&\cdots&0\\B_{k+1}&B_{k+2}&B_{k+3}&\cdots&0\\\vdots&\vdots&\vdots&\ddots&0\\B_{k+1}&B_{k+2}&B_{k+3}&\cdots&B_{k+N_p}\end{bmatrix} \tag{7}$$

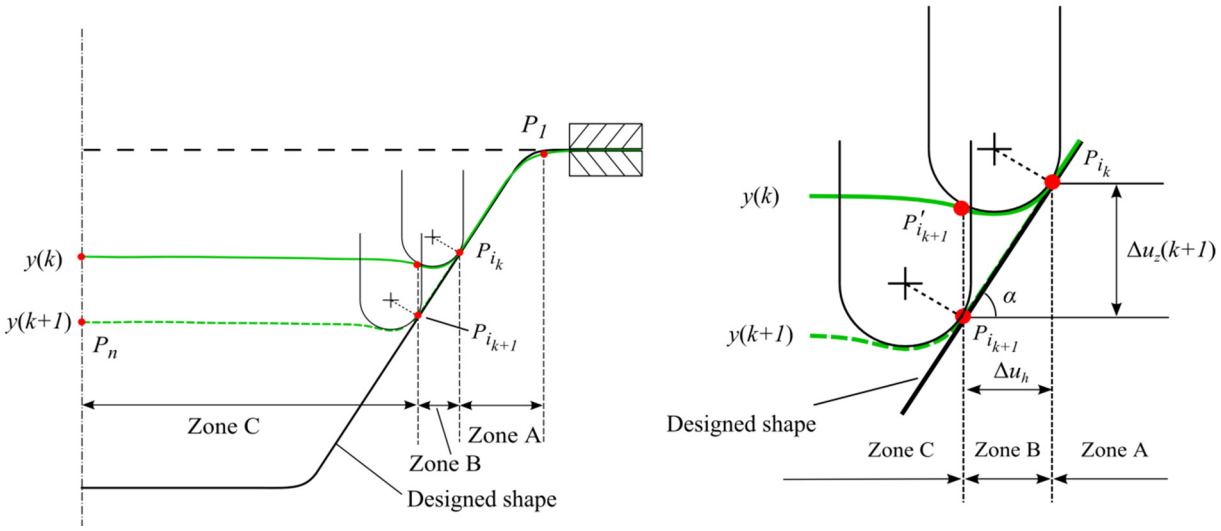

Figure 4 Incremental deformation of the metal blank between two neighbouring steps.

Actually, the coefficient matrix determines how the profile state changes when the tool is driven by future input moves. Figure 4 illustrates the deformation of the metal blank from step k to k+1 in an example case. This can be generalised to any other shapes that can be produced via ISF. The black line is the designed shape. As for the profile of each step, there are *n* points on the profile to represent the profile state. The sequence number of these points increases from 1 to n from the top edge to the centre. We denote the point of tangency, where the tool is tangent to the wall, at step k and step k+1 as P_{i_k} and $P_{i_{k+1}}$, respectively. $P'_{i_{k+1}}$ is the projection of $P_{i_{k+1}}$ onto profile $y(k)$. The profile $y(k+1)$ can be divided into three zones, namely Zone A ($P_1 \sim P_{i_k}$), Zone B ($P_{i_k} \sim P_{i_{k+1}}$), and Zone C ($P_{i_{k+1}} \sim P_n$). As the tool moves down from contour k to contour k+1, the material in Zone C will be pushed down by approximately the step depth size (Δu_z) and the material in Zone B will be pushed and pulled down along the wall while the material in Zone A has been already formed and will be deformed very slightly, which can be ignored. That is, the effect of tool movement on the material in Zone A is not very significant between two neighbouring steps so that we make a simplification without taking the effect in Zone A into account at each step.

Based on this, some simplifications are made to obtain the coefficients, B_{k+1}. More specifically, the B_{k+1} values of state points within Zone A can be estimated as 0 while those values of points within Zone C can be estimated as 1. Regarding Zone B, the area wrapped by profiles, namely $y(k)$ and $y(k+1)$, can be simplified as a triangle. The B_{k+1} values at point P_{i_k} and $P_{i_{k+1}}$ are 0 and 1, respectively. A linearization method is used to get the B_{k+1} values. In this zone, the B_{k+1} value linearly increases from 0 to 1 with the slope value as $\tan\alpha$, where α is the local wall angle. Consequently, b^i_{k+1} is expressed in the following equation. In general, there are only a few number of points belongs to Zone B.

$$b_{k+1}^{i}=\begin{cases}0, & 0<i<i_k\\ f_{b_{k+1}}(i), & i_k\le i\le i_{k+1}\\ 1, & i_{k+1}<i\le n\end{cases} \tag{7}$$

where $f_{b_{k+1}}$ is a linear function and the dependent variable increases from 0 to 1 in $[i_k, i_{k+1}]$.

Then, all $B_{k+j}=\left[b_{k+j}^{1}, b_{k+j}^{2}, \ldots, b_{k+j}^{n-1}, b_{k+j}^{n}\right]^T, j=1,2,\ldots,N_p$ can be obtained in the way described above.

2.3 Quadratic Programming for MPC solution

The optimisation problem solved at each step of the MPC control process is a Quadratic Programming (QP) problem. It involves optimising a quadratic objective function subject to equality and inequality constraints that are affine. It is a special type of convex optimization problem. A standard quadratic programming problem can be formulated in the form [20],

$$\min \frac{1}{2}x^T Px+q^T x+r \tag{8}$$

$$\text{subject to } Gx\preceq h \text{ (inequality constraints)}$$

$$Bx=c \text{ (equality constraints)}$$

where P, q, r, G, h, B and c are compatible matrices or vectors. Specifically, P should be symmetric and positive semidefinite to ensure that the objective is convex quadratic.

In the developed MPC algorithm, the optimization problem at each step is a typical QP problem. Therefore, QP is used to get the optimal input ΔU for the receding optimisation problem in constrained MPC control of ISF. At step k, the cost function can be expressed as,

$$J=\| \hat{Y}-W \|^2+\lambda \Delta U^T \Delta U \tag{9}$$

By putting (6), (8) and (9) together, the cost function can be written as,

$$\begin{aligned} J &=\| Y+B\Delta U-W \|^2+\lambda \Delta U^T \Delta U \\ &=U^T(B^T B+\lambda I)\Delta U+2(Y-W)^T A\Delta U+(W-Y)^T(W-Y) \\ &=\frac{1}{2}\Delta U^T P\Delta U+q^T \Delta U+r \end{aligned} \tag{10}$$

where $P=2(B^T B+\lambda I), q^T=2(Y-W)^T B, r=(W-Y)^T(W-Y)$.

Figure 5 illustrates the flow chart of MPC control process in ISF. The target profile states and initial toolpath are system inputs. At step *k*, after the measurement of currently formed shape state, the optimal input ($\Delta U^*(k)$) is obtained by solving a QP problem. Only the first move of $\Delta U^*(k)$ will be applied in the next step. Then, the optimisation process will be repeated until the part with good geometric accuracy has been formed.

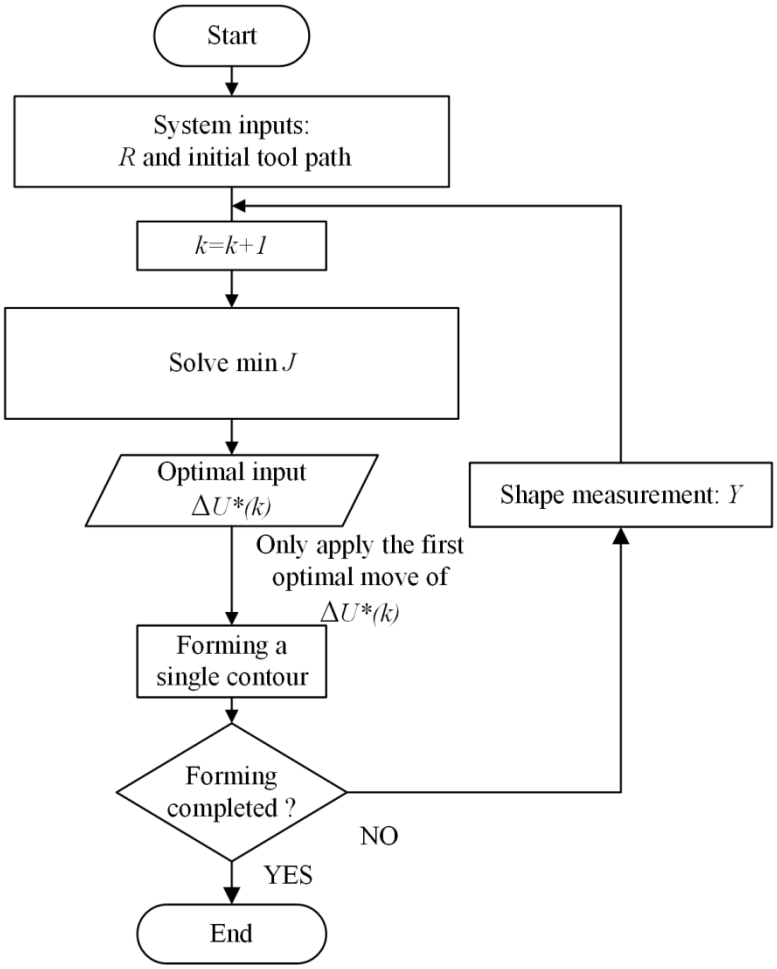

Figure 5 Flow chart for MPC application to ISF.

2.4 Experiment setup

The ISF forming platform used in the lab is an AMINO® DLNC-PC ISF machine, as shown in Figure 6. This is a dedicated machine, with a FANUC controller for numerical control, designed for the ISF process by Amino Corporation. In the experimental design, the sheet blank is clamped between clamping blocks and a steel backing plate to prevent any movement of the blank edges during forming process. The metal blank, with 1.6 mm in thickness and 300 mm × 300 mm in size, is made of aluminium (7075-O), a metal material used in automotive and aviation applications. A 30 mm diameter cylindrical steel tool with a ball end is used to deform the blank. The tip of the tool is tungsten carbide and the body is made of K110 steel which was hardened and tempered to HRC60. Lubricant (oil-Shell Tellus Oil 68) is used to reduce the wear and friction between the tool and the metal blank.

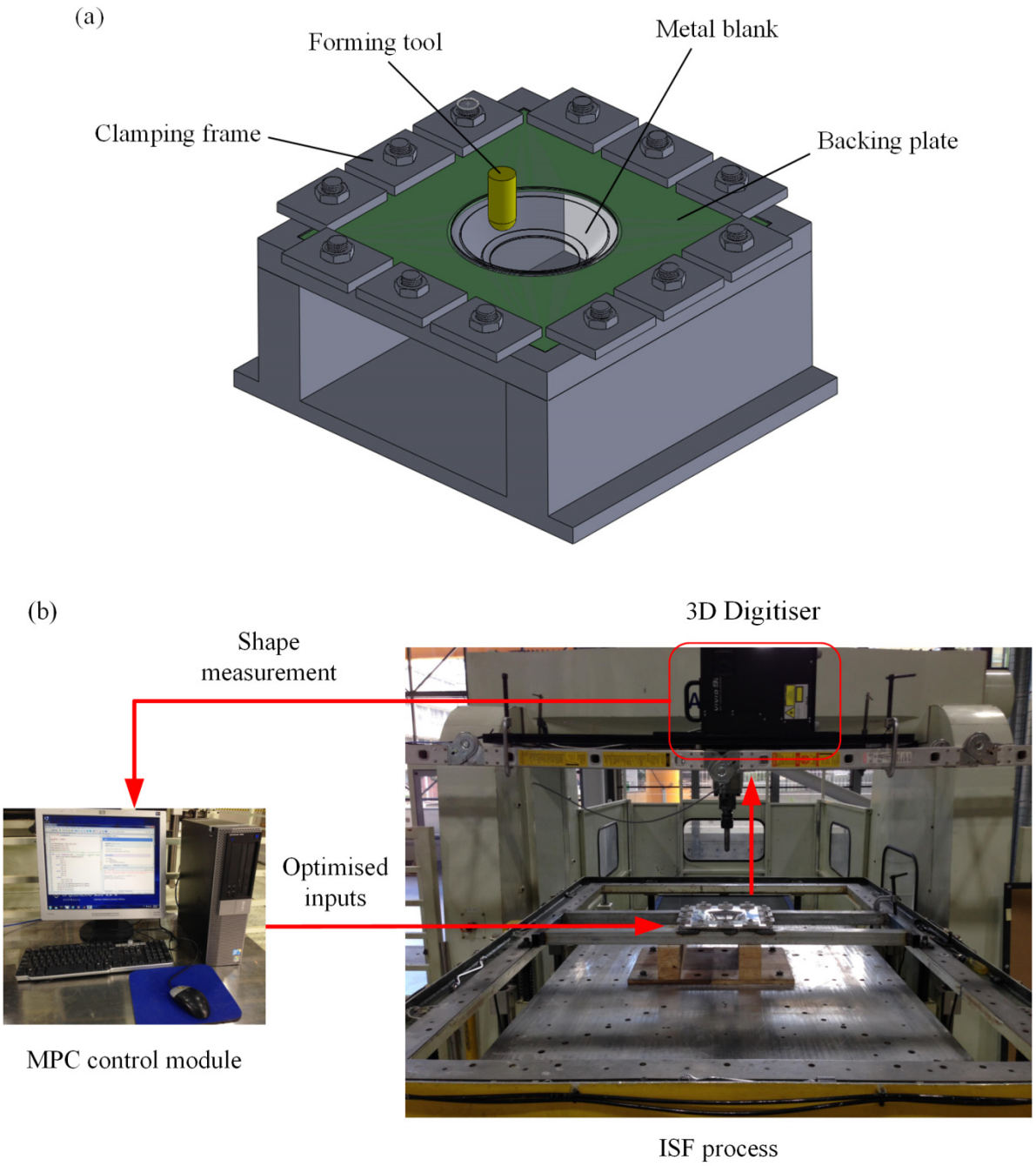

Figure 6 (a) Single point incremental forming setup. (b) ISF with closed-loop feedback control.

To evaluate the geometric accuracy, the 3D geometry of formed parts can be measured using a Non-contact 3D Digitiser (VIVID 9i), as shown in Figure 6. The scanning accuracy is within ±0.05mm, which is accurate enough for the ISF shape measurement. Scanning a formed shape at each step only takes about 2.5 seconds. GEOMAGIC Qualify is used to produce 3D geometry data of the scanned shape and analyse the dimensional error between deformed test parts and designed CAD models. Specifically, both produced and designed profiles are given in large sets of points in the same Cartesian coordinate system.

In this work, the cross-sectional profile along a defined section plane is used to evaluate the geometric accuracy since test shapes are symmetric. A system plane (plane XOZ) across the symmetric axis of the test shape is set as the section plane. The deviation in Z direction between the designed and fabricated profiles is calculated as the geometric error in the cross-sectional comparison.

To validate the developed closed-loop feedback control strategy, a truncated cone and a truncated pyramid, two commonly used shapes in the validation of ISF processes, were chosen as benchmark shapes for the experiments. CAD models of the test shapes are designed in SOLIDWORKS. The parameter settings of experiments are summarised in Table 1. The designed depth is consistent with previous approaches [9, 19].

Table 1 Experimental parameter settings

ISF Parameters	**Truncated cone (Case 1); Truncated pyramid (Case 2)**
Wall angle (°)	50
Designed depth (mm)	30
Feed rate (mm/min)	4000
Initial sheet thickness (mm)	1.6
Tool diameter (mm)	30
Step depth / Δu_z (mm)	2 (open loop); varying (controlled)

In this work, the initial toolpath used for feedback control is generated using a CAD/CAM software, Unigraphix NX7.5 (UG NX7.5) from Siemens. Figure 7 illustrates the initial toolpaths of test shapes. Both of them are parallel contour toolpaths with a constant step depth.

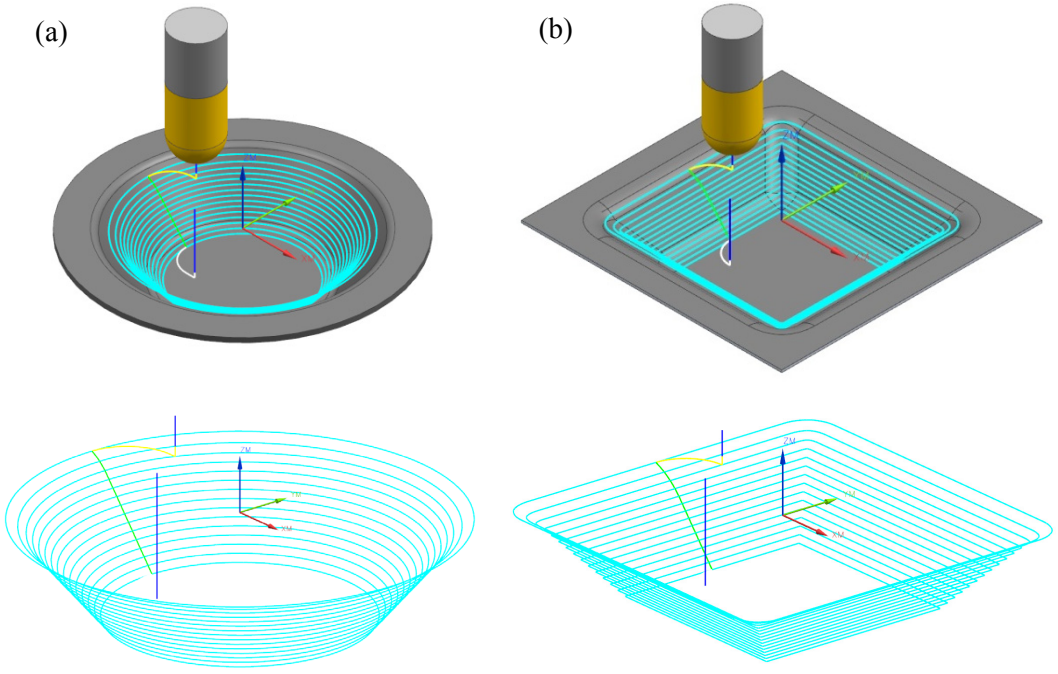

Figure 7 Illustration of initial toolpaths of test shapes: (a) Truncated cone; (b) Truncated Pyramid.

3. Results

The geometry of the deformed components is measured at each step. To demonstrate the feedback control strategy is effective, the formed shape at each step is compared with the one formed in open loop ISF and the target one via cross-sectional profile comparison. Specifically, dimensional errors of the whole shape in both ISF with and without control are analysed by using contour graphs. In addition, history of the average depth at the bottom and its error along the steps are compared to provide the evolution of the control action and its effectiveness.

3.1 Case 1: Truncated Cone

The test shape in case 1 is a truncated cone. The results are shown in Figure 8-12. In the first two steps of the forming process, dramatic springback was observed when the tool is released due to a large proportion of elastic deformation in the early forming stage. The formed shape is nearly flat and much shallower compared with the one with target depth. This makes it difficult to capture the shape features for the comparison work. Therefore, control actions are conducted from the end of the third step after measuring the formed shape at this step.

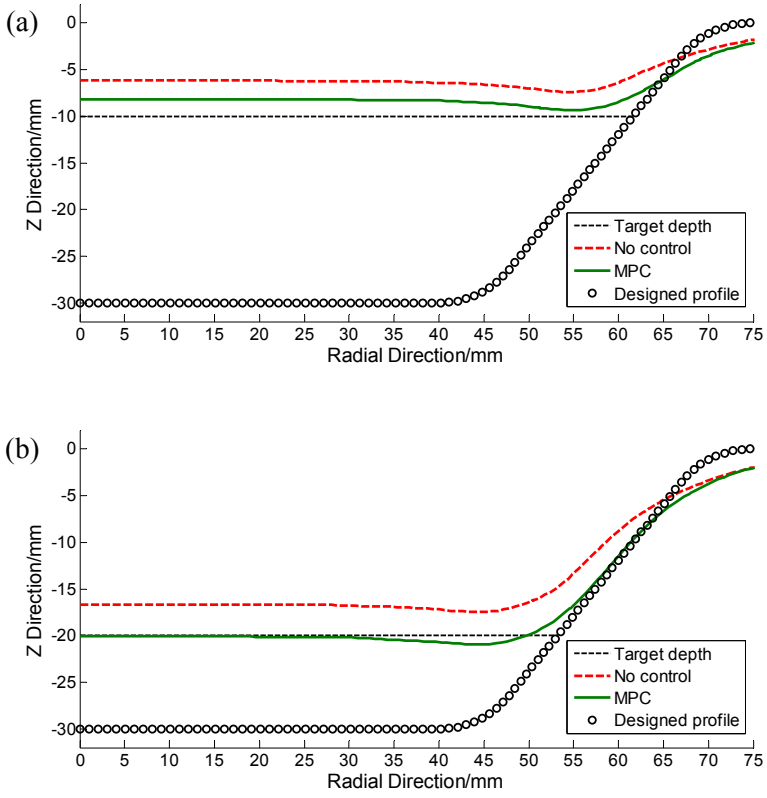

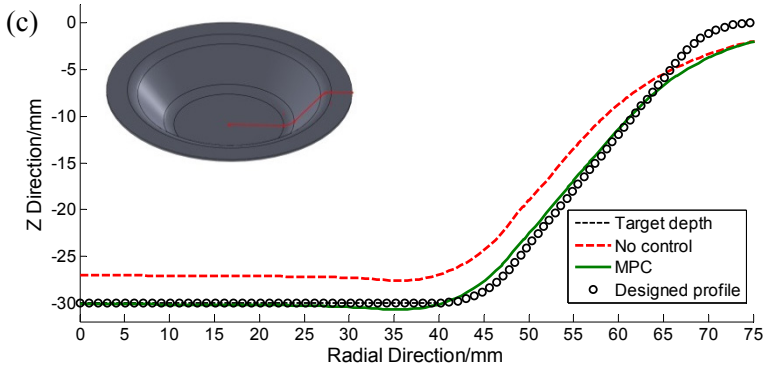

Figure 8 Cross-sectional comparison at three steps: (a) Step 5; (b) Step 10; (c) Final Step.

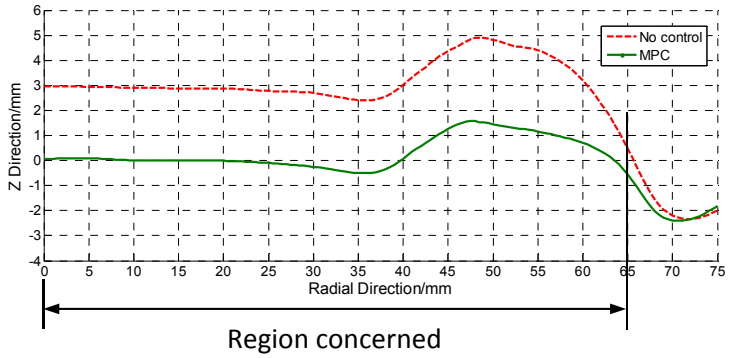

Figure 9 Error distribution of truncated cone finally formed.

In Figure 8, formed shapes in ISF with MPC control and without control are compared together with the designed one by using cross-sectional profiles at three different steps. For the validation of the developed MPC feedback control strategy, the number of steps is set as 15. In this paper, we only present the profile comparison at 5th, 10th and final steps that represent the early stage, the middle and the end of the control process, respectively. Figure 8(a) shows that in the early stage of the MPC control process, the errors between the formed profile and the target are reduced but still need to be improved. This is also shown in Figure 10 which shows the history of the average depth at the bottom and its error during the ISF processes. Figure 8(b) and (c) illustrate that the dimensional accuracy have been significantly improved compared with that in open loop ISF. The error distributions of the final profiles are shown in Figure 9. The final formed shape and the designed one are well-matched in the region concerned (the bottom area and the wall area). The geometric errors at the bottom have been greatly reduced.

To provide an overview of the effectiveness of the developed feedback control strategy, the average depth of the part bottom, is analysed along the steps, as shown in Figure 10. More specifically, the average depth is the average of the formed depth of points at the bottom plane.

Step depth, is optimised from the third step to the end. From step 3 to step 7, the formed depth is getting closer to the target one at each step. From then on, the error between the formed depth and the designed one is greatly reduced (within ±0.2mm). Optimised inputs at different steps are varying while the inputs are set as constant at 2mm in open loop ISF, as illustrated in Figure 11.

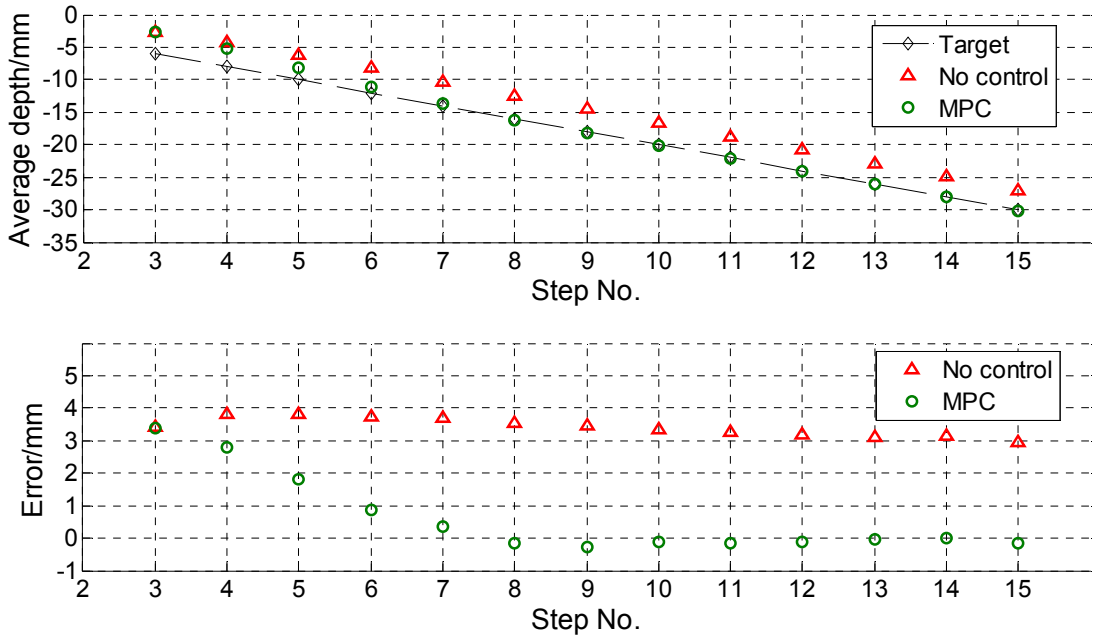

Figure 10 History of average depth of the part bottom and its error along the steps.

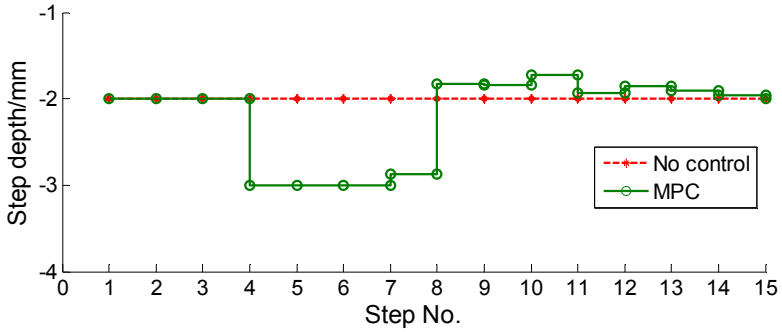

Figure 11 Inputs along the steps.

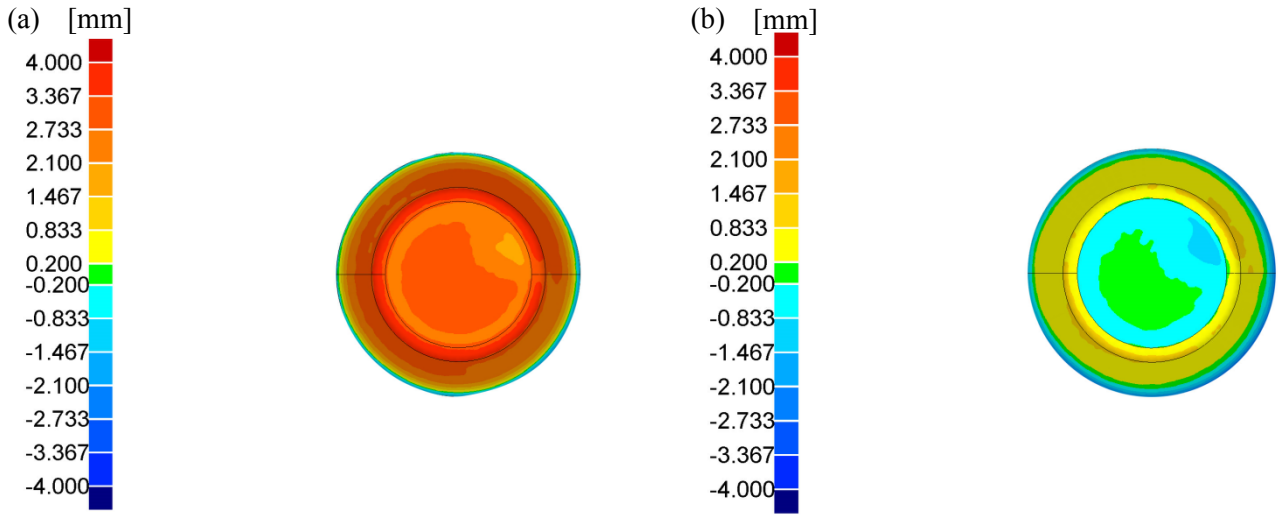

Figure 12 Top view of accuracy colour plots: (a) Formed cone in uncontrolled ISF; (b) Formed cone in ISF with MPC control.

To examine the global geometric accuracy, parts formed in both uncontrolled and controlled ISF are compared with the nominal model through colour contour plots. The scanned point cluster can be directly compared with the CAD file in 3D comparison module of Geomagic Qualify. Figure 12 shows the global dimensional accuracy in normal direction in these two processes. Results in the figures indicate that the geometric deviations in ISF with MPC control has been reduced a lot in comparison with that in uncontrolled ISF. More specifically, the geometric error in the bottom area has been reduced from ±3.0mm to ±0.25mm. Improved geometric accuracy also has been observed in the wall area but does not reach the accuracy level of the bottom area. This is due to the fact that the horizontal increment values are kept the same as those used in the uncontrolled ISF process and only the step depth values are optimised during the forming process with control. For the geometric error around the clamped edges, the area with dark blue colour in contour plots, is uncontrollable in SPIF, the accuracy in this area is not considered in this paper.

Figure 8 and Figure 12 also show that changes of step depth values have direct influence on the deformation of the wall area. In a single step with the horizontal increment set as unchanged, the wall area will be stretched down further by the tool as current step depth increases, and vice versa. Similarly, the wall area of formed shape can be driven closer to the target one through adjusting the horizontal increment values. The geometric accuracy of the wall area could be further improved by optimising the horizontal increment and step depth at the same time. Overall, this will be covered by future work.

3.2 Case 2: Truncated pyramid

The results for the truncated pyramid are shown in Figure 13-17. Like case 1, the control actions were also conducted after measuring the formed part at the third step. The cross-sectional comparison of formed profiles at three steps is shown in Figure 13. Figure 13(a) illustrates that geometric errors are reduced in the early stage of the feedback control process but are still relatively large. This is also shown in Figure 15 that plots the history of the average depth and its error during the ISF processes. Figure 13(b) and (c) represent the stable stages of the control process. Figure 14 shows corresponding error distributions of the final profiles in Figure 13(c). The dimensional accuracy has been greatly enhanced compared with that in open loop ISF. The final formed shape and the designed one are well-matched at the bottom.

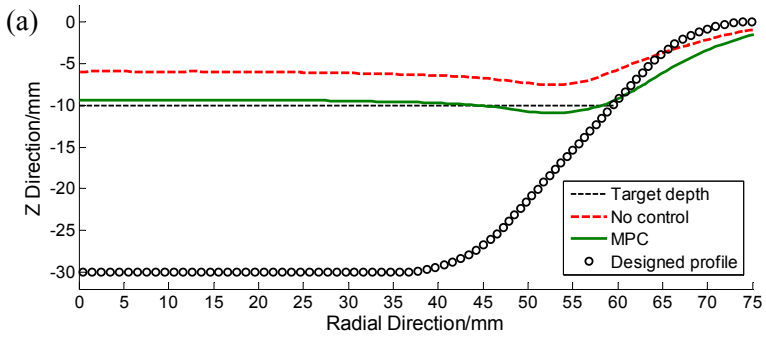

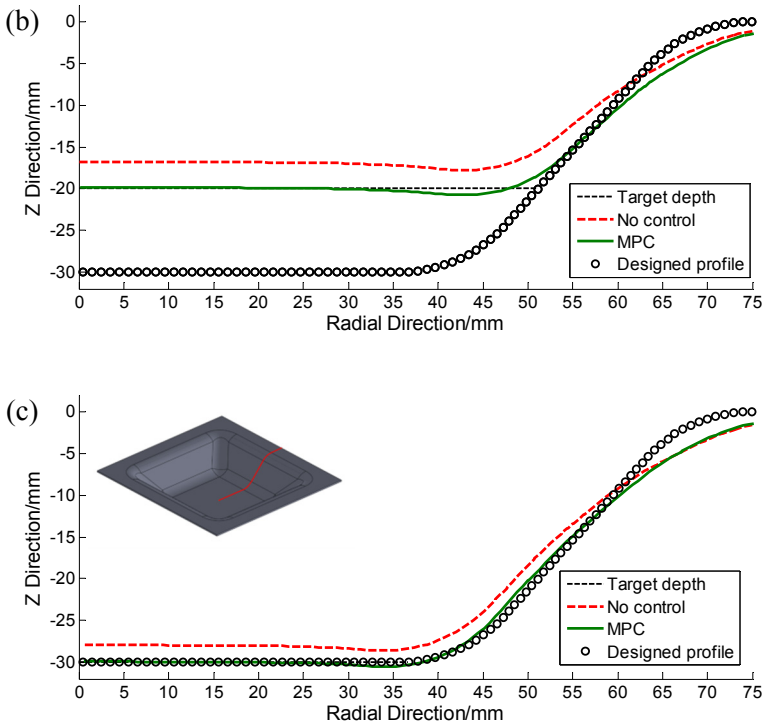

Figure 13 Cross-sectional comparisons at three steps: (a) Step 5; (b) Step 10; (c) Final Step.

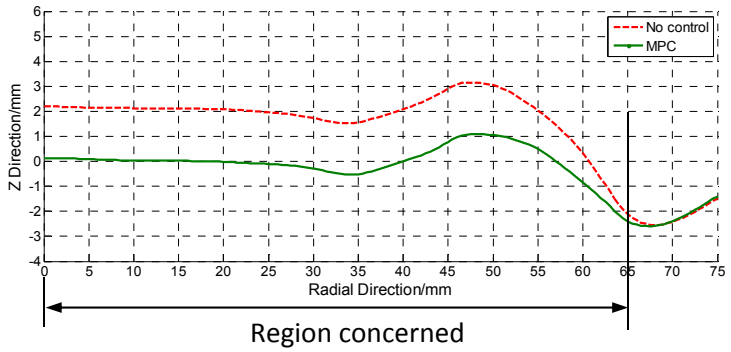

Figure 14 Error distribution of truncated pyramid finally formed.

Figure 15 illustrates the average depth of the bottom along the steps. This demonstrates the effectiveness of developed feedback control strategy. The input, namely step depth, is optimised from the third step to the end. From step 3 to step 7, the formed depth is getting closer to the target one at each step. From then on, the error between the formed depth and the designed one is greatly reduced (within ±0.2mm). Optimised inputs at different steps are varying while the inputs are set as constant at 2mm in open loop ISF, as illustrated Figure 16.

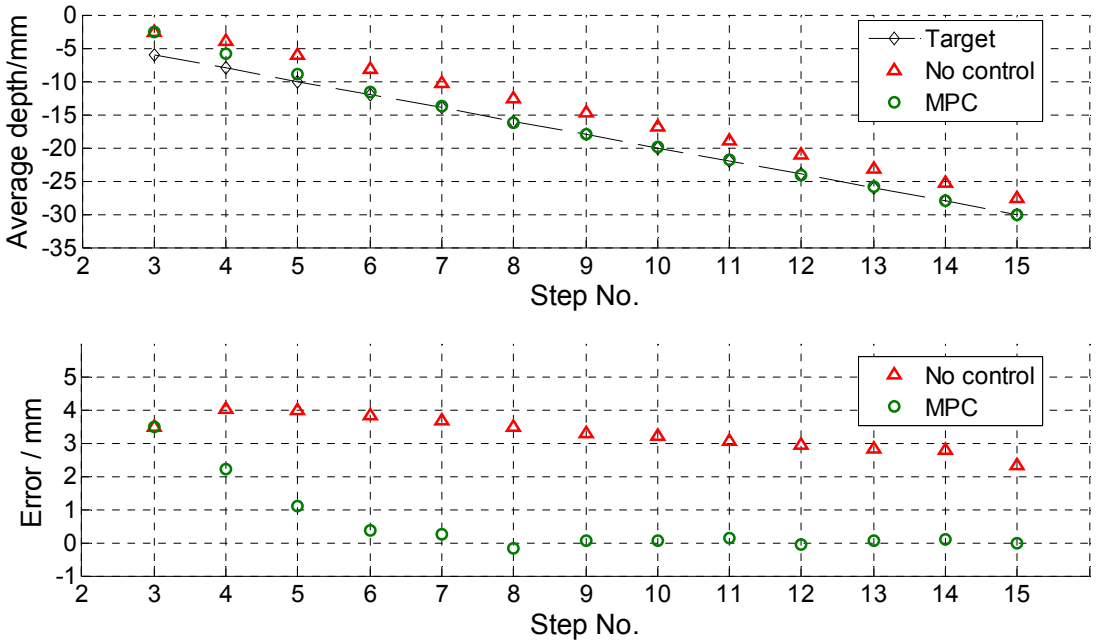

Figure 15 History of average depth of the part bottom and its error along the steps.

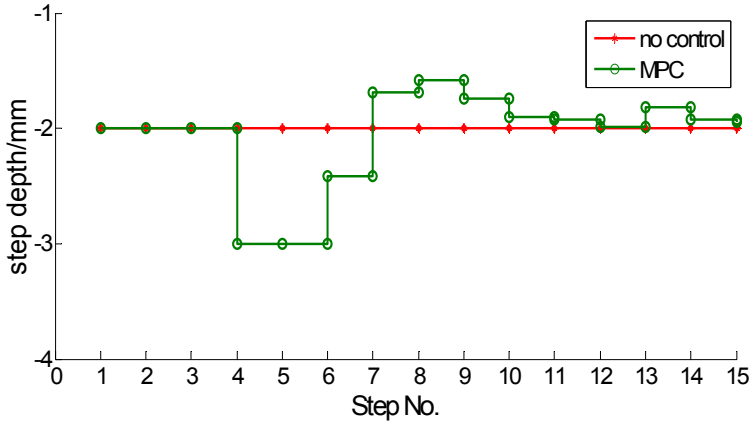

Figure 16 Inputs along the steps.

In Figure 17, the global geometric accuracy of the formed pyramid is evaluated by comparing parts formed in both uncontrolled and controlled ISF with the designed one. The colour contour plots show the distribution of geometric deviations. The geometric accuracy in the bottom area has been significantly improved via feedback control of ISF. The accuracy level at the bottom can reach ±0.3 mm compared with that in open loop ISF (±3.0mm). The accuracy near clamped edges is not considered in this work due to fact that the geometric errors in this area are uncontrollable in SPIF.

Regarding the wall area excluding the four corners, the geometric inaccuracy has also been reduced from ±3.0mm to ±1.0mm. That is, the wall area of the part obtained in controlled ISF is less accurate than its bottom area. This is due to the fact that only the step depth is optimised during the forming process with control. Larger geometric errors can be observed in the four corners of the formed pyramid in Figure 17(a). These errors are reduced in controlled ISF but still are relatively large, as shown in Figure 17(b). Further improvement of the inaccuracy in the wall area will be included in the scope of future work in which the horizontal increment will be optimised as well based on

current work. As for the nonaxisymmetric shapes, some key features, such as the corners of the truncated pyramid, will be taken into consideration in the module of horizontal increment optimisation.

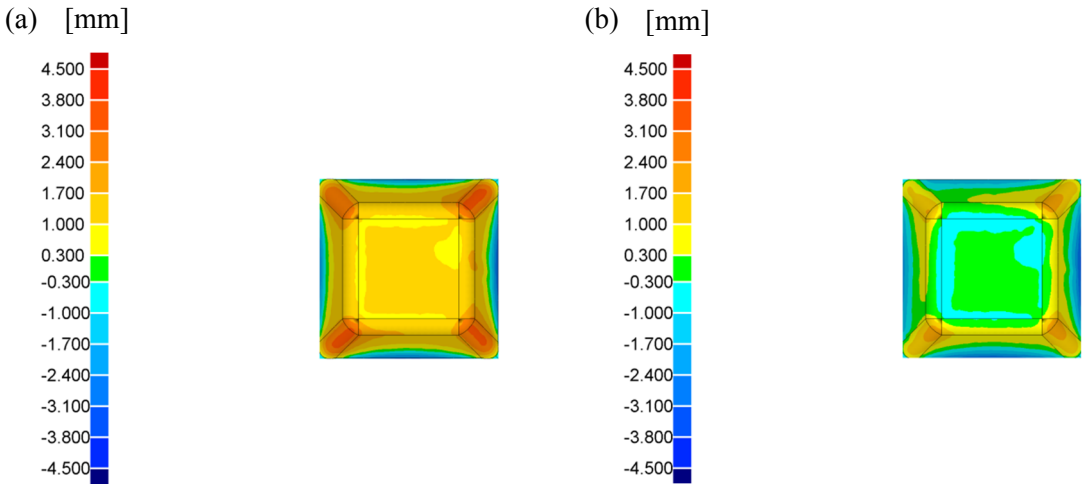

Figure 17 Top view of accuracy colour plots: (a) uncontrolled ISF; (b) ISF with MPC control;

Overall, these indicate that the average geometric deviation in ISF with MPC control has been greatly reduced in comparison with that in uncontrolled ISF. The formed cone and pyramid in ISF with feedback control are shown in Figure 18 (a) and (b), respectively.

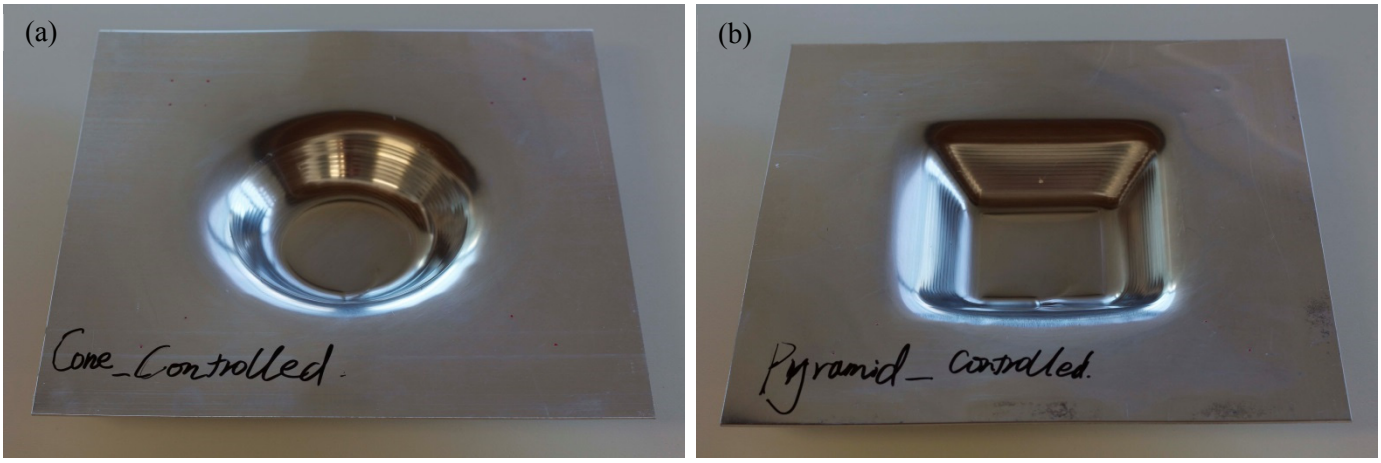

Figure 18 Formed parts in ISF with feedback control.

4. Conclusion and future work

As geometric accuracy significantly limits the development and application of ISF, many attempts have been conducted to achieve better geometric accuracy. Toolpath control and optimisation has been considered as a promising approach in terms of controlling the geometric accuracy in ISF. In this paper, a novel MPC control approach for ISF has been developed and validated. The predictive control model is based on the incremental deformation mechanism of ISF. Step depth of the toolpath

was optimised at each forming step by solving a receding optimal problem, based on shape state feedback during the forming process. Two different shapes were formed in experiments to validate the developed control method. Results show that the geometric accuracy in ISF with feedback control has been greatly improved. As for the bottom areas, the geometric errors of the truncated cone and pyramid have been reduced from ±3.0mm to ±0.25mm and ±0.3mm, respectively. Enhanced geometric accuracy in the wall areas of the formed parts also has been achieved and the wall areas were are not as accurate as the bottom areas. Overall, the developed MPC control strategy for the ISF process is effective and could contribute to the improvement of geometric accuracy in ISF.

As for current work, only step depth ($\triangle u_z$) is optimised during the forming process, which leads to significant accuracy improvement in vertical direction (bottom area). The geometric accuracy of the wall area also has been improved and it could be further improved by adjusting the horizontal step increment ($\triangle u_h$) values. In the future, the MPC control model will be further developed by optimising two key parameters of toolpath, step depth horizontal step increment, together with experimental validation in forming more general shapes. Besides this, the proposed MPC strategy will be combined with multistage ISF to further correct the errors in the areas which has already been deformed.

Acknowledgements

China Scholarship Council (CSC) is acknowledged for the scholarship support.

References

1. Bahloul, R., H. Arfa, and H. BelHadjSalah, *A study on optimal design of process parameters in single point incremental forming of sheet metal by combining Box–Behnken design of experiments, response surface methods and genetic algorithms.* The International Journal of Advanced Manufacturing Technology, 2014. **74**(1-4): p. 163-185.
2. Filice, L., G. Ambrogio, and M. Gaudioso, *Optimised tool-path design to reduce thinning in incremental sheet forming process.* International Journal of Material Forming, 2013. **6**(1): p. 173-178.
3. Smith, J., et al., *Deformation mechanics in single-point and accumulative double-sided incremental forming.* The International Journal of Advanced Manufacturing Technology, 2013. **69**(5-8): p. 1185-1201.
4. Attanasio, A., et al., *Asymmetric two points incremental forming: Improving surface quality and geometric accuracy by tool path optimization.* Journal of Materials Processing Technology, 2008. **197**(1-3): p. 59-67.
5. Leszak, E., *Apparatus and process for incremental dieless forming*. 1967, Google Patents.
6. Rous, P., *Machines for shaping sheet metal*. 1960, Google Patents.
7. Micari, F., G. Ambrogio, and L. Filice, *Shape and dimensional accuracy in Single Point Incremental Forming: State of the art and future trends.* Journal of Materials Processing Technology, 2007. **191**(1-3): p. 390-395.
8. Al-Ghamdi, K. and G. Hussain, *The pillowing tendency of materials in single-point incremental forming: Experimental and finite element analyses.* Proceedings of the Institution of Mechanical Engineers, Part B: Journal of Engineering Manufacture, 2014.
9. Wang, H. and S. Duncan. *Optimization of tool trajectory for Incremental Sheet Forming using closed loop control*. in *Automation Science and Engineering (CASE), 2011 IEEE Conference on*. 2011.
10. Attanasio, A., E. Ceretti, and C. Giardini, *Optimization of tool path in two points incremental forming.* Journal of Materials Processing Technology, 2006. **177**(1-3): p. 409-412.

11. Allwood, J.M., D. Braun, and O. Music, *The effect of partially cut-out blanks on geometric accuracy in incremental sheet forming.* Journal of Materials Processing Technology, 2010. **210**(11): p. 1501-1510.
12. Bambach, M., B. Taleb Araghi, and G. Hirt, *Strategies to improve the geometric accuracy in asymmetric single point incremental forming.* Production Engineering, 2009. **3**(2): p. 145-156.
13. Ambrogio, G., L. Napoli, and L. Filice, *A novel approach based on multiple back-drawing incremental forming to reduce geometry deviation.* International Journal of Material Forming, 2009. **2**(1): p. 9-12.
14. Ambrogio, G., et al., *Influence of some relevant process parameters on the dimensional accuracy in incremental forming: a numerical and experimental investigation.* Journal of Materials Processing Technology, 2004. **153–154**(0): p. 501-507.
15. Hirt, G., et al., *Forming strategies and Process Modelling for CNC Incremental Sheet Forming.* CIRP Annals - Manufacturing Technology, 2004. **53**(1): p. 203-206.
16. Behera, A.K., et al., *Tool path compensation strategies for single point incremental sheet forming using multivariate adaptive regression splines.* Computer-Aided Design, 2013. **45**(3): p. 575-590.
17. Fu, Z.M., et al., *Tool path correction algorithm for single-point incremental forming of sheet metal.* International Journal of Advanced Manufacturing Technology, 2013. **64**(9-12): p. 1239-1248.
18. Allwood, J.M., et al., *Closed-loop feedback control of product properties in flexible metal forming processes with mobile tools.* CIRP Annals - Manufacturing Technology, 2009. **58**(1): p. 287-290.
19. Wang, H. and S. Duncan. *Constrained model predictive control of an incremental sheet forming process*. in *Control Applications (CCA), 2011 IEEE International Conference on*. 2011.
20. Boyd, S. and L. Vandenberghe, *Convex optimization*. 2009: Cambridge university press.

Paper 3

Two-directional toolpath correction in single point incremental forming using Model predictive control

Lu, H., Kearney, M., Liu, S., Daniel, W. J., & Meehan, P. A.

The International Journal of Advanced Manufacturing Technology

2016, Pages: 1-16.

Two-directional toolpath correction in single point incremental forming using model predictive control

Haibo Lu [a, *], Michael Kearney [a], Sheng Liu [a], William J.T. Daniel [a] and Paul A. Meehan [a]

[a] School of Mechanical & Mining Engineering, University of Queensland, St Lucia, Brisbane, QLD 4072, Australia

* Corresponding author. Tel.: +61 3346 9570.

E-mail addresses: h.lu2@uq.edu.au, luhaibocsu@gmail.com (H. Lu)

Keywords: Incremental sheet forming; Model predictive control; Geometric accuracy; Two-directional toolpath correction

Abstract

Incremental Sheet Forming (ISF) is an emerging forming technology that promises high flexibility and formability. These properties make it suited for small scale and customised production. However, the poor geometric accuracy of ISF limits the wide application of this flexible forming technology. This paper presents a two-directional toolpath correction approach to enhance ISF forming accuracy using a Model Predictive Control (MPC) algorithm. A toolpath optimisation method for vertical toolpath correction has been validated in our previous work [1], and it helps to reduce errors in the base of the test shapes to a suitable level while its major limitation is that horizontal geometric errors are relatively large. This paper extends our previous work [1] by augmenting the vertical control module with a new control module for horizontal toolpath correction. The proposed control algorithm was experimentally validated in single point incremental sheet forming (SPIF) using two forming case studies. In the first case study (a truncated pyramid), two control approaches with different assumptions for the horizontal springback distribution along the horizontal cross-sectional profile were tested and compared. Then, the developed MPC control algorithm was applied to form a more complex asymmetric shape. Results show that the developed strategy can reduce the forming errors in the wall and base of the formed shape compared to the existing works. The ISF process with MPC control leads to significant accuracy improvement in comparison with the typical ISF process that is without toolpath control.

1 Introduction

Flexible forming technologies are becoming an increasingly significant part of the manufacturing industry because small batch and customised production have become a significant component in the market, and it is predicted that the proportion of customised production will increase in the future. Single point incremental forming (SPIF) is a flexible sheet forming processes for quick and low-cost production for small batch manufacturing since it possesses the dieless nature and guarantees high flexibility in the fabrication of sheet parts. SPIF uses a simple tool with a smooth end to deform sheets along a toolpath typically generated from CAM software. In SPIF, the part is incrementally fabricated by orderly accumulation of plastic deformations localised around the ball end of the tool. With no needs of any dedicated tooling or dies, SPIF can be quickly adjusted for new and modified product shapes via toolpath alteration. However, SPIF still suffers from some drawbacks including long processing time and low geometric accuracy. The latter one is the major cause of low take-up of SPIF in the forming industry. Micari et al. [2] summarised that three types of geometric inaccuracies in SPIF are the sheet bending effect, the pillow effect, and springback. The geometric inaccuracy caused by the sheet bending effect can be partially reduced by using a backing plate underneath the metal blank, but it is still uncontrollable in SPIF. Therefore, this kind of error will not be considered in this work. Sheet springback, which results from the sudden decrease of stress as the deformation load from the tool is released, accounts for the majority of SPIF defects. To address the limitation of poor geometric accuracy primarily caused by the springback, a number of mitigation approaches have been presented in the literature. Attanasio et al. [3] performed a set of experiments to optimise two process parameters, namely the scallop height and step depth; Ambrogio et al. [4] developed a two-pass approach by adding a back-drawing ISF stage after the typical SPIF process to improve geometric accuracy; Araghi et al. [5] proposed a hybrid ISF approach by combining ISF with stretch forming; Behera et al. [6] developed a multi-stage strategy based on intelligent sequencing and multi-step mesh morphing techniques and Bambach et al. [7] demonstrated that a multi-stage strategy with stress relief annealing can reduce the geometric errors in ISF.

An alternative approach reported in the literature is to improve the low geometric accuracy of ISF through toolpath correction. Recently, some off-line approaches were presented to correct the ISF toolpath. Ambrogio et al. [8] modified the ISF toolpath by using a larger wall

angle to form the first half of the shape in terms of depth, which is a preliminary attempt on toolpath optimisation. In [9], an iterative approach was presented to optimised the toolpath based on the springback of formed parts in the trial fabrication. Similarly, Behera et al. [10] developed a multivariate adaptive regression splines (MARS) correction strategy for toolpath compensation in ISF. Fiorentino et al. [11] used an iterative control algorithm based on an artificial cognitive system for toolpath correction. On the other hand, some studies on the in-process toolpath correction for accuracy improvement in ISF have been reported recently. The on-line toolpath correction method measures the progress of the formed part and corrects the toolpath in-process to improve the forming accuracy. Based on spatial impulse responses of the system obtained from the ISF process without control, Allwood et al. [12] used a feedback control strategy to reduce geometric errors. Wang et al. [13, 14] reported a MPC control strategy for improving the poor accuracy in SPIF via toolpath optimisation. The predictive model for this work is also empirically determined. The results showed that final geometric errors were reduced at the base of the formed shapes using the control strategy while the errors in the wall areas of the test shape are still relatively large. What's more, the error distribution map of the whole part was not reported in these studies [12-14].

In our previous work [1], an MPC control strategy for ISF toolpath optimisation, using an analytical model for shape prediction, was presented to improve geometric accuracy through optimising step depth during the forming process. Results show that good accuracy improvement has been made in the bottom areas of the test shapes with the use of the developed control strategy. As for the wall areas of the test shapes, geometric errors are still relatively large. Specially, the corners of the pyramid still have relatively low accuracy. This is due to the fact that this work only dealt with toolpath optimisation in the vertical direction without considering toolpath correction in the horizontal direction. This finding is consistent with the results presented in [14].

In this paper, a two-directional MPC control algorithm is developed to control and correct the toolpath in the vertical and the horizontal directions. This work extends our previous work by augmenting the existing vertical MPC controller with a horizontal controller with the view to further reduce the errors of the wall and corner areas of the test part. Two key toolpath parameters, the horizontal step increment and the step depth, are optimised by solving optimisation problems at each step following a receding horizon control framework. Compared with previous studies on toolpath optimisation, analytical models, based on the

incremental nature of the ISF deformation, were used for shape state predictions. During the forming process, the shape state predictions are obtained based on the shape measurement in the past and future toolpath parameters. Control actions are computed in two separate modules, namely vertical and horizontal MPC modules. Two case studies were performed in the SPIF process for experimental validation. After testing and comparing two models with different assumptions for the horizontal springback distribution in the first case study, the developed control algorithm with the interpolated horizontal model was applied in the fabrication of an asymmetric shape to verify its effectiveness.

2 Model Predictive Control of ISF

MPC [15] is a control strategy that uses a predictive model of the system under control to choose inputs that optimise the performance, such as minimising geometric errors in ISF, while ensuring system constraints are satisfied over a prediction horizon. In this work, there are two separate MPC modules to deal with the optimisation of two critical toolpath parameters, the horizontal step increment (Δu_h) and the step depth (Δu_z), as shown in Figure 1. During the forming process with control, each MPC time-step is taken to be the forming of a single contour. The number of steps taken to form the shape depends on the designed depth of the shape and the initial Δu_z value. The forming of a single contour depends on the values of Δu_z and Δu_h computed in the control strategy. The ISF process with MPC control is shown in Figure 1.

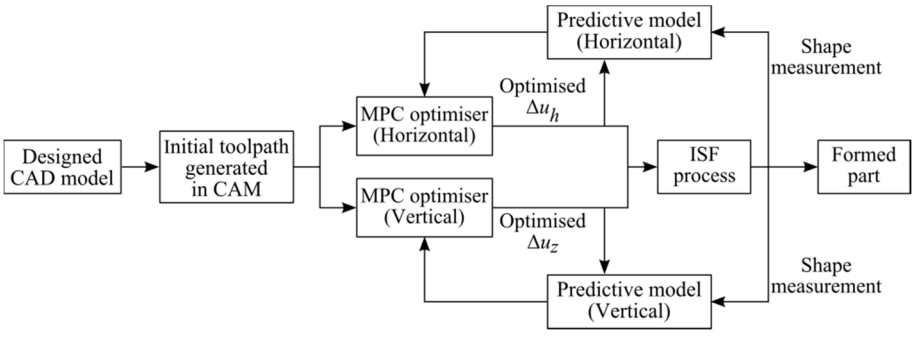

Figure 1 Structure of the ISF process with MPC control.

Figure 2 illustrates the implementation of the MPC algorithm in ISF. The system inputs include the target shape states in two directions (W_z and W_h) and toolpath contours generated from CAM software. After forming the contour *k*, the formed shape is measured and the

measured profile state is then used in the predictive models to predict the shape states of next several steps in terms of the vertical and horizontal directions. Then, the MPC optimisers will determine a sequence of control inputs that minimise the difference between the target shape states and the predicted shape states. Optimised inputs of next N_p steps ($\Delta U_z^*(k)$ and $\Delta U_h^*(k)$) will be obtained by solving the optimisation problems in each of the two control modules. For each direction, only the first element of the optimised parameters will be used to correct the toolpath in the following single step. The entire control process is then repeated at each subsequent step (forming contour) until the shape is formed.

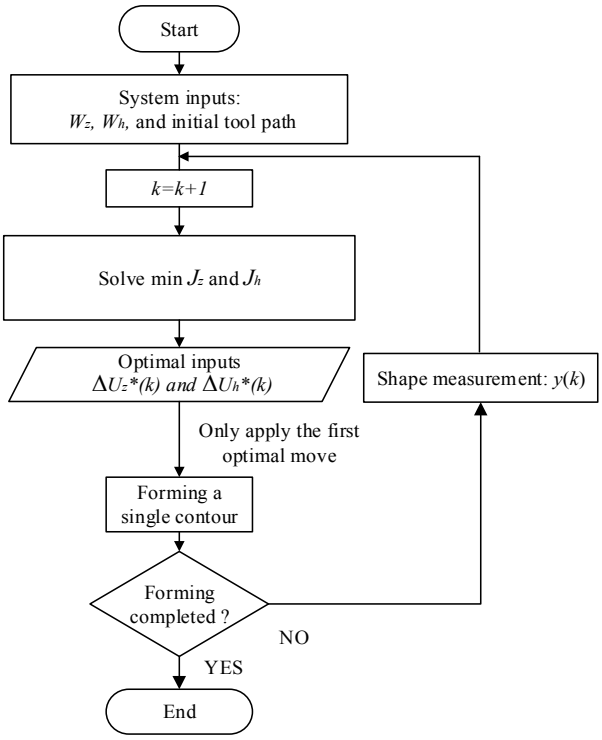

Figure 2 Application of the MPC control algorithm in ISF.

2.1 MPC algorithm with two-parameter optimisation

2.1.1 Two critical parameters of ISF

The parallel contour toolpath is the common toolpath type used in ISF and typically contains a sequence of horizontal contours. The horizontal step increment (Δu_h) and the step depth (Δu_z) are the critical toolpath parameters in ISF, shown in Figure 3. There are a number of contour points on each single contour and their coordinates are defined in a cylindrical

coordinate system. $X_k^j(r_k^j, \theta_k^j, z_k^j)$ is a contour point on contour *k*. At a single step, e.g., step *k+1*, $\Delta u_z(k+1)$ is a scalar because all the points of a single contour are on the same z-level plane, and it can be expressed as,

$$\Delta u_z(k+1) = z_{k+1} - z_k \tag{1}$$

where z_{k+1} and z_k are the *z* coordinates of X_k^j and X_{k+1}^j, respectively. Δu_h is a vector that captures the radial distances between points of interest on two successive contours. Δu_h of step *k+1* can be expressed by the following equation,

$$\Delta u_h(k+1) = \left[\Delta u_h^1(k+1), \Delta u_h^2(k+1), \ldots, \Delta u_h^j(k+1), \ldots, \Delta u_h^m(k+1)\right] \tag{2}$$

where *m* is the number of points on a single contour, and $\Delta u_{h\,k+1}^{\;j}$ is the radial distance between the *j*th pair of points (X_k^j and X_{k+1}^j) on two neighbouring contours, as shown in Figure 3.The value of Δu_z is typically defined by the user. The values of Δu_h are computed, according to the Δu_z value and the part design, in the CAM software. However, the initial contour toolpath without control typically leads to low geometric accuracy caused by the springback. This paper aims to control and optimise both Δu_z and Δu_h to improve the ISF accuracy.

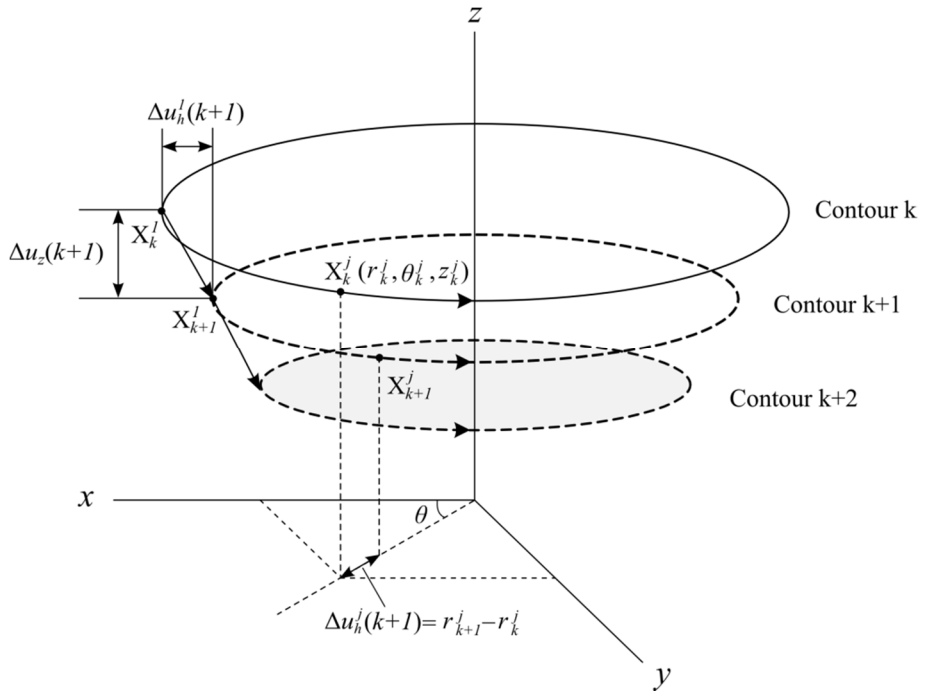

Figure 3 Two critical parameters of the typical ISF toolpath.

2.1.2 Vertical direction optimisation

This control module for vertical direction optimisation was built, based on the MPC algorithm in our previous work [1], to optimise Δu_z for accuracy improvement in the vertical direction. In ISF, Δu_z is the determinant of vertical movement of the tool between successive contours and it has direct effect on vertical deformation of metal sheet. The cross-sectional profile through the centre axis is used to represent the shape state. After forming step *k*, the vertical profile state is measured as $y_z(k) \in R^n$,

$$y_z(k) = \left[y_z^1(k), y_z^2(k), \ldots, y_z^i(k), \ldots, y_z^n(k) \right]^T \tag{3}$$

where *n* is the number of profile points and $y_z^i(k)$ is the *z*-coordinate of the *i*th point (P_i) on the profile, as shown in Figure 4.

The forming mechanism in ISF is complex so that it is difficult to find an accurate analytical model to describe the system $y_z(k+1) = f(y_z(k), \Delta u_z(k+1))$ for on-line toolpath correction [1]. The finite element method could properly model the forming process. However, it usually takes long time [16, 17], from several hours to several days, for the simulation of ISF

processes so that this method is not suitable for online toolpath correction. Using the linear predictive model in [1] for shape state prediction in the vertical direction, the vertical profile state at step *k+1* can be predicted as,

$$\hat{y}_z(k+1|k) = y_z(k) + B_z(k+1)\Delta u_z(k+1) \tag{4}$$

where $B_z(k+1)$ is the coefficient vector that captures the influence of the input Δu_z on the deformation of next step in the linear model.

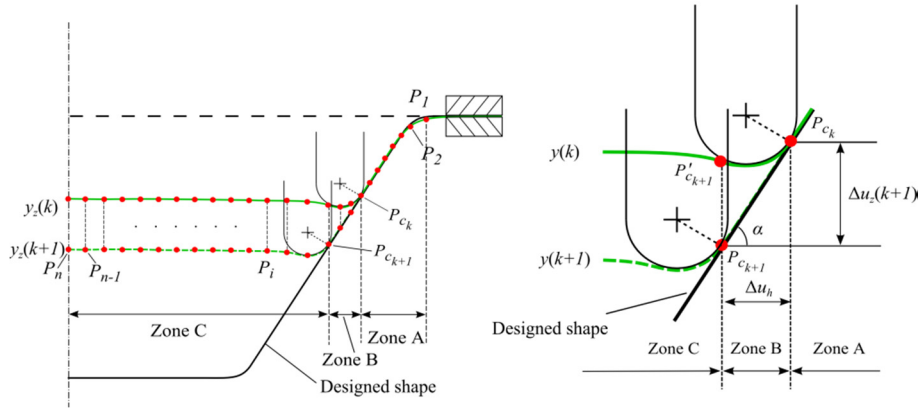

Figure 4 Incremental deformation between two neighbouring steps (refer to [1]).

Figure 4 shows how the vertical cross-sectional profile varies with the vertical input between two consecutive steps. This can be generalised to a large number of shapes fabricated in ISF. The green lines are the formed profiles $y_z(k)$ and $y_z(k+1)$ and the black line represents the ideal profile in design. P_1 and P_n are the first point and the last point on the formed profile, respectively. P_{c_k} and $P_{c_{k+1}}$ are the contact points and are geometrically detected because they are where the ball end of the tool tangentially touches the local wall. The profile $y_z(k+1)$ consists of three zones, namely Zone A ($P_1 \sim P_{c_k}$), Zone B ($P_{c_k} \sim P_{c_{k+1}}$), and Zone C ($P_{c_{k+1}} \sim P_n$). Based on the simplifications in the linear predictive model in [1], the metal sheet will be pushed down with the increase in depth as Δu_z in Zone C. Since Zone A is a formed region and will not be formed by the tool in the future, the deformation of material in this region will be slight and will be ignored. The metal blank in Zone B will be pushed down and stretched by the single tool following the predefined slope of the forming step. Therefore, all the

elements in $B_z(k+1)=\left[b_z^1(k+1),b_z^2(k+1),\ldots,b_z^n(k+1)\right]^T$ can be computed in Equation (5). Generally, Zone B contains only a few points.

$$b_z^i(k+1)=\begin{cases}0, & 1\le i<c_k \quad (\text{Zone A})\\ \dfrac{i-c_k}{i-c_{k+1}}, & c_k\le i<c_{k+1} \quad (\text{Zone B})\\ 1, & c_{k+1}\le i\le n \quad (\text{Zone C})\end{cases} \tag{5}$$

where i is the index number of the profile points. c_k and c_{k+1} are the index number of points P_{c_k} and $P_{c_{k+1}}$, respectively. Consequently, all the B_z values of the future N_p steps, $B_z(k+j)=\left[b_z^1(k+j),b_z^2(k+j),\ldots,b_z^n(k+j)\right]^T$, $j=1,2,\ldots,N_p$, can be obtained similarly.

This simplified model has been verified as reasonable from the results of our previous work [1]. In addition, this simplification has been justified through experimental validation, as discussed in Section 3.1. Using the linear predictive model in Equation (4), the profile states in the prediction horizon, namely the future N_p steps, can be predicted as,

$$\hat{Y}_z(k)=Y_z(k)+B_z\Delta U_z(k) \tag{6}$$

where $\hat{Y}_z(k)=\left[\hat{y}_z(k+1|k),\hat{y}_z(k+2|k),\ldots,\hat{y}_z(k+N_p|k)\right]^T$ contains the state predictions in the prediction horizon, $Y_z(k)=[y_z(k),y_z(k),y_z(k),\ldots,y_z(k)]^T$ is the measured profile shape at time-step k, $\Delta U_z(k)=\left[\Delta u_z(k+1),\Delta u_z(k+2),\ldots,\Delta u_z(k+N_p)\right]^T$ is the input sequence over the prediction horizon, and B_z is the coefficient matrix to predict how future inputs influence the changes of the vertical profile state in the predictive model. B_z is expressed as,

$$B_z=\begin{bmatrix}B_{z\,k+1} & 0 & 0 & \cdots & 0\\ B_{z\,k+1} & B_{z\,k+2} & 0 & \cdots & 0\\ B_{z\,k+1} & B_{z\,k+2} & B_{z\,k+3} & \cdots & 0\\ \vdots & \vdots & \vdots & \ddots & 0\\ B_{z\,k+1} & B_{z\,k+2} & B_{z\,k+3} & \cdots & B_{z\,k+N_p}\end{bmatrix} \tag{7}$$

and $B_{z\,k+j}=\left[b_{z\,k+j}^{\,1},b_{z\,k+j}^{\,2},\ldots,b_{z\,k+j}^{\,n}\right]^T$, $j=1,2,\ldots,N_p$.

At step k, the optimisation problem in the vertical control module is summarised as,

$$\min J_z = \left\| \hat{Y}_z - W_z \right\|^2 + \lambda_z \Delta U_z^T \Delta U_z \tag{8}$$

$$\text{subject to } \hat{y}_z(k+j \mid k) = y_z(k) + \sum_{i=1}^{j} B_z(k+i)\Delta u_z(k+i), j = 1,2,\ldots,N_p$$

$$\Delta u_{z\min} \le \Delta u_z(k+j) \le \Delta u_{z\max}, j = 1,2,\ldots,N_p$$

where J_z is the cost function; W_z is the vertical profile states in design; $\Delta U_z(k) = \left[\Delta u_z(k+1), \Delta u_z(k+2), \ldots, \Delta u_z(k+N_p)\right]^T, k = 1,2,\ldots,N$ is the input sequence; N is the number of steps; The second item of J_z is added to limit the fluctuation of the control inputs; λ_z is a non-negative weighting factor and is set as 0.2, which is the same as in [1]. The solution of Equation (8) can be found by solving a quadratic programming (QP) problem [1], which is programed in Python.

2.1.3 Horizontal direction optimisation

Results of previous studies from [1, 13, 14] indicate that the MPC control strategy with optimising vertical step depth only can greatly reduce geometric errors in the base area of the formed parts. However, the reduction in the geometric error in the wall areas of the formed part was more modest, especially the corners of the formed truncated pyramid. In this work, a new horizontal MPC module is added into the control strategy with the aim to reduce the wall and corner geometric errors.

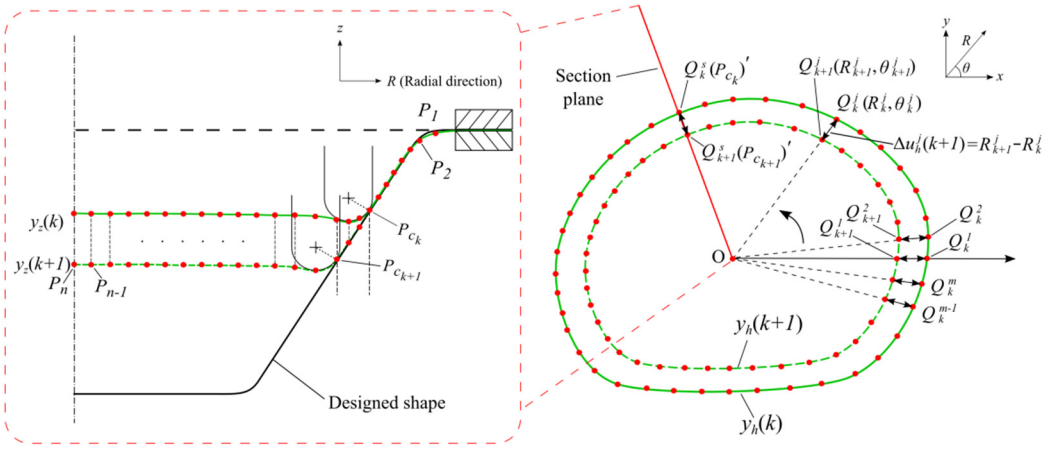

Figure 5 Incremental deformation in the horizontal direction.

Figure 5 illustrates the incremental deformation between two forming contours in the horizontal direction. In the top view, the vertical cross-sectional profile is obtained in a vertical section through points Q_k^s and Q_{k+1}^s, which are the contact points P_{c_k} and $P_{c_{k+1}}$ in the section view, respectively. Meanwhile, the horizontal cross-sectional profile $y_h(k)$ is on the horizontal section plane through the contact point (P_{c_k}). The horizontal cross-sectional profile is represented by a number of profile points for optimisation. The number of profile points, *m*, is determined by the complexity of the target shape and generally increases as the shape complexity increases. Q_k^j and Q_{k+1}^j is the *j*th pair of points on $y_h(k)$ and $y_h(k+1)$, respectively. At step *k*, the radial coordinate (R_k^j) of each profile point (Q_k^j) is the profile state of this point. Therefore, the horizontal profile state at step *k* is measured as $y_h(k)$ expressed as follows,

$$y_h(k)=\left[y_h^1(k),y_h^2(k),\ldots,y_h^j(k),\ldots,y_h^m(k)\right] \tag{9}$$

where $y_h^j(k)=R_k^j$, *m* is the number of profile points on the profile.

In consideration of the incremental nature of ISF, the horizontal distance between Q_k^j and Q_{k+1}^j is taken to be the horizontal input $\Delta u_h^j(k+1)$, the *j*th element of $\Delta u_h(k+1)$. At step *k*, the horizontal profile state of next step can be predicted by,

$$\hat{y}_h(k+1|k)=y_h(k)+\Delta u_h(k+1) \tag{10}$$

where $\hat{y}_h(k+1)=\left[\hat{y}_h^1(k+1),\hat{y}_h^2(k+1),\ldots,\hat{y}_h^j(k+1),\ldots,\hat{y}_h^m(k+1)\right]$ is the predicted profile state, and $\Delta u_h(k+1)=\left[\Delta u_h^1(k+1),\Delta u_h^2(k+1),\ldots,\Delta u_h^j(k+1),\ldots,\Delta u_h^m(k+1)\right]$ is the horizontal step increment of step *k+1*.

Similarly, the profile predictions along the prediction horizon can be expressed as,

$$
\begin{aligned}
&\hat{y}_h(k+1\,|\,k) = y_h(k) + \Delta u_h(k+1) \\
&\hat{y}_h(k+2\,|\,k) = \hat{y}_h(k+1\,|\,k) + \Delta u_h(k+2) \\
&\qquad\qquad = y_h(k) + \Delta u_h(k+1) + \Delta u_h(k+2) \\
&\quad \vdots \\
&\hat{y}_h(k+N_p\,|\,k) = y_h(k) + \Delta u_h(k+1) + \Delta u_h(k+2) + \ldots + \Delta u_h(k+N_p)
\end{aligned}
\tag{11}
$$

Equation (11) can also be written as,

$$
\hat{Y}_h(k) = Y_h(k) + L_h \Delta U_h(k) \tag{12}
$$

where $\hat{Y}_h(k) = \left[\hat{y}_h(k+1\,|\,k), \hat{y}_h(k+2\,|\,k), \ldots, \hat{y}_h(k+N_p\,|\,k)\right]$ is the collection of predicted profile states of next N_p steps, $Y_h(k) = [y_h(k), y_h(k), y_h(k), \ldots, y_h(k)]$ is the measured profile state at step k, $\Delta U_h(k) = \left[\Delta u_h(k+1), \Delta u_h(k+2), \ldots, \Delta u_h(k+N_p)\right]$ is the input sequence over the prediction horizon, and L_h is the coefficient matrix to determine how the horizontal profile state varies with the horizontal input in the next N_p steps. By collecting Equation (11) together, L_h is expressed in Equation (13).

$$
L_h = \begin{bmatrix}
I_{m\times m} & 0 & 0 & 0 \\
I_{m\times m} & I_{m\times m} & 0 & 0 \\
\vdots & \vdots & \ddots & 0 \\
I_{m\times m} & I_{m\times m} & I_{m\times m} & I_{m\times m}
\end{bmatrix} \tag{13}
$$

At each step, the control problem in the horizontal module can be summarised as:

$$
\min\ J_h = \left\| \hat{Y}_h - W_h \right\|^2 + \lambda_h \left\| \Delta U_h - \Delta U_{h0} \right\|^2 \tag{14}
$$

$$
\text{subject to } \left| \Delta u_h(k+i) - \Delta u_{h\,0}(k+i) \right| \le e, i = 1, 2, \ldots, N_p
$$

$$
\hat{y}_h(k+i\,|\,k) = y_h(k) + \sum_{i=1}^{j} \Delta u_h(k+1), j = 1, 2, \ldots, N_p
$$

where J_h represents the cost function, W_h is the horizontal profile state in design, the last item of J_h is to limit the variation range of the control inputs around the initial inputs, λ_h is

the non-negative weighting factor and $\lambda_h = 0.7$ has been adopted after tuning in this work, $\Delta u_{h0}(k+i)$ is the initial horizontal step increment in the initial toolpath, and e is the inequality constraints of the horizontal inputs and is set as 0.5. The optimisation problem given in Equation (14) is a typical QP problem and can be solved using the method in [1].

2.2 Case study 1

In this case, the developed control algorithm is validated by forming a truncated pyramid (Figure 6), which is a typical test in ISF because it has flat wall areas as well as relatively sharp corners where the shape bends significantly. The yellow area is the concerned region.

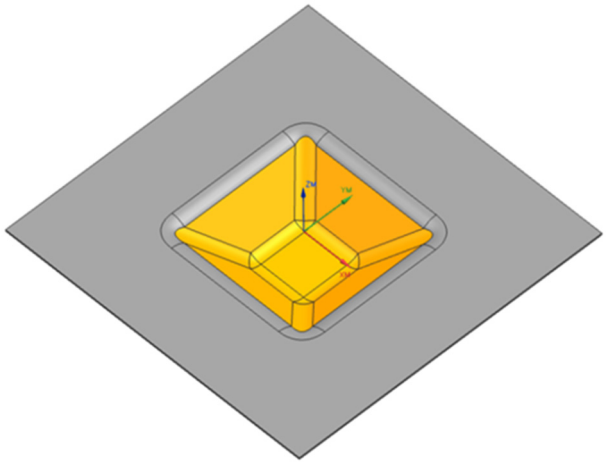

Figure 6 Test shape in case study 1.

To optimise Δu_z, the vertical cross-sectional profile is obtained in a section through the corner of the pyramid, as shown in Figure 7. The optimization of Δu_h will only consider one eighth of the shape due to its symmetry. Two models with different assumptions of the horizontal springback distribution were utilised to simplify the optimisation problem in the control process. The first model assumes that the horizontal component of the springback is uniformly distributed along the horizontal cross-sectional profile at each step. The second model assumes that the horizontal springback linearly varies with the radial coordinate of the point on the horizontal cross-sectional profile. The use of a simplified model allows the entire horizontal contour to be adjusted based upon the optimised Δu_h values of only a few profile points rather than all the profile points.

2.2.1 Uniform horizontal springback

In the first model, under the assumption of uniform horizontal springback, the correction of the springback is taken to be uniformly distributed along the cross-sectional profile, as shown in Figure 7. That is, the optimised contour is assumed to be obtained by slightly enlarging or shrinking the initial contour by a constant scale factor. Therefore, this scale factor can be calculated using a profile point in any radial direction. In Figure 7, $X_k^j(r_k^j,\theta_k^j)$ is the point on the initial contour k and $Q_k^j(R_k^j,\theta_k^j)$ is the point on the profile $y_h(k)$.

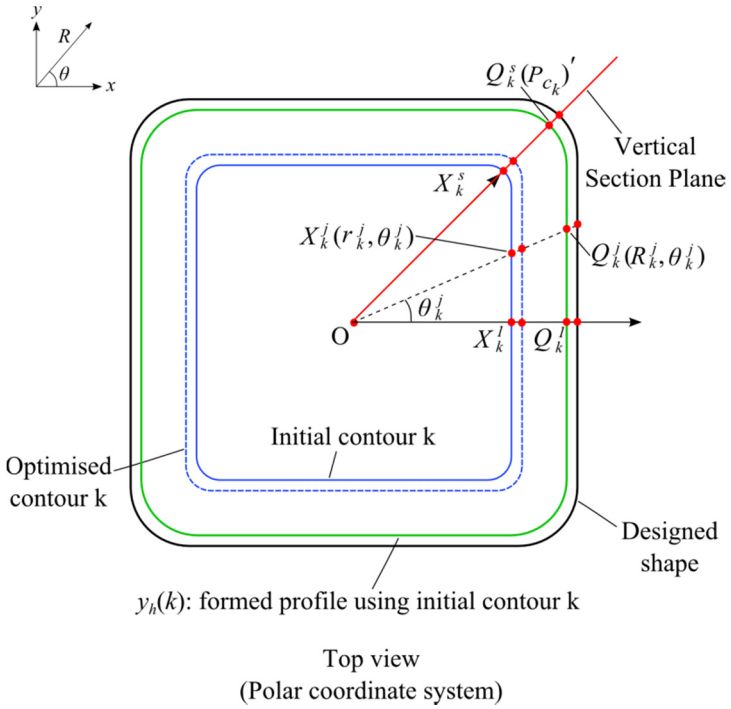

Figure 7 Optimisation of contour in the horizontal direction.

The scale factor can be calculated in the following equation.

$$\beta_k = r^{*j}_k / r^j_k = \left[r^j_k + (\Delta u^{*j}_h(k) - \Delta u^j_h(k)) \right] / r^j_k = 1 + (\Delta u^{*j}_h(k) - \Delta u^j_h(k)) / r^j_k \qquad (15)$$

where β_k is the scale factor; r^j_k is the radial coordinate of point X^j_k on the initial contour k; r^{*j}_k is the radial coordinate of point X^{*j}_k on the optimised contour. $\Delta u^j_h(k)$ and $\Delta u^{*j}_h(k)$ are respectively the initial horizontal input and the optimised input in the radial direction of $\theta = \theta^j_k$.

In this case, the profile point at the corner, namely point $Q_k^s(R_k^s, \theta_k^s = 45°)$, is chosen for calculating the scale factor. Q_k^s is also where the shape is vertically sectioned to get the vertical profile. Therefore, β_k is calculated as,

$$\beta_k = 1 + (\Delta u^{*s}_h(k) - \Delta u^s_h(k)) / r^s_k \tag{16}$$

where $\Delta u^s_h(k)$ and $\Delta u^{*s}_h(k)$ are respectively the initial horizontal input and the optimised one in the direction of $\theta = \theta^s_k$. The horizontal input in any direction can be obtained from Equations (15) and (16),

$$\Delta u^{*j}_h(k) = \Delta u^j_h(k) + r^j_k(\Delta u^{*s}_h(k) - \Delta u^s_h(k)) / r^s_k,\ j = 1, 2, \ldots, m \tag{17}$$

Therefore, the optimisation of $\Delta u^*_h(k) = \left[\Delta u^{*1}_h(k), \Delta u^{*2}_h(k), \ldots, \Delta u^{*j}_h(k), \ldots, \Delta u^{*m}_h(k)\right]$ shrinks to an optimal problem requiring the optimisation of $\Delta u^{*s}_h(k)$ with the use of the horizontal MPC module.

2.2.2 Interpolated horizontal springback

From the results in our previous work by [1], it appeared that while there was significant error at the corner of the pyramid, the use of the MPC module for vertical toolpath correction was able to reduce errors in the middle of the wall to be fairly low, as shown in Figure 8. This suggests that the horizontal springback is not uniformly distributed along the horizontal profile, which is consistent with other sheet forming processes, such as air bending [18]. A model with varying horizontal springback is developed to correct the horizontal errors. More specifically, the horizontal springback distribution is assumed to vary linearly between the springback of point $Q_k^1(R_k^1, \theta_k^1 = 0°)$ and point $Q_k^s(R_k^s, \theta_k^s = 45°)$ based on the radial coordinates of the points, as shown in Figure 8.

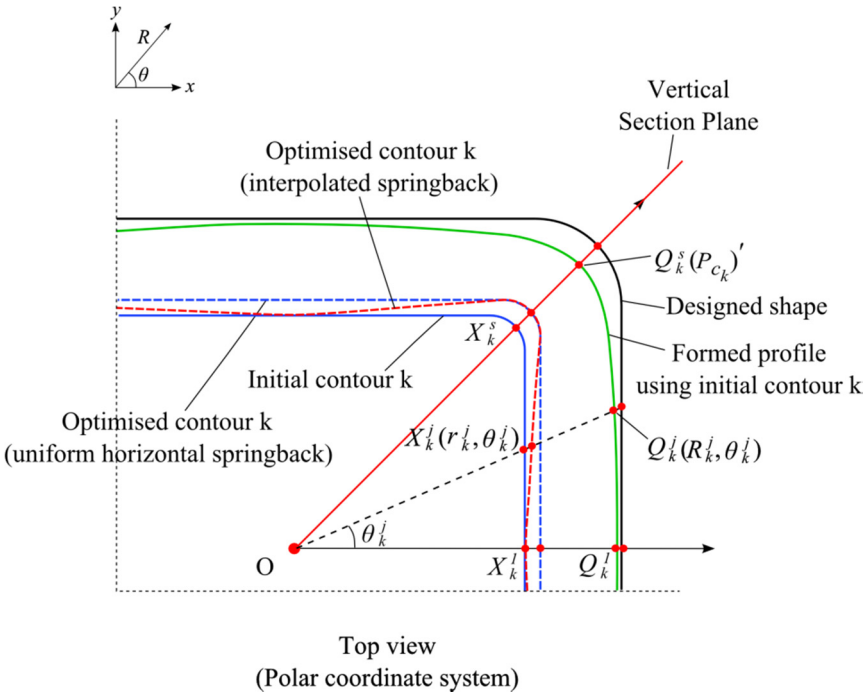

Figure 8 Optimisation of contour at step *k* (enhanced model).

To control the springback effect, the contour is adjusted based on the model with varying springback distribution. Consequently, the scale factor β_k for adjusting the initial contour varies at different radial directions and can be expressed as,

$$\beta_k = \left[\beta_k^1, \beta_k^2, \ldots, \beta_k^j, \ldots, \beta_k^m\right] \tag{18}$$

For the linearly interpolated horizontal springback model, only springback at the two radial directions ($\theta = \theta_k^1$ and $\theta = \theta_k^s$) will be detected and the springback at any radial direction ($\theta = \theta_k^j$) is estimated by a linear interpolation based on the radial coordinates. Therefore, the scale factor value β_k^j can be obtained using the following equation,

$$\beta_k^j = \beta_k^1 + (\beta_k^s - \beta_k^1)(r_k^j - r_k^1)/(r_k^s - r_k^1) \tag{19}$$

Also, β_k^j can be expressed in a generalisation of Equation (16),

$$\beta_k^j = 1 + (\Delta u^{*j}_h(k) - \Delta u_h^j(k))/r_k^j \tag{20}$$

Similarly,

$$\beta_k^s = 1 + (\Delta u^{*s}_h(k) - \Delta u^s_h(k)) / r^s_k \tag{21}$$

From the results of our previous work [1], geometric accuracy in the middle of four pyramid walls was greatly improved to the desirable level (± 0.3 mm) when only Δu_z is optimised and Δu_h is kept unchanged from the initial CAD toolpath. The radial direction $\theta = \theta^1_k$ corresponds to the middle of the pyramid wall. Therefore, β^1_k is taken to be 1. It means that the position of the contour point in this direction will not be adjusted while optimising the contour.

By combining Equations (19), (20) and (21) together, the optimal input at any radial direction can be obtained using the linear interpolation,

$$\Delta u^{*j}_h(k) = \Delta u^j_h(k) + (\Delta u^{*s}_h(k) - \Delta u^s_h(k)) \frac{r^j_k (r^j_k - r^1_k)}{r^s_k (r^s_k - r^1_k)},\ j = 1, 2, \ldots, m \tag{22}$$

Once again, the optimisation of $\Delta u^*_h(k) = \left[\Delta u^{*1}_h(k), \Delta u^{*2}_h(k), \ldots, \Delta u^{*j}_h(k), \ldots, \Delta u^{*m}_h(k) \right]$ shrinks to an optimal problem for optimising $\Delta u^{*s}_h(k)$. After $\Delta u^{*s}_h(k)$ is calculated in the horizontal MPC module at each step, the optimised contour can be obtained for springback correction. Hence, the computational complexity for using either of the two springback models is identical.

2.3 Case study 2

To further validate the developed MPC control algorithm, another case study was performed using a more complex asymmetric shape. The test shape is an asymmetric cone, as shown in Figure 9, with the wall angle varying at different radial directions from the centre.

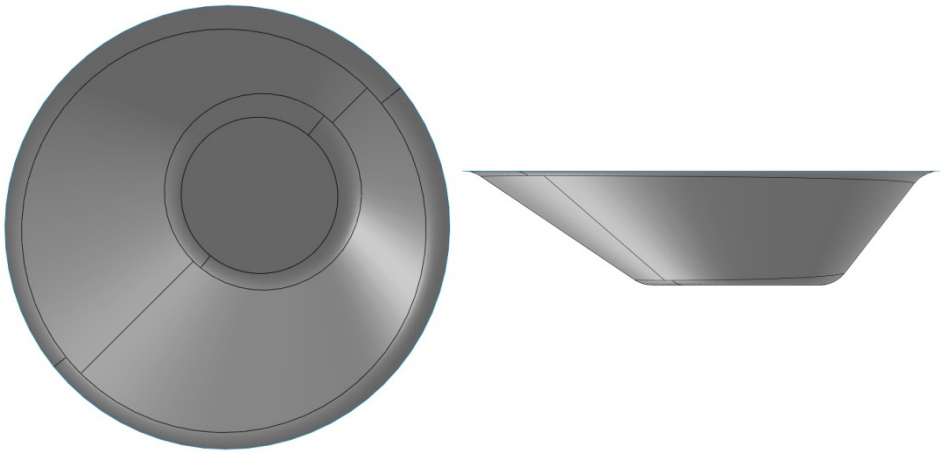

Figure 9 Test shape in case study 2.

In the vertical optimisation, the formed shape is sectioned through point $Q_k^s(R_k^s, \theta_k^s = 45°)$, as shown in Figure 10, to get the vertical cross-sectional profiles. As for the horizontal optimisation, the model with interpolated horizontal springback distribution was used to estimate the horizontal errors. The optimised Δu_h values in five selected radial directions ($\theta = 0°, 45°, 90°, 180°, 270°$), which are marked by arrow lines in Figure 10, are computed directly in the horizontal MPC optimiser. The optimised Δu_h values in other radial directions are calculated using linear interpolation between the sample points, that is, using an appropriate modification to Equation (22) for each inter-sample segment.

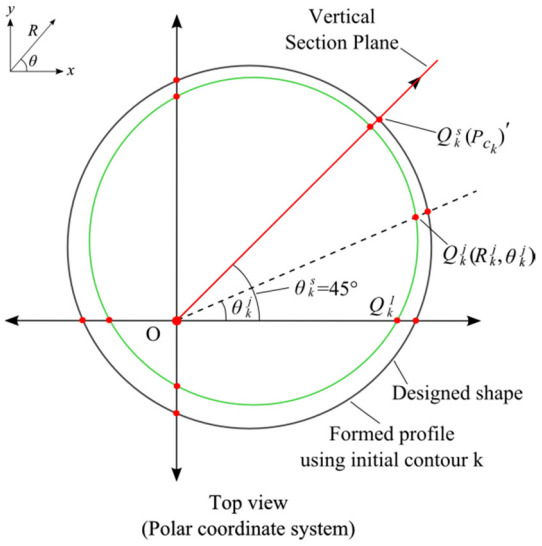

Figure 10 Application of the horizontal model with interpolated springback.

2.4 Set-up in experiments

The present work was conducted on an AMINO® ISF machine, shown in Figure 11. A 3D Digitiser (VIVID 9i), with the scanning accuracy within ±0.05 mm, was utilised to scan the 3D geometry of formed parts. In the SPIF process, a 3 mm thick steel backing plate and clamping blocks were used to clamp the sheet blank. Besides this, the backing plate can also provide a rigid support for the undeformed areas of the blank. This helps to reduce geometric inaccuracies caused by the sheet bending effect. The test material is aluminium (7075-O). The initial blank is a 300 mm × 300 mm square and the thickness is 1.6 mm. A ball-ended tool with a 30 mm diameter was used in the experiments. Lubricating oil was used for lubrication during the forming process.

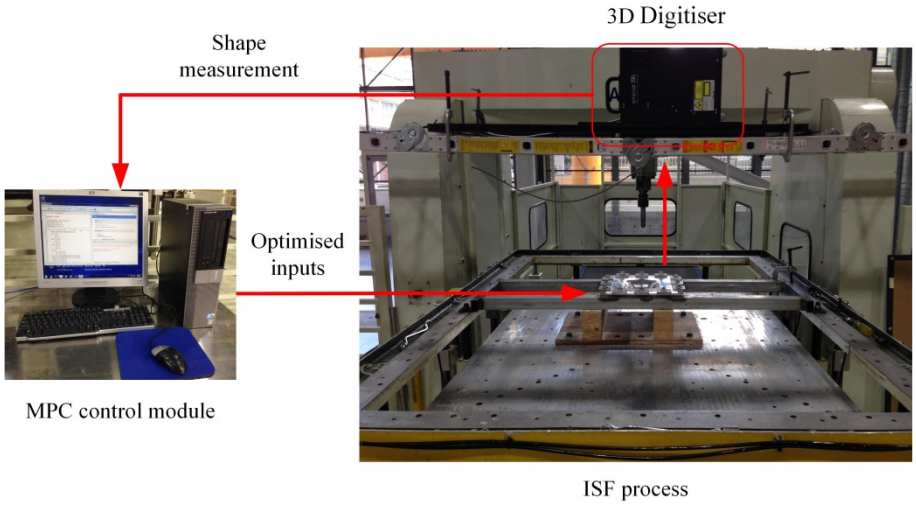

Figure 11 Experimental set-up of the ISF system with MPC control.

Figure 11 illustrates the experimental implementation of the manufacturing system with MPC control in the lab. The geometric data of scanned formed parts is collected and analysed in GEOMAGIC Qualify. Cross-sectional profiles for feedback control are obtained in sections in different directions. In the first three steps of the forming process, the metal blank is formed without control and the MPC control modules are turned on when the forming of third step is finished, since the formed shape at the early stage is too shallow to accurately capture the formed features. After solving the optimisation problems in the control modules by the QP method [1], optimised toolpath parameters are used for the forming of next contour. The CAD shapes are designed in SOLIDWORKS. Unigraphix NX7.5 is used to generate the contour toolpath with a fixed Δu_z for typical ISF with no toolpath control. Table 1 illustrates

detailed parameter settings of the experiments and the MPC controllers. The depth of the shape design is consistent with the work by [13, 14].

Table 1 Parameter settings in experiment

Parameters	Truncated pyramid	Asymmetric Cone
Tool diameter (mm)	30	20
Raw thickness (mm)	1.6	1.6
Feed rate (mm/min)	4000	4000
Total depth (mm)	35	35
Wall angle (°)	40	Varying at different radial directions
Prediction Horizon (N_p)	6	6

3 Results and discussions

3.1 Justification of the predictive model

To model the forming process for MPC control, simplifications were made to predict the formed vertical profiles during the control process. Before analysing the results of MPC control strategies, the simplified model (Figure 4) used for vertical profile predictions was experimentally justified in forming the test shape in case study 1. In the typical ISF process without toolpath control, the formed shape of each step was measured during the forming process. To validate this model, the predicted profile of next step was compared with the formed profile of next step (Figure 12a). The predicted profile of next step was obtained in the predictive model based on the formed profile of the current step. The comparisons from two example steps show that the majority of the predicted profile of the next step matches well with the formed one while the prediction error near the position where the tool touches the blank, namely Zone B in Figure 4, is relatively large. However, there are only a few profile points within this region so that it will not significantly affect the optimisation in the control strategy.

Figure 12b illustrates how the prediction error changes along the steps in terms of the centre point in Figure 12a. The prediction error is defined as the difference between the predicted *z*-coordinate of the centre point and the formed one at each step. As discussed previously in Section 2.4, the control strategy in the vertical direction was applied after the first three steps so that the prediction of the profile begins from the 4th step. The prediction error is relatively large at the early stage of the forming process, which is due to the fact that the springback is

relatively large in the first few steps. As the formed depth increases, the prediction error begins to fluctuate in a small range (-0.05~+0.12mm) from about the 10th step. This illustrates that the prediction error will not accumulate due to the feedback of measured shape state at each time-step. The prediction errors cannot be ignored, especially in the first few steps, but the influence of the prediction errors can be partially compensated in the MPC optimiser by updating the feedback of the measured shape state and control actions at each step. Therefore, the simplifications in the model can be considered as reasonable for in-process feedback control of ISF.

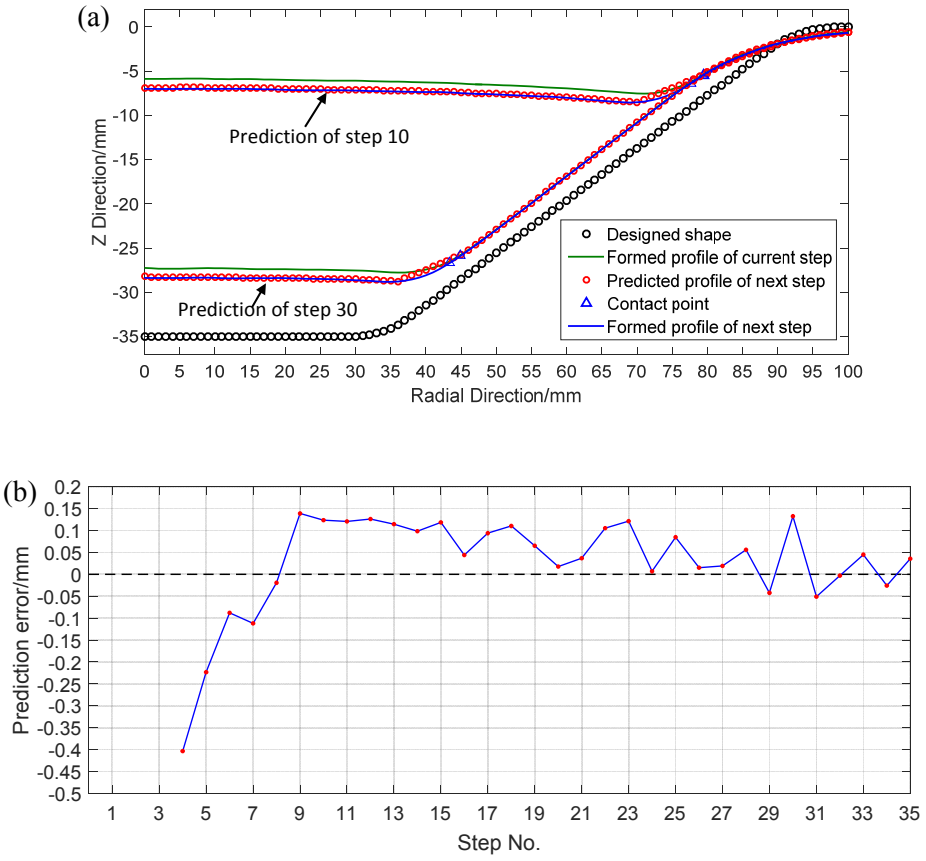

Figure 12 Experimental justification of the predictive model in typical ISF (no control):

(a) Comparison of the predicted profile and formed file at two example steps;

(b) Prediction errors at the centre point of the cross-sectional profile at different steps.

3.2 Case study 1

To verify the developed control algorithm, the test shape is formed in four tests using different strategies (Table 2). Control strategy MPC-0 is the one reported in our previous work by [1]. It only deals with the optimisation of Δu_z. In the two-directional MPC strategy,

two parameters are optimised at the same time. To determine Δu_h at each step, strategy MPC-1 uses a simplified model with uniform horizontal springback while an enhanced model with interpolated horizontal springback is used in strategy MPC-2. In the experimental verification of the MPC strategy, the cross-sectional profile through the centre axis and two corners is chosen as the shape state for feedback control. The profile provides the vertical states of all the points for vertical optimisation. Control actions are conducted after the measured state and the target state are compared and computed in the MPC optimisers.

Table 2 Different strategies

Strategies	Δu_z	Δu_h
No control (typical ISF)	from CAM (1mm)	from CAM
MPC-0 (previous work [1])	MPC-vertical	from CAM
MPC-1	MPC-vertical	MPC-horizontal (uniform horizontal springback)
MPC-2	MPC-vertical	MPC-horizontal (interpolated horizontal springback)

After experimental justification of the predictive model, the results obtained from the four strategies are analysed and compared in several aspects. Figure 13a shows the comparison of profiles from cross-sections through the corners and the corresponding error distributions. The deviations in the *z* direction are regarded as the geometric errors. The results shows that errors formed from the typical ISF process are quite large and those in the wall area reach about 3mm. In Strategy MPC-0, errors at the bottom are greatly reduced to ± 0.3 mm while those on the wall are also reduced, compared with those in uncontrolled ISF, and are still relatively large (± 1 mm). With the addition of the horizontal MPC module, significant accuracy improvement (within ± 0.3 mm) is achieved in both the bottom and wall areas in MPC-1 and MPC-2. The errors beyond the region concerned are caused by the bending effect and will not be discussed in this work since this is uncontrollable in SPIF [13].

However, in MPC-1, the model with an assumption of uniform horizontal springback fails to obtain high-level accuracy on the wall in terms of the cross-section through the centre and the middle of the wall. Figure 14a and b show that the accuracy of the wall area gets worse in MPC-1 compared with MPC-0. In MPC-1, each contour was horizontally enlarged in a constant scale based on the horizontal error of cross-sectional profile through the corners. This leads to too much deformation on the planar walls of the pyramid shape because the

horizontal springback values on the planar walls are less than those at the curved corners where there are larger residual stresses. Using an enhanced model that better accounts for the spatial variance of horizontal springback, MPC-2 helps to address the issue in MPC-1 and greatly reduces the error on the planar walls, as shown in Figure 14b. In all three controlled processes, accuracy at the bottom have been improved to the range of ± 0.3 mm. Figure 15a illustrates the vertical inputs along all the steps and Figure 15b and Figure 15c show how the horizontal input differs from the initial one at each step at the radial directions through the corner and the wall middle, respectively.

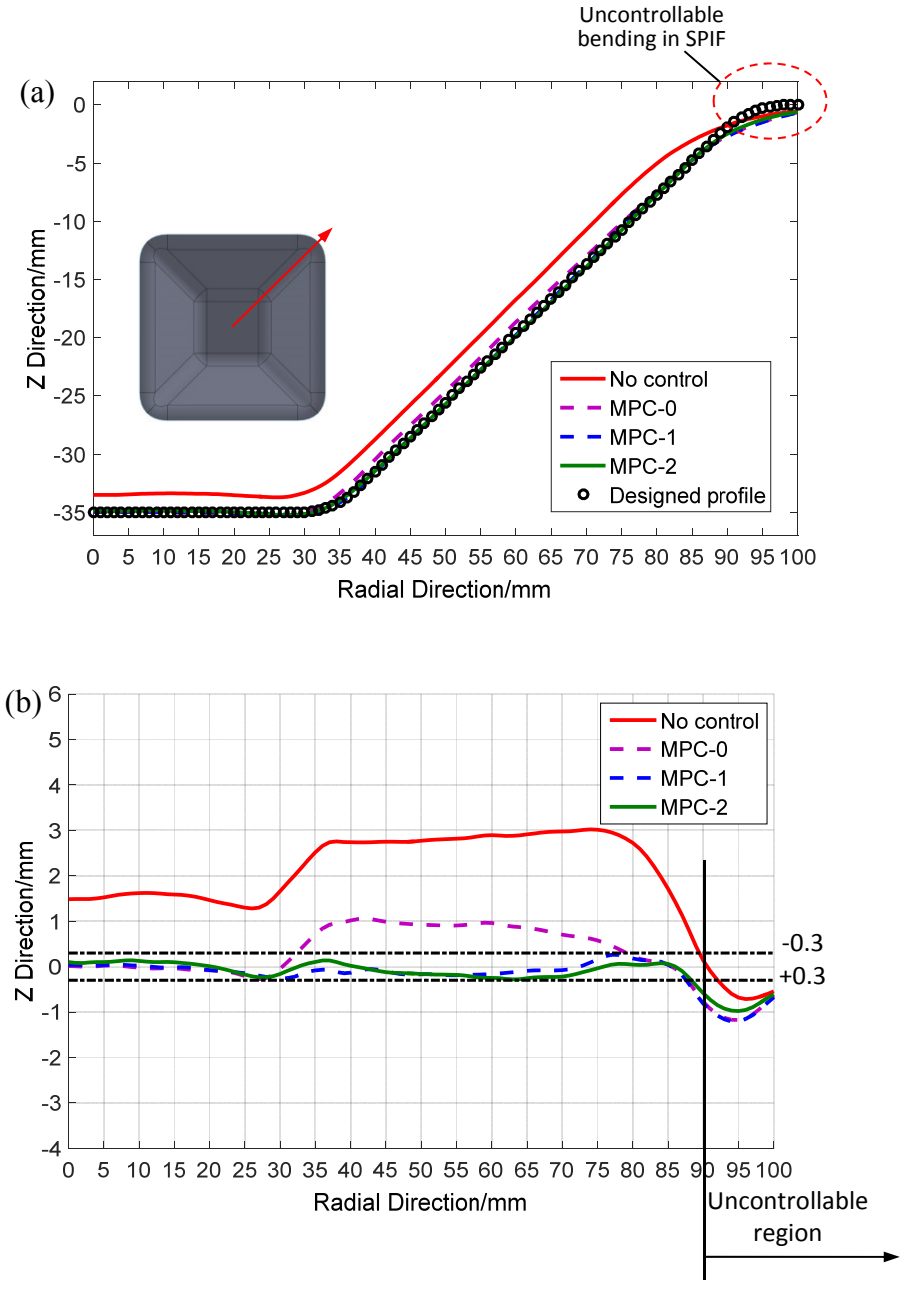

Figure 13 : (a) Cross-sectional profiles through the corners; (b) Corresponding error distribution.

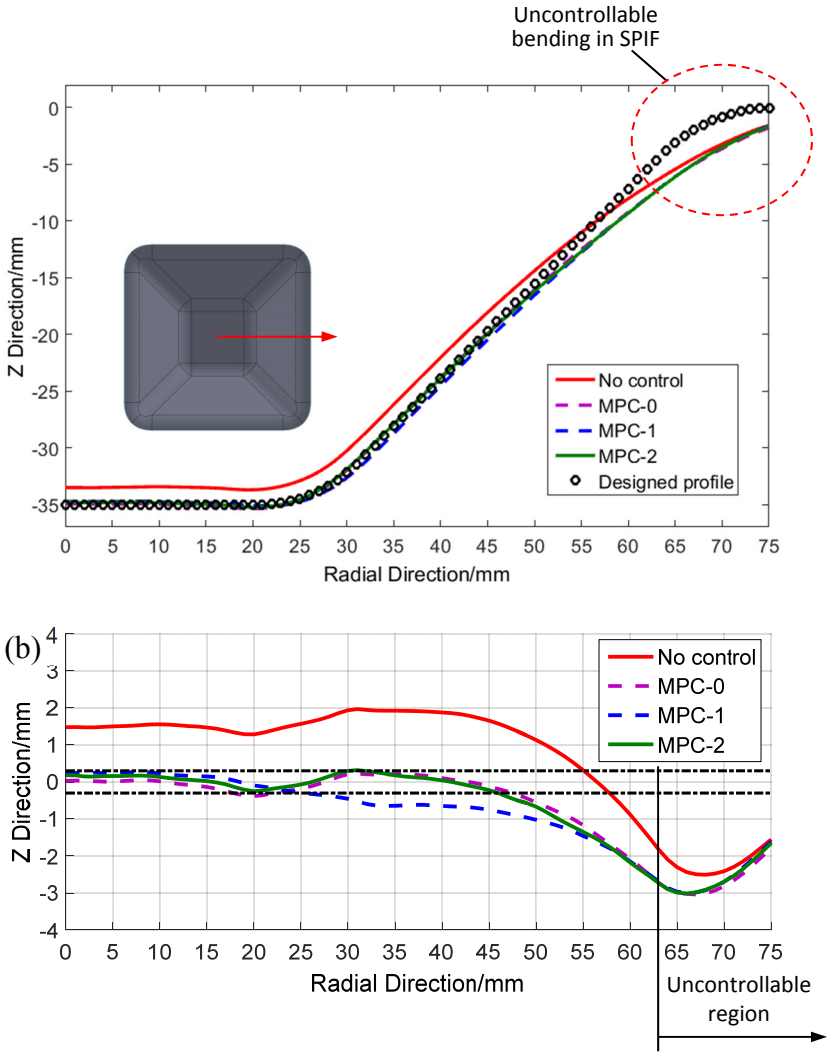

Figure 14: (a) Cross-sectional profiles through the middle of walls; (b) Corresponding error distribution.

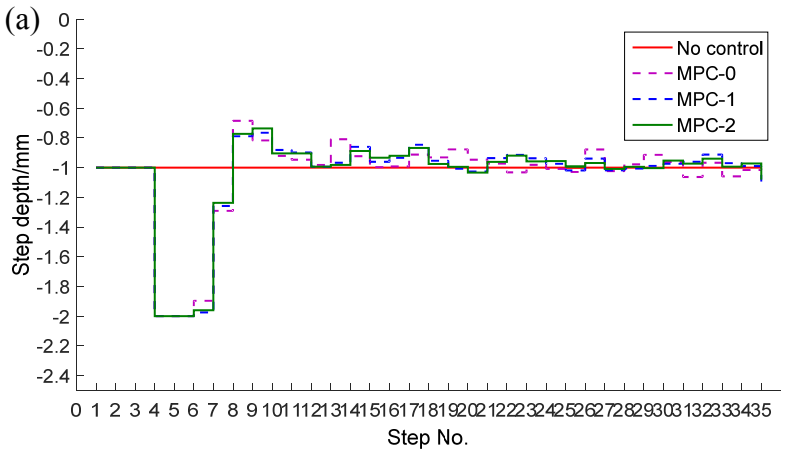

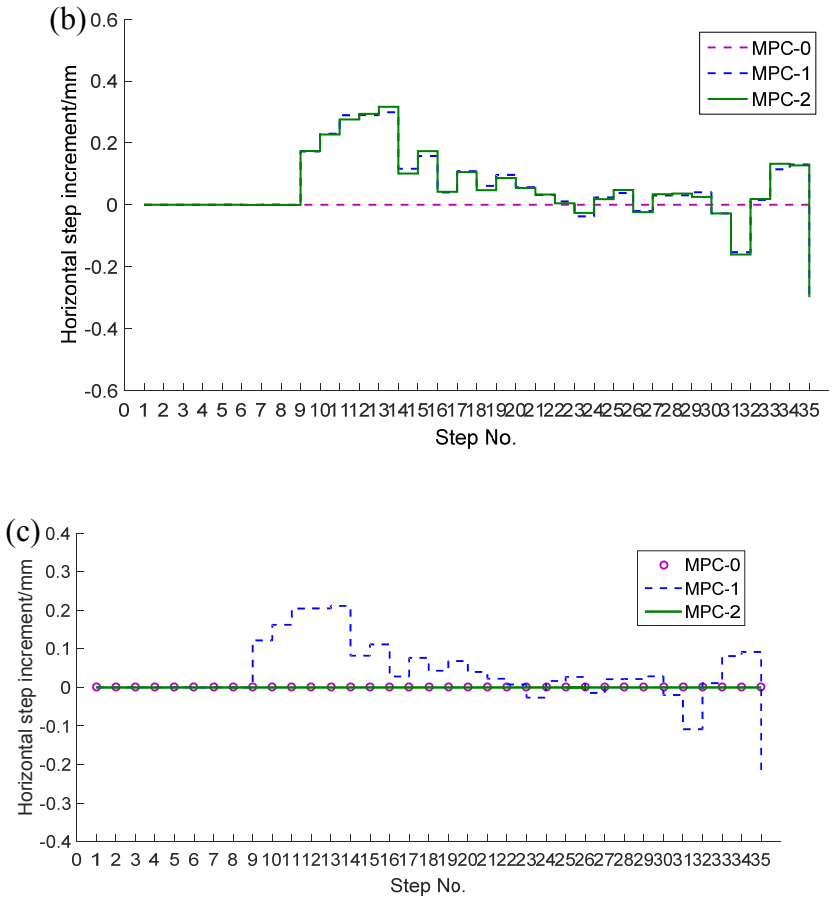

Figure 15 Inputs along the steps: (a) Step depth;
(b) Horizontal step increment through the corner (deviations from initial inputs);
(c) Horizontal step increment through the wall middle (deviations from initial inputs).

To fully evaluate the geometric accuracy from different strategies, error maps of the formed parts, in the unclamped condition, are presented in Figure 16. The scanned shape and the CAD file are compared in the 3D comparison module of Geomagic Qualify. In additional to these maps, horizontal sections were made through a horizontal plane with the depth of 25mm to quantify the horizontal error distribution more clearly. Horizontal cross-sectional profiles along a section trajectory (from A to B in Figure 16 b, c, and d) and the corresponding error distributions are compared in terms of strategy MPC-0, strategy MPC-1, and strategy MPC-2, as shown in Figure 17.

Compared with uncontrolled ISF with no toolpath control (Figure 16a), large accuracy improvements have been observed at the bottom area and part of wall areas in strategy MPC-0 while errors around the corners have been reduced to some extent and still need to be further reduced (Figure 16b). Figure 17 shows that most of the wall areas have high accuracy (+0.3mm) but errors around the corners have reached the level of +1.5mm.

In strategy MPC-1, a horizontal optimisation module was added to improve the poor accuracy in the horizontal direction. Figure 16c shows that errors around corners are significantly lessened and the accuracy at the bottom area remains similar to MPC-0. This indicates that the horizontal module in strategy MPC-1 helps to increase the geometric accuracy around the corners and it does not have significant influence on the vertical optimisation. This means the varying of Δu_h in a range at one step does not substantially influence the formed depth of bottom areas. Figure 17 shows that a new problem occurred associated with MPC-1. The errors of main wall areas have increased to a higher level (-1.0 mm) from strategy MPC-0 as these areas were over-deformed beyond the walls of the part design. Figure 17 also shows that the horizontal errors are not uniformly distributed along the section trajectory at a certain z-level, which demonstrates that the springback is not uniformly distributed in the horizontal direction.

With the use of strategy MPC-2, the bottom area and most part of the wall areas have high accuracy ($\pm$0.3 mm) while small part of the wall areas near the corner is less accurate but still have improved accuracy ($\pm$0.5 mm), as illustrated in Figure 16d and Figure 17. This can be due to the fact that the estimation of the distribution of springback effect along the horizontal profile is not perfect. This limitation might be solved when many more sample points on the horizontal profile are considered for the estimation of horizontal errors in various radial directions. Overall, these show that strategy MPC-2 with an interpolated springback model can give better evaluation of the horizontal springback distribution than MPC-1 with a uniform springback model. Compared with uncontrolled ISF and our previous work by [1], the dimensional accuracy of the formed part has been greatly improved in the concerned areas.

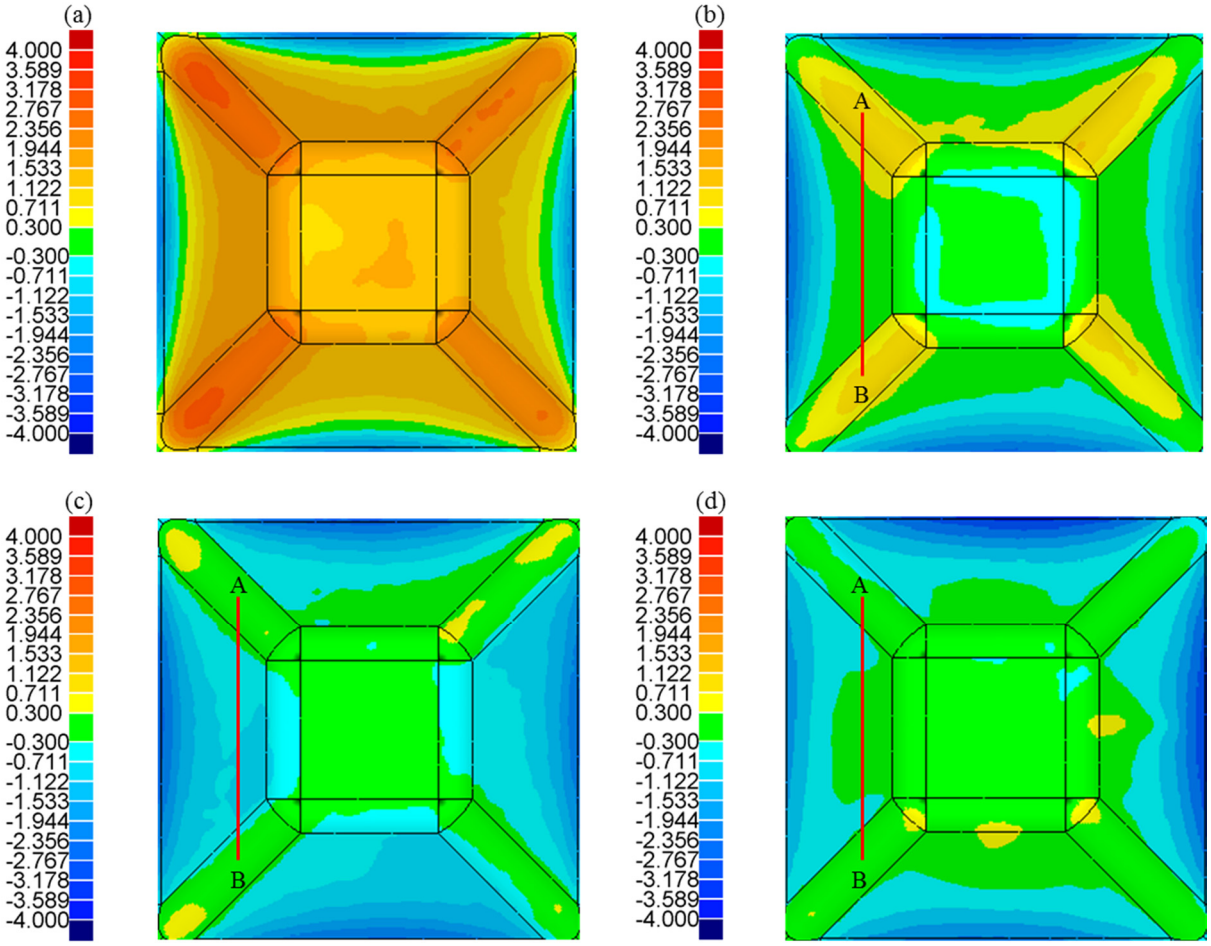

Figure 16 Geometric error maps of the formed parts: (a) No control; (b) MPC-0; (c) MPC-1; (d) MPC-2.

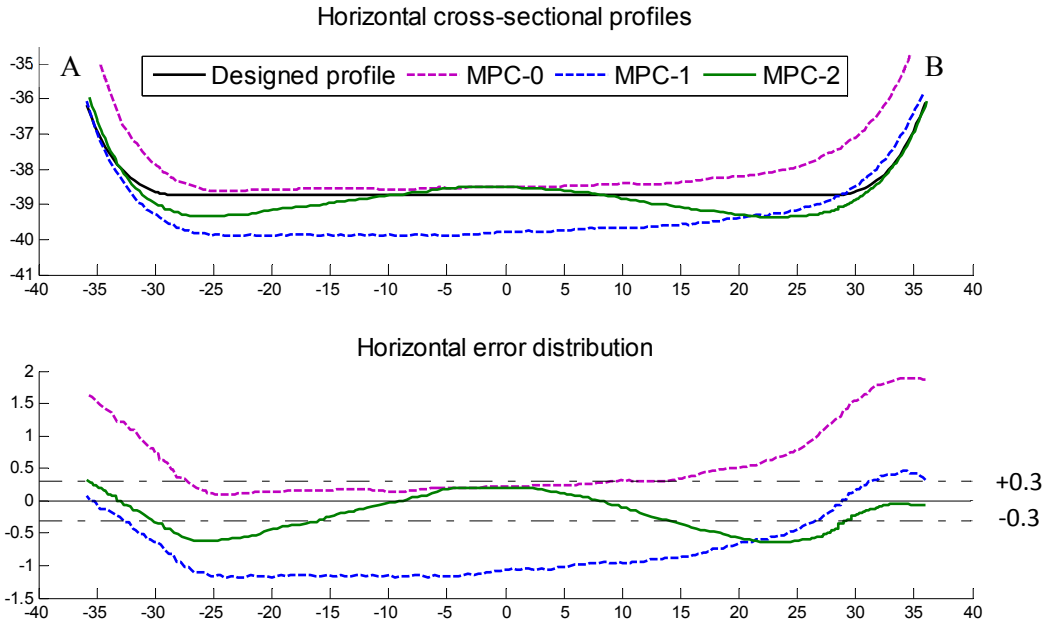

Figure 17 Comparison of horizontal cross-sectional profiles and the corresponding error distributions.

3.3 Case study 2

The developed MPC control algorithm was applied to form an asymmetric cone to demonstrate the applicability of the developed control strategy to asymmetric shapes. More specifically, strategy MPC-2 using the model with interpolated horizontal springback was used in this case study. To compare typical ISF with no toolpath control and controlled ISF, the geometric accuracy of formed shapes in the unclamped condition are analysed in terms of the geometric error maps. At the same time, the influence of the release of clamping plates on the formed shapes was analysed.

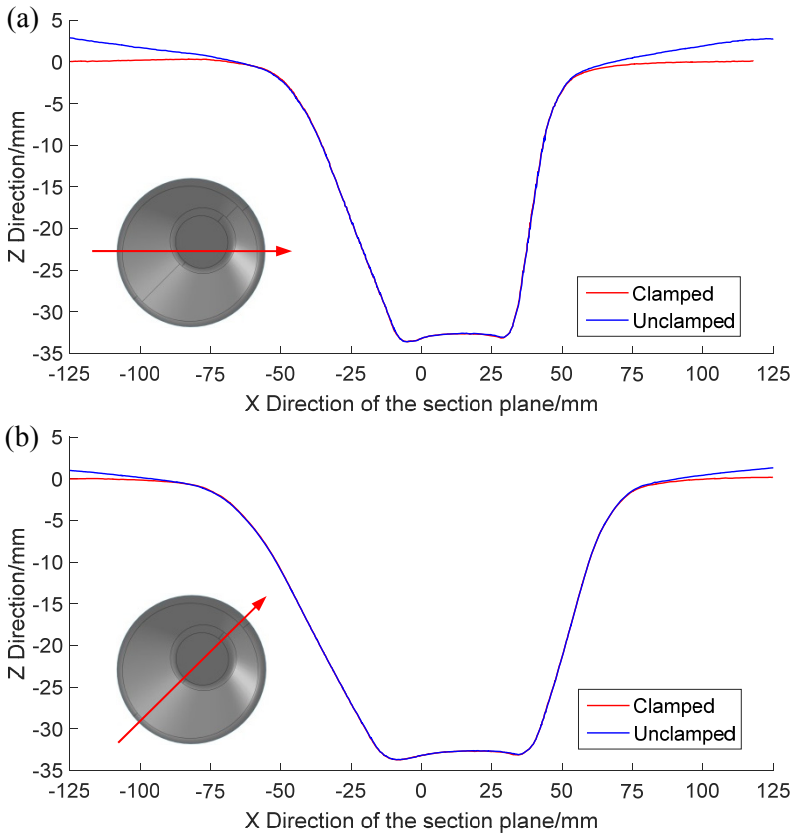

Figure 18 Comparison of the formed shapes in clamped and unclamped conditions: (a) Section through plane XOZ ($\theta = 0°$); (b) Section through the radial direction $\theta = 45°$.

Figure 18 shows that there is large springback at the clamped edges of the metal blank after the removal of clamping plates, which is caused by the residual stress around the clamped areas. In contrast, the release of clamping plates nearly has no influences on the concerned region of formed part. These results indicate that the formed region should not be too close to the clamped edges when choosing the size of the metal blank for part fabrication.

The error distributions of the whole parts are shown in Figure 19. In the base and most wall areas of the formed part, the geometric accuracy is greatly improved from ±3 mm to ±0.3 mm with the use of the MPC control strategy. In Figure 19b, an annulus zone in light blue colour can be observed at the bottom, which is the "pillow effect" that occurs at the flat base of the part formed in SPIF [2]. This area is where the tool travels at the final step and it is lower than the centre area of the bottom due to the residual stress. The "pillow effect" can also be observed in Figure 18 and Figure 19a. This work focused on reducing the geometric errors caused by springback so that the errors caused by "pillow effect" will not be studied here. In some very small areas of the wall, the geometric errors have been reduced but remain slightly larger than the desirable level. These can be due to fact that current model with interpolated horizontal springback does not fully capture how the horizontal springback is actually distributed along the horizontal profiles. Nevertheless, the developed two-directional control algorithm leads to an order of magnitude overall improvement in geometric accuracy compared with ISF without toolpath control.

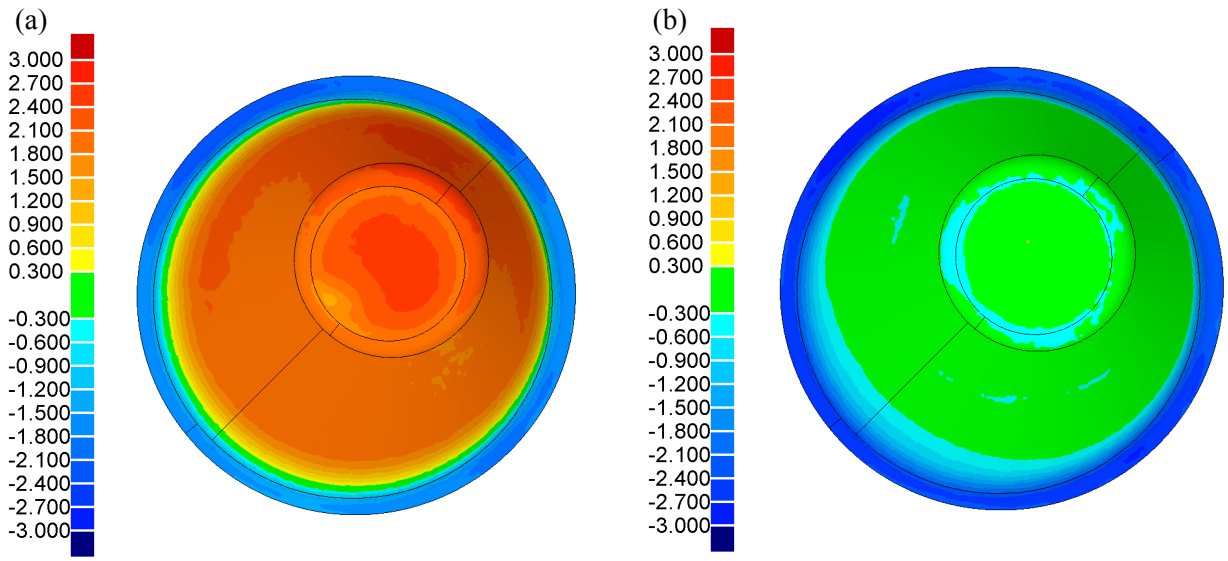

Figure 19 Comparison of the formed parts in terms of the geometric error map: (a) No control; (b) Control strategy MPC-2.

4 Conclusions and future work

To address the limitation of poor geometric accuracy in ISF processes, reported attempts for accuracy improvement have concentrated on toolpath optimisation/correction. In this paper, a two-directional MPC control algorithm for in-process toolpath correction in ISF has been developed and validated in two case studies. With two separate MPC modules in vertical and

horizontal directions, the toolpath was corrected by optimising Δu_z and Δu_h at each step during the forming process. In the first case study, two different simplifying models for the horizontal optimisation were tested in strategy MPC-1 and strategy MPC-2, respectively. Results show that our previous control strategy (MPC-0) leads to significant error reduction in the bottom area from ± 3 mm (No control) to ± 0.3mm while one of its limitation is that errors around the pyramid corners are relatively large (+1.5 mm). The two-directional strategy MPC-1 can help to improve the geometric accuracy around the corners while the wall areas were excessively formed. Strategy MPC-2 contributes to addressing the major limitation of strategy MPC-0 as well as the shortcoming of MPC-1. Then, control strategy MPC-2 was further validated in case study 2 for forming an asymmetric cone. The geometric errors in the base and most wall areas have been reduced from ± 3 mm (No control) to ± 0.3 mm (MPC-2). The two-directional control strategy provides a useful feedback control method to improve the accuracy via toolpath correction in SPIF. What's more, the ISF process with MPC control offers a good attempt for accurate manufacturing via in-process control and/or optimisation.

The interpolated springback model in strategy MPC-2 can provide better evaluation of the distribution of horizontal springback than the uniform springback model in strategy MPC-1. However, the primary limitation of the current work is that the interpolated model still cannot fully capture how the horizontal springback is distributed along the horizontal profile because only serveal profile points in the predefined radial directions are utilised to evaluate the horizontal errors using an interpolation method. In the future, this limitation might be overcomed in the generalisation of the current horizontal model by using many more profile points for more accurate evaluation of the horizontal springback distribution. Besides this, the integration of the developed control algorithm and multi-stage strategy in ISF may offer a means of reducing geometric errors in the region that has already been formed.

Acknowledgements

This research is partially supported by the China Scholarship Council (CSC) scholarship.

References

[1] H. Lu, M. Kearney, Y. Li, S. Liu, W.T. Daniel, P. Meehan, Model predictive control of incremental sheet forming for geometric accuracy improvement, The International Journal of Advanced Manufacturing Technology, (2015) 1-14.
[2] F. Micari, G. Ambrogio, L. Filice, Shape and dimensional accuracy in Single Point Incremental Forming: State of the art and future trends, Journal of Materials Processing Technology, 191 (2007) 390-395.
[3] A. Attanasio, E. Ceretti, C. Giardini, Optimization of tool path in two points incremental forming, Journal of Materials Processing Technology, 177 (2006) 409-412.
[4] G. Ambrogio, L. Napoli, L. Filice, A novel approach based on multiple back-drawing incremental forming to reduce geometry deviation, International Journal of Material Forming, 2 (2009) 9-12.
[5] B.T. Araghi, G.L. Manco, M. Bambach, G. Hirt, Investigation into a new hybrid forming process: Incremental sheet forming combined with stretch forming, Cirp Ann-Manuf Techn, 58 (2009) 225-228.
[6] A.K. Behera, B. Lauwers, J.R. Duflou, Tool path generation for single point incremental forming using intelligent sequencing and multi-step mesh morphing techniques, International Journal of Material Forming, 8 (2014) 517-532.
[7] M. Bambach, B. Taleb Araghi, G. Hirt, Strategies to improve the geometric accuracy in asymmetric single point incremental forming, Production Engineering, 3 (2009) 145-156.
[8] G. Ambrogio, I. Costantino, L. De Napoli, L. Filice, L. Fratini, M. Muzzupappa, Influence of some relevant process parameters on the dimensional accuracy in incremental forming: a numerical and experimental investigation, Journal of Materials Processing Technology, 153–154 (2004) 501-507.
[9] G. Hirt, J. Ames, M. Bambach, R. Kopp, R. Kopp, Forming strategies and Process Modelling for CNC Incremental Sheet Forming, CIRP Annals - Manufacturing Technology, 53 (2004) 203-206.
[10] A.K. Behera, J. Verbert, B. Lauwers, J.R. Duflou, Tool path compensation strategies for single point incremental sheet forming using multivariate adaptive regression splines, Computer-Aided Design, 45 (2013) 575-590.
[11] A. Fiorentino, G.C. Feriti, C. Giardini, E. Ceretti, Part precision improvement in incremental sheet forming of not axisymmetric parts using an artificial cognitive system, Journal of Manufacturing Systems, 35 (2015) 215-222.
[12] J.M. Allwood, O. Music, A. Raithathna, S.R. Duncan, Closed-loop feedback control of product properties in flexible metal forming processes with mobile tools, CIRP Annals - Manufacturing Technology, 58 (2009) 287-290.
[13] H. Wang, S. Duncan, Optimization of tool trajectory for Incremental Sheet Forming using closed loop control, in: Automation Science and Engineering (CASE), 2011 IEEE Conference on, 2011, pp. 779-784.
[14] H. Wang, S. Duncan, Constrained model predictive control of an incremental sheet forming process, in: Control Applications (CCA), 2011 IEEE International Conference on, 2011, pp. 1288-1293.
[15] E.F. Camacho, C.B. Alba, Model predictive control, Springer Science & Business Media, 2013.
[16] S.B.M. Echrif, M. Hrairi, Research and Progress in Incremental Sheet Forming Processes, Mater Manuf Process, 26 (2011) 1404-1414.
[17] Y. Li, Z. Liu, W.J.T. Daniel, P.A. Meehan, Simulation and Experimental Observations of Effect of Different Contact Interfaces on the Incremental Sheet Forming Process, Mater Manuf Process, 29 (2014) 121-128.
[18] K. Yilamu, R. Hino, H. Hamasaki, F. Yoshida, Air bending and springback of stainless steel clad aluminum sheet, Journal of Materials Processing Technology, 210 (2010) 272-278.

Paper 4

Part accuracy improvement in two point incremental forming with a partial die using a model predictive control algorithm

Lu, H., Kearney, M, Wang C., Liu, S., & Meehan, P. A

Precision Engineering: Journal of the International Societies for Precision Engineering and Nanotechnology

2017, Volume: 49, Pages: 179-188.

Part accuracy improvement in two point incremental forming with a partial die using a model predictive control algorithm

Haibo Lu [a,*], Michael Kearney [a], Chenhao Wang [a], Sheng Liu [a] and Paul A. Meehan [a]

[a] School of Mechanical & Mining Engineering, University of Queensland, St Lucia, Brisbane, QLD 4072, Australia

* Corresponding author. Tel.: +61 (0)7 3346 9570.

E-mail addresses: h.lu2@uq.edu.au, luhaibocsu@gmail.com (H. Lu)

Keywords: Two point incremental forming; Model predictive control; Geometric accuracy; Toolpath correction.

Abstract

As a flexible forming technology, Incremental Sheet Forming (ISF) is a promising alternative to traditional sheet forming processes in small-batch or customised production but suffers from low part accuracy in terms of its application in the industry. The ISF toolpath has direct influences on the geometric accuracy of the formed part since the part is formed by a simple tool following the toolpath. Based on the basic structure of a simple Model Predictive Control (MPC) algorithm designed for Single Point Incremental Forming (SPIF) in our previous work [1] that only dealt with the toolpath correction in the vertical direction, an enhanced MPC algorithm has been developed specially for Two Point Incremental Forming (TPIF) with a partial die in this work. The enhanced control algorithm is able to correct the toolpath in both the vertical and horizontal directions. In the newly-added horizontal control module, intensive profile points in the evenly distributed radial directions of the horizontal section were used to estimate the horizontal error distribution along the horizontal sectional profile during the forming process. The toolpath correction was performed through properly

adjusting the toolpath in two directions based on the optimised toolpath parameters at each step. A case study for forming a non-axisymmetric shape was conducted to experimentally validate the developed toolpath correction strategy. Experiment results indicate that the two-directional toolpath correction approach contributes to part accuracy improvement in TPIF compared with the typical TPIF process that is without toolpath correction.

1. Introduction

ISF is a flexible sheet forming technology that offers a promising alternative to traditional sheet forming processes for the cost-effective production of small-batch or customised parts. Without using dedicated dies, it uses a simple tool with a hemispherical end to form the sheet parts. By travelling along a 3D CAM toolpath on the surface of the sheet, the tool end deforms the sheet incrementally with the plastic deformation localised near the tool end [2] during the forming process. The two main variations of ISF are SPIF and TPIF. The main difference is that TPIF uses simple dies besides the forming tool (Figure 1b and c) while SPIF (Figure 1a) only uses a single tool to form the parts. To be more specific, TPIF can be classified into two types, namely TPIF with a full die and TPIF with a partial die, as shown in Figure 1b and c. The simple dies are generally made of cheap materials like timber or resin [3] so that the cost in the fabrication and storage of dies is not huge. With the use of supporting dies, TPIF generally leads to better geometric accuracy of the formed parts than SPIF [4].

The major limitation of ISF is the poor geometric accuracy of the formed parts. The errors are usually caused by the sheet springback and sheet bending. The sheet springback accounts for the geometric inaccuracies in the most areas of the formed parts. In addition, the “pillow effect”, an unwanted curved surface, typically occurs on the flat

base of the part formed in SPIF [5]. In order to improve the poor geometric accuracy, some attempts have been presented in the literature, including experimental investigation of process parameters [4, 6], hybrid ISF processes [7-9], the use of partially cut-out blanks [10], and a multi-stage strategy [3].

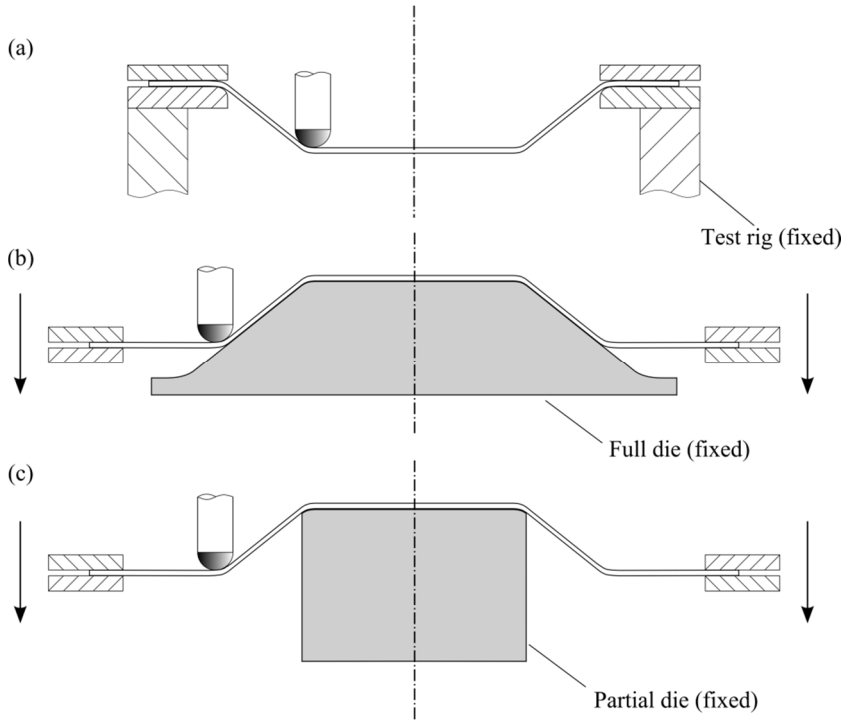

Figure 1 Typical ISF variations.

Recently, many studies concentrated on the toolpath correction/optimisation. The ISF toolpath can be corrected by using error compensation based on trial fabrications [11], a feature-based toolpath generation strategy [12], a Multivariate Adaptive Regression splines (MARS) correction strategy [13], iterative algorithms based on a transfer function [14], and an artificial cognitive system [15]. Moreover, some in-process toolpath correction approaches were performed in SPIF based on a control strategy using spatial impulse responses of the process [16] and a MPC strategy [17]. In particular, the MPC control strategy reported in [17] only dealt with the optimisation of the step depth, which is one of the two critical toolpath parameters in ISF. The

predictive model in the control algorithm was obtained based on the formed shape in SPIF without toolpath control. In our previous work [1], a different MPC control strategy was developed to improve geometric accuracy via in-process toolpath correction. The MPC control algorithm used an analytical predictive model to vertically correct the toolpath by optimising the step depth during the forming process. The results showed that the geometric errors were improved in the base areas of the formed part, but the errors in the part wall areas were still relatively large since the proposed control algorithm only dealt with toolpath correction in the vertical direction. Additionally, obvious "pillow effect" was observed at the flat bases of the parts formed in the SPIF processes. The "pillow effect" is one of typical geometric inaccuracies in SPIF, however, there is no notable "pillow effect" in TPIF with the use of dies to support the flat base [18].

Currently, there are not many studies that have been reported on in-process toolpath correction in TPIF. In TPIF with a single full die, it is difficult to correct the geometric errors by freely adjusting the toolpath because the tool movement is greatly limited by the full die with a definite shape as shown in Figure 1b. A possible way for toolpath correction in TPIF with a full die is to use different full dies with modified shapes at the intermediate stages of the forming process. It would be time-consuming to fabricate multiple full dies for forming a part. On the contrary, TPIF with a partial die is more flexible and the toolpath can be freely adjusted in a large range for geometric accuracy improvement.

This paper presents a MPC control algorithm for TPIF with a partial die to improve geometric accuracy via in-process toolpath correction in the horizontal and vertical directions. Based on our previous work for SPIF toolpath correction only in the vertical

direction [1], an enhanced MPC algorithm has been developed specially for TPIF with a partial die to correct the toolpath through optimising the step depth and the horizontal step increment. In particular, a horizontal control module is added in the enhanced MPC algorithm for toolpath correction in the horizontal direction. In the horizontal control module, intensive profile points in the evenly distributed radial directions of the horizontal section were used to estimate the horizontal error distribution along the horizontal sectional profile during the forming process, which provide an achievable method to estimate the horizontal error distribution in forming general shapes. Two analytical models, based on the deformation nature in TPIF with a partial, were used for shape state predictions in two directions so that in-process toolpath control and correction can be directly conducted. During the forming process, shape measurement is performed at each time-step to provide shape feedback in the control algorithm. In the two (vertical and horizontal) separate MPC modules, optimised values of step depth and horizontal step increment are used to correct the toolpath in the vertical and horizontal directions, respectively. A non-axisymmetric shape was used to experimentally validate the developed control strategy. The experimental results were analysed by comparing the typical TPIF process and the TPIF process with toolpath correction in terms of horizontal sectional profiles, the error colour map, and the percentage distribution of geometric deviations. This work offers an achievable approach on in-process toolpath control/correction in TPIF with improved geometric accuracy on the final parts.

2. MPC control strategy for TPIF with a partial die

MPC is an advanced control technology and it is able to use linear models to deal with the control of constrained non-linear systems in various industry processes [17, 19]. This control technology is used to drive the system state following the target trajectory

by minimising the predicted states and the target states in a finite horizon. Suppose a nonlinear system is modelled as,

$$y(k+1) = f(y(k), \Delta u(k)). \tag{1}$$

The optimisation problem solved by MPC at each time instant is expressed in the following equation,

$$\min\ J(k) = \left\| \hat{Y}(k) - W(k) \right\|^2 + \lambda \left\| \Delta U(k) \right\|^2, \tag{2}$$

$$\text{subject to} \quad \hat{y}(k+1 \mid k) = Ay(k) + B\Delta u(k)$$

$$\Delta u_{\min} \le \Delta u \le \Delta u_{\max}$$

where $J(k)$ is the cost function, $\hat{Y}(k) = \left[\hat{y}(k+1 \mid k), \hat{y}(k+2 \mid k), \ldots, \hat{y}(k+N_p \mid k) \right]^T$ contains the predicted system outputs and $\hat{y}(k+1 \mid k) = Ay(k) + B\Delta u(k)$ is the linear simplification of the system, $W = \left[w(k+1), w(k+2), \ldots, w(k+N_p) \right]^T$ is the target trajectory, $\Delta U = \left[\Delta u(k+1), \Delta u(k+2), \ldots, \Delta u(k+N_p) \right]^T$ collects the system inputs over the prediction horizon (N_p).

The process model is dynamic because the prediction model at each sampling instant is updated based on the currently measured state and the estimated future inputs. Control actions over the finite horizon are obtained by solving an optimisation problem at the current sampling instant but only the first move of the control actions will be applied in the future.

The in-process toolpath correction strategy for TPIF with a partial die is developed based on a two-directional MPC control algorithm. The basic concept of toolpath correction in TPIF is illustrated in Figure 2. There are geometric errors on the formed part using the initial toolpath. By correcting the toolpath based on shape feedback in the MPC controlled process, the geometric errors can be reduced on the final parts. More specifically, the toolpath is corrected in two perpendicular directions during the forming process. This is achieved by properly modifying the values of two critical toolpath parameters, namely the horizontal step increment (Δu_r) and the step depth (Δu_z) in Figure 4, based on the optimisation in the MPC algorithm.

Figure 3 illustrates the structure of feedback control of TPIF using the two-directional MPC control algorithm. The forming process consists of a number of forming steps and each forming step corresponds to the forming a single contour. The control algorithm takes each forming step as a time-step. At time-step k, the measured shape states of currently formed shape are imported to the predictive models for shape state predictions of future several steps in the two directions. To drive the predicted shape states as close as to target shape states, the MPC optimisers will optimise Δu_z and Δu_r of the next several steps, however only the optimised Δu_z and Δu_r of the following single step ($k+1$) are used to correct the toolpath. In this way, the control of toolpath parameters will be repeated step by step till the end of the whole forming process.

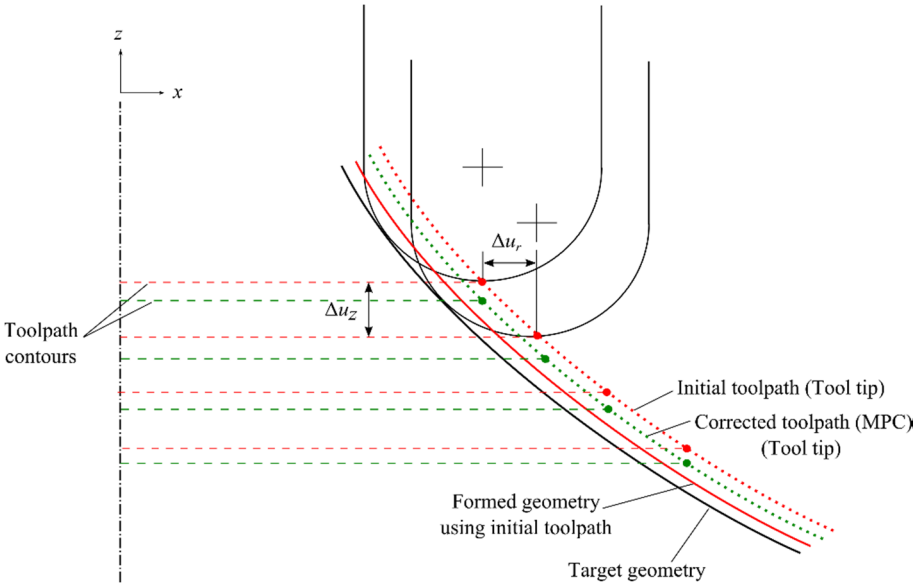

Figure 2 Toolpath correction by using a MPC control algorithm (section view).

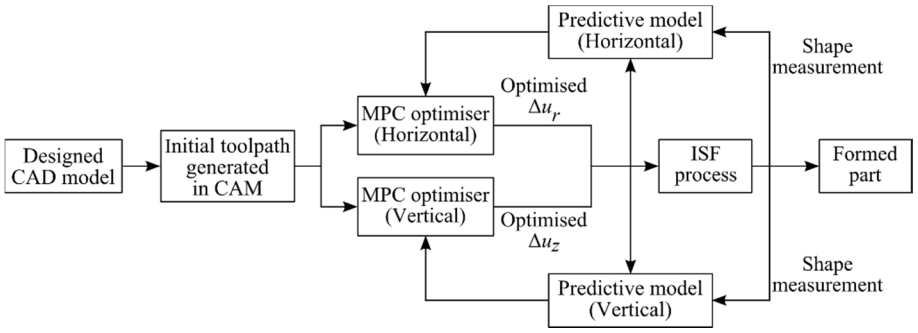

Figure 3 MPC control of two toolpath parameters in ISF.

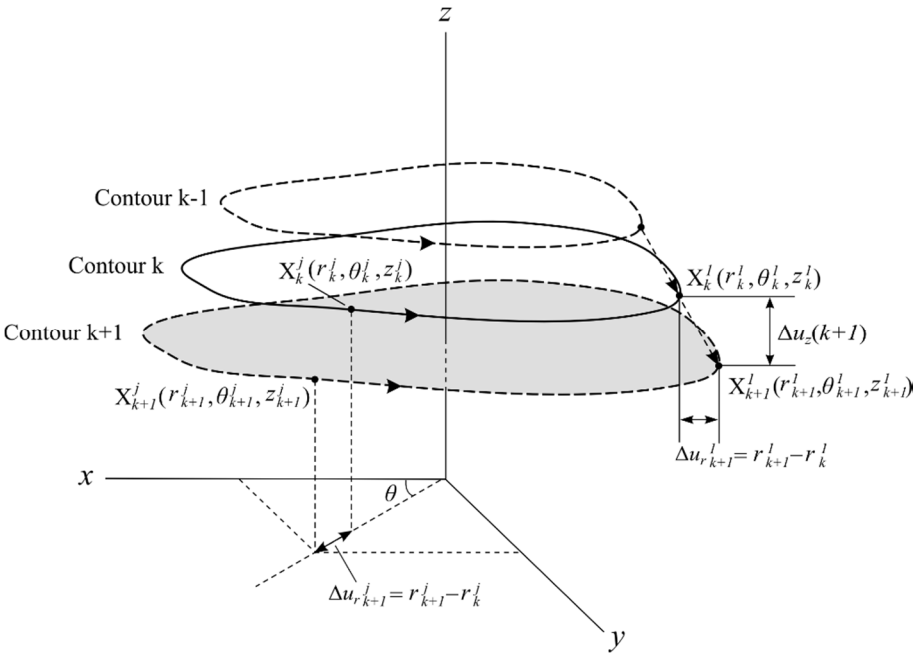

Figure 4 Two critical parameters of the contour toolpath.

There are no specialised modules for generating ISF toolpath in commercial CAM softwares. The most commonly-used toolpath type in ISF is the parallel contour toolpath generated in the milling module of CAM softwares [20]. It consists of a certain number of contours that are parallel to each other, as shown in Figure 4. In this control model, each contour is represented by a certain number (m) of contour points defined in the cylindrical coordinate system. Therefore, the toolpath can be horizontally corrected in enough number of radial directions when forming general shapes, such as non-axisymmetric shapes. Δu_r collects the radial distances between on two successive contours in terms of the predefined contour points (Figure 4). Δu_r can be represented as,

$$\Delta u_r(k+1) = \left[\Delta u_r^1(k+1), \Delta u_r^2(k+1), \ldots, \Delta u_r^j(k+1), \ldots, \Delta u_r^m(k+1)\right], \tag{3}$$

$$\text{and } \Delta u_r^j(k+1) = r_{k+1}^j - r_k^j, j = 1,2,...,m$$

where m is the number of contour points at each step, $\Delta u_r^j(k+1)$ is the radial distance between corresponding profile points from two neighbouring contours.

Step depth, Δu_z, is the vertical depth that the tool travels down between two consecutive steps. In particular, the number of contours depends on the Δu_z value and the total depth of the shape design. Therefore, the number of steps is also determined by Δu_z and the shape depth since the forming of a single contour is taken as a time-step. At each step, the z coordinates of all contour points on a single contour are the same since these points are on the same z-level plane. This can be expressed as,

$$\Delta u_z(k+1) = z_{k+1} - z_k . \quad (4)$$

Between two neighboring contours of the toolpath, Δu_z and Δu_r account for the tool movements in the vertical direction and the horizontal direction, respectively. Therefore, two separate MPC control modules are designed to optimise the two parameters separately.

2.1 MPC control algorithm in TPIF

A simple MPC control algorithm that only optimises Δu_z in SPIF was demonstrated in our previous study [1] that it was able to properly correct the toolpath in the vertical direction. Toolpath correction in the vertical direction leads to geometric accuracy improvement in the base area of the formed parts whilst the part accuracy in the wall areas requires further improvement. This is consistent with the work reported in [17]. In this work, an enhanced MPC algorithm has been developed specially for TPIF with a partial die to correct the toolpath in the vertical direction as well as the horizontal direction. To be more specific, a new horizontal MPC module is added into the control algorithm to correct the toolpath in both the horizontal and vertical directions to reduce dimensional deviations of the formed part. The predictive models in the vertical and horizontal control modules are analytical models that are built based on the deformation nature of TPIF with a partial die in terms of the two directions.

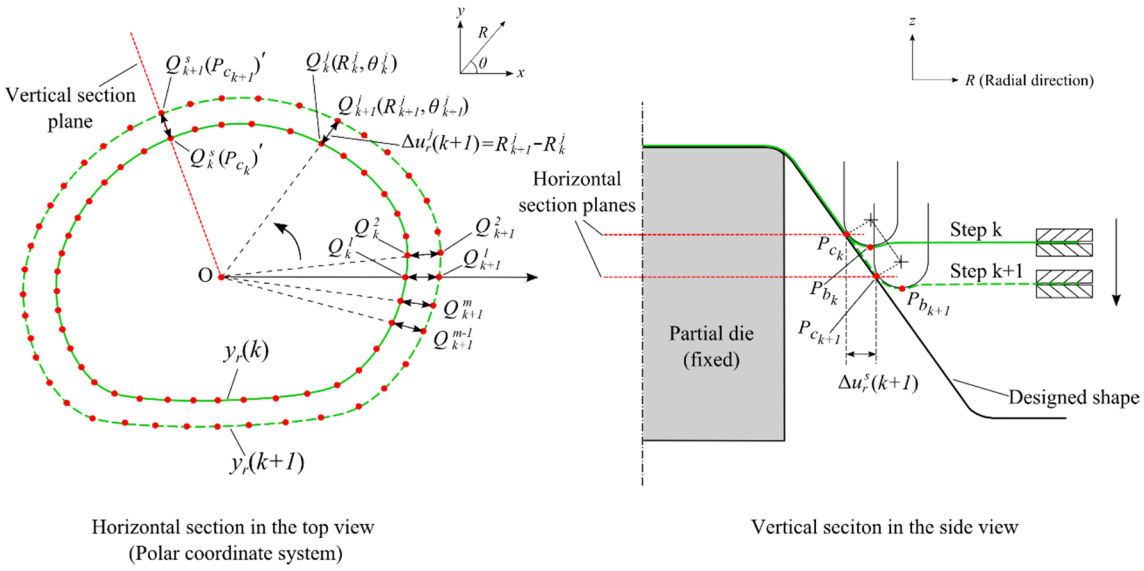

Figure 5 Cross-sectional profiles of formed shapes during TPIF.

Figure 5 shows the cross-sectional profiles of the formed shape in two directions during the forming process of TPIF. At each step, the formed shape is scanned and sectioned horizontally and vertically to get the cross-sectional profiles in the horizontal and vertical directions, respectively. The locations of the contact point P_{c_k} and the bottom point P_{b_k} are geometrically identified based on the local feature of the currently formed shape after scanning the formed shape. The cross-sectional profiles in the two directions are taken as the shape states for optimisation in the control modules. Each vertical sectional profile is obtained in a vertical section plane through a predefined radial direction $\theta_k^s = \theta_k^j (j = 1, 2, \cdots, m)$. On the vertical sectional profiles, contact points P_{c_k} and $P_{c_{k+1}}$ in the side view are the points Q_k^s and Q_{k+1}^s in the top view, respectively. The top view illustrates the horizontal sections, which corresponds to the horizontal section planes in the side view, at two neighbouring steps.

Since the deformation models for building the predictive models in the vertical and horizontal modules are different and they are obtained by sectioning the part in the

vertical and horizontal directions, respectively, the two control modules are described and explained separately for clear understanding.

2.1.1 Horizontal control module

The newly-added horizontal MPC module is aimed to optimise Δu_r for toolpath correction in the horizontal direction. In the horizontal model, the horizontal sectional profile at each step is represented by intensive profile points in different radial directions, as seen in the top view of Figure 5. This method can provide proper accuracy for the estimation of horizontal error distribution in forming general shapes. As a matter of the resolution for representing a curve, more profile points can give more accurate estimation of the formed sectional profiles, especially. To guarantee enough accuracy in representing the formed profiles and the horizontal error distribution, the horizontal sectional profile at each step is sampled in 360 uniformly distributed radial directions in this study, as shown in the top view of Figure 5. That is, the number of profile points is set as m=360. At time-step k, $Q_k^j(R_k^j, \theta_k^j)$ is the jth profile point of horizontal profile $y_r(k)$ and its radial coordinate (R_k^j), is taken as the profile state of this point. Consequently, the horizontal profile state of step k is defined in the following equation,

$$y_r(k) = \left[y_r^1(k), y_r^2(k), \ldots, y_r^j(k), \ldots, y_r^m(k) \right]. \tag{5}$$

From the definition of Δu_r (Figure 4), namely the horizontal distance that the tool moves between two consecutive steps, the horizontal distance between Q_k^j and Q_{k+1}^j can be taken to be $\Delta u_r^j(k+1)$, as shown in the side view of Figure 5. In TPIF, the part is formed incrementally step by step with the sizes of Δu_r and Δu_z typically being small. Consequently, the amounts of springback in two neighbouring steps are very close to

each other and can be taken to be equal to each other. Based on this, a linear model is built for MPC control to predict the horizontal profile states during the forming process. Since the linear model is dynamic and the feedback of the measured shape state is updated at each step, the prediction errors brought by the linear model can be partially compensated. Therefore, the linearisation can be taken as reasonable for in-process control in ISF. After the shape measurement at step *k*, the state of point Q_{k+1}^{j} can be predicted in the next equation.

$$\hat{y}_r^j(k+1) = y_r^j(k) + \Delta u_r^j(k+1) \tag{6}$$

Taking into account the profile points in all radial directions, the profile state of next step can be estimated as,

$$\hat{y}_r(k+1|k) = y_r(k) + \Delta u_r(k+1), \tag{7}$$

where $\hat{y}_r(k+1) = \left[\hat{y}_r^1(k+1), \hat{y}_r^2(k+1), \ldots, \hat{y}_r^j(k+1), \ldots, \hat{y}_r^m(k+1)\right]$ is the predicted profile state of next step, $\Delta u_r(k+1) = \left[\Delta u_r^1(k+1), \Delta u_r^2(k+1), \ldots, \Delta u_r^j(k+1), \ldots, \Delta u_r^m(k+1)\right]$ is the horizontal step increment of next step.

In the future several steps, the predicted profile states can also be obtained in the following equation,

$$\begin{aligned}
&\hat{y}_r(k+1|k) = y_r(k) + \Delta u_r(k+1) \\
&\hat{y}_r(k+2|k) = \hat{y}_r(k+1|k) + \Delta u_r(k+2) \\
&\qquad\qquad = y_r(k) + \Delta u_r(k+1) + \Delta u_r(k+2) \\
&\quad \vdots \\
&\hat{y}_r(k+N_p|k) = y_r(k) + \Delta u_r(k+1) + \Delta u_r(k+2) + \ldots + \Delta u_r(k+N_p)
\end{aligned}, \tag{8}$$

where N_p is the prediction horizon in MPC control and is set as 6 in this work after tuning.

By collecting Equation (8) together, the matrix-vector form of this equation can be obtained,

$$\hat{Y}_r(k) = Y_r(k) + L_r \Delta U_r(k), \tag{9}$$

where $Y_r(k) = [y_r(k), y_r(k), \ldots, y_r(k)]^T$ is the measured profile states at current step, $\hat{Y}_r(k) = \left[\hat{y}_r(k+1|k), \hat{y}_r(k+2|k), \ldots, \hat{y}_r\left(k+N_p|k\right)\right]^T$ is the collection of the predictions of future horizontal profile states, $\Delta U_r(k) = \left[\Delta u_r(k+1), \Delta u_r(k+2), \ldots, \Delta u_r(k+N_p)\right]^T$ stands for the horizontal inputs of next N_p steps; L_h is the coefficient matrix that indicates how the horizontal input influences the horizontal profile state in the future N_p steps and it is expressed in the next equation,

$$L_r = \begin{bmatrix} I & 0 & 0 & 0 \\ I & I & 0 & 0 \\ \vdots & \vdots & \ddots & 0 \\ I & I & \cdots & I \end{bmatrix}. \tag{10}$$

At time-step *k*, the control problem in the horizontal module can be summarised as an optimisation problem to optimise the horizontal toolpath inputs through minimising the difference between the predicted profile states and target profile states in the prediction horizon:

$$\min J_r = \left\| \hat{Y}_r - W_r \right\|^2 + \lambda_r \left\| \Delta U_r - \Delta U_{r0} \right\|^2, \tag{11}$$

$$\text{subject to } \hat{y}_r(k+j \mid k) = y_r(k) + \sum_{i=1}^{j} \Delta u_r(k+i), j = 1,2,\ldots,N_p$$

$$\left|\Delta u_r(k+j) - \Delta u_{r\,0}(k+j)\right| \le e, j = 1,2,\ldots,N_p$$

where J_r stands for the cost function, W_r is the target profile states in the horizontal direction, ΔU_r contains the horizontal inputs of several future steps, ΔU_{r0} is the collection of the initial horizontal inputs in the initial toolpath. Besides the minimisation of the difference between $\hat{Y}_r(k)$ and W_r, another item is added in the cost function to limit the control inputs in a predefined range around the initial inputs with *e* is set as 0.5, λ_r is the weighting coefficient and is adopted as 0.7 in this work after tuning;

2.1.2 Vertical control module

To optimise Δu_z for toolpath correction in the vertical direction, the vertical MPC module is developed based on a different deformation model that only uses one specified point to represent the vertical shape state in the vertical module while the control structure is similar to the horizontal control module.

In the side view of Figure 5, the vertical cross-sectional profile at each step is a curve which also can be represented by a number of points. At step *k*, P_{c_k} is the contact point where the flat local wall is tangent to the hemispherical end of the tool while P_{b_k} is the point where the bottom point of the ball end touches the metal blank. Due to the springback, the formed depth of the shape is generally smaller than the target depth. This control module is to drive the metal blank to the target depth by using the optimised Δu_z. That is, the vertical control module aims to drive the bottom point on

the cross-sectional profile to the target position. Considering the vertical sectional profiles in all the radial directions ($\theta_k = \theta_k^1, \theta_k^2 \cdots, \theta_k^j, \cdots, \theta_k^m$) in the top view of Figure 5, the *z* coordinates of the bottom points of these vertical sectional profiles are taken as the shape state, $y_z(k)$, in the vertical direction.

$$y_z(k) = \left[y_z^1(k), y_z^2(k), \ldots, y_z^j(k), \ldots, y_z^m(k) \right] \tag{12}$$

Based on the incremental nature of TPIF, the shape is formed incrementally step by step and the size of Δu_z typically is small. Therefore, the amounts of springback in two neighbouring steps are very close to each other and can be considered to be equal to each other for building a linear model for MPC control. Under this simplification, the vertical distance between P_{b_k} and $P_{b_{k+1}}$ in the radial direction $\theta = \theta_k^s$ will be the step depth of step *k+1*, as expressed in the following equation,

$$\Delta u_z^s(k+1) = \hat{y}_z^s\left(k+1 \mid k\right) - y_z^s(k). \tag{13}$$

In the contour toolpath, the contours are parallel to each other. The contour points of each contour are on the same z-level plane, which is consistent with the way they are defined in the initial contour toolpath. Therefore, the $\Delta u_z(k+1)$ values in all the radial directions are the same. That is, $\Delta u_z(k+1) = \left[\Delta u_z^1(k+1), \Delta u_z^2(k+1), \ldots, \Delta u_z^j(k+1), \ldots, \Delta u_z^m(k+1) \right]$ can be expressed as,

$$\Delta u_z(k+1) = \Delta u_z^s(k+1) I_{1\times m} \ . \tag{14}$$

Based on this, the optimised $\Delta u_z(k+1)$ can be obtained in the optimisation of just one element, namely $\Delta u_z^s(k+1)$, in a selected radial direction. In this work, the radial direction through the middle of one of the curved fillets ($\theta_k^s=45°$) was used for optimising $\Delta u_z(k+1)$ in the vertical control module.

Consequently, only one element of $y_z(k)=\left[y_z^1(k), y_z^2(k), \ldots, y_z^j(k), \ldots, y_z^m(k)\right]$, namely $y_z^s(k)$, is investigated in the vertical control module. The vertical shape state at each step can be simplified as,

$$y_z(k)=y_z^s(k)\,. \tag{15}$$

$y_z^s(k)$ can be obtained in the cross-sectional profile in the selected radial direction ($\theta_k^s=45°$) after measuring the formed shape at step *k*. The vertical state of next step can be predicted as,

$$\begin{aligned}\hat{y}_z(k+1\,|\,k) &= y_z(k)+\Delta u_z^s(k+1)\\ &= y_z^s(k)+\Delta u_z^s(k+1)\end{aligned}\,, \tag{16}$$

where $\hat{y}_z(k+1)$ is the predicted profile state of next step. Similarly, the vertical shape states over the prediction horizon can be obtained by,

$$\begin{aligned}\hat{y}_z(k+1\,|\,k) &= y_z^s(k)+\Delta u_z^s(k+1)\\ \hat{y}_z(k+2\,|\,k) &= \hat{y}_z(k+1\,|\,k)+\Delta u_z^s(k+2)\\ &= y_z^s(k)+\Delta u_z^s(k+1)+\Delta u_z^s(k+2)\\ &\vdots\\ \hat{y}_z(k+N_p\,|\,k) &= y_z^s(k)+\Delta u_z^s(k+1)+\Delta u_z^s(k+2)+\Delta u_z^s(k+N_p)\end{aligned}\,. \tag{17}$$

Equation (17) can be gathered into the matrix-vector form,

$$\hat{Y}_z(k) = Y_z(k) + L_z \Delta U_z(k), \tag{18}$$

where $\hat{Y}_z(k) = \left[\hat{y}_z(k+1|k), \hat{y}_z(k+2|k), \ldots, \hat{y}_z(k+N_p|k) \right]^T$ collects the state predictions of future N_p steps, $Y_z(k) = [y_z^s(k), y_z^s(k), \ldots, y_z^s(k)]^T$ is the measured shape state at time-step k, $\Delta U_z(k) = \left[\Delta u_z^s(k+1), \Delta u_z^s(k+2), \ldots, \Delta u_z^s(k+N_p) \right]^T$ is the vertical toolpath inputs, L_z is a matrix obtained by collecting Equation (17) together and is expressed as,

$$L_z = \begin{bmatrix} 1 & 0 & 0 & 0 \\ 1 & 1 & 0 & 0 \\ \vdots & \vdots & \ddots & 0 \\ 1 & 1 & \cdots & 1 \end{bmatrix}. \tag{19}$$

To the drive the formed depth as close as possible to the target depth at each step, the control problem in the vertical control module at time-step k can also be summarised as an optimisation problem in the following equation. The second item is used to limit the size of vertical toolpath inputs that are negative at all steps. λ_z is set as 0.2, which is the same as in [1].

$$\min J_z = \left\| \hat{Y}_z - W_z \right\|^2 + \lambda_z \Delta U_z{}^T \Delta U_z \tag{20}$$

$$\text{subject to } \Delta U_z(k) = \left[\Delta u_z^s(k+1), \Delta u_z^s(k+2), \ldots, \Delta u_z^s(k+N_p) \right]^T, k = 1, 2, \ldots, N$$

$$\hat{y}_z(k+j|k) = y_z^s(k) + \sum_{i=1}^{j} \Delta u_z^s(k+i), j = 1, 2, \ldots, N_p$$

$$\Delta u_{z\min} \le \Delta u_z(k+j) \le \Delta u_{z\max}, j = 1, 2, \ldots, N_p$$

where J_z is the cost function, W_z is the target vertical states, N is the number of steps. The min and max values of Δu_z are 0.5mm and 2 mm, respectively.

In summary of Section 2.1, two separate MPC control modules have been developed to get the optimal Δu_r and Δu_z for in-process toolpath correction at each step. To solve the optimisation problems in the two control modules, the cost functions can be transformed into typical Quadratic Programming (QP) problems and would be solved using the method in our previous study [1]. After solving the optimisation problems, ΔU_z^* and ΔU_r^*, the optimised toolpath inputs over the next N_p steps, will be obtained. Only the first optimal move, namely the optimised toolpath inputs in the next one step, will be applied to form the contour in the next single step. Control actions will be conducted using the two-directional MPC control algorithm at each subsequent step until the shape is finally formed.

2.2 Application in TPIF with a partial die

The developed control strategy was applied to TPIF using a partial die to form parts. The implementation of the control system in the lab is shown in Figure 6. After the forming of a certain step was finished, currently formed shape was measured by a 3D digitiser. The shape states of current shape used for feedback control were generated by sectioning the scanned geometry. The shape states then were imported into the MPC control module where toolpath parameters were optimised in the well-defined optimisers. As a result, the metal blank was deformed by the tool following a corrected toolpath in the next step. As the tool formed down step by step, the toolpath was continuously corrected based on the shape feedback to get improved geometric accuracy in the final part.

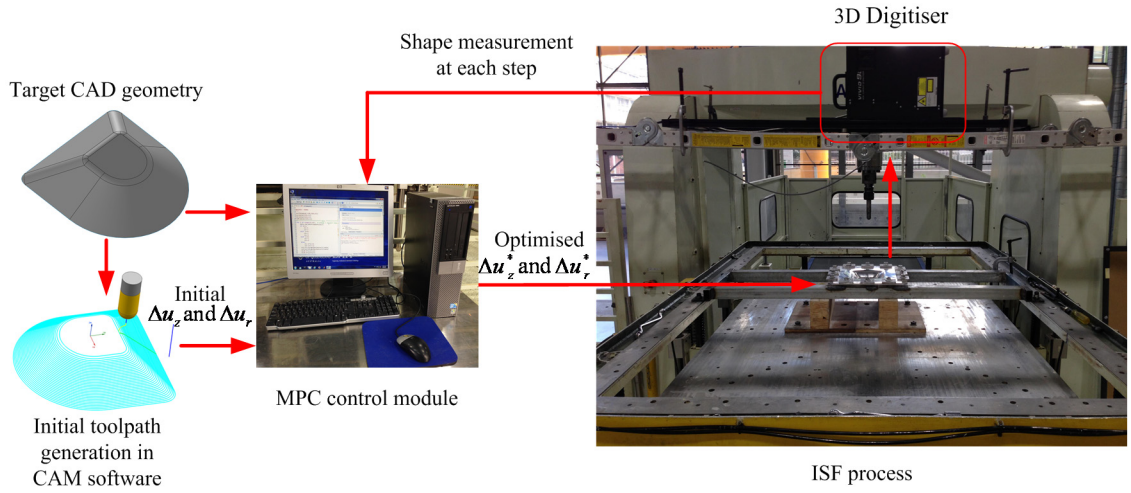

Figure 6 Structure of the closed-loop control system for ISF.

3. Experimental validation

The developed control strategy for TPIF with a partial die was experimentally validated in forming a non-axisymmetric shape. The control system for TPIF is built based on an ISF machine from AMINO® Corporation (Figure 6). During the forming process with control, the shape measurement of the formed parts for feedback is completed using a 3D Digitiser (VIVID 9i) placed on the top of the forming platform. It takes about 2.5 seconds for each scan and the scanning accuracy is in the range of ±0.05 mm, which is of sufficient accuracy for shape measurement in ISF. Then, the geometric data of scanned formed parts is collected in GEOMAGIC Qualify and is imported to the control algorithm programmed in Python. When the forming process is completed, the 3D comparison between the scanned formed part and the designed CAD model is performed using GEOMAGIC Qualify. The experiment results from uncontrolled and controlled TPIF processes were compared and analysed in terms of the geometric accuracy.

3.1 Case studies

The test shape used for the experiments was a non-axisymmetric shape, which contains both flat and curved walls (Figure 7). The wall angle was 40° and the total depth was 35mm. There are a number of z-level contours in the initial toolpath, as shown in Figure 7. The initial step depth was set as 1mm. Consequently, the number of steps in the forming process was calculated as 35. The metal sheet used for tests was made of aluminium (AA 7075-O) and the raw thickness was 1.6 mm. The unformed blank size was 300 mm × 300 mm. A ball-ended tool with a 20 mm diameter was used in the experiments. The feed rate in the forming process was 4000 mm/min. Based on the test shape, a partial die (Figure 8) made of timber was fabricated for the TPIF forming process in the test. Lubricating oil was used for lubrication during the forming process.

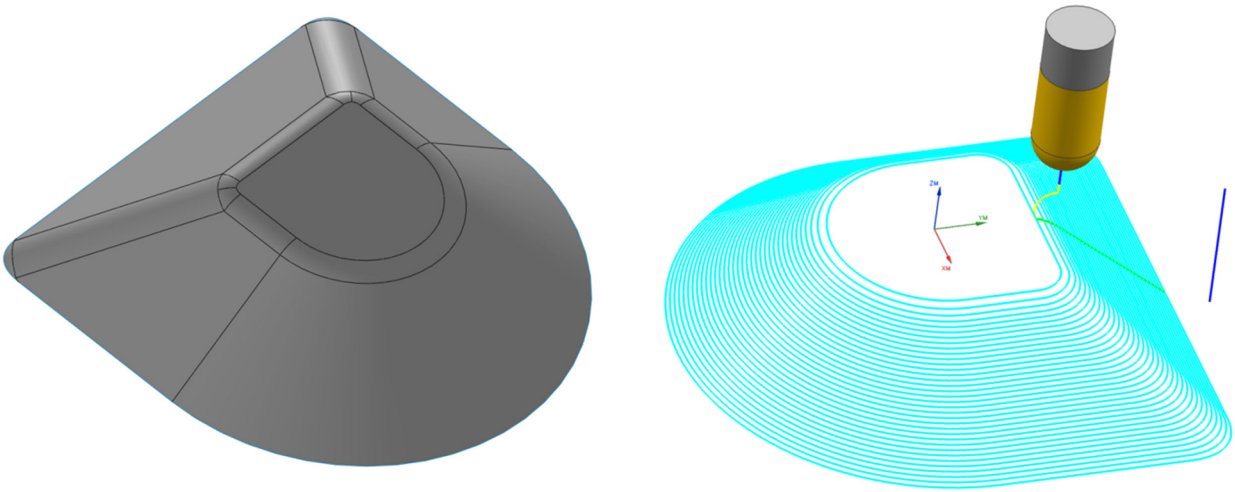

Figure 7 Test shape and the initial toolpath from CAM software.

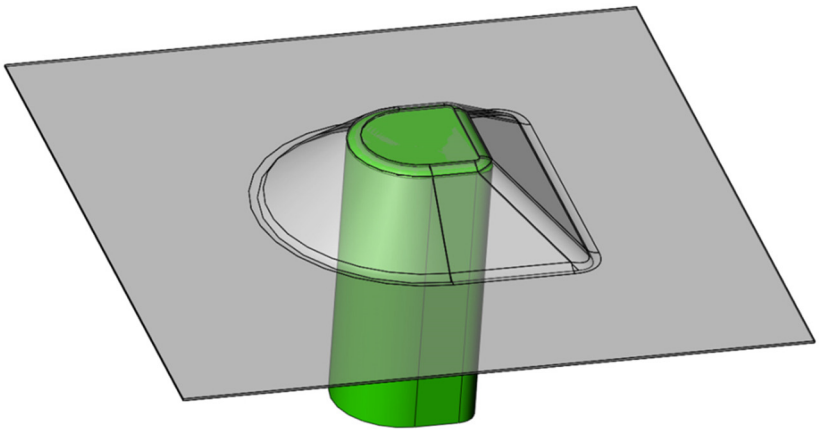

Figure 8 The partial die used in the TPIF process.

3.2 Results and discussion

In this section, the results of toolpath correction in TPIF are firstly illustrated by the comparison of initial toolpath and the corrected toolpath. Figure 9 shows the contours of the corrected toolpath and initial toolpath in terms of three sample steps (10th, 20th, and 30th). The initial depth of the contours at the three steps are z=-10, -20, -30mm, respectively, since the initial step depth was set as 1mm. From the comparison in the isometric view and the top view, it can be observed that the toolpath is corrected in the horizontal and vertical directions. This is achieved based on the optimised Δu_z and Δu_r at each step during the forming process.

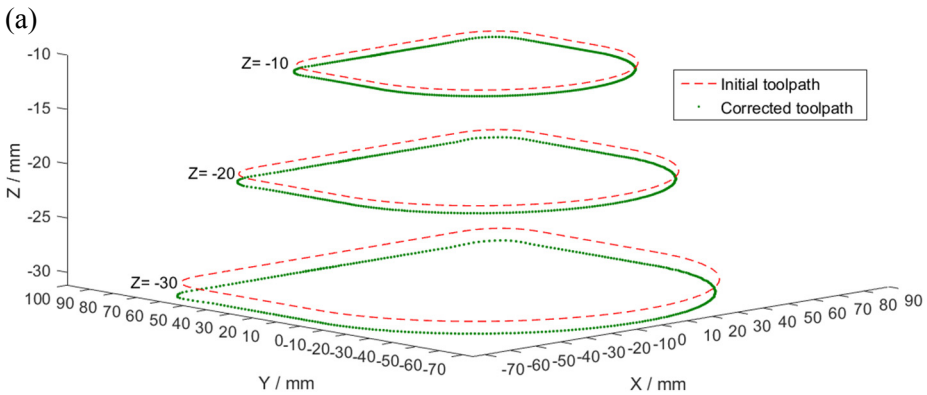

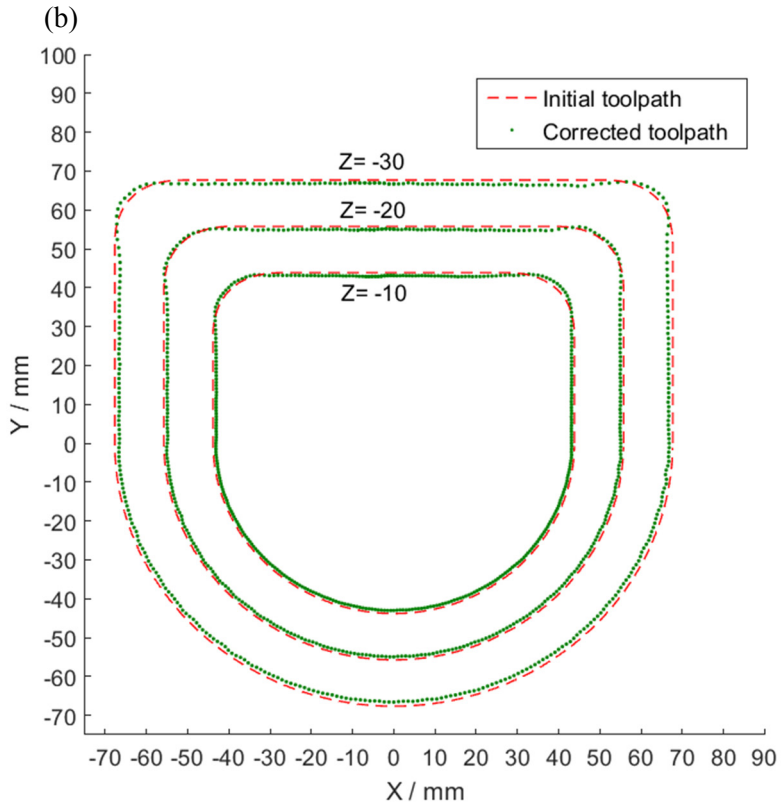

Figure 9 Contours of the corrected toolpath and the initial toolpath at three sample steps: (a) Isometric view; (b) Top view;

To analyse the geometric accuracy of uncontrolled and controlled TPIF processes, formed parts in the unclamped condition are compared using horizontal sectional profiles (Figure 10) and error distribution colour maps from the top view (Figure 11). The sectional profiles in Figure 10 were obtained in the horizontal sections at three z levels (z=-10, -20, -30mm).

In the TPIF process without toolpath control, the formed part has low geometric accuracy in the wall areas and the errors reach as large as 3 mm near the outside (bottom) edges, as shown in Figure 10 and Figure 11a. This is mainly caused by the sheet springback. However, from the top view (Figure 11), the inside base area (top) supported by the partial die is of high accuracy ($\pm$0.3 mm) in both controlled and

uncontrolled TPIF processes. Also, there is no notable “pillow effect”, which occurs in the flat base of the formed part in SPIF, observed in the base areas in the TPIF processes.

Compared with the part formed in uncontrolled TPIF, the part formed with MPC control has improved accuracy in most areas, as shown in Figure 11b. This can also be demonstrated by the comparison of the sectional profiles (Figure 10). In particular, there is significant improvement (from ±3 mm to ±0.3 mm) on the geometric accuracy in terms of the wall areas. Nevertheless, the accuracy in the certain areas of the corner fillets is still out of the desirable range and is slightly worse than the result from TPIF without toolpath control. In the areas of corner fillets, the local curvature of the shape changes rapidly in a relatively small range since the fillet radius equals the tool radius in the shape design. This could cause sudden changes of the strain when the tool deforms this area. As a result, the springback in the corner fillet areas varies rapidly so that the springback would be more complex and more difficult to capture. The springback of these areas was not well compensated in the current control model, which is the primary limitation of the current work.

Figure 12 shows the comparison of deviation distributions (percentage) between TPIF processes with and without control. More specifically, the formed shape was scanned into a large number of scatter points. This figure illustrates how dimensional deviations of all the points are distributed in different deviation ranges in the form of percentage distribution. The percentage of deviations ranging from +0.6 mm to +3.0 mm is greatly shortened from 78% to 8.5% with the use of MPC control algorithm. The percentage of deviations in the range ±0.3 mm significantly increases from 19.5% to 70%. Compared

with uncontrolled TPIF, the deviations of the points are more intensively distributed near the desirable range in terms of the TPIF with toolpath control.

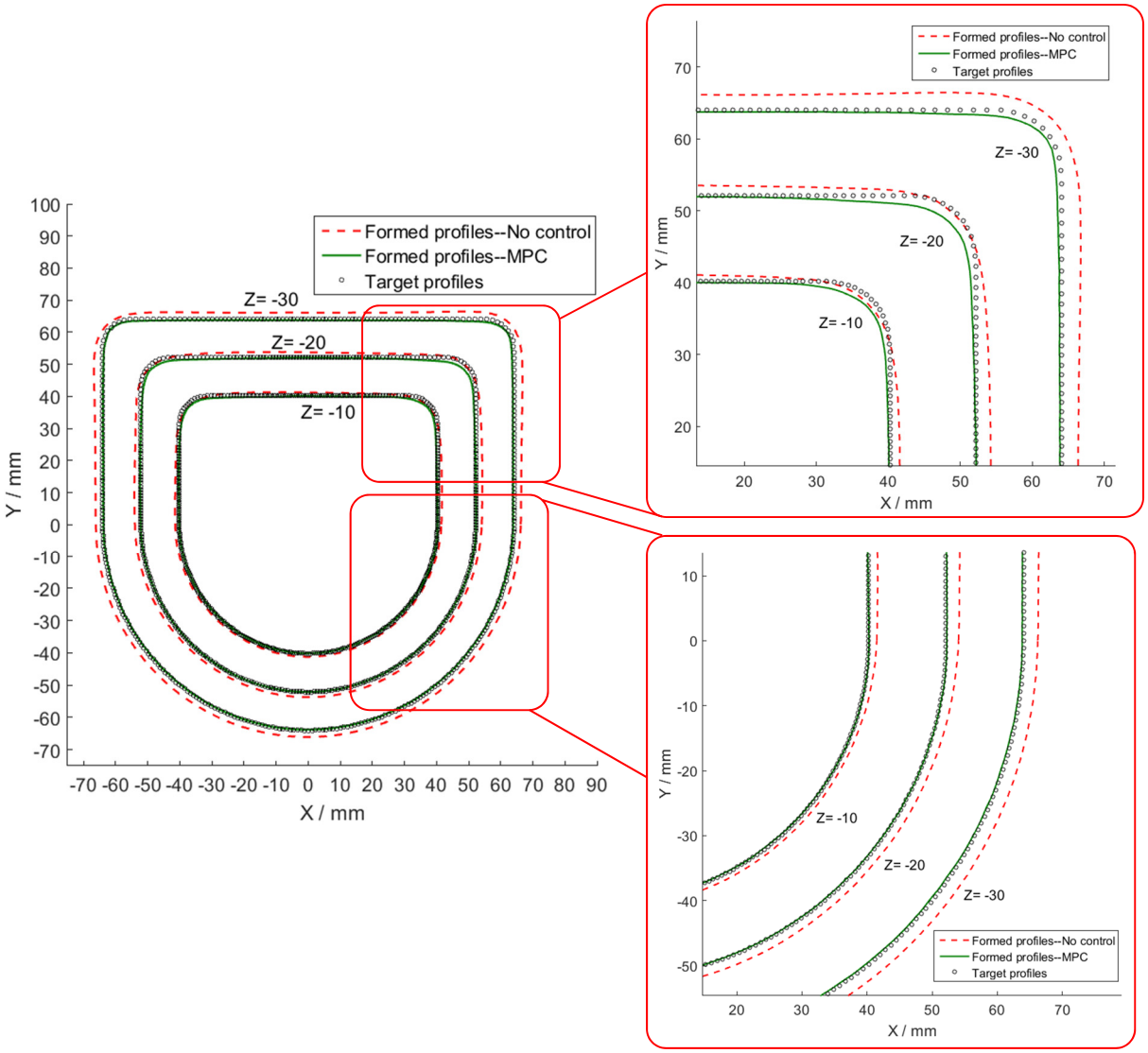

Figure 10 Comparison of sectional profiles from three horizontal sections.

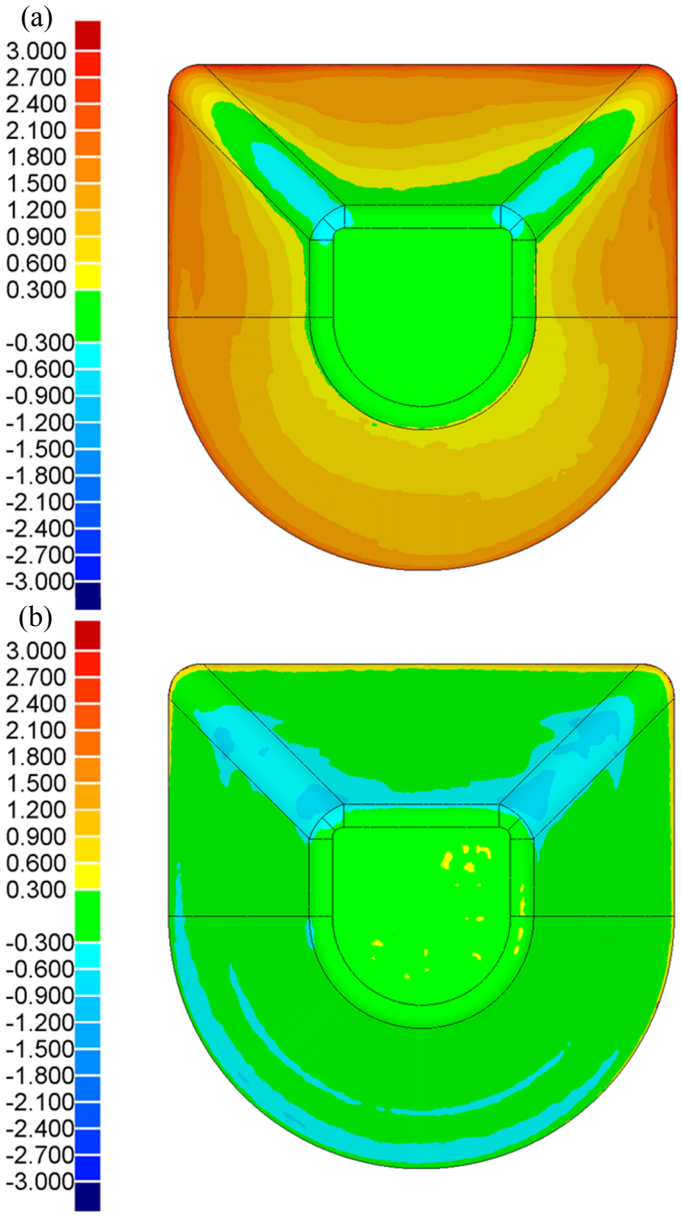

Figure 11 Geometric accuracy colour maps: (a) No control; (b) MPC control.

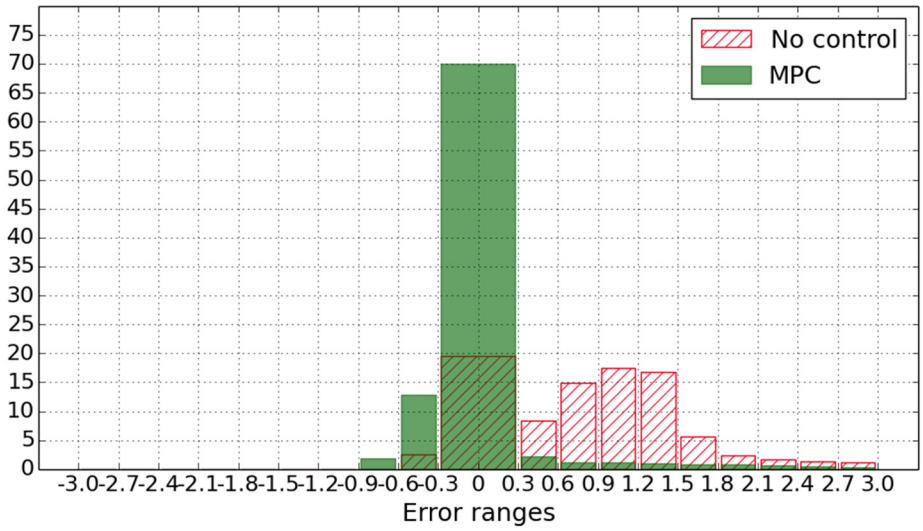

Figure 12 Deviation distributions (percentage) of different error ranges in the colour maps.

4. Conclusions and Future work

This paper reports an in-process toolpath correction strategy specially developed for TPIF with a partial die using MPC control for its ability to use linear models to achieve good control of constrained nonlinear systems in various industries [17, 19]. The MPC control algorithm was developed based on the deformation nature of TPIF with partial die, and a simple MPC algorithm for SPIF in our previous work [1]. The control algorithm presented in this paper is able to deal with toolpath correction in the horizontal and vertical directions through optimising two toolpath parameters (Δu_r and Δu_z) in two separate control modules. This toolpath correction strategy was experimentally tested to form a non-axisymmetric shape. Compared with the typical TPIF process that has no toolpath correction, fairly good improvement in geometric accuracy was achieved with the use of the toolpath correction strategy in TPIF with a partial die while the geometric accuracy in the partial fillet areas requires further

improvement. This work provides a helpful approach to achieve in-process toolpath control/correction in TPIF.

One of the primary limitations of this work is that current control approach is not able to perfectly compensate the springback in the partial corner fillet areas of the test shape. The springback in the fillet areas with high curvature could be more complex because the local curvature changes rapidly in a small range and rapid changes of the strain could occur when the tool deforms the corner fillets. In the current control model, the Δu_z values of the contour points in different radial directions on each contour are taken to be constant, which follows the way of defining Δu_z in the typical contour toolpath. To effectively correct the errors in the areas with high curvature, such as corner fillets, the z positions of the contour points on each contour might need to be adjusted differently in different radial directions.

In the future, this limitation might be solved by using more complex predictive models and the further development of current MPC control algorithm through using varying Δu_z values in different radial directions at each step as well as coupling two toolpath parameters in the control algorithm. What's more, the geometric errors in the region that has already been formed might be further corrected by the integration of the MPC control algorithm with a multi-stage toolpath.

Acknowledgements

China Scholarship Council (CSC) is acknowledged for the scholarship support.

References

[1] Lu H, Kearney M, Li Y, Liu S, Daniel WT, Meehan P. Model predictive control of incremental sheet forming for geometric accuracy improvement. The International Journal of Advanced Manufacturing Technology. 2015:1-14.
[2] Li Y, Daniel WJT, Meehan PA. Deformation analysis in single-point incremental forming through finite element simulation. The International Journal of Advanced Manufacturing Technology. 2016:1-13.
[3] Bambach M, Taleb Araghi B, Hirt G. Strategies to improve the geometric accuracy in asymmetric single point incremental forming. Production Engineering. 2009;3:145-56.
[4] Attanasio A, Ceretti E, Giardini C, Mazzoni L. Asymmetric two points incremental forming: Improving surface quality and geometric accuracy by tool path optimization. Journal of Materials Processing Technology. 2008;197:59-67.
[5] Fiorentino A, Feriti GC, Giardini C, Ceretti E. Part precision improvement in incremental sheet forming of not axisymmetric parts using an artificial cognitive system. Journal of Manufacturing Systems. 2015;35:215-22.
[6] Li Y, Lu H, Daniel WT, Meehan P. Investigation and optimization of deformation energy and geometric accuracy in the incremental sheet forming process using response surface methodology. The International Journal of Advanced Manufacturing Technology. 2015;79:2041-55.
[7] Araghi BT, Manco GL, Bambach M, Hirt G. Investigation into a new hybrid forming process: Incremental sheet forming combined with stretch forming. Cirp Ann-Manuf Techn. 2009;58:225-8.
[8] Taleb Araghi B, Göttmann A, Bambach M, Hirt G, Bergweiler G, Diettrich J, et al. Review on the development of a hybrid incremental sheet forming system for small batch sizes and individualized production. Production Engineering. 2011;5:393-404.
[9] Ambrogio G, Napoli L, Filice L. A novel approach based on multiple back-drawing incremental forming to reduce geometry deviation. International Journal of Material Forming. 2009;2:9-12.
[10] Allwood JM, Braun D, Music O. The effect of partially cut-out blanks on geometric accuracy in incremental sheet forming. Journal of Materials Processing Technology. 2010;210:1501-10.
[11] Hirt G, Ames J, Bambach M, Kopp R, Kopp R. Forming strategies and Process Modelling for CNC Incremental Sheet Forming. CIRP Annals - Manufacturing Technology. 2004;53:203-6.
[12] Lu B, Chen J, Ou H, Cao J. Feature-based tool path generation approach for incremental sheet forming process. Journal of Materials Processing Technology. 2013;213:1221-33.
[13] Behera AK, Verbert J, Lauwers B, Duflou JR. Tool path compensation strategies for single point incremental sheet forming using multivariate adaptive regression splines. Computer-Aided Design. 2013;45:575-90.
[14] Fu ZM, Mo JH, Han F, Gong P. Tool path correction algorithm for single-point incremental forming of sheet metal. Int J Adv Manuf Tech. 2013;64:1239-48.
[15] Fiorentino A, Giardini C, Ceretti E. Application of artificial cognitive system to incremental sheet forming machine tools for part precision improvement. Precision Engineering. 2015;39:167-72.
[16] Allwood JM, Music O, Raithathna A, Duncan SR. Closed-loop feedback control of product properties in flexible metal forming processes with mobile tools. CIRP Annals - Manufacturing Technology. 2009;58:287-90.
[17] Wang H, Duncan S. Constrained model predictive control of an incremental sheet forming process. Control Applications (CCA), 2011 IEEE International Conference on2011. p. 1288-93.

[18] Reddy NV, Lingam R, Cao J. Incremental Metal Forming Processes in Manufacturing. In: Nee AYC, editor. Handbook of Manufacturing Engineering and Technology: Springer London, 2014. p. 411-52.
[19] Camacho EF, Bordons C, Camacho EF, Bordons C. Model predictive control: Springer London, 2004.
[20] Malhotra R, Reddy NV, Cao JA. Automatic 3D Spiral Toolpath Generation for Single Point Incremental Forming. J Manuf Sci E-T Asme. 2010;132.